

**THE DISTRIBUTION OF CHARGE AND ACIDIC FUNCTIONAL
GROUPS IN NATURAL ORGANIC MATTER: THE DEPENDENCE
ON MOLECULAR WEIGHT AND pH.**

**A Dissertation
Presented to the
Academic Faculty**

by

Jason Duane Ritchie

**In Partial Fulfillment
of the Requirements for the Degree
of Doctor of Philosophy In the
School of Earth and Atmospheric Sciences**

**Georgia Institute of Technology
December 2005**

Copyright © Jason Duane Ritchie 2005

**THE DISTRIBUTION OF CHARGE AND ACIDIC FUNCTIONAL
GROUPS IN NATURAL ORGANIC MATTER: THE DEPENDENCE
ON MOLECULAR WEIGHT AND pH.**

Approved by:

Prof. E. Michael Perdue, Advisor and committee chair

School of Earth and Atmospheric Sciences

Georgia Institute of Technology

Prof. Michael Bergin, committee member

School of Earth and Atmospheric Sciences

Georgia Institute of Technology

Prof. Ching-Hau Huang, committee member

School of Civil and Environmental Engineering

Georgia Institute of Technology

Prof. Ellery Ingall, committee member

School of Earth and Atmospheric Sciences

Georgia Institute of Technology

Prof. Martial Taillefert, committee member

School of Earth and Atmospheric Sciences

Georgia Institute of Technology

Date approved: August 16, 2005

To my soul mate and only love,
I finally made it, now our lives truly begin.

ACKNOWLEDGEMENT

I would like to express my sincere gratitude to my academic advisor, Dr. E. Michael Perdue, for his dedication to bringing this project to fruition. During the last seven years, Dr. Perdue has provided me with excellent guidance in the development of my laboratory and research skills. Because of Dr. Perdue, I was given the opportunity to co-author a review chapter on natural organic matter in the very prestigious *Treatise on Geochemistry* series.

I would also like to thank Dr. Michael Bergin, Dr. Ching-Hua Huang, Dr. Ellery Ingall, and Dr. Martial Taillefert for serving as my committee members. I also thank the administrative and office staff in the School of Earth and Atmospheric Sciences (Rita Anderson, Susan Ryan, Laura Cederquist, Kathy Plummer, and Keith Anderson), and Chair Dr. Judith Curry, for generously supporting my efforts to complete my studies, research, and teaching assignments. Numerous faculty, research staff, and graduate students in the School of Earth and Atmospheric Sciences assisted me in this work. I sincerely thank Dr. Lu (Lucy) Sun, Jean-Francois Koprinjak, Meg Grantham, and Amy Sullivan for their respective laboratory expertise. I thank Dr. Scott Sandholm for the donation of surplus parts and equipment for the repair of the spectrophotometer.

I was fortunate to collaborate with numerous scientific professionals at the GSF Forschungszentrum für Umwelt und Gesundheit (Munich, Germany): Prof. Dr. Philippe Schmitt-Kopplin, Dr. Norbert Hertkorn, Heidi Neumeir, Moritz Frommberger, and Agnes Fekete. Dr. Schmitt-Kopplin's expertise in capillary electrophoresis and his generous assistance was invaluable. I also thank Dr. Paul Bloom, University of Minnesota, for

providing both financial support and samples of the IHSS standards.

I must give a special acknowledgement to the Chemistry Department at Frostburg State University (Dr. Donald Weser, Dr. James Martin, Dr. Paul Hunt, Dr. Mary Mumper, and Dr. Fred Senese) and to my mentor, Dr. Robert Larivee, who convinced me that a scientist will only be happy if he (or she) does science, and does science well.

TABLE OF CONTENTS

Acknowledgement	iv
List of Tables	xiii
List of Figures	xvii
Summary	xxiv
 Chapter 1. INTRODUCTION	 1
1.1 The acid-base chemistry of natural organic matter.	1
1.2 Research objectives.	4
 Chapter 2. BACKGROUND	 7
2.1 Terminology.	7
2.2 Size-exclusion Chromatography (SEC).	7
2.2.1 Size-exclusion chromatography of NOM.	7
2.2.2 Calibration of SEC systems.	11
2.2.3 Methods of detection.	12
2.3 The acid-base chemistry of natural organic matter.	13
2.3.1 Indirect and direct titration methods.	13
2.3.2 Organic charge and charge density.	15
2.3.3 Quantifying titration data of NOM.	17
2.4 Capillary electrophoresis of NOM.	19

2.4.1	Variables that effect capillary electrophoretic separations.	20
2.4.2	The effective mobility scale.	24
2.4.3	Charge-to-size relationship in CE.	26
2.4.4	Capillary electrophoresis of NOM.	28
2.4.5	Shapes of electropherograms.	31
2.4.6	Capillary electrophoresis of NOM samples of different molecular weight.	32
Chapter 3. METHODS FOR CHEMICAL AND INSTRUMENTAL ANALYSES		34
3.1	Instrumentation, chemicals, and solutions.	34
3.2	Preparative fractionation of the Suwannee River NOM by size-exclusion chromatography (SEC).	38
3.2.1	Preparation of solutions.	38
3.2.2	Preparation of resin and SEC column.	39
3.2.3	Fractionation of the Suwannee River NOM.	40
3.2.4	Division of fractions.	42
3.2.5	Final processing of SRNOM fractions.	43
3.3	Determination of molecular weights (MW) by SEC.	43
3.3.1	Preparation of solutions.	44
3.3.2	Preparation of resin and column for SEC.	45
3.3.3	Protocol for SEC at pH 6.8.	45
3.3.4	Protocol for SEC at pH 9.3.	45
3.3.5	Calibration of SEC system.	46

3.3.6	Evaluation and modeling of absorbance and online-TOC chromatograms.	46
3.3.7	The 3-Gaussian (3-G) models for UV-absorbance and TOC chromatograms.	49
3.3.8	Number-average (M_n) and weight-average (M_w) molecular weights.	50
3.4	Elemental analysis.	52
3.4.1	Organic elements.	52
3.4.2	Inorganic elements.	52
3.5	UV-visible spectroscopy.	53
3.5.1	Measurements of UV-visible absorbance.	53
3.5.2	Specific UV absorptivity (SUVA).	53
3.5.3	E_4/E_6	55
3.6	Acid-base chemistry by direct titrations.	56
3.6.1	Direct titration method.	56
3.6.2	Calculations of organic charge and charge density.	57
3.6.3	The modified Henderson-Hasselbalch (H-H) model.	60
3.6.4	Concentrations of acidic functional groups by the pH method.	60
3.6.5	Titration of a mixture of seven simple organic acids (SOA).	61
3.7	Capillary electrophoresis (CE).	61
3.7.1	Preparation of CE system.	61
3.7.2	Electrophoretic separations and detection.	62

3.7.3	Baseline corrections of CE chromatograms.	63
3.7.4	The effective mobility scale.	65
3.7.5	Qualitative comparisons of electropherograms.	65
3.7.6	The 3-Gaussian-3-Lorentzian (3-GL) model.	68
Chapter 4.	RESULTS AND DISCUSSION OF CHEMICAL ANALYSES.	70
4.1	Preparative size-exclusion chromatography.	70
4.1.1	Characteristics of preparative SEC chromatograms.	70
4.1.2	Division of fractions.	77
4.1.3	Recovery and yields of the fractions.	80
4.2	Determination of molecular weights by SEC.	82
4.2.1	Calibration of SEC system.	82
4.2.2	Absorbance and online-TOC chromatograms.	85
4.2.3	The mode MW.	90
4.2.4	The 3-Gaussian (3-G) model.	92
4.2.5	Average MWs and ranges of MWs.	92
4.2.6	Literature reports of M_n and M_w .	98
4.2.7	Reconstructing absorbance of the SRNOM.	100
4.3	Elemental analysis.	103
4.3.1	Elemental composition.	103
4.3.2	The elemental compositions of dry, ash-free samples.	106
4.3.3	Literature reports of elemental data.	110
4.3.4	Elemental data and MW.	110

4.4	UV-visible spectrophotometry.	113
4.4.1	The absorbance of UV-visible light.	113
4.4.2	Reconstructing the UV-visible spectrum of the SRNOM.	116
4.4.3	Specific UV absorptivity (SUVA) and E_4/E_6 .	116
4.4.4	Literature reports of SUVA and E_4/E_6 .	122
4.5	Acid-base chemistry by direct titrations.	122
4.5.1	Comparison of forward and reverse titrations.	122
4.5.2	Reconstructing the titration curves of the SRNOM.	126
4.5.3	The modified Henderson-Hasselbalch (H-H) model parameters.	128
4.5.4	pH method for Q_1 and Q_2 .	131
4.5.5	The consequences of hysteresis.	135
4.5.6	Literature reports of acidic functional groups.	138
4.6	Capillary electrophoresis.	140
4.6.1	Overview of CE electropherograms.	140
4.6.2	Comparison of electropherograms between samples.	154
4.6.3	Peak effective mobilities (μ_p).	155

Chapter 5. A PROBABILISTIC APPROACH FOR CHARACTERIZING THE DISTRIBUTION OF CHARGE IN NOM. 160

5.1	Molecular Weight, capillary electrophoresis, and titration data.	160
5.1.1	Probability of molecular weight, $P(MW)$.	160

5.1.2	Probability of effective mobility, $P(\mu)$.	164
5.1.3	Charge density (Q_{pH}) and the z/MW ratio.	165
5.1.4	The conservation of mass and charge.	166
5.2	The Charge Distribution Model (CDM).	170
5.2.1	Input data.	170
5.2.2	z-matrix.	170
5.2.3	P-matrix.	172
5.2.4	Optimization of k_{pH} .	175
5.3	Results of the Charge Distribution Model.	175
5.3.1	Optimized values of k_{pH} .	175
5.3.2	Charge distribution histograms.	177
5.3.3	Molar distribution histograms.	189
5.4	The most probable distribution of charge.	199
5.4.1	Minimum probable charges.	199
5.4.2	Maximum probable charges.	202
5.4.3	Distribution of carboxyl groups.	205
5.4.4	Distribution of phenolic functional groups.	209
Chapter 6. APPLICATIONS OF THE MOST PROBABLE DISTRIBUTION OF CHARGE.		213
6.1	Accurate calculations of ionic strength at high NOM concentrations.	213
6.2	Treatment of ionic strength by the major proton-binding models.	220
6.2.1	Model V and Model VI.	221

6.2.2	The NICA-Donnan model.	227
6.3	The complexity of NOM and the distribution of charge.	230
6.4	Considerations for the most probable distribution of charge.	232
6.5	The most probable distribution of charge and SEC.	235
Chapter 7. CONCLUSION		239
7.1	Chemical analyses.	239
7.2	The most probable distribution of charge.	242
7.3	The application of the most probable distribution of charge.	243
7.4	Final thoughts about the most probable distribution of charge and future research.	244
Appendix		247
References		276
Vita		289

LIST OF TABLES

Table 2.1	The terminology commonly used in the literature for various forms of natural organic matter.	8
Table 3.1	The inventory of laboratory instruments and hardware used.	35
Table 3.2	The inventory of chemicals that were used.	36
Table 3.3	The stock solutions and recipes for the working solutions that were used.	37
Table 3.4	Data for the MW standard compounds used for the calibration of the SEC for MW determination. Data for the polystyrene sulfonate standards were provided by Polysciences, Inc. (Warren, PA).	47
Table 4.1	The division of the preparative SEC chromatogram for the SRNOM elution performed on February 19, 2001 (see Figure 4.4).	79
Table 4.2	The final recoveries of the % area by absorbance, total mass, and total carbon for Fractions 1-7 after the completion of the 70 separations of the SRNOM by preparative SEC.	81
Table 4.3	The parameters for the three-Gaussian model (3-G) for absorbance and TOC chromatograms.	93
Table 4.4	The number-average (M_n) and weight-average (M_w) molecular weights, and the minimum and maximum MWs for the SRNOM and Fractions 1-7 as determined by semi-analytical SEC at pH 6.8 and pH 9.3. Average MWs have units of g mol^{-1} . Polydispersity (P) is calculated as M_w/M_n . Minimum and maximum MWs have units of Daltons.	96
Table 4.5	The average MWs for the Suwannee River fulvic acid (SRFA), humic acid (SRHA), and other Suwannee River NOM samples (SRNOM) as reported in the literature. Average MWs have units of g mol^{-1} .	99

Table 4.6	The raw elemental composition for the SRNOM and Fractions 1-7 as reported by Huffman Laboratory (Golden, Colorado) in June, 2001.	104
Table 4.7	The inorganic ions in the ash portion of each sample.	105
Table 4.8	Elemental analyses on a dry, ash-free basis.	107
Table 4.9	The mass yield (g) and % mass yield of the organic forms of carbon, hydrogen, nitrogen, and oxygen that were recovered in Fractions 1-7 compared to those in the SRNOM separated during the preparative SEC.	108
Table 4.10	The elemental data for the Suwannee River fulvic acid (FA), humic acid (HA), and NOM as reported in the literature.	111
Table 4.11	The specific UV absorptivity (SUVA) at 254 nm ($\text{L gC}^{-1} \text{ cm}^{-1}$) and the E_4/E_6 values for the SRNOM and Fractions 1-7 at pH 6.8 and pH 9.3.	117
Table 4.12	The specific UV absorptivity (SUVA) at 254 nm ($\text{L gC}^{-1} \text{ cm}^{-1}$) and the E_4/E_6 values for the IHSS standard collection and other soil FAs and HAs as reported in the literature.	121
Table 4.13	The estimates of acid functional groups by pH-cutoff method and the Henderson-Hasselbalch (H-H) model parameters for the SRNOM, Fractions 1-7, and the mixture of seven simple organic acids (SOA).	129
Table 4.14	The downward drift in pH and differences in acidic functional group concentrations for the SRNOM and Fractions 1-7 caused by hysteresis.	136
Table 4.15	The concentrations of acidic functional groups (mmol gC^{-1}) for the Suwannee River fulvic acid(s) and humic acid(s) that were determined by direct titration methods as reported in the literature.	139
Table 5.1	The probabilities of MWs ($P(\text{MW})$), effective mobilities ($P(\mu)$), and the charges ($P(z)$) of solutes for the SRNOM at pH 4.87.	169
Table 5.2	The schematic representation of the z-matrix.	171

Table 5.3	The schematic representation of the P-matrix.	173
Table 5.4	The most probable ranges of MWs contained within the charge distribution histograms for integer charges (z) between -1.0 and -10.0 for the SRNOM (Figure 5.3).	187
Table 6.1	The mole % of solutes ($\%n_z$) that have charges (z) between -0.5 and -15.0 in the SRNOM (as shown in molar distribution histograms in Figure 5.11).	217
Table A.1	The parameters for the electrophoresis of the SRNOM.	247
Table A.2	The parameters for the electrophoresis of Fraction 1.	248
Table A.3	The parameters for the electrophoresis of Fraction 2.	249
Table A.4	The parameters for the electrophoresis of Fraction 3.	250
Table A.5	The parameters for the electrophoresis of Fraction 4.	251
Table A.6	The parameters for the electrophoresis of Fraction 5.	252
Table A.7	The parameters for the electrophoresis of Fraction 6.	253
Table A.8	The parameters for the electrophoresis of Fraction 7.	254
Table A.9	The parameters for the 3-Gaussian-3-Lorentzian (3-GL) model for the SRNOM.	255
Table A.10	The parameters for the 3-Gaussian-3-Lorentzian (3-GL) model for Fraction 1.	256
Table A.11	The parameters for the 3-Gaussian-3-Lorentzian (3-GL) model for Fraction 2.	257
Table A.12	The parameters for the 3-Gaussian-3-Lorentzian (3-GL) model for Fraction 3.	258
Table A.13	The parameters for the 3-Gaussian-3-Lorentzian (3-GL) model for Fraction 4.	259
Table A.14	The parameters for the 3-Gaussian-3-Lorentzian (3-GL) model for Fraction 5.	260

Table A.15	The parameters for the 3-Gaussian-3-Lorentzian (3-GL) model for Fraction 6.	261
Table A.16	The parameters for the 3-Gaussian-3-Lorentzian (3-GL) model for Fraction 7.	262
Table A.17	Chain calculation for the most probable distribution of solutes with carboxyl groups and solutes with carboxyl and phenolic groups in the SRNOM.	263

LIST OF FIGURES

Figure 2.1	The standard titration curves for the IHSS Suwannee River fulvic acid and leonardite humic acid (Ritchie and Perdue, 2003).	18
Figure 2.2	The capillary electropherograms for the Suwannee River NOM at pHs 4.87, 11.40, and 8.62 (this work). Peak A in the bottom graph is a suspected system peak (Schmitt-Kopplin and Junkers, 2003). Peaks B and C are suspected “fingerprint” peaks due to polysubstituted aromatic acids formed from the degradation of lignin (Schmitt-Kopplin <i>et al.</i> , 1998b).	29
Figure 3.1	The capillary electrochromatogram for Fraction 3 at pH 8.37.	64
Figure 3.2	The procedure for correcting baselines of CE chromatograms (top graph). The baseline-corrected CE chromatogram for Fraction 3 at pH 8.37 (bottom graph).	66
Figure 3.3	The capillary electropherogram for Fraction 3 at pH 8.37 after baseline correction and conversion of the x-axis to the effective mobility scale.	67
Figure 4.1	The preparative SEC chromatogram for the fractionation of the Suwannee River natural organic matter (SRNOM), performed on February 19, 2001.	71
Figure 4.2	The minimum, maximum, and average chromatograms for 70 elutions of 4 g L ⁻¹ SRNOM on the preparative SEC system.	73
Figure 4.3	pH of the eluent during preparative SEC. The solid black line is the average pH of the last four elutions of the SRNOM on the preparative SEC column that was completed on April 17, 18, and 19, 2001. The dashed line is the outline of the average chromatograms for the same samples.	75

Figure 4.4	The division of the preparative SEC chromatogram for the SRNOM, performed on February 19, 2001. The chromatogram was divided into six areas of approximately equal absorbance at 350 nm—Fractions 1-6. Fraction 7 contained all organic material that eluted from the column after the total column volume.	78
Figure 4.5	The calibration curves for the SEC system for the determination of the molecular weights at pH 6.8 and pH 9.3. The dashed vertical lines represent the retention times of the void volume and total column volume. PSS are the polystyrene sulfonate salt standards. MTB and 4HBA are the methylthymol blue dye and 4-hydroxybenzoic acid.	83
Figure 4.6	The absorbance (thin gray line) and online-TOC chromatograms (black lines) for the SRNOM and Fractions 1-7 as determined by SEC at pH 6.8. The absorbance values in the absorbance chromatograms were multiplied by 10 for better resolution.	86
Figure 4.7	The absorbance chromatograms for the SRNOM and Fractions 1-7 as determined by SEC at pH 9.3.	87
Figure 4.8	The mode MWs for the SRNOM and Fractions 1-7 at pH 6.8 and 9.3 (top graph). The correlation between mode MWs at pH 9.3 for Fractions 1-6 and their respective “midpoint” retention times during the fractionation of the SRNOM by preparative SEC (bottom graph). The dashed vertical lines represent the retention times of the void volume and the total column volume for the column used in the preparative SEC.	91
Figure 4.9	The best-fit 3-G models (dashed lines) for the SRNOM and Fraction 1 are superimposed on the absorbance chromatograms (solid black line) as determined by SEC at pH 6.8.	94
Figure 4.10	The absorbance and online-TOC chromatograms for the SRNOM (solid lines) at pH 6.8 compared to the reconstructed absorbance and online-TOC chromatograms (dashed lines) created from the weighted sums of chromatograms for Fractions 1-7.	101

Figure 4.11	The absorbance chromatogram for the SRNOM (solid line) at pH 9.3 compared to the reconstructed absorbance chromatogram (dashed line) that was created from the weighted sums of absorbance chromatograms for Fractions 1-7.	102
Figure 4.12	The O/C and N/C ratios for the SRNOM and Fractions 1-7 as a function of their weight-average (M_w) MWs. The linear trend line for O/C was fit through data for Fractions 1-6. The linear trend line for N/C was fit through data for Fractions 1-5.	112
Figure 4.13	The UV-visible absorbance profiles for the SRNOM and Fractions 1-7 as determined at pH 6.8 (solid black line) and pH 9.3 (thin gray line). The working solution of each sample was prepared at 15 mgC L ⁻¹ with 0.1 ionic strength.	114
Figure 4.14	The UV-visible absorbance profiles for the SRNOM sample (solid lines) at pH 6.8 and 9.3 compared to the reconstructed absorbance profile (dashed lines) that were created from the weighted sums of absorbance profiles for Fractions 1-7.	115
Figure 4.15	The specific UV absorptivity (SUVA) at 254 nm and 280 nm for the SRNOM and Fractions 1-7 as a function of weight-average (M_w) MWs. The linear trend lines were fit through data for Fractions 2-7. The dashed line is the empirical relationship between SUVA at 280 nm and M_w as observed by Chin <i>et al.</i> (1994).	118
Figure 4.16	The E_4/E_6 values for the SRNOM and Fractions 1-7 as a function of their N/C and H/C ratios (mol/mol). The linear trend lines were fit through data for Fractions 1-7.	120
Figure 4.17	The standard forward and reverse titration curves for a mixture of seven simple organic acids (SOA). One 10-ml aliquot of SOAs was sequentially titrated forward (3 times) with NaOH and backward (2 times) with HCl, with 30-minute intervals between each titration.	123

Figure 4.18	The forward (lower) and reverse (upper) titration curves for the SRNOM and Fractions 1-7. The modified Henderson-Hasselbalch (H-H) models for the forward and reverse titrations (dashed lines) are superimposed over the titration curves (solid black lines).	124
Figure 4.19	The forward and reverse titration curves for the SRNOM sample (solid line) compared to the reconstructed titration curves (dashed lines) that were created from the weighted sums of forward and reverse titration curves for Fractions 1-7.	127
Figure 4.20	The carboxyl concentrations (pH method) for forward and reverse titrations for the SRNOM and Fractions 1-7 with respect to their weight-average MWs (M_w). The linear trend lines for all graphs are for Fractions 1-6.	133
Figure 4.21	The phenolic concentrations (pH method) for forward and reverse titrations for the SRNOM and Fractions 1-7 with respect to their weight-average MWs (M_w). The linear trend lines for all graphs are for Fractions 1-6.	134
Figure 4.22	The subset of six capillary electropherograms for the SRNOM.	142
Figure 4.23	The subset of six capillary electropherograms for Fraction 1.	143
Figure 4.24	The subset of six capillary electropherograms for Fraction 2.	144
Figure 4.25	The subset of six capillary electropherograms for Fraction 3.	145
Figure 4.26	The subset of six capillary electropherograms for Fraction 4.	146
Figure 4.27	The subset of six capillary electropherograms for Fraction 5.	147
Figure 4.28	The subset of six capillary electropherograms for Fraction 6.	148

Figure 4.29	The subset of six capillary electropherograms for Fraction 7.	149
Figure 4.30	The comparison of peak effective mobilities (μ_p) for the SRNOM and Fractions 1-7 as a function of increasing pH	156
Figure 4.31	The comparison of peak effective mobilities (μ_p) for the SRNOM and Fractions 1-7 as a function of increasing charge density (Q_{pH}). Q_{pH} was calculated using the modified Henderson-Hasselbalch (H-H) model for reverse titrations.	157
Figure 5.1	$P(MW)$ is the probability of MWs based on the mole distribution of MWs derived from the 3-G model for the SRNOM. $P(\mu)$ is the probability of effective mobilities (μ_{eff}) as derived from the 3-GL model for the electropherogram of the SRNOM at pH 4.87.	163
Figure 5.2	The optimized values of k_{pH} for the SRNOM and Fractions 1-7 as a function of pH.	176
Figure 5.3	The subset of charge distribution histograms for the SRNOM.	178
Figure 5.4	The subset of charge distribution histograms for Fraction 1.	179
Figure 5.5	The subset of charge distribution histograms for Fraction 2.	180
Figure 5.6	The subset of charge distribution histograms for Fraction 3.	181
Figure 5.7	The subset of charge distribution histograms for Fraction 4.	182
Figure 5.8	The subset of charge distribution histograms for Fraction 5.	183
Figure 5.9	The subset of charge distribution histograms for Fraction 6.	184
Figure 5.10	The subset of charge distribution histograms for Fraction 7.	185

Figure 5.11	The subset of mole distribution histograms for the SRNOM.	191
Figure 5.12	The subset of mole distribution histograms for Fraction 1.	192
Figure 5.13	The subset of mole distribution histograms for Fraction 2.	193
Figure 5.14	The subset of mole distribution histograms for Fraction 3.	194
Figure 5.15	The subset of mole distribution histograms for Fraction 4.	195
Figure 5.16	The subset of mole distribution histograms for Fraction 5.	196
Figure 5.17	The subset of mole distribution histograms for Fraction 6.	197
Figure 5.18	The subset of mole distribution histograms for Fraction 7.	198
Figure 5.19	The %molar abundances of solutes in the SRNOM and Fractions 1-7 that have -0.5 and -1.0 charges.	200
Figure 5.20	The maximum probable charges in the SRNOM and Fractions 1-7.	203
Figure 5.21	The most probable distribution of solutes with carboxylic acid groups in the SRNOM and Fractions 1-7.	208
Figure 5.22	The most probable distribution of total acidic functional groups in the SRNOM and Fractions 1-7. Black bars represent the % of solutes with only carboxyl groups. Gray bars represent the % of solutes with carboxyl and ≥ 1 phenolic groups.	210

Figure 6.1	The effect of the SRNOM at four different concentrations on the ionic strength of aqueous solutions prepared in 10^{-3} and 10^{-1} M 1:1 background electrolyte at 25 °C. The horizontal dashed line represents the concentration of the 1:1 background electrolyte.	218
Figure 6.2	The effect of ionic strength on the calculation of the Donnan volume (V_D) used in Models V and VI (Tipping and Hurley, 1992; Tipping, 1998) over a continuum of 1:1 background electrolyte concentrations [BGE]. The effect of NOM on the calculation of ionic strength is neglected. The horizontal dashed line represents the uppermost limit allowed for the Donnan volume in Models V and VI at 20% of the total solution volume. $M_n = 1500$ (for a fulvic acid). $r = 0.8$ nm.	223
Figure 6.3	The effect of the SRNOM (at pH 3.55 and pH 10.40) on the calculation of the Donnan volume (V_D) used in Models V and VI (Tipping and Hurley, 1992; Tipping, 1998) over a continuum of 1:1 background electrolyte concentrations [BGE]. The horizontal dashed line represents the uppermost limit allowed for the Donnan volume in Models V and VI at 20% of the total solution volume. $M_n = 1500 \text{ g mol}^{-1}$ (for a fulvic acid), $r = 0.8$ nm.	224
Figure 6.4	The effect of the Suwannee River NOM on the calculation of the Donnan volume (V_D) used in the NICA-Donnan model (Kinniburgh <i>et al.</i> , 1996; Benedetti <i>et al.</i> , 1996; Milne <i>et al.</i> , 2001) for a continuum of 1:1 background electrolyte concentrations [BGE]. The empirical constant b is set to 0.87 (Milne <i>et al.</i> , 2001).	228
Figure 6.5	The qualitative comparison of the distribution of charge in Fractions 1-6 with respect to their retention times during fractionation by preparative SEC.	236

SUMMARY

The Suwannee River natural organic matter (SRNOM) was fractionated by preparative size-exclusion chromatography (SEC) into seven molecular weight (MW) fractions. The SRNOM and its MW fractions were subsequently analyzed for their concentrations of acidic functional groups by direct titrations, average MWs and MW distributions by semi-analytical SEC, and charge-to-MW distributions by capillary electrophoresis.

Carboxyl concentrations in the MW fractions were inversely proportional to their average MWs. Conversely, the phenolic concentrations, though smaller than the carboxyl concentrations, were proportional to average MWs. Hysteresis—the non-overlap between sequential forward and reverse titrations—was observed for the SRNOM and its MW fractions, where the reverse titrations predicted a greater concentration of carboxylic acid groups than the forward titration. Because hysteresis is thought to be caused by the base-catalyzed hydrolysis of esters, this suggests that ester groups in the SRNOM are distributed over all MWs.

Data for direct titrations, MW distributions, and capillary electrophoresis were evaluated by a computational scheme that solves for the most probable distribution of acidic functional groups and charges on solutes in the SRNOM and the MW fractions as a function of pH. Depending on the MW ranges of the samples, solutes in the SRNOM and the MW fractions are predicted to have from one to a maximum of 25 carboxyl groups per solute. Most phenolic groups are predicted to be on solutes that have a minimum of two carboxyl groups. At low pH, all samples have high relative abundances

of solutes with the lowest charges. The charges of solutes are predicted to increase with increasing pH due to the sequential ionization of acidic functional groups. Depending on the MW ranges of the samples, the maximum probable charges of solutes in the SRNOM and the fractions at high pH are -12 to -30. By knowing the most probable distribution of charge and abundances of acidic functional groups, researchers will make better estimates of thermodynamic parameters and models that describe equilibria between metals and natural organic matter in the environment.

Chapter 1.

INTRODUCTION

1.1 The acid-base chemistry of Natural Organic Matter.

Natural organic matter (NOM) is a very complex mixture of naturally-occurring organic solutes that form from the degradation and dispersion of refractory biomatter in soil, freshwater, groundwater, and marine environments (Stevenson, 1994). Aquatic and soil NOM are readily soluble, have a relatively high density of acidic functional groups, strongly absorb UV and visible light, add color to natural waters, and form the basic substrate upon which soil and aquatic micro fauna and bacteria feed. NOM contains a high density of acidic functional groups (primarily carboxylic and phenolic acids) that have a high affinity to complex metal ions (Khanna and Stevenson, 1962; Schnitzer and Skinner, 1962; Randhawa and Broadbent, 1965; Stevenson, 1977; Sposito *et al.*, 1978; Shuman, 1992). Metals and metalloids in soils and natural waters are considered as toxins or pollutants when high concentrations. The speciation of metals in soils and natural waters is dependent on pH, temperature, the presence of various inorganic and organic ligands and physical surfaces to which they complex, and oxidation-reduction (redox) chemistry. Extensive databases describe metal reactivity and metal speciation with inorganic ligands in natural water systems, and the thermodynamics of those interactions are understood (Stumm and Morgan, 1996; Morel and Hering, 1997). NOM is also sensitive to changes in pH, temperature, and ionic strength—all of which directly affect the protonation-deprotonation equilibria of acidic functional groups on NOM

solutes and the NOM's ability to complex metals. Therefore, the acid-base chemistry of NOM must be first understood in order to understand and correctly characterize metal-NOM interactions.

Direct titration is the most prevalent method for the characterization of the acid-base chemistry of NOM. It is common practice to titrate solutions of purified NOM samples at high concentrations (100 to 2000 mg L⁻¹). Only under carefully controlled experimental conditions in the laboratory—fixed temperature in the presence of high concentrations of common inert salts (e.g., NaCl) used as background ionic strength adjusters—can the acid-base chemistry of NOM can be characterized with sufficient accuracy.

Due to the complexity of NOM, and the fact that the majority of solutes in NOM cannot be resolved on the molecular level, the acid-base properties of NOM are indirectly calculated based on the known inorganic species in aqueous solution. All aqueous solutions must be electrically neutral (equation 1.1),

$$(1.1) \quad [H^+] + \sum_i m_i [Cations^{m+}] = [OH^-] + \sum_i n_i [Anions^{n-}] + \sum_i z_i [Org_i^{z_i-}]$$

where $\sum_i m_i [Cations^{m+}]$ and $\sum_i n_i [Anions^{n-}]$ are the molar concentrations and charges of the known cations and anions in aqueous solution. $[H^+]$ and $[OH^-]$ are calculated from the measured pH in conjunction with their respective activity coefficients, γ . The term $\sum_i z_i [Org_i^{z_i-}]$ is the total contribution of charge by the NOM to the aqueous solution (eq

L⁻¹). By rearranging equation 1.1, $\sum_i z_i [Org_i^{z_i-}]$ is calculated as the charge deficit between the total positively and negatively charged inorganic ions in solution (equation 1.2).

$$(1.2) \quad \sum_i z_i [Org_i^{z_i-}] = \left([H^+] + \sum_i m_i [Cations^{m+}] \right) - \left([OH^-] + \sum_i n_i [Anions^{n-}] \right)$$

NOM is a complex mixture of organic acids and their conjugate bases, therefore the quantity $\sum_i z_i [Org_i^{z_i-}]$ is negative and has the identity

$$(1.3) \quad \sum_i z_i [Org_i^{z_i-}] = \sum_i z_1 [Org_{n1}^{z_1}] + \sum_i z_2 [Org_{n2}^{z_2}] + \sum_i z_3 [Org_{n3}^{z_3}] \dots + \sum_i z_{\max} [Org_{n \max}^{z_{\max}}]$$

where the right side of equation 1.3 represents the molar concentrations and charges (from the lowest charge, z_1 , to the maximum charge, z_{\max}) of all ionized solutes in the NOM. During the course of a direct titration from low pH to high pH (e.g. 3 to ~11.), $\sum_i z_i [Org_i^{z_i-}]$ will increase (become more negatively charged) due to the ionization of an increasing number of acidic functional groups in the whole NOM. Additionally, the charges (z) of the solutes in the NOM (right side of equation 1.3) will also increase as more acidic functional groups on those solutes ionize with increasing pH.

Direct titrations can only determine the total charge contribution of the whole NOM to the bulk aqueous solution $\left(\sum_i z [Org_i^{z_i-}] \right)$ at each pH during the titration.

Direct titrations can provide neither the information regarding the molar concentrations of the individual organic acids in the NOM nor the pH dependent distribution of charges on those acids (right side of equation 1.3).

1.2 Research Objectives.

Proton-binding and metal-binding equilibria of NOM are thermodynamic processes driven by the activities of the H^+ , the dissolved metal species in solution, and the solutes in NOM. The calculation of activities in thermodynamic equilibria requires knowledge of the ionic strength of the aqueous solution. The ionic strength can only be calculated if the molar concentrations of all ionic species and their respective charges are known, including those for all ionized solutes in NOM. The molar concentrations of solutes in NOM, their respective charges, and their distributions as a function of pH is currently unknown. Additionally, the contribution of NOM to the ionic strength of aqueous solution being titrated, even when NOM is in very high concentrations, is often ignored (Marshall *et al.*, 1995). The major models for proton and metal-binding titrations of NOM (i.e. Models V and VI, NICA-Donnan model, Gaussian distribution model) use empirical constants to correct for ionic strength effects and make simplistic assumptions about the charges of NOM solutes.

The objective of this research is to characterize the acid-base chemistry of the Suwannee River natural organic matter (SRNOM) to approximate:

1. The most probable distribution of acidic functional groups on NOM solutes.
2. The most probable distribution of charge on NOM solutes due to the ionization of the acidic functional groups as a function of pH (between pH 3 and 11).

3. The dependence of the MW of NOM solutes on the distribution of acidic functional groups.
4. The effect of NOM on the calculations of ionic strength for aqueous solutions.

The research was completed in several key stages between October 2000 and December 2004. The primary methods used to realize the goals for this work are size-exclusion chromatography, direct titrations, and capillary electrophoresis. Size-exclusion chromatography characterizes the molecular weight distribution. Direct titrations characterize the overall acid-base chemistry and total charge of the NOM as a function of pH. Capillary electrophoresis characterizes the charge-to-mass distribution of NOM solutes as a function of pH. Results from all three methods were integrated into a computational scheme that simultaneously solves for the most probable (1) distribution of charge as a function of pH, (2) the relative abundances of solutes with those charges, and (3) the dependence of MW on the distribution of acidic functional groups within the NOM. To the knowledge of this author, the attempt to characterize the distribution of acidic functional groups and the most probable charges in natural organic matter by integrating those techniques has never been attempted.

This research is intended to be the foundation for future work in environmental research concerning metal-NOM interactions. The application of information gained by knowing the most probable distribution of acidic functional groups in natural organic matter, the distribution of charge as a function of pH, and the effect of NOM on the ionic strength of aqueous solutions will, in due time, improve the knowledge of the thermodynamics behind proton and metal-binding by NOM. It is imperative, however, that natural organic matter must be considered and treated, first-and-foremost, as a very

heterogeneous mixture.

Chapter 2.

BACKGROUND

2.1 Terminology.

The terminology used in the literature for NOM and related organic matter is very broad and will not be discussed in detail in this document. The most common terms for various forms of organic matter and brief definitions of each are shown in Table 2.1.

2.2 Size-exclusion Chromatography (SEC).

The basic premise of a SEC technique is that solutes migrate through a porous gel or functionalized stationary phase, and are separated by their effective size, which is proportional to molecular weight (MW) at high ionic strengths (De Haan *et al.*, 1987; Barth *et al.*, 1998). Smaller solutes readily diffuse into the micro-cavities of, and into pore spaces between stationary phase particles, resulting in longer retention times on the column. Larger solutes are prohibited by size from entering micro-cavities and pores, so they remain entrained in the mobile phase and have little affinity for retention on the column. The net result is that largest solutes migrate through the column at the flow rate of the mobile phase, and the progressively smaller solutes have longer retention times on the column (Kuo and Provder, 1987; Pelekani *et al.*, 1999).

2.2.1 Size-exclusion chromatography of NOM.

The use of gel permeation chromatography (GPC) and size-exclusion

Table 2.1. The terminology commonly used in the literature for various forms of natural organic matter.

Term	Abbr.	Definition
Natural organic matter	NOM	Generic term for organic matter isolated from soil or aquatic environments.
Humic substances	HS	The assemblage of organic compounds in NOM that cannot be identified or classified. HS does not include amino acids, sugars, lipids, lignin phenols, and polycarboxylic aromatic acids.
Particulate organic matter	POM	All organic matter in aquatic environments with nominal size $> 1 \mu\text{m}$.
Colloidal organic matter	COM	All organic matter in aquatic environments with nominal size between 1 and $0.45 \mu\text{m}$.
Dissolved organic matter	DOM	All organic matter isolated from aquatic environments with nominal size $< 0.45 \mu\text{m}$.
Aquatic humus	AqH	Interchangeable with DOM. Commonly used in the 1970's-1980's.
Yellow organic acids	YOA	Interchangeable with DOM. Commonly used in 1950's-1960's.
Marine organic matter	MOM	Organic matter isolated from marine and brackish environments $< 0.2 \mu\text{m}$
Soil organic matter	SOM	All organic matter isolated from soil environments.
Humic acid	HA	Fraction of DOM, SOM, or MOM that sorbs to XAD-8 resin, insoluble at $\text{pH} < 2$.
Fulvic acid	FA	Fraction of DOM, SOM, and MOM that sorbs to XAD-8 resin, soluble at all pHs.
Transphilic acid	Hyl	Fraction of DOM, SOM, and MOM that does not sorb to XAD-8 resin, soluble at all pHs.
Humin	Hum	Fraction of SOM that is insoluble at all pHs.
Kerogen		Highly weathered residual organic matter associated with shale and slate that is not soluble in organic solvents.
Coal		Mineralized organic matter

chromatography (SEC) for the analysis of aquatic and soil NOM has been an art in progress since the mid 1960's. The early attempts to characterize NOM by GPC with the series of Sephadex gels in the 1960's and 1970's (Gjessing and Lee, 1967; Ghassemi and Christman, 1968; Schnitzer and Skinner, 1968; Swift and Posner, 1971; Cameron *et al.*, 1972; Hall and Lee, 1972; Kemp and Wong, 1974; Beck *et al.*, 1974) often yielded convoluted results. In those studies, mobile phases tended to be poorly buffered with respect pH or had low ionic strengths. The resulting chromatograms were irregularly shaped with multiple peaks due to the non-size exclusion effects (Barth, 1987; Perminova *et al.*, 1998).

Automated high-pressure size-exclusion chromatography (HPSEC) in the 1990's and 2000's have been used to rapidly and reliably separate NOM samples by size or MW (Chin and Gschwend, 1991; Chin *et al.*, 1994; Perminova *et al.*, 1998; Pelekani *et al.*, 1999; Cabaniss *et al.*, 2000; Specht and Frimmel, 2000). Good separation of NOM solutes by size relies on uniform, well-buffered mobile phases to prevent gradients in ionic strength and pH, minimize non-ideal solute-solute interactions, and suppress solute-stationary phase interactions (Chin *et al.*, 1994) that plagued earlier GPC experiments. The most common mobile phases used in HPSEC studies of NOM are 0.05-0.1 M NaCl or KCl ($I = 0.05$ to 0.1) at neutral pHs buffered by dilute phosphate, borate, or carbonate salts (Janos, 2003). De Nobili and Chen (1999) advise that the NOM sample is to be prepared at the same ionic strength, background matrix, and pH as the mobile phase to prevent gradients within the column. Under very controlled conditions, as suggested by Chin *et al.* (1994) and De Nobili and Chen (1999), HPSEC chromatograms of NOM (intensity of detection method vs. retention time) are broad, unimodal curves with minor

topographical features such as shoulders and tailing, revealing a very polydisperse mixture with a wide range of MWs. Cabaniss *et al.*, (2000) characterized NOM samples as having a log-normal Gaussian distribution of MWs. HPSEC can, however, produce dubious results based on poor calibration, poor choices of mobile phase, and faults in detection (Perminova *et al.*, 1998; Pelekani *et al.*, 1999; Varga *et al.*, 2000). Some researchers contend that separation of NOM solutes is strongly influenced by properties other than MW.

Perminova *et al.* (1998) and Pelekani *et al.* (1999) tested the separation efficiency of their HPSEC systems with small neutral organic compounds and small organic acids (MWs from 60 to ~400 Da). They observed that those compounds tended to elute from their HPSEC columns at significantly different retention volumes than predicted by their MWs. Pelekani *et al.* (1999) observed that retention times were directly correlated to the charge-to-mass ratio of their small organic compounds. Compounds with multiple ionized groups eluted first at much shorter retention times than predicted by their MWs, neutral compounds eluted at longer retention times than predicted by their MWs. Additionally, Perminova *et al.* (1998) stated that factoring octanol-water partitioning constants (K_{OW}) in conjunction with charge-to-mass due to the ionization of their organic compounds was a better predictor of retention time. In contrast, Huber *et al.* (1994) and Huber and Frimmel (1996) proposed that the HPSEC fractionation of NOM was more influenced by functionality of organic solutes rather than by MW exclusively. According to Huber and colleagues, HPSEC with TOC detection revealed that marine NOM might be fractionated (in order of increasing retention time) into large organic colloids, polysaccharide structures, humic-like material (humic acids and fulvic acids), lipids and

amino acids, phenols, and non-ionic compounds (see Figure 2 in Huber and Frimmel, 1996).

2.2.2 Calibration of SEC systems.

The calibration of SEC systems requires special consideration. It is recommended that calibration be performed using a single series of MW standards whose shape, charge density, and specific volumes do not change as a function of MW (Kuo and Provder, 1987; De Nobili and Chen, 1999). Synthetic polyanions are the MW standards of choice, starting in the 1960's with GPC through modern research with HPSEC systems. Perminova and coworkers (1998) criticized the use of synthetic polyanions—such as polystyrene sulfonate salts (PSS) and polymethacrylic acid (PMA)—as calibration standards because the polyanions will have potential non-ideal interactions with stationary phases and distributions of acidic functional groups that differ greatly from NOM. Additionally, if the same SEC system is calibrated using two or more different series of MW standards of comparable MWs, each set of standards will give a different calibration equation. This will result in different estimations of the MW distribution and average MWs of the NOM (Chin and Gschwend, 1991; Perminova *et al.*, 1998; Perminova *et al.*, 2003).

The main difficulty is selecting a suite of model compounds, either natural or synthetic, that closely mimics the physicochemical properties of NOM under the necessary experimental conditions. No series of MW standards absolutely replicates the behavior of all solutes within NOM (Kemp and Wong, 1974). Because a significant quantity of NOM has MWs < 1000, the accurate calibration of SEC systems may also

require the use of smaller organic acids and compounds to better resolve calibration curves at the low MW region < 1000 Da (De Nobili and Chen, 1999; Pelekani *et al.*, 1999; and Zhou *et al.*, 2000). This work will rely on a series of PSS salts and two smaller organic acids as calibration compounds (Zhou *et al.*, 2000).

2.2.3 Methods of detection.

The most prominent method of detection in SEC systems for NOM is ultraviolet (UV) absorbance, typically at λ 200-280 nm. New technologies for fluorescence, refractive index, and online-TOC (total organic carbon) detection have gained prominence in recent years. Evidence shows that the ability of NOM to absorb light is greatly influenced by MW and structural features of NOM solutes, which may result in over-estimation and under-estimation of the concentrations of some MW classes of NOM (Chin *et al.*, 1994; O'Loughlin and Chin, 2001; Her *et al.*, 2002). Hibbert *et al.* (2001) elaborated on errors in UV detection with HPLC due to non-ideal solute-solvent interactions, contamination, and peak broadening. Tandem UV and online-TOC or simultaneous UV and fluorescence detection have been used by Huber *et al.* (1990), Huber and Frimmel (1996), Müller and Frimmel (2002), Specht and Frimmel (2000), Her *et al.* (2002), Egeberg and Alberts (2003), and Her *et al.*, (2003). The overall shapes and retention times of their NOM chromatograms by UV and the other detection methods tend to be comparable, but all of the aforementioned research groups observed various discrepancies between UV chromatograms and chromatograms of the other detection methods. Typically, higher average MWs are calculated from UV chromatograms than from TOC or fluorescence chromatograms.

2.3 The Acid-base Chemistry of Natural Organic Matter.

Natural organic matter was discussed in the introduction as a complex mixture of organic solutes that have a high density of acidic functional groups. It is widely accepted that NOM contains two major types of acidic functional groups, carboxylic and phenolic acids (Schnitzer and Khan, 1972; Stevenson, 1994). Amine and thiol groups, considered to be less abundant due to the low nitrogen and sulfur contents of NOM, may contribute significantly to the binding of "soft" metal cations such as Hg(I), Hg(II), and Cd(II) (Li *et al.*, 1998; Woolard and Linder, 1999; Smith *et al.*, 2002). Sierra *et al.* (2004) addressed the possibility that amide and amine nitrogen groups may dominate the acid-base chemistry of terrestrial HAs at high pHs.

2.3.1 Indirect and direct titration methods of NOM.

From the 1950's to the 1980's, the dominant method for measuring the concentrations of acidic functional groups in NOM was the use of barium hydroxide for the total acidity of NOM and calcium acetate for the carboxyl content (Blom *et al.*, 1957; Brooks and Sternhell, 1957; Schnitzer and Gupta, 1965). Phenolic content is calculated as the difference between the total acidity and the carboxylic acid content. In short, the two protocols require that the NOM be exposed to concentrated $\text{Ba}(\text{OH})_2$ or $\text{Ca}(\text{O}_2\text{CCH}_3)_2$ for 24 hours, at which time the reactive mixture is first filtered to remove the precipitated Ba-NOM or Ca-NOM complexes. The remaining solutions are then titrated to a fixed pH endpoint with acid or base. The $\text{Ba}(\text{OH})_2$ filtrate is back titrated with HCl to pH 8.4, the acetate filtrate is titrated with NaOH to its endpoint at pH 9.8.

The operational problems and limitations of these methods are discussed in detail elsewhere (Dubach *et al.*, 1964; Van Dijk, 1966; Holtzclaw and Sposito, 1979; Perdue *et al.*, 1980; Perdue, 1985). Only the quantities of carboxyl groups, phenolic groups, and the total acidity of NOM are determined by the indirect titration method.

Starting in the 1960's, direct or potentiometric titrations of NOM became increasingly desirable for NOM, though not as common as the indirect titration methods. Direct titrations provide more detail about the thermodynamics of the acid-base chemistry of NOM, because pH is monitored continuously as titrant is incrementally added, typically between pH 3-11. During forward titrations with a strong base (from low pH to high pH), acidic functional groups dissociate with increasing pH and produce an increasingly negative charge on the NOM. Reverse titrations (from high pH to low pH) with strong acids reprotonate acidic functional groups. The titration curves of NOM are smooth and continuous, lacking distinct inflection points, as would be seen in the titration curves of pure weak acids.

Unlike the established methods for indirect titrations with barium hydroxide and calcium acetate, there is no standardized protocol for conducting direct titrations on NOM (Antweiler, 1991; Santos *et al.*, 1999), nor is there any standardized mathematical treatment of experimental titration data (Marshall *et al.*, 1995). The determination of the concentrations of carboxyl and phenolic groups, estimates of average acid-dissociation constants, and the interpretation of titration curves are left to the discretion of the researcher.

There is much uncertainty about the acid-base chemistry of NOM, as determined by direct titration methods. The ionization of acidic functional groups is strongly

affected by the background solution chemistry (i.e. ionic strength, types of background salts, and temperature) of NOM solutions being titrated. It is well known that titrations performed on solutions with higher concentrations of background electrolytes yield larger net charges on the NOM over all pHs than titrations performed at lower background electrolyte concentrations (Khalaf *et al.*, 1975; Ephraim *et al.*, 1996; Christensen *et al.*, 1998). Ephraim *et al.* (1996) stated that the ionic strength effect on NOM was greater for samples with larger molecular weights and higher polydispersities. The shapes of titration curves at different ionic strengths are usually parallel, due to electrostatic effects controlled by the ionic strength of the bulk solution (Benedetti *et al.*, 1996). This effect is assumed to be independent of pH (Benedetti *et al.*, 1996). Very little is currently known about the direct effect of the NOM on the ionic strength on aqueous solutions.

Additionally, numerous researchers have observed hysteresis—the non-overlapping titration curves of sequential forward and reverse titrations (Davis and Mott, 1981; Varney *et al.*, 1983; Paxeus and Wedborg, 1985; Bowles *et al.*, 1989; Antweiler, 1991; Leenheer *et al.*, 1995; Marshall *et al.*, 1995). Although the exact mechanism for the observed hysteresis is not known, the two most prevalent hypotheses are conformational changes due to electrostatic repulsion (Varney *et al.*, 1983; Paxeus and Wedborg, 1985) and base-catalyzed hydrolysis of esters (Bowles *et al.*, 1989; Antweiler, 1991). All of the aforementioned researchers agree that hysteresis is attributed to physical or chemical changes, or a combination of both, of the NOM, beyond the effect of simple solution chemistry and proton association-dissociation reactions.

2.3.2 Organic charge and charge density.

In direct titration methods, pH is monitored continuously as incremental volumes of titrant (base or acid) are added a solution containing a known concentration of NOM. At a given pH, the molar concentrations of ions from the background electrolyte and titrant, H^+ and OH^- , and the concentration of NOM ($g\ L^{-1}$) in solution are known and are corrected for dilution. The charge contribution of NOM to the solution $\left(\sum_i z_i [Org_i^{z_i-}]\right)$ ($eq\ L^{-1}$) must be calculated using the known molar concentrations and charges of the other ions in solution with an electroneutrality equation (equation 1.2).

$\sum_i z_i [Org_i^{z_i-}]$ is pH dependent—an increase in pH with the addition of base (forward titration) will cause more acidic functional groups to ionize, thus increasing $\sum_i z_i [Org_i^{z_i-}]$. A decrease in pH with the addition of acid (reverse titration) will cause acidic functional groups to become reprotonated, thus decreasing $\sum_i z_i [Org_i^{z_i-}]$. Therefore, each step in pH during the course of a direct titration (forward or reverse) requires a new calculation of $\sum_i z_i [Org_i^{z_i-}]$ that is specific to that pH, using equation 1.2.

It is customary to normalize the values of $\sum_i z_i [Org_i^{z_i-}]$ ($eq\ L^{-1}$) calculated at each pH to the dilution-corrected mass concentration of NOM ($g\ L^{-1}$) in the solution to yield the charge density, Q_{pH} ($eq\ g^{-1}$ or $mol\ g^{-1}$).

$$(2.1) \quad Q_{pH} = \frac{\sum_i z_i [Org_i^{z_i-}]}{[NOM]}$$

Q_{pH} is the concentration of ionized acidic functional groups per unit mass of the total NOM at a given pH. Q_{pH} is a concentration-independent value because it is charge normalized to the mass of NOM. If a NOM sample is titrated at two different concentrations (e.g. 100 and 1000 mg L⁻¹), the normalization of $\sum_i z_i [\text{Org}_i^{z_i-}]$ from both of those titrations to the dilution-corrected concentrations of the NOM yield identical values of Q_{pH} . Although Q_{pH} is technically negative, it is customary to report Q_{pH} as its absolute value. Values of Q_{pH} over the entire range of pHs of the titration are then plotted against pH to give the standard titration curve for an NOM sample (Figure 2.1). Standard titration curves, such as those shown in Figure 2.1 for the Suwannee River fulvic acid (FA) and leonardite humic acid (HA), are continuously increasing functions with increasing pH.

2.3.3 Quantifying titration data of NOM.

During the late 1980's and early 1990's, numerous models were developed for the interpretation of proton and metal binding to NOM. The most commonly used models are the Model V and Model VI (Tipping and Hurley, 1992; Tipping, 1998), the NICA and NICA-Donnan models (Kinniburgh *et al.*, 1996; Benedetti *et al.*, 1996; Milne *et al.*, 2001), and the Gaussian distribution model (Perdue and Lytle, 1983; Perdue *et al.*, 1984; Dobbs *et al.*, 1989). All of the models replicate the shapes of titration curves (and metal-binding titration curves) equally well. The models assign the “best-fit” estimates of carboxyl and phenolic group concentrations (Q_1 and Q_2), mean proton-binding and metal-binding affinities (pK_a and pK_M), and other parameters that allow for wide distributions of binding affinities by non-identical carboxyl or phenolic acid groups. The models

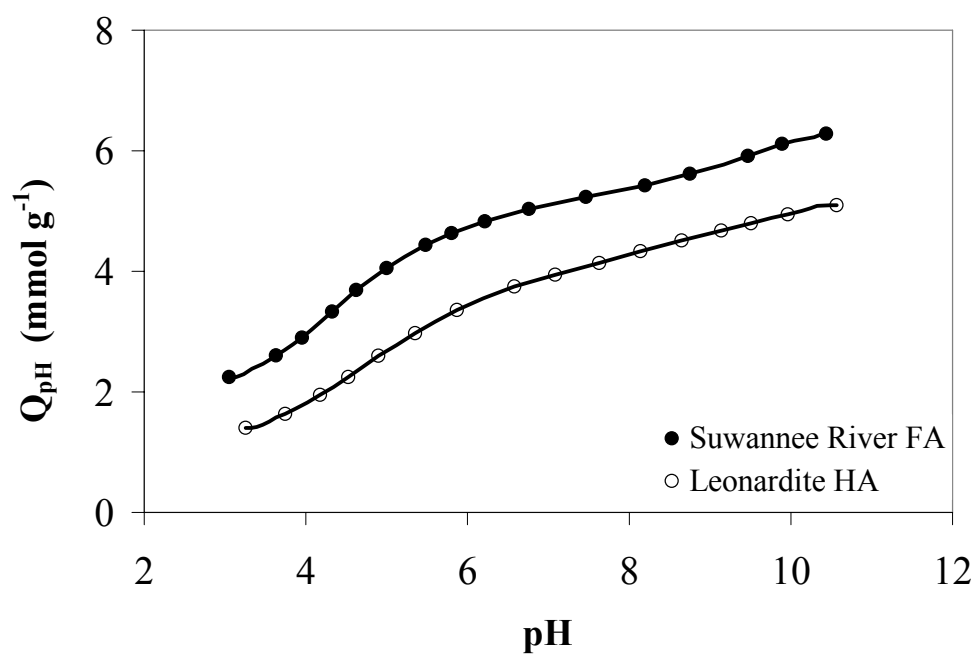


Figure 2.1. The standard titration curves for the IHSS Suwannee River fulvic acid and leonardite humic acid (Ritchie and Perdue, 2003).

differ in their mathematical treatments of experimental titration data, the number of empirical constants used, and computational algorithms. Two different models potentially could generate grossly different estimates of acid group concentrations and thermodynamic constants for the same titration data set and yet fit the titration curves to the same degree (Ritchie and Perdue, 2003).

Some researchers prefer to use a purely empirical approach to estimate the concentrations of acidic groups average proton-binding affinities directly from titration curves. In the pH method, pH cut-offs are assigned that define regions of titration curves as exclusive to only carboxyl or only phenolic acid groups (Reuter, 1980; Thurman, 1985; Bowles *et al.*, 1989; Cabaniss, 1991; Santos *et al.*, 1999; Ritchie and Perdue, 2003). For example, Bowles *et al.* (1989) titrated the Suwannee River fulvic acid (SRFA) between pH 2.5-12.0 and designated the carboxyl content to be equal to Q_{pH} at pH 8.0 and the phenolic content to be 2 times the difference in Q_{pH} between pH 8.0 and 10.0. Bowles *et al.* (1989) assumed that only carboxyl acid groups ionized below pH 8.0 and only phenolic groups ionized between pH 8.0 and 12.0. This would force the mean pK_a of phenolic acids to equal 10.0 and the mean pK_a of carboxyl groups to equal the pH at which $\frac{1}{2}$ of Q_{pH} at pH 8.0 was accrued.

2.4 Capillary Electrophoresis of NOM.

Electrophoresis is the transport of electrically charged compounds in solution under the influence of an electric field (Kuhn and Hoffstetter-Khun, 1993). A capillary is filled with a carrier solution that contains a background electrolyte (BGE) that conducts the electric current and provides pH buffering. The two ends of the capillary are

submerged into two separate reservoirs, containing the same carrier solution as in the capillary, one at the cathode and the other at the anode. The application of an electric field induces the solvent in the carrier solution to migrate by electroosmotic pressure toward the cathode at a constant velocity called under electroosmotic flow (EOF). The ionic species in the carrier solution and sample zone will also to migrate, relative to the EOF, to their corresponding electrodes—cations migrate to the cathode, anions migrate to the anode. The texts by Kuhn and Hoffstetter-Kuhn (1993) and Foret *et al.* (1993) thoroughly detail the principles of physical chemistry that apply to capillary electrophoresis.

2.4.1 Variables that affect capillary electrophoretic separations.

The migration time and the mobilities of analytes in a sample are greatly affected by the strength of the electric field across the capillary (E), pH, ionic strength (I) of the carrier solution, chemical composition of the carrier solution, length of the capillary (L), variations in sample injection, the modification of the carrier solution, and the formation of system peaks in the sample zone. Slight variations of one or more of the above will significantly lower the reproducibility of the separations. The first seven variables will be discussed briefly. The phenomenon of system peaks will be discussed in more detail.

Electric field strength. An increase in E will increase EOF and reduce migration times of samples in the capillary to the detector. Increases or decreases in E have little effect on the peak geometry of the sample (Garrison *et al.*, 1995).

pH. Silanol groups on the inner walls of fused silica capillaries accumulate an increasing negative charge with increases in pH (PZC ~ pH 3-5). The more negatively

charged the inner walls of the capillary become, the more polarized the solvent of the carrier solution becomes and EOF will increase (Garrison *et al.*, 1995). pH will also affect the charge density of weak acid anions in the sample, changing their charges and their mobilities.

Ionic strength. An increase in the concentration of the BGE in the carrier solution—with pH held constant—will decrease the actual mobility of acid anions in the sample, causing them to elute at shorter migration times. The relative decrease in the actual mobility of the ion is a function of its charges (Friedl *et al.*, 1995; Reijenga *et al.*, 1996). Ions with -1 charges are least affected, and the relative decrease in mobility increases with increasing charges of the acid anion: $-2 < -3 < -4 < -5 < -6$ (Friedl *et al.*, 1995).

Capillary length. An increase in the length of the capillary will linearly increase the retention time of EOF and geometrically increase the retention time of ions in the sample (Schmitt-Kopplin *et al.*, 2001).

Sample injection. Variations in the volume of sample introduced into the capillary will result in small increases or decreases in length of capillary occupied by the sample. This will result in variations of the sample's peak height, width, and area when detected at the detector (van der Moolen *et al.*, 1996).

Modification of the carrier solution. During the course of an electrophoretic separation, the carrier solution may become modified. The electrolysis of water will occur in the reservoirs of carrier solution at the electrodes—induced by the net accumulation of carrier solution anions at the anode and carrier solution cations at the cathode from the capillary—forming H^+ at the anode and OH^- at the cathode to neutralize

the excess ions. H^+ and OH^- are also mobile under an electric field, and will migrate at their respective velocities toward the opposite electrodes. H^+ and OH^- have significantly greater specific conductances than ions in the BGE and will affect pH-buffering in the capillary. The pH, conductivity of the carrier solution, and chemistry of the carrier solution will gradually change with time forming gradients within the capillary. Carrier solutions will become increasingly modified at longer separation times at higher voltages (Bello, 1996). A major consequence of this perturbation is a non-steady baseline at longer migration times (Colyer *et al.*, 1995).

Sample zones and system peaks. Initially, the capillary is filled with a carrier solution containing a BGE that will provide pH-buffering and a constant conductivity. The sample is injected into the capillary at the anode end of the capillary, followed by a small volume of carrier solution. Then, the ends of the capillary are submerged into two different reservoirs containing the identical carrier solutions at the electrodes. Prior to the application of the electric field across the capillary, the capillary will have three distinct zones with two boundaries: a zone of carrier solution to the front of the sample zone, the sample zone, and a zone of carrier solution behind the sample zone. The sample zone is a homogenous mixture of an analyte (coion) and its counterion (Boden and Bächmann, 1996), and should not occupy more than 3-4% of the total length of the capillary. The sample zone represents the only discontinuity of the carrier solution in the length of the capillary (Gaš and Kenndler, 2004).

The BGE in the carrier solution will be a weak, protolyzing electrolyte (weak acid or weak base) that will properly buffer the pH in the capillary (Poppe, 1992). The sample zone will generally have different concentrations of ions, specific conductances, and

chemical compositions than the carrier solution. Beckers and Boček (2003) recommend that both the carrier solution's BGE and the sample have the same counterion. For example, if the sample contains one pure compound, such as the benzoate ion, the analyte will be prepared as Na^+ -benzoate. The choice of BGE in the carrier solution should be a weak acid and its Na^+ -conjugate base, like acetic acid and Na^+ -acetate or NaHCO_3 . However, the coions in the sample zone (benzoate) and the carrier solution (acetate or bicarbonate) are different, thus there will be an initial vacancy of the carrier solution's coion in the sample zone.

All ions will begin to migrate axially through the capillary at their respective actual mobilities upon application of the electric field—counterions (Na^+) toward the cathode in the direction of EOF, coions (benzoate and acetate) toward the anode against EOF but not at the same migration velocity. As ions from carrier solution migrate through the boundaries into the sample zone, or vice versa, the concentrations of coions and counterions in the sample zone change as the ions mix. However, a uniform specific conductance and electroneutrality must be maintained through the capillary according to the Kohlraush regulating function (Beckers, 1994; Beckers and Boček, 2003), in spite of all ions being in motion. If the specific conductance of the sample zone differs significantly than the specific conductance of the carrier solution, the coion in the sample will be forced to become non-uniformly redistributed within the moving sample zone. The coion will become concentrated in one part of the sample zone and diluted in the other to equalize the specific conductance of the sample zone to that of the carrier solution (Boden and Bachmann, 1996; Gebauer and Boček, 1997, Beckers and Boček, 2003). This will lead to the observed distortion of the geometry of the sample peak at the

detector. These distorted peaks are called system peaks. System peaks are the result of non-ideal interactions between the sample zone and the carrier solutions in electrophoretic separations.

2.4.2 The effective mobility scale.

Experimental data for electrophoretic separations are often reported in terms of detector response (y-axis) vs. migration time in the capillary (x-axis). In this work, these will be referred to as the capillary electrochromatogram, or CE chromatogram. The true velocity of the analyte in the capillary is dependent on (1) the migration velocity of the ion induced by the electric field and (2) the velocity and direction of the EOF driving the carrier solution toward the cathode (Kuhn and Hoffstetter-Kuhn, 1993; Foret *et al.* 1993). A gradual change or shift in one or more variables listed in section 2.4.1 within the time frame of an electrophoretic separation, or between several separations under the same apparent experimental conditions, may generate significantly different and non-reproducible results when analyzed on the time scale (Schmitt-Kopplin *et al.*, 2001). Therefore, it is advantageous for the conversion of all experimental electrophoretic data to the effective mobility (μ_{eff}) scale.

The velocity of the EOF in the capillary is determined with the use of an EOF marker, a neutral compound that will passively migrate in the same direction and at the same velocity as the carrier solution. The migration velocity (v_{EOF}) and the actual mobility of the EOF (μ_{EOF}), in the capillary are calculated as

$$(2.2) \quad v_{EOF} = \frac{L_D}{t_{EOF}}$$

and

$$(2.3) \quad \mu_{EOF} = \frac{L_D L_T}{E t_{EOF}}$$

where L_D is the length of the capillary to the detector (cm), L_T is the total length of the capillary (cm), E is the voltage across the capillary (V), and t_{EOF} is the migration time of the EOF marker to the detector. The migration velocity (v_i) and the actual mobility (μ_i) of an ion species during the electrophoretic separation is calculated as

$$(2.4) \quad v_i = \frac{L_D}{t_R}$$

and

$$(2.5) \quad \mu_i = \frac{L_D L_T}{E t_R}$$

where L_D , L_T , and E have the same meaning as in equations 2.2 and 2.3, and t_R is the retention time of the ion species in the capillary. Therefore, the effective mobility (μ_{eff_i}) of an ion species in reference to the EOF of the carrier solution, is the difference in the absolute mobility of the charged species and the mobility of the EOF marker.

$$(2.6) \quad \mu_{eff_i} = \mu_i - \mu_{EOF}$$

If equations 2.3 and 2.5 are substituted into equation 2.6, μ_{eff_i} of any ion species undergoing electrophoretic separation in a capillary at a particular set of solution conditions (e.g. ionic strength, pH, voltage) can be calculated using equation 2.7.

$$(2.7) \quad \mu_{eff_i} = \left(\frac{L_D L_T}{E} \right) \times \left(\frac{1}{t_{EOF}} - \frac{1}{t_{m_i}} \right)$$

Electrophoretic separations plotted as detector response (y-axis) vs. effective mobility (x-axis) in this work will be referred to as the CE electropherogram.

The effective mobility scale allows for intercomparison between electrophoretic separations that were performed at different capillary lengths (with voltage and pH held constant) and electric field strengths (with capillary length and pH held constant) because the mobilities of solutes in the sample become normalized relative to the EOF (Schmitt-Kopplin *et al.*, 2001). Capillary length and electric field strength are parameters that affect the performance of the electrophoretic system—both neutral EOF marker and the sample will experience the same influence from both. pH, however, requires special consideration. pH only affects the separation of the ions in the sample because changes in pH change the charges (z_i) of those ions. The neutral EOF marker feels no effect.

2.4.3 Charge-to-size relationship in CE.

Offord (1966) observed that the mobilities (μ_i) of large polypeptides in an

electrophoretic separation are directly proportional to the ratio of the solutes' charge-to-hydrodynamic size—the apparent size of a solute is the core molecule plus the diffuse layer around the molecule that contains solvating water and the enrichment of counterions. When ionic strength is greater than the critical ionic strength (De Haan *et al.*, 1987 estimated the critical ionic strength to be ~ 0.02), the hydrodynamic radius of a solute approaches the radius of the core molecule, and the size of the solute becomes directly proportional to the MW of the solute.

Offord (1966), then Rickard *et al.* (1991), tested several empirical relationships between calculated μ_i and the MWs of their compounds. They suggested that μ_i is actually a function of the solute's hydrodynamic surface area ($4\pi r_g^2$), assuming that their polypeptides were rigid spheres. Offord's (1966) equation is

$$(2.8) \quad \mu_i = k \frac{z}{MW^{2/3}}$$

where k is a constant, z is the charge of the solute, and $MW^{2/3}$ is the proportionality of the solute's MW to its hydrodynamic surface area. The constant k equals $(6\pi\eta)^{-1}$, where η is the viscosity of the solvent in the carrier solution.

Offord's (1966) equation is very useful for the determination of charge (z) of unknown, pH-active compounds that are in very small supply (Miller *et al.*, 2002). Titration methods require relatively large quantities of sample (mg) whereas HPSEC and electrophoresis require very small quantities (μg). If the MW of a compound is accurately determined by HPSEC, then z and the acid-base chemistry of that compound

can be characterized at a single pH or over a wide range of pHs (Glück *et al.*, 1996). This approach is most often used for the discovery, separation, and acid-base characterization of various compounds in the pharmaceutical and chemical engineering industries (Mrestani *et al.*, 1998; Barbosa *et al.*, 1999; Lin and Chem, 2000; Miller *et al.*, 2002).

2.4.4 Capillary electrophoresis of NOM.

The vast majority of capillary electrophoretic separations of NOM have been performed since the review article of Duxbury (1989). The review article by Schmitt-Kopplin and Junkers (2003) catalogued and reviewed 55 CE studies involving various NOM, FAs, and HAs that were performed between 1991 and 2002. The majority of the studies catalogued by Schmitt-Kopplin and Junkers (2003) were intended to “fingerprint” NOM samples from different sources based on the recognition of unique peaks in CE electropherograms.

Electropherograms of NOM samples are often described as “humic humps” (Schmitt-Kopplin and Junkers, 2003)—very broad, continuous unimodal distributions with minor topographical features like sharp peaks and tailing (see examples of CE electropherograms in Figure 2.2). CE electropherograms nearly resemble SEC chromatograms in shape (De Nobili *et al.*, 1999). Schmitt-Kopplin *et al.* (1999b) described CE electropherograms as “polydisperse” mixtures of z/MW due to the wide ranges of observed μ_{eff} .

Schmitt-Kopplin and colleagues used Offord’s equation (applying it to the effective mobility scale) under the assumption that solutes in NOM have spheroid geometries. It is often assumed, for simplicity, that all solutes NOM are able to collapse

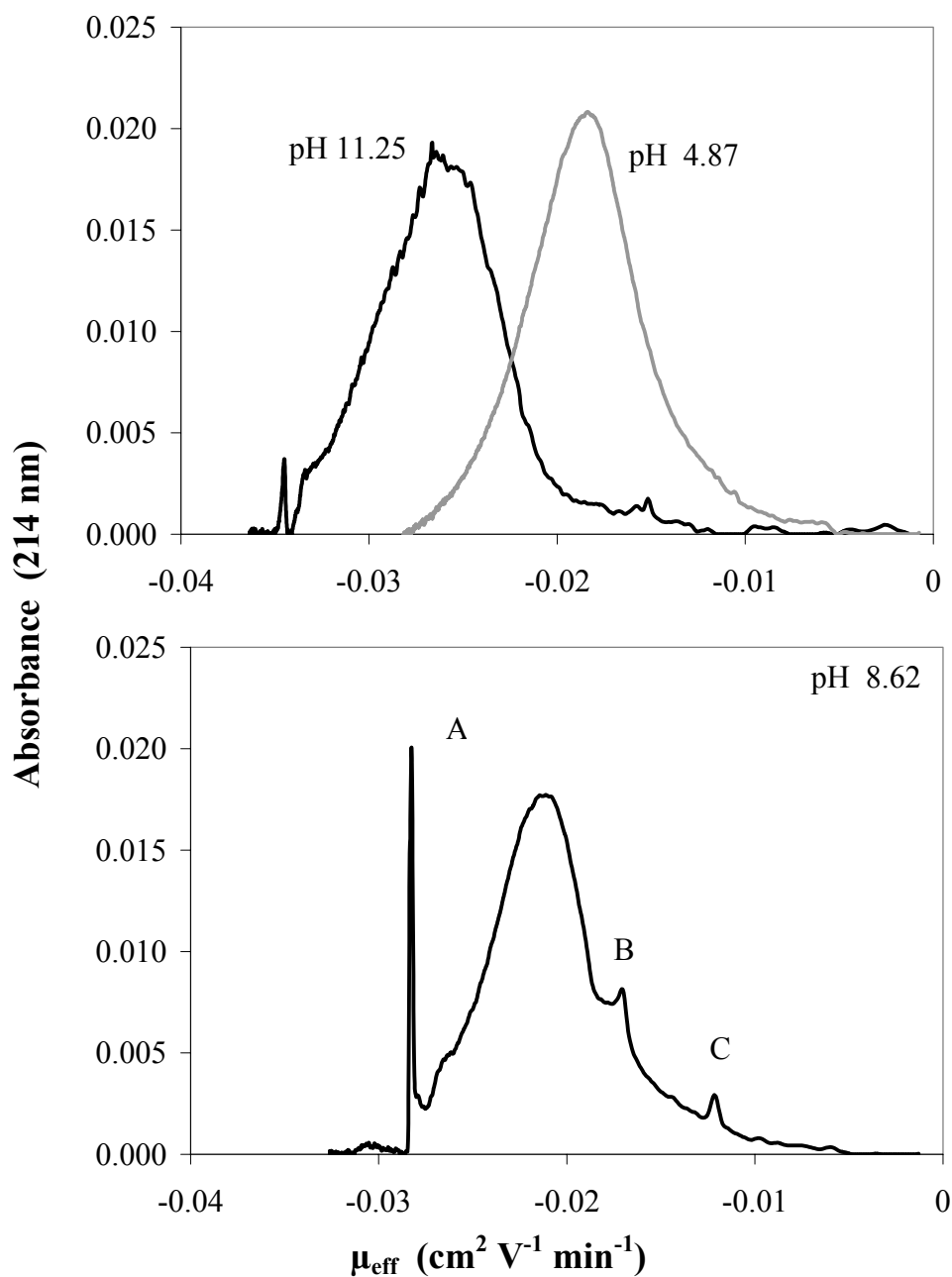


Figure 2.2. The capillary electropherograms for the Suwannee River NOM at pHs 4.87, 11.40, and 8.62 (this work). Peak A in the bottom graph is a suspected system peak (Schmitt-Kopplin and Junkers, 2003). Peaks B and C are suspected “fingerprint” peaks due to polysubstituted aromatic acids formed from the degradation of lignin (Schmitt-Kopplin *et al.*, 1998b).

into spherical geometries at relatively high ionic strengths. However, it is very unlikely that all NOM solutes are flexible and large enough to reconfigure themselves into spheres. Rigid aromatic molecules (e.g. fragments of lignin polymers) will tend to have geometries ranging from near-planar to irregularly branched. Therefore, k may differ from $(6\pi\eta)^{-1}$ and the $2/3$ coefficient for MW may not absolutely hold true for all solutes in the NOM. Miller *et al.* (2002) discussed variations in k and coefficients for MW in their work with pharmaceutical compounds.

At a given pH, any discrete value of μ_{eff} may contain one to dozens of different solutes, all of which will have the identical value of $z/MW^{2/3}$, but not necessarily the same z or MW. The molar concentrations, values of z , and the MWs of all solutes in NOM that have the identical value of $z/MW^{2/3}$ cannot be resolved from the electropherogram or μ_{eff} —the UV absorbance (detection) at a value of μ_{eff} is only proportional to the total weighted-sum of all of the organic anions that have the identical value of $z/MW^{2/3}$.

The ranges of μ_{eff} and the observed distribution of $z/MW^{2/3}$ in CE electropherograms of NOM are pH dependent. If capillary electrophoresis is performed at several different pHs, increases in pH of the separations will cause NOM to become more negative by ionizing more acidic functional groups, increasing Q_{pH} of the whole NOM and z of the individual acids. As a result, the ranges of μ_{eff} in the CE electropherograms are translated to greater negative mobilities, often accompanied by changes in the shape of the electropherograms (Figure 2.2). Due to the vast complexity

of NOM wide and the variability of acidic functional groups in NOM, it cannot be assumed, however, that the charge of every organic anion in the NOM mixture will increase with increasing pH. The gradual translation of CE electropherograms to increasingly negative mobilities in response to the increase in pH is a cumulative effect.

2.4.5 Shapes of electropherograms.

CE electropherograms resemble smooth, pseudo-Gaussian distributions in the pH range of 5 to 11 when CE is performed in carrier solutions with inert buffering salts like acetate and carbonate—examples of which can be seen in the works of Schmitt-Kopplin *et al.* (1998b and 1999b). CE electropherograms on NOM samples often contain sharp peaks and shoulders that jut out of the “humic hump” or the tails of the electropherograms. Borate and phosphate salts were used in earlier analyses of NOM by CE as buffering agents in the carrier solutions, causing very large peaks in electropherograms that were actually artifacts due to NOM-buffer interactions. Borate forms organic-borate esters with carbohydrates (Hoffstetter-Kuhn *et al.*, 1991), cis-diol (Schmitt-Kopplin *et al.*, 1998c), and lactone compounds (Schmitt-Kopplin *et al.*, 1998a).

The very large peaks that are often found on the high mobility (most negative) or low mobility (least negative) shoulders of CE electropherograms are considered system peaks (Schmitt-Kopplin and Junkers, 2003)—non-ideal interactions between sample and carrier solution. Schmitt-Kopplin and Junkers (2003) advise that these peaks (peak A in bottom graph of Figure 2.2) do not represent the separation of NOM solutes based on

$\frac{z}{MW^{2/3}}$, and should be discounted.

The smaller peaks and shoulders that are often present on the “humic hump”, not

designated as system peaks, will be called in this work “fingerprint” peaks. When electrophoretic separations of NOM are performed in inert carrier solutions of acetate or carbonate salts, Schmitt-Kopplin *et al.* (1998b) attributed fingerprint peaks (peaks B and C in bottom graph of Figure 2.2) to abundant polysubstituted aromatic compounds from the degradation of lignin. Schmitt-Kopplin *et al.* (1998b) compared the effective mobilities of these smaller peaks in CE electropherograms of NOM with effective mobilities of small, polysubstituted aromatic acids under the same experimental conditions. The relative positions of fingerprint peaks in the NOM electropherograms and in the electropherogram of the aromatic acids were comparable.

2.4.4 Capillary electrophoresis of NOM samples of different molecular weight.

Schmitt-Kopplin *et al.* (1999b) fractionated the Scheyern soil HA by sequential stage ultrafiltration (UF) into five MWs fractions (< 10 kDa, 10-50 kDa, 50-100 kDa, and >300 kDa), then analyzed the fractions by capillary electrophoresis in carbonate buffer at pH 9.03. The electropherograms of the five fractions were within the range of μ_{eff} for the electropherogram of the unfractionated Scheyern soil HA. The electropherogram for the smallest fraction (< 10 kDa) was translated to the greatest negative mobilities and had the narrowest distribution of the five MW fractions. This suggests that solutes with smaller MWs will carry relatively larger charges. The electropherograms of the MW fractions were positioned at progressively lower negative mobilities and become increasingly wider as the nominal MW ranges of the fractions increased. The fraction with the greatest MWs (> 300kDa) was centered at the lowest mobility range and had the

widest distribution. This would suggest that solutes with the largest nominal MWs will have relatively smaller charges. None of the fractions contained a unique range of mobility. All of the electropherograms overlapped to some degree. At least 2-4 prominent fingerprint peaks were observed at the same μ_{eff} in the electropherograms of the MW fractions.

Chapter 3.

METHODS FOR CHEMICAL AND INSTRUMENTAL ANALYSES

3.1 Instrumentation, Chemicals, and Solutions.

The physical and chemical analyses of the Suwannee River natural organic matter (SRNOM) required the acquisition and use of numerous laboratory instruments (Table 3.1), glassware and specialty items (Table 3.1), and chemicals (Table 3.2).

The SRNOM sample used in this study was isolated by the reverse osmosis method (Serkiz and Perdue, 1990; Sun *et al.*, 1995) in May 1999 from the Suwannee River (Fargo, GA, USA). The SRNOM (1R101N) is a commercially available sample of the International Humic Substances Society (IHSS).

Stock and working solutions of the SRNOM and Fractions 1-7 were required for their physical and chemical analyses. The concentrations and chemical compositions of stock and working solutions of the samples, as well as mobile phases for chromatography, solutions for spectroscopic analyses, and titrants for acid-base chemistry are reported in Table 3.3.

The Solver tool in Microsoft Excel was used for various modeling tasks in this research. These include the 3-Gaussian (3-G) model (Section 3.3.6), the modified Henderson-Hasselbalch (H-H) model (Section 3.6.3), the 3-Gaussian-3-Lorentzian (3-GL) model (Section 3.7.6), and various sub-routines in the Charge Distribution Model (Chapter 5). The operational settings for Solver were: target by minimization; maximum

Table 3.1. The inventory of laboratory instruments and hardware used.

Instrument	Manufacturer	Model
Atomic absorbance spectrophotometer	Perkin Elmer	3100
Capillary electrophoresis system	Beckmann	2100
Combination pH electrode	Orion	8103
Diode array spectrophotometer	Hewlett-Packard	HP8451a
Fraction collector	Eldex	UFC-3780
Freeze drier	Labconco	77535
Gas regulator	Fisher Scientific	FS50
Organic carbon analyzer	Sievers-Ionics	TOC-800
Peristaltic pump	Masterflex	7524-10
pH meter	Orion	720A
Submersible magnetic stirrer	Troemner	700
Temperature controller	Tronac	PTC41

Hardware	Manufacturer	Model
Column, 30 x 0.6 cm	Amersham Pharmacia	6-30
Column, 60 x 1.6 cm	Amersham Pharmacia	16-60
Freeze drier sample flasks	Labconco	75000 series
Norprene peristaltic tubing	Masterflex-Norton	06240-14
Pyrex syringe, 10 ml	Fischer Scientific	P-440
Quartz flow cell, 1-cm	Hellma	710-QS
Quartz cuvette, 1-cm	Beckman	75170
Teflon tubing, 1.6 mm ID	Nalgene	
Teflon vessel, 25 ml	Savillex	

Table 3.2. The inventory of chemicals that were used.

Chemical or Analyte	Manufacturer	Purity
Ammonium molybdate	Fisher Scientific	LG
Barium chloride	Fisher Scientific	LG
1,2,4,5 benzenetetracarboxylic acid	Sigma Aldrich	LG
Benzoic acid	Sigma Aldrich	LG
Calcium standard, 1000 mg L ⁻¹	Fisher Scientific	LG
Cation exchange resin, analytical	Biorad	
Cation exchange resin, coarse	Biorad	
Ethanol , 95% v/v	Fisher Scientific	LG
Hydrochloric acid, 1.00 N std.	Fisher Scientific	AG
4-Hydroxybenzoic acid	Sigma Aldrich	LG
Iron standard, 1000 mg L ⁻¹	Fisher Scientific	LG
Magnesium standard, 1000 mg L ⁻¹	Fisher Scientific	LG
Methylthymol blue dye	Sigma Aldrich	LG
Ninhydrin	Sigma Aldrich	LG
Nitrogen gas	AirGas	GC
Oxalic acid	Sigma Aldrich	LG
pH buffers: 3.00, 4.00, 7.00, 10.00	Fisher Scientific	LG
pH buffer: phosphate dry	Fisher Scientific	LG
Phthalic acid	Sigma Aldrich	LG
Polystyrenesulfonate salts: 18, 4.6, 1.8 kDa	Polysciences, Inc.	AG
Propanol, 70% v/v	Fisher Scientific	LG
Potassium dihydrogen phosphate granules	Fisher Scientific	LG
Potassium hydrogen phthalate	Sigma Aldrich	LG
Silicon standard, 1000 mg L ⁻¹	Fisher Scientific	LG
Sodium bicarbonate granules	Sigma Aldrich	LG
Sodium carbonate granules	Sigma Aldrich	LG
Sodium chloride granules	Sigma Aldrich	LG
Sodium hydroxide, 1.00 N std.	Fisher Scientific	AG
Sodium hydroxide pellets	Fisher Scientific	LG
Sodium nitrate granules	Fisher Scientific	LG
Sodium sulfate granules	Fisher Scientific	LG
Superdex-30 TM resin	Amersham Pharmacia Biotech	
Ultrapure water	Fisher Sci.	HPLC
Vanillin	Sigma Aldrich	LG

LG: laboratory grade. AG: analytical grade. HPLC: HPLC grade. GC: GC grade.

Table 3.3. The stock solutions and recipes for the working solutions that were used.

Stock Solution	Concentration	Working Solution
Mobile phase: preparative SEC		
Sodium bicarbonate	1.00 mol L ⁻¹	267 ml NaHCO ₃ + 67 ml Na ₂ CO ₃ , dilute to 4.0 L with DI water
Sodium carbonate	0.33 mol L ⁻¹	
Cleaning solution for Superdex-30 resin		
Ethanol	95% v/v	150 ml ethanol + 120 ml propanol, dilute to 500 ml with DI water
Propanol	70% v/v	
Mobile phase: MW determination		
Phosphate buffer	7.0 g L ⁻¹	200 ml phosphate buffer + 100 ml NaCl, dilute to 2.0 L with ultrapure water
Sodium chloride	2.0 mol L ⁻¹	
Titrants: acid-base chemistry		
Sodium hydroxide	1.00 mol L ⁻¹	100 ml NaOH, dilute to 1.00 L with degassed ultrapure water
Hydrochloric acid	1.00 mol L ⁻¹	100 ml HCl, dilute to 1.00 L with ultrapure water
Sample solutions for MW and UV-visible spectroscopy		
SRNOM	0.169 gC L ⁻¹	pH 6.8: 2.50 ml phosphate buffer + 1.25 ml NaCl + volume of sample, dilute to 25 ml with ultrapure water. DOC = 15.0 mgC L ⁻¹ .
Fraction 1	0.148 gC L ⁻¹	
Fraction 2	0.162 gC L ⁻¹	
Fraction 3	0.177 gC L ⁻¹	
Fraction 4	0.192 gC L ⁻¹	pH 9.3: volume of stock solution, dilute to 25 ml with carbonate buffer.
Fraction 5	0.193 gC L ⁻¹	
Fraction 6	0.176 gC L ⁻¹	
Fraction 7	0.113 gC L ⁻¹	

time = 500 seconds; maximum iteration limit = 1000 calculations; precision = 10^{-10} ; tolerance = 10^{-10} ; convergence = 10^{-10} ; forward derivative; tangent estimation; and Newton search.

3.2 Preparative Fractionation of the Suwannee River NOM by Size-Exclusion Chromatography (SEC)

Preparative fractionation is a large-scale separation scheme in which the resulting fractions of the whole mixture are collected in sufficient quantities that they can be analyzed chemically. The preparative fractionation in this work is intended to fractionate the SRNOM into smaller fractions that will contain discrete ranges of unique MWs. Each molecular weight fraction and the unfractionated SRNOM will subsequently undergo chemical analyses. The results of those chemical analyses for the fractions and the SRNOM will be compared and described as a function their MW ranges and average MWs.

3.2.1 Preparation of solutions.

The mobile phase for the preparative SEC was prepared from NaHCO_3 and Na_2CO_3 (Table 3.3). The resulting ionic strength of the mobile phase was 0.10 with a buffered pH of 9.1-9.2. The SRNOM solutions for SEC were prepared by dissolving 400 mg of freeze-dried, oven-dried SRNOM powder into 100 ml of the $\text{NaHCO}_3/\text{Na}_2\text{CO}_3$ mobile phase. The pH of the SRNOM solution was adjusted to pH 9.1-9.2 with 2.0 ml 0.1 M NaOH. The SRNOM solution was shaken on an Innova platform shaker for 24 hours at room temperature prior to the first SEC separation. The SRNOM solution was

stored in a refrigerator at 4° C at the end of each working day. In the mornings prior to SEC, the SRNOM solution was gently warmed to room temperature by submerging the storage bottle in warm tap water. The bulk concentrations of the SRNOM solutions for preparative SEC were estimated to contain 0.400 g of sample in 102.0 ml ($\sim 3.92 \text{ g L}^{-1}$).

3.2.2 Preparation of resin and SEC column.

The stationary phase was Superdex-30TM (Amersham Pharmacia Biotech, Stockholm, Sweden) developed for separation of large globular proteins and polypeptides. According to Amersham technical support, Superdex-30TM is slightly cationic with a MW exclusion of $>30,000 \text{ Da}$ and a lower MW separation limit of $\sim 300 \text{ Da}$.

The SEC column was prepared by slowly pouring the resin slurry into the column in 20-30 ml doses. Layering and stratified packing were avoided by gently raising the bed with a bottom-to-top flux of DI water to cause resettling as the new addition of resin slurry was added. Once all of the resin was added, the top fittings and cap were secured to the column and DI water was continuously flowed through the column from top to bottom as bed height of the resin was slowly adjusted and compressed from the bottom. The resin bed length was 52.1 cm with an inner diameter of 1.60 cm, which corresponded to a total bed volume of 105 cm^3 . The void space in the preparative SEC column was determined by continuously pushing a 0.01 M potassium hydrogen phthalate (KHP) solution through the SEC system and measuring the absorbance at 350 nm in 30-second intervals until KHP was detected in the effluent. The void space of the column/resin was approximately 37.5 cm^3 .

The resin was initially cleaned with ethanol/propanol (Table 3.3) at a flow rate of 2 ml min^{-1} . The resin was then rinsed with 1 liter of deionized water, followed by 100 ml of the general purpose 0.1 M NaOH then another 1 liter of deionized water after which the ethanol odor was eliminated. Every two weeks, the resin was cleaned thoroughly by the same cleaning regimen. The column was prepared at the beginning of each working day for use again by forward eluting 100-150 ml of $\text{NaHCO}_3/\text{Na}_2\text{CO}_3$ mobile phase solution prior loading the next sample. The column was cleaned after daily use by eluting 100 ml of deionized water followed by 50 ml of general purpose 0.1 M NaOH and 70-80 ml of $\text{NaHCO}_3/\text{Na}_2\text{CO}_3$ mobile phase solution or until the pH reached ~ 9.2 .

3.2.3 Fractionation of the Suwannee River NOM.

The flow rate of the mobile phase through the column and system was set to 2.0 ml min^{-1} after allowing the peristaltic pump to run and for a minimum of 30-45 minutes. The Hewlett-Packard diode array spectrophotometer was allowed to warm 30 minutes prior to sample injection. The zero-baseline for the spectrophotometer was established after 70-80 ml of fresh mobile phase had passed through the column. The spectrophotometer was repeatedly zeroed every minute until the change in absorbance units was less than 0.0005 absorbance units over a period of five minutes. The Eldex fraction collector was programmed to rotate to a new fraction tube every 90 seconds starting at the point of sample injection. The spectrophotometer was programmed to record absorbance at 350 nm at 90-second intervals starting after a 45-second delay from the point of injection of sample. Measurements of absorbance would be recorded at the point when each fraction tube in the Eldex collector was half filled.

Common wavelengths for the detection of NOM by absorbance in SEC and HPSEC studies are 220, 254, or 280 nm. Due to the “super-loading” of NOM into the SEC system, maximum absorbance readings at 254 and 280 nm would be > 3.0 , exceeding the instrument’s specifications for reliable measurements. Preliminary testing of the SEC system with a 1 g L^{-1} NOM solution showed that the chromatograms at 254 and 350 nm were almost identical in peak retention time and shape, with the chromatogram at 350 nm being $\sim 30\%$ less in magnitude. It was assumed that detection at 350 nm detection would produce the same chromatogram as detection at 254 nm.

A 3.8 ml aliquot of SRNOM sample was loaded into the Teflon injection loop with a clean Pyrex syringe. At time zero, the 3.8 ml aliquot of SRNOM was manually injected into the mobile phase stream that led directly into the SEC column. The Eldex fraction collector and spectrophotometer were simultaneously engaged. The eluting sample/mobile phase from the column was collected in 3-ml aliquots in 90-second time intervals on the Eldex fraction collector after passing through the HP spectrophotometer where the absorbance at $\lambda = 350 \text{ nm}$ was taken. The time delay between the absorbance measurement in the quartz flow-through cell of the spectrophotometer and the collection of that portion of a sample in the fraction collector was ~ 10 seconds.

Preliminary testing of the chromatography system had revealed undesired tailing and non-reproducible chromatograms between tandem injections. The probable cause was thought to be either strongly sorbed NOM on the surface of the resin that was subsequently flushed from the stationary phase during the next elution, or very slow-moving small NOM molecules. The technical support department at Amersham Pharmacia Biotech provided information that the Superdex resins were slightly cationic,

which may facilitate sorption of anions to the surface of the resin. A non-intrusive cleaning step was developed to minimize this effect and flush all or a majority of the sorbed organic matter from the column between tandem preparative SEC separations.

The cleaning procedure was initiated at fraction tube 35, 54 minutes after the beginning of the elution. A 10-ml aliquot of 0.10 M NaOH was injected into the mobile phase stream, followed by 20 ml of mobile phase. At fraction tube 50 (75 minutes), 20 ml of deionized water was injected into the mobile phase stream, followed by mobile phase. The high pH aliquot should have completely ionized the sorbed NOM and made it mobile while the near zero ionic strength aliquot should have pushed the smaller slower molecules through the resin faster than at the 0.10 ionic strength of the carbonate mobile phase. Flow was never disrupted and fractions were collected up to 90-105 tubes (135 to 158 minutes) when the absorbance dropped below 0.001 absorbance units. The eluting mobile phase was collected for an additional 15 minutes after the last fraction tube in a 500 ml bottle. A total of 70 elutions of $\sim 4 \text{ gL}^{-1}$ SRNOM were performed over a 10 week period. The pHs of each fraction tube for the final four elutions were measured.

3.2.4. Division of fractions.

The preparative SEC chromatograms for each elution were plotted as absorbance vs. retention time. Individual chromatograms for the 70 elutions were set against a square grid and the area of the whole profile was integrated for percent area within vertical columns corresponding to individual fraction tubes. The main peak, almost Gaussian in shape, of each elution profile was divided as closely as possible into six equal areas based on absorbance. The seventh fraction contained all material eluted after

the “Gaussian” portion of the chromatograms. Each of the liquid fractions based on division by area of absorbance for all 70 elutions were combined into their respective fractions. The fractions from the preparative SEC were designated as Fractions 1-7.

The division of the SRNOM chromatogram, and the subsequent division of the liquid sample from the separation, into the seven fractions was to ensure adequate sample size when all SEC separations were completed. After 70 elutions, nearly 1 gram of sample was fractionated, which would allow for approximately 170 mg of sample in each fraction.

3.2.5 Final processing of SRNOM fractions.

Fractions 1-7 were individually desalted by slowly pushing the liquid fractions containing high concentrations of sodium and carbonate upward through ~100 ml of H⁺-saturated coarse cation exchange resin (Biorad). The desalted fractions were collected in clean plastic bottles and subsequently freeze-dried on a Labconco freeze drier. The recovered freeze-dried powders for Fractions 1-7 were vacuum-dried at 60° C for 6-8 hours. The oven-dried powders were then weighed on the Sartorius balance and the gross dry weights of Fractions 1-7 were recorded. The dry freeze-dried products were transferred to clean amber bottles for storage.

3.3 Determination of Molecular Weights (MW) by SEC.

The MW distributions and the average MWs for the SRNOM and Fractions 1-3 were determined by semi-analytical SEC using the same Superdex-30TM resin as used for

the preparative fractionation. SEC was performed at pH 6.8 in a phosphate/NaCl buffer—most common conditions for MW studies (Janos, 2003). SEC was also performed at pH 9.3 in carbonate buffer—same conditions as the original preparative fractionation.

3.3.1 Preparation of solutions.

The mobile phases and the working solutions of Fractions 1-7 and the SRNOM for the determination of MWs are shown in Table 3.3. Polystyrenesulfonate (PSS) sodium salts (18KDa, 4.6KDa, and 1.8KDa) were purchased from Polysciences, Inc. (Warrington, PA). The exact masses and polydispersities for each molecular weight standard (according to the manufacturer's literature) are listed in Table 3.4. Additional standards of methylthymol blue (MTB) dye (MW = 798.0) and 4-hydroxybenzoic acid (MW = 137.1), both from Sigma Aldrich, were used to extend the calibration curve to MW values < 1000 Da. 20.0 mg of each PSS solid was transferred to a clean 25.0-ml volumetric flasks. 20.0 ml of mobile phase buffer was transferred to each volumetric flask and the contents were shaken vigorously until all solids dissolved. The pH of each solution was measured to be 6.7-6.8 or 9.2-9.3 without adjustment, and then each flask was diluted to the mark with buffered mobile phase. Each PSS solution was transferred to a clean glass bottle. The bottles were wrapped in aluminum foil and stored at room temperature in a drawer so that no direct light would contact the solutions. MTB and 4-hydroxybenzoic acid were prepared in the same pH 6.8 and 9.3 buffers at a concentration of 2 mgC L⁻¹.

3.3.2 Preparation of resin and columns.

SEC at pH 6.8 was performed in 30.0 cm x 1.60 cm column, and SEC at pH 9.3 was performed in 30.0 cm x 1.0 cm column (Amersham Pharmacia Biotech). The columns were packed and the void volumes of the columns were determined according to procedure in section 3.2.2. The total volumes of the resin beds in the SEC columns were 60.3 and 23.6 cm³, respectively. The void volumes of the SEC columns were 19.0 ± 0.1 and 8.1 ± 0.2 cm³.

3.3.3 Protocol for SEC at pH 6.8.

A 1.0-ml aliquot of each PSS molecular weight standard, MTB, 4-hydroxy benzoic acid, and each sample was injected separately into the SEC column at a flow rate of 1.3 ml min⁻¹. The sample/mobile phase eluted from the SEC column then passed in tandem through the quartz flow cell in the Hewlett Packard 8451a to the Sievers TOC 800 Turbo. The flow rates for the sample intake, oxidant, and acid mixing in the Sievers TOC 800 Turbo were preset to 1.1 ml min⁻¹, 0.5 μ l min⁻¹, and 0.2 μ l min⁻¹ respectively. The time offset between the real-time absorbance detection and the online TOC detection was ~4.5 minutes. Absorbance at 254 nm (610 nm for the MTB) was measured and recorded every 15 seconds from the time of injection. The detection by online-TOC (mgC L⁻¹) was measured and recorded every 3-7 seconds. The chromatograms for online TOC detection were corrected by subtracting 4.5 minutes from the retention times in order to match the UV detection chromatograms.

3.3.4 Protocol for SEC at pH 9.3.

A 0.5-ml aliquot of each PSS molecular weight standard, MTB, 4-hydroxy benzoic acid, and each sample was injected separately into the SEC column at a flow rate of 2.0 ml min⁻¹. The sample/mobile phase eluted from the SEC column then passed through the quartz flow cell in the Hewlett Packard 8451a where absorbance at 254 nm (610 nm for the MTB) was measured and recorded every 15 seconds from the time of injection. Online-TOC detection was not used due to the very high concentration of carbonate.

3.3.5 Calibration of SEC system.

Three elutions of each MW standard were performed on each SEC system, two elutions prior to the samples and one after the samples. The average and standard deviations for the peak retention times for each standard were calculated. The linear calibration curves and the calibration equations for the SEC systems were determined by plotting the log M_p values (shown in Table 3.4) against the average peak retention times for absorbance (at pH 6.8 and 9.3) and TOC detection (at pH 6.8). The retention times for all absorbance and TOC chromatograms for the SRNOM and Fractions 1-7 will be transformed to the Log MW scales using the respective calibration equations.

3.3.6 Evaluation of absorbance and online-TOC chromatograms.

The retention time scale (x-axis) of all absorbance and TOC chromatograms for the SRNOM and Fractions 1-7 were first transformed according to their respective calibration curves and were plotted as absorbance vs. log MW and TOC (mgC L⁻¹) vs. log MW. Each chromatogram was truncated to contain absorbance and TOC values

Table 3.4. Data for the MW standard compounds used for the calibration of the SEC for MW determination. Data for the polystyrene sulfonate standards were provided by Polysciences, Inc. (Warren, PA).

Standard	M_w	M_n	M_p	P
PSS 18,000 Da	15200	13800	15800	1.10
PSS 4,600 Da	5180	4600	4880	1.13
PSS 1,800 Da	1430	1200	1370	1.19
4-Hydroxybenzoic Acid		138		1
Methylthymol blue (MTB)		798		1

M_w : weight average molecular weight. M_n : number average molecular weight. M_p : peak molecular weight. P: polydispersity, M_w/M_n

between log MW 4.370 and 1.775, which corresponds to MW values of 22,900 and 60 Da, respectively—the predicted MW range between the total void volume and the total column volume.

Absorbance was assumed to be proportional to the mass concentration of solutes eluting from the SEC column and TOC was the direct measurement of the organic carbon concentration of solutes that eluted from the SEC column. As discussed in section 2.2.3, UV detection in SEC and HPSEC methods may be compromised by the MWs of solutes and possible structures in the NOM that may disproportionately absorb UV light stronger than other structures. Although the pitfalls of UV detection are known and considered, the assumption will be made, for simplicity, that all solutes will absorb UV light equally and that the variation in absorbance signal is due to concentration of the sample in the eluent. Likewise, online-TOC detection can only measure the organic carbon concentration of eluent (mgC L^{-1}) and not the absolute concentration of the NOM or each fraction (mg L^{-1}) in the eluent. The assumption will be made that TOC of the eluent will be directly proportional to the mass concentration.

The SEC chromatograms for Fractions 1-7 and the SRNOM were evaluated for their MWs that correspond to the peak absorbance and peak TOC. These will be called the mode MWs and will be used for qualitative comparisons between the samples. In theory, a mode MW (as determined by SEC at pH 9.3) would be a good indicator of the approximate MW that corresponds to the retention time of the center of the fraction when collected during preparative SEC. The chromatograms were also evaluated for their maximum and minimum MWs. The maximum MW is the MW that corresponds to the retention time of the first detection by absorbance or online-TOC.

3.3.7 The 3-Gaussian (3-G) models.

The UV absorbance and TOC chromatograms for Fractions 1-7 and the SRNOM sample were modeled using the Solver tool in Microsoft Excel in which three overlapping Gaussian distributions were generated whose weighted sums would replicate the absorbance and TOC chromatograms (equations 3.1 and 3.2),

$$(3.1) \quad Abs_{\text{Log MW}_i} = \frac{A_1}{\sigma_1 \sqrt{2\pi}} \exp \left[-\frac{1}{2} \left(\frac{\mu_1 - \text{Log MW}_i}{\sigma_1} \right)^2 \right] + \frac{A_2}{\sigma_2 \sqrt{2\pi}} \exp \left[-\frac{1}{2} \left(\frac{\mu_2 - \text{Log MW}_i}{\sigma_2} \right)^2 \right] + \frac{A_3}{\sigma_3 \sqrt{2\pi}} \exp \left[-\frac{1}{2} \left(\frac{\mu_3 - \text{Log MW}_i}{\sigma_3} \right)^2 \right]$$

$$(3.2) \quad \text{TOC}_{\text{Log MW}_i} = \frac{A_{\text{TOC}1}}{\sigma_1 \sqrt{2\pi}} \exp \left[-\frac{1}{2} \left(\frac{\mu_1 - \text{Log MW}_i}{\sigma_1} \right)^2 \right] + \frac{A_{\text{TOC}2}}{\sigma_2 \sqrt{2\pi}} \exp \left[-\frac{1}{2} \left(\frac{\mu_2 - \text{Log MW}_i}{\sigma_2} \right)^2 \right] + \frac{A_{\text{TOC}3}}{\sigma_3 \sqrt{2\pi}} \exp \left[-\frac{1}{2} \left(\frac{\mu_3 - \text{Log MW}_i}{\sigma_3} \right)^2 \right]$$

where μ_i is the mean log MW, σ_i is the standard deviation, A_i and $A_{\text{TOC}i}$ are the weighted areas of each Gaussian distribution. The resulting 3-G models were plotted as absorbance vs. log MW and TOC vs. log MW at 0.005 log MW unit intervals between log MW 4.370 and 1.775 (22,900 and 60 Da).

The 3-G models were used to simply reproduce the chromatograms for the determination of the average MWs of the samples and for future use in Chapter 5. Solver freely generated all parameters in equations 3.1 and 3.2 to get the best fit to the experimental absorbance and TOC data. Three overlapping Gaussian functions were

optimal for reproducing each chromatogram (R^2 values between experimental SEC data and the 3-G models were > 0.999 for all samples). One Gaussian function or two overlapping Gaussian functions could not adequately reproduce the chromatograms. Four overlapping Gaussian function reproduced the chromatograms equally well as three Gaussian functions.

3.3.8 Number-average (M_n) and weight-average (M_w) molecular weights.

The SEC chromatograms were based on UV absorbance and TOC detection, both assumed to be proportional to mass concentrations of the SRNOM and Fractions 1-7 in the eluent at the detector. Both sets of SEC chromatograms were transformed into their respective mole distributions because the rigorous calculations of M_n and M_w require that the MW distributions must be evaluated on their mole distributions of MW. First, absorbance values were determined using the 3-G models at every 0.005 log MW interval. Next, the corresponding TOC concentration (gC L^{-1}) at each log MW_i was calculated from absorbance at 254 nm using equation 3.3,

$$(3.3) \quad [TOC_i] = \frac{Abs_i}{SUVA_{\lambda=254}}$$

where $SUVA_{\lambda=254}$ is the specific UV absorptivity ($\text{L gC}^{-1} \text{ cm}^{-1}$) of the SRNOM and Fractions 1-7 at 254 nm, determined using the protocol in section 3.5.2. The resulting TOC concentrations at each log MW_i value were then converted into their respective NOM concentrations (g L^{-1}) using equation 3.4,

$$(3.4) \quad [NOM_i] = [TOC_i] \times \frac{100}{\%C}$$

where the %C is the weight percent carbon (dry, ash-free) in each fraction and the SRNOM as determined by elemental analysis (section 3.4.1). The molar concentration, n_i (mol L⁻¹) of solutes at each log MW_i value were calculated from the [NOM_i] using equation 3.5,

$$(3.5) \quad n_i = \frac{[NOM_i]}{MW_i}$$

where MW_i is the absolute MW value (g mol⁻¹). The data for the TOC chromatograms were also transformed into their respective mole distributions of MW using only equations 3.4 and 3.5 since they were initially in TOC units. Finally, M_n and M_w values were calculated using the rigorous formulas based on their mole distributions of MW, equations 3.6 and 3.7 (Swift, 1989).

$$(3.6) \quad M_n = \frac{\sum n_i MW_i}{\sum n_i}$$

$$(3.7) \quad M_w = \frac{\sum n_i MW_i^2}{\sum n_i MW_i}$$

The polydispersity of each molecular weight distribution was calculated as

$$(3.8) \quad P = \frac{M_w}{M_n}$$

3.4 Elemental Analysis.

3.4.1 Organic elements.

The elemental analysis was performed at the Huffman Laboratory, Golden, Colorado. 10 mg of each sample was oven-dried at 60° C for 24 hours, or for a longer length of time until all moisture in the samples was lost. The samples were then combusted in an elemental analyzer to measure the weight percent of carbon, nitrogen, hydrogen, and inorganic ash. The weight percent of oxygen was indirectly calculated as the difference between the total dry mass (100%) and the sum of %C, %H, %N, and % inorganic ash contents.

3.4.2 Inorganic elements.

The stock solutions for the SRNOM and Fractions 1-7 (Table 3.3) were used for the analysis of the inorganic elements. A 1:5 dilution for each sample was required for the Na analysis. The major cations (Na, K, Ca, Mg, and Fe) were determined by flame atomic absorption (FAA) spectroscopy. Sulfate and H_4SiO_4 were determined by colorimetric methods (Colovos *et al.*, 1976; Clesceri *et al.*, 1989). The inorganic elements were reported as the mole ratio of carbon-to-element.

A 15-ml aliquot of each stock solution (Table 3.3) to be used for analysis by direct titration was analytically desalted by quickly eluting the 15-ml volume through 5

ml of H^+ -saturated analytical cation exchange resin (Biorad). The sodium contents of the analytically desalted samples were determined by FAA spectroscopy.

3.5 UV-Visible Spectrophotometry.

3.5.1 Measurements of UV-visible absorbance.

The absorbance properties of the SRNOM and Fractions 1-7 in the UV-visible wavelengths were measured at pH 6.8 and 9.3. The working solutions of the SRNOM and Fractions 1-7 for UV-visible spectroscopy were the same pH 6.8 and 9.3 solutions for MW determination by SEC (Table 3.3). Blanks at each pH were prepared by diluting 2.5 ml of DI water to 25.0 ml with the respective buffers. The UV-visible spectra of each sample were measured on the Hewlett Packard 8451a diode array spectrophotometer in a quartz cell with a 1.0-cm optical path. Five spectra were measured for each sample at the spectral range 200-720 nm. The mean and standard deviations of the absorbance values at each wavelength for each sample were calculated. The absorbance profiles for the SRNOM and Fractions 1-7 were plotted as mean absorbance vs. wavelength. Because the chemical compositions of the working solutions were prepared uniformly at 15 mgC L^{-1} , the UV-visible spectra for the SRNOM and Fractions 1-7 were directly compared.

3.5.2 Specific UV absorptivity (SUVA).

Specific UV absorptivity (SUVA), which is similar to molar absorptivity (a.k.a. extinction coefficient), is defined as the optical density or the absorbance of the organic solutes at a defined wavelength normalized to unit mass at a cell length of 1 cm (Orlov,

1966; Schnitzer and Khan, 1972). According to Stevenson (1994), values of SUVA for humic and fulvic acids tend to increase with increasing MW, increasing %C content (per unit mass), and with greater % aromatic and pi-bonded C-C structures. Humic acids tend to have larger MWs, are darker, absorb light more strongly, and have the greater SUVA values than fulvic acids (Orlov, 1966).

The SUVA values ($\text{L gC}^{-1} \text{ cm}^{-1}$) for each sample at pH 6.8 and 9.3 were calculated using equation 3.9,

$$(3.9) \quad SUVA = \frac{Abs_{\lambda=254}}{[TOC] \times b}$$

where $Abs_{\lambda=254}$ is the mean absorbance of the sample at wavelength 254 nm, $[TOC]$ is the total organic carbon concentration of the samples (i.e. 0.0150 gC L^{-1}), and b is the length of the quartz cuvette (1.0 cm).

Chin *et al.* (1994) preferred using 280 nm instead of 254 nm for their SUVA values for the suite of samples in their study, stating that 280 nm better correlated to M_w and to the aromaticity of their samples. They observed the relationship between $SUVA_{\lambda=280}$ and M_w to be

$$(3.10) \quad SUVA_{\lambda=280} = \frac{M_w - 490}{47.92}$$

Experimental SUVA values at 280 nm at pH 6.8 were compared with $SUVA_{\lambda=280}$ values that were calculated from the M_w values for the SRNOM and Fractions 1-7 and equation

3.10—the empirical relationship between $SUVA_{280}$ and M_w made by Chin *et al.* (1994).

3.5.3 E_4/E_6 .

The E_4/E_6 ratio has been used as a qualitative descriptor of the degree of humification (degradation of organic matter due to the length of residence time in the environment) for soil organic matter (Stevenson, 1994) and has been applied for comparison purposes to broad collections of organic matter from soil and aquatic environments (Senesi *et al.*, 1989). It was observed by Chen *et al.* (1977), Senesi *et al.* (1989), Baes and Bloom (1990), and Stevenson (1994) that humic acids tend to have lower E_4/E_6 values than fulvic acids, and the E_4/E_6 tends to be independent of NOM concentration. Stevenson (1994) stated that E_4/E_6 tends to be inversely proportional to the MWs and the quantity of aromatic and pi-bonded structures in the organic matter—greater MWs and greater %aromatic and pi-bonded structures have lower E_4/E_6 values—though Chen *et al.* (1977) contends that there is no direct relationship between E_4/E_6 and aromaticity of soil FAs and HAs.

The E_4/E_6 values for Fractions 1-7 and the SRNOM were calculated using equation 3.11,

$$(3.11) \quad \frac{E_4}{E_6} = \frac{Abs_{\lambda=440}}{Abs_{\lambda=640}}$$

the ratio of the absorbances at 440 and 640 nm.

3.6 Acid-base Chemistry by Direct Titrations.

3.6.1 Direct titration method.

A 10.0-ml aliquot of each analytically desalted stock solution (see Table 3.3) was transferred to a clean 25-ml Teflon vessel. 1.11 ml of 1.00 molar NaNO_3 was added to the 10.0 sample to give 0.1 molar background salt and an initial ionic strength of 0.1. The Teflon vessel was placed into a temperature-controlled water bath held constant at 25 ± 0.02 °C. The void space inside the vessel was continuously purged with flowing GC-grade N_2 gas. An Orion combination pH electrode—filled with 5.0 M NaNO_3 electrolyte and previously calibrated with pH 2.00, 3.00, 4.00, 7.00, and 10.00 buffers—was inserted through the lid of the Teflon vessel into the solution. The sample was allowed to stir under N_2 atmosphere at 25 °C for 5 minutes prior to the forward titration. A Gilmont microburette was filled with the 0.100 M NaOH titrant and the tip was inserted into the sample solution.

The initial pH of the solution was recorded prior to the addition of base. The 0.100 molar NaOH titrant was added to the solution in 6 -10 μL increments every 15 seconds up to the maximum pH of 10.5. pH was recorded 15 seconds after each addition of titrant. At the end of the forward titration (pH 10.5), the microburette was carefully removed from the solution. The titrated sample was allowed to stir continuously under N_2 atmosphere for exactly 30 minutes.

As discussed in section 2.3.1, hysteresis—the non-overlapping titration curves of sequential forward and reverse titrations—is often observed for direct titrations. It is the opinion of this author that base-catalyzed ester hydrolysis is the major cause of observed hysteresis (Bowles et al., 1989; Antweiler et al., 1991). The analysis of NOM samples by

^{13}C -NMR, for the most part, reveal greater quantities of carboxyl-like structures in NOM than the total quantity of carboxyl groups that were titrated by either indirect or direct titration methods (Hatcher *et al.*, 1981; Thorn, 1989; Rasyid *et al.*, 1992). The majority of these other carboxyl-like structures in the δ 160-190 ppm range are most likely esters. Hydrolyzed esters will yield new carboxylic acids and alcohols. The addition of new carboxylic acids to the NOM will increase the overall charge of the NOM and cause the reverse titration to have greater charge densities than the forward titrations.

By allowing the samples to stir continuously for 30 minutes at alkaline pHs, a portion of esters (if present) would hydrolyze and hysteresis would be observed when the samples undergo the reverse titrations. The effect of hysteresis on titration data for the SRNOM and the fractions of different MWs was of interest.

After the 30-minute interval at alkaline pH, the same microburette containing 0.100 M HCl titrant was inserted into the vessel, and the pH of the solution was recorded prior to the beginning of the reverse titration. The HCl titrant was added to the solution in 6-10 μL increments every 15 seconds to the minimum pH of 3.0.

3.6.2 Calculations of organic charge and charge density.

The sodium concentration in each sample from the ash content was zero after analytical desalting (verified by flame atomic absorbance spectroscopy). The sulfate and silica in the samples were measured by colorimetric methods, and their concentrations and charge contribution to the acid-base chemistry of the samples were accounted for in calculation steps in the following paragraphs. Due to the addition of base and acid titrants during the course of this work, all concentrations of ions and DOC in the solution

were dilution-corrected.

First, the initial estimation of the total organic charge concentration, $\sum_i z_i [Org_i^{z_i-}]$ (eq L⁻¹), at any pH during either the forward or reverse titration was calculated using the electroneutrality equation, equation 3.12,

$$(3.12) \quad \sum_i z_i [Org_i^{z_i-}] = [Na^+] + \{H^+\} - [Cl^-] - [NO_3^-] - 2[SO_4^{2-}] - [H_3SiO_4^-] - \{OH^-\}$$

where $\{H^+\}$ and $\{OH^-\}$ were the activities of hydrogen and hydroxide as measured directly by the pH electrode, and $[Na^+]$, $[Cl^-]$, and $[NO_3^-]$ were the dilution-corrected molar concentrations of inorganic ions from the background electrolyte and titrants. Although the ionic strength was predicted to remain near 0.10 due to the background electrolyte, the ionic strength (I) at each pH was calculated using equation 3.13.

$$(3.13) \quad I = \frac{1}{2} \left([Na^+] + [NO_3^-] + [Cl^-] + 2[SO_4^{2-}] + [H_3SiO_4^-] + \{H^+\} + \{OH^-\} + \sum_i z_i [Org_i^{z_i-}] \right)$$

Because the charges (z_i) of the NOM anions are unknown, z_i was set to equal -1. The solutions of NOM and Fractions 1-7 were prepared at relatively dilute concentrations (113 to 193 mgC L⁻¹), thus the assumed effect of the organic samples on the overall ionic strength of the solution would be minimal. Once the initial ionic strength was calculated, the activity coefficients (γ) for H⁺ and OH⁻ were calculated using the Davies equation (Davies, 1962), equation 3.14,

$$(3.14) \quad \log \gamma_H = \log \gamma_{OH} = -0.509 \times I^2 \times \left[\frac{\sqrt{I}}{1 + \sqrt{I}} - 0.30I \right]$$

and the molar concentrations of H^+ and OH^- were calculated from their activities as

$$[H^+] = \frac{\{H^+\}}{\gamma_H} \quad \text{and} \quad [OH^-] = \frac{\{OH^-\}}{\gamma_{OH}} \quad ..$$

Next, $\sum_i z_i [Org_i^{z_i-}]$ at each pH in the titrations was recalculated using the molar concentrations of H^+ and OH^- (equation 3.15).

$$(3.15) \quad \sum_i z_i [Org_i^{z_i-}] = [Na^+] + [H^+] - [Cl^-] - [NO_3^-] - 2[SO_4^{2-}] - [H_3SiO_4^-] - [OH^-]$$

The calculations of I , γ_H and γ_{OH} , and $[H^+]$ and $[OH^-]$ were iteratively performed, using equations 3.14-3.15, until the change in $\sum_i z_i [Org_i^{z_i-}]$ was less than 1%. Finally, the resulting $\sum_i z_i [Org_i^{z_i-}]$ calculated at each pH was normalized to the dilution-corrected DOC concentration ($gC L^{-1}$) of the sample being titrated (equation 3.16) to define the charge density, Q_{pH} . Q_{pH} is the density of ionized sites per unit mass of carbon ($mmol gC^{-1}$).

$$(3.16) \quad Q_{pH} = 1000 \times \frac{\sum_i z_i [Org_i^{z_i-}]}{[DOC]}$$

Q_{pH} for titration data will be reported as positive values.

3.6.3 The modified Henderson-Hasselbalch (H-H) model.

The Q_{pH} values for both forward and reverse titrations for the SRNOM and Fractions 1-7 were plotted as the standard titration curves, Q_{pH} vs. pH, and were modeled using a modified Henderson-Hasselbalch (H-H) model (Katchalsky and Spitnik, 1947; Ritchie and Perdue, 2003).

$$(3.17) \quad Q_{pH} = \left(\frac{Q_1}{1 + (K_1[H^+])^{1/n_1}} \right) + \left(\frac{Q_2}{1 + (K_2[H^+])^{1/n_2}} \right)$$

For consistency in this study, the H-H model (equation 3.17) assumes that there are two major classes of acidic functional groups, carboxyl and phenolic, that have the maximum concentrations (Q_1) and (Q_2), respectively, in units of mmol gC⁻¹. K_1 and K_2 represent mean proton-binding affinities by the two classes of binding sites. The parameters n_1 and n_2 are empirical constants ($5 \geq n \geq 1$) that reflect the range of mean log K values within each distribution of proton-binding sites. The optimum set of all parameters in equation 3.17 for each titration curve for the SRNOM and Fractions 1-7 was generated using the Solver tool in Microsoft Excel.

3.6.4 Concentrations of acidic functional groups by the pH method.

The concentrations of the acidic functional groups, carboxyl (Q_1) and phenolic (Q_2), were estimated using the pH method. Q_1 is defined as the value of Q_{pH} at pH 8.0. Q_2 is defined as two times the increase in Q_{pH} between pH 8.0 and pH 10.0 (Bowles *et*

al., 1989; Ritchie and Perdue, 2003). The benefit of the pH method is its simplicity: Q_1 and Q_2 values are evaluated directly from the experimental data without the use of a model. The pH method, however, assumes that there is no overlap between carboxyl and phenolic groups—only carboxyl groups are ionized below pH 8.0; only phenolic groups are ionized above pH 10.0.

3.6.5 Titrations of a mixture of seven simple organic acids (SOA).

A solution of seven simple organic acids (SOA) was prepared with approximately 1×10^{-3} M benzoic acid, 1×10^{-3} M 4-hydroxybenzoic acid, 1×10^{-3} M salicylic acid, 0.8×10^{-3} M 1,2,4,5-benzene tetracarboxylic acid, 1.0×10^{-3} M phthalic acid, 2.0×10^{-3} M vanillin, and 1.7×10^{-3} M oxalic acid in 0.10 M NaNO₃. The TOC of the SOA mixture was measured on the Sievers TOC-800 carbon analyzer. One 10-ml aliquot of the SOA was repetitively titrated forward with base and back with acid for a total of five titrations, using the same titration protocol and conditions as used for the SRNOM and Fractions 1-7.

The seven model organic acids in the SOA have a total of 12 carboxylic groups and three phenolic groups that have overlapping acid dissociation constants between pH 1 and 12.3. Because the seven model organic acids do not contain esters, no hysteresis is expected to be observed between their sequential forward and reverse titration curves.

3.7 Capillary Electrophoresis (CE).

3.7.1 Preparation of CE system.

Approximately 1.0 mg of each freeze-dried sample was dissolved into 1.0 ml of 0.1 M NaOH and shaken for several seconds on a vortex shaker. The alkaline solutions were then centrifuged for 2-4 minutes at ~5000 RPM to remove any undissolved material. The liquid containing the dissolved NOM or one of the fractions was carefully drawn out of the centrifuge tube with a micropipette and stored in a clean 2-ml borosilicate vial. A 2-ml volume of 10^{-3} molar mesityl oxide, the neutral EOF marker, was freshly prepared each day prior to all work. pH-buffered carrier solutions were prepared minutes before each electrophoretic separation by mixing various ratios of acetic acid/ Na^+ -acetate (for pHs < 7) and $\text{NaHCO}_3/\text{Na}_2\text{CO}_3$ (for pHs > 7) until the desired pH was achieved. The total concentrations of the buffers in the carrier solutions ranged from ~0.025 to 0.050 mol L^{-1} , with ionic strengths from ~ 0.025 to 0.06.

The fused silica capillary was carefully cut to the desired length of 27, 37, or 57 cm. A small flame was used to partially melt the capillary to form a detection “window” at the 20, 30, or 50 cm mark. The capillary was then mounted into the Beckman P/ACE 2100 CE with the detection “window” positioned 7 cm before the cathode needle. Prior to the first CE separation, the capillary was flushed with 0.1 M NaOH for 5 minutes. Between each CE separation, the capillary was flushed with 0.1 M NaOH for 5 minutes followed by a 2-minute rinse with the carrier solution for the next separation.

3.7.2 Electrophoretic separations and detection.

The two ends of the capillary were submerged in two different reservoirs of the same freshly-prepared carrier solution, one at the anode and one at the cathode. The carrier solution was pushed under pressure to fill the entire length of the capillary. The

EOF marker was then injected for 2 seconds under pressure into the capillary at the anode end. Sample was then injected for 10 seconds immediately behind the EOF marker. The EOF marker and sample initially occupied $\sim 4\%$ of the total column length prior to separation.

The anode and cathode needles were lowered into the pH buffer vials and the potential across the capillary (20, 25, or 30 kV) was engaged. Temperature of the capillary was thermostated at 30°C to eliminate the effects of coulombic heating. The migrating EOF and sample were detected at the “window” as absorbance at 214 nm. Absorbance measurements were taken every 0.5 to 1 second. The experimental data for each CE chromatogram, absorbance vs. retention time, were acquired by the Beckman Gold software and were formatted into small text files.

3.7.3 Baseline corrections of the CE chromatograms.

The text files for each CE chromatogram were imported into the GelTreat program (Kudryavtsev, University of Moscow, Russia), a data analysis package for chromatography and separation chemistry (Kudryavtsev *et al.*, 2000). The CE chromatograms were plotted in GelTreat as absorbance vs. retention time (Figure 3.1). The EOF marker would always migrate through the capillary as a very narrow sharp peak, and typically appear as the tallest peak at a very short retention time. All UV-absorbing material detected prior to the EOF peak (velocities greater than EOF) was designated as having a positive mobility and being positively charged. All UV-absorbing material detected after the EOF peak (velocities less than EOF) was designated as having a negative mobility and being negatively charged.

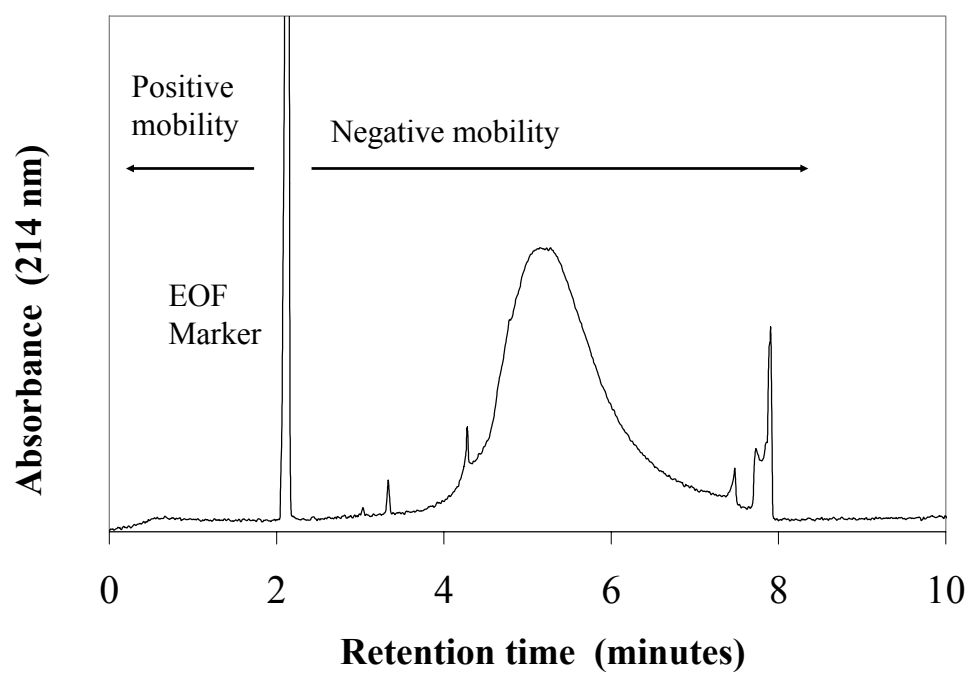


Figure 3.1. The capillary electrochromatogram for Fraction 3 at pH 8.37.

The baseline for each CE chromatogram was corrected using the non-linear spline tool in GelTreat (Kudryavtsev *et al.*, 2000; Schmitt-Kopplin *et al.*, 2001). The spline's vertical and horizontal position on the CE chromatogram, and the spline's degree of curvature, were adjusted by adding and spacing 5 to 10 nodes (Figure 3.2, top graph). The GelTreat program automatically truncated the CE chromatograms at the spline and the relative heights of absorbance for the chromatograms were automatically adjusted (Figure 3.2, bottom graph).

3.7.4 The effective mobility scale.

The data for the baseline-corrected CE chromatograms were transformed into their respective baseline-corrected CE electropherograms by the GelTreat program. GelTreat first evaluated the region of the CE chromatograms within ± 0.5 minutes of the EOF peak to find the maximum absorbance value. GelTreat defined the migration time of the peak EOF to the detector, t_{R_0} , to be the zero-mobility, μ_0 . The effective mobilities, μ_{eff_i} ($\text{cm}^2 \text{ V}^{-1} \text{ min}^{-1}$), for all retention times greater than the EOF peak were calculated using equation 2.7. The resulting data for the baseline-corrected CE electropherograms were plotted as absorbance vs. μ_{eff} (Figure 3.3).

3.7.5 Qualitative comparisons of electropherograms.

For simplicity, the peak mobility (μ_p)—the effective mobility corresponding to the maximum absorbance of an electropherogram—was used as a proxy for the mean μ_{eff} of each electropherogram. μ_p was determined for the “humic hump”, or main body, of the electropherogram. μ_p was not assigned at the μ_{eff} of the discrete peaks (system

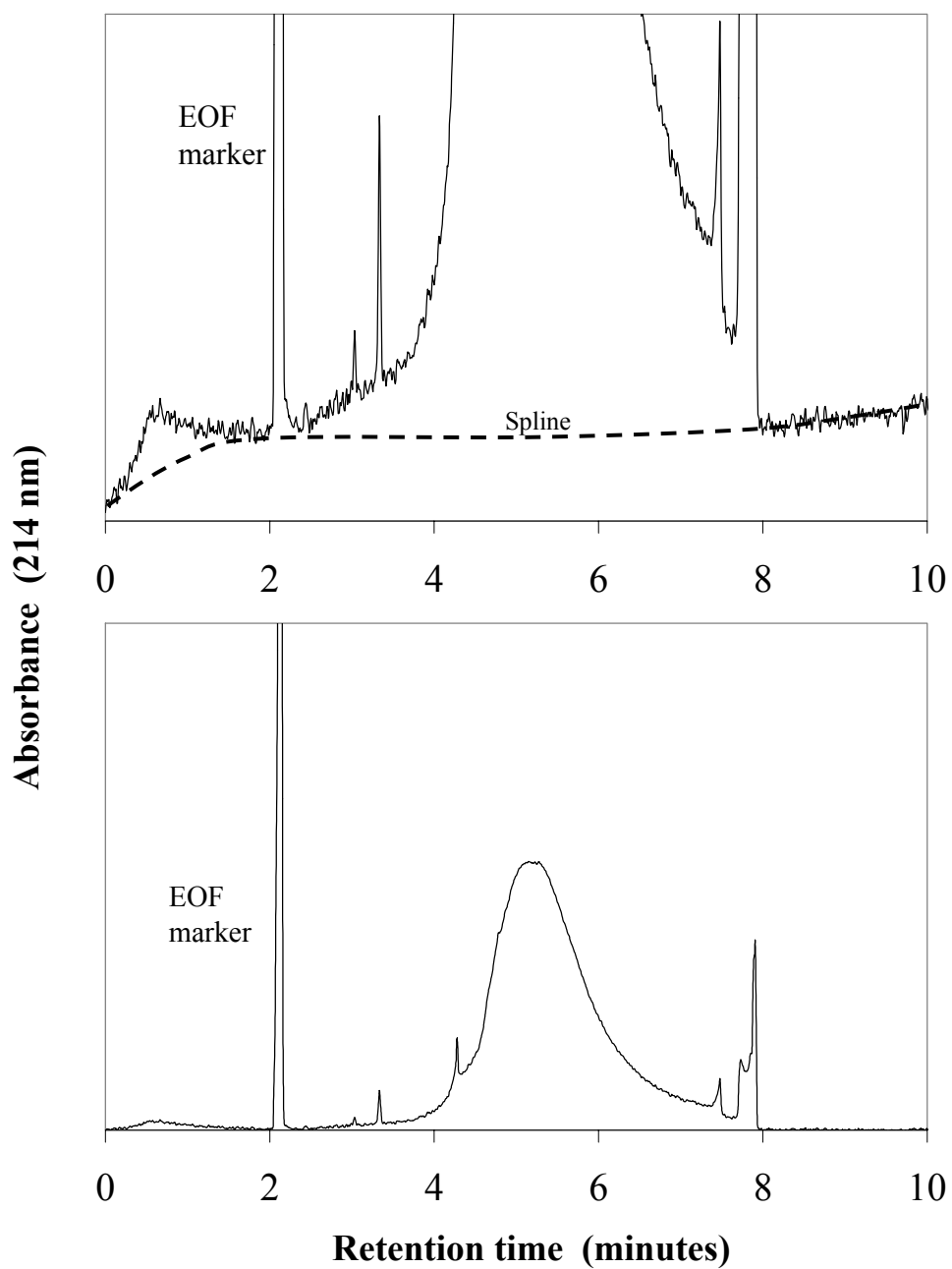


Figure 3.2. The procedure for correcting baselines of CE chromatograms (top graph). The baseline-corrected CE chromatogram for Fraction 3 at pH 8.37 (bottom graph).

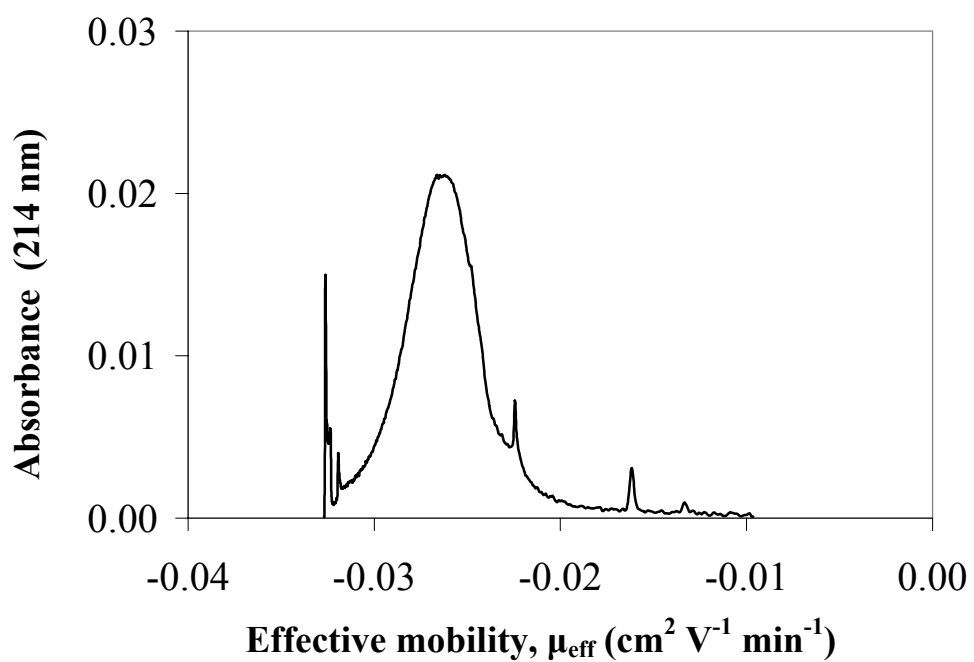


Figure 3.3. The capillary electropherogram for Fraction 3 at pH 8.37 after baseline correction and conversion of the x-axis to the effective mobility scale.

peaks or “fingerprints”) in the humic hump, even if they had greater absorbance than the maximum absorbance of the humic hump.

3.7.6 The 3-Gaussian-3-Lorentzian (3-GL) model.

Each set of data for the baseline-corrected CE electropherograms contained between 1000 and 2500 data points, making data files very large and cumbersome to manipulate. Additionally, there was no consistent scaling of the mobility axes between baseline-corrected CE electropherograms that could be used in a quantitative comparison of either (1) CE electropherograms of the same sample at different pHs or (2) CE electropherograms of different samples at the same pH.

The shapes and the topography of the CE electropherograms could not be adequately reproduced using a single Gaussian or Lorentzian distribution (or two overlapping Gaussian or Lorentzian distributions)—the detail of the skewedness, tailing, and peaks of the CE electropherogram were considered important and would be lost. By combining the weighted sums of three overlapping Gaussian and Lorentzian distributions, the overall shape of the electropherogram and the anomalous peaks could be adequately reproduced (R^2 values between the experimental data and the 3-GL models were > 0.980).

First, the data for each baseline-corrected CE electropherogram were truncated at the lower mobility limit = $-0.001 \text{ cm}^2 \text{ V}^{-1} \text{ min}^{-1}$. This would remove any bias from the EOF peak. The upper limit for each CE electropherogram was the most negative mobility at which an absorbance signal was detected. Next, the Solver tool in Excel was used to generate the “best-fit” 3-GL model parameters, (equation 3.18),

(3.18)

$$Abs_{\mu_{eff_i}} = \frac{A_{G1}}{\sigma_{G1}\sqrt{2\pi}} \exp\left[-\frac{1}{2}\left(\frac{\mu_{eff_i} - \bar{\mu}_{eff,G1}}{\sigma_{G1}}\right)^2\right] + \frac{A_{G2}}{\sigma_{G2}\sqrt{2\pi}} \exp\left[-\frac{1}{2}\left(\frac{\mu_{eff_i} - \bar{\mu}_{eff,G2}}{\sigma_{G2}}\right)^2\right] + \frac{A_{G3}}{\sigma_{G3}\sqrt{2\pi}} \exp\left[-\frac{1}{2}\left(\frac{\mu_{eff_i} - \bar{\mu}_{eff,G3}}{\sigma_{G3}}\right)^2\right] \\ + \frac{A_{L1}}{2\pi} \left[\frac{\sigma_{L1}}{(\mu_{eff_i} - \bar{\mu}_{eff,L1})^2 + (\sigma_{L1}/2)^2} \right] + \frac{A_{L2}}{2\pi} \left[\frac{\sigma_{L2}}{(\mu_{eff_i} - \bar{\mu}_{eff,L2})^2 + (\sigma_{L2}/2)^2} \right] + \frac{A_{L3}}{2\pi} \left[\frac{\sigma_{L3}}{(\mu_{eff_i} - \bar{\mu}_{eff,L3})^2 + (\sigma_{L3}/2)^2} \right]$$

A_{Gi} weighted areas of Gaussian functions
 A_{Li} weighted areas of Lorentzian functions
 $\bar{\mu}_{eff,Gi}$ mean effective mobilities for Gaussian functions
 $\bar{\mu}_{eff,Li}$ mean effective mobilities for Lorentzian functions
 σ_{Gi} standard deviations for Gaussian functions
 σ_{Li} standard deviations for Lorentzian functions

The solver tool was allowed to fit all 18 parameters in equation 3.18, no parameters were manually fixed. The only limits applied to the solver tool was to generate only values of $\bar{\mu}_{eff,Gi}$ and $\bar{\mu}_{eff,Li}$ contained between -0.0400 and -0.0005 cm² V⁻¹ min⁻¹—the acceptable range of mobilities as observed for this experimental work, and as suggested by Schmitt-Kopplin and colleagues (1999a) as seen for other NOM samples. The Gaussian functions gave the 3-GL models the general shape of the CE electropherograms and the Lorentzian functions tended to form the prominent fingerprint or suspected system peaks. The 3-GL models for each CE electropherogram were plotted as absorbance vs. μ_{eff} for the mobility range -0.001 to -0.0400 cm² V⁻¹ min⁻¹ at every 0.0001 increment, so all model CE electropherograms had the same mobility scale and the total number of data points per CE electropherogram was reduced to 392 with very little loss of information.

Chapter 4.

RESULTS AND DISCUSSION OF CHEMICAL ANALYSES

4.1 Preparative Size-Exclusion Chromatography (SEC).

4.1.1 Characteristics of preparative SEC chromatograms.

Seventy elutions of the Suwannee River NOM were performed on the SEC system over a period of 10 weeks. Data for each elution were plotted as a smooth curve of absorbance (350 nm) vs. retention time. An example of a typical preparative SEC chromatogram for the SRNOM is shown in Figure 4.1.

The chromatograms for the SRNOM consist of a wide, unimodal peak, almost Gaussian in shape, and closely resembled HPSEC chromatograms reported for raw Suwannee River water (Chin *et al.*, 1994) and for the Suwannee River fulvic and humic acids (Perminova *et al.*, 1998; Zhou *et al.*, 2000; O'Loughlin and Chin, 2001; Her *et al.*, 2002; Her *et al.*, 2003). A distinct hump or shoulder is observed on the leading edge of the main peak for most of the chromatograms, typically between the retention times of 19-21 minutes. Every chromatogram has a very distinct shoulder on the tailing edge of the main peak between retention times of 50-55 minutes. This shoulder is immediately followed by a long, drawn-out tail that gradually decreases to an absorbance of ~zero at 135-150 minutes.

The tail contains two or three conspicuous humps that are thought to be NOM released from the surface of the resin by the cleaning steps with 0.1 molar NaOH and DI water. According to technical support personnel at Amersham Pharmacia Biotech, the surface of SuperdexTM-30 resin is slightly cationic and becomes nearly neutral in charge

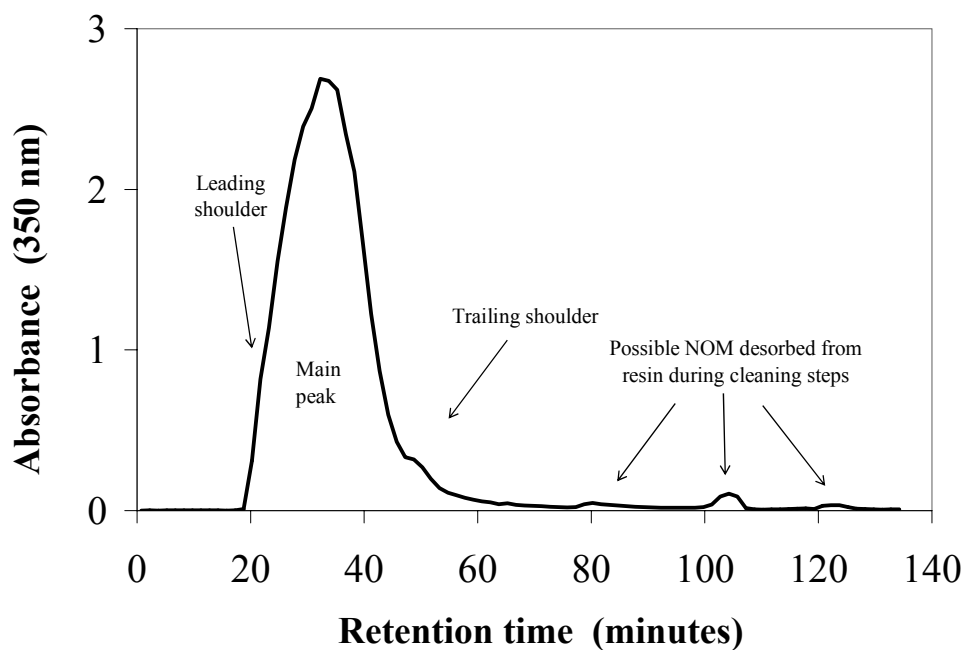


Figure 4.1. The preparative SEC chromatogram for the fractionation of the Suwannee River natural organic matter (SRNOM), performed on February 19, 2001.

above pH 7, which may have enhanced the retention of negatively-charged molecules and the sorption of neutral molecules to the resin, especially at the very high NOM concentrations used in this work. The sorption of NOM to the resin was observed during preliminary testing of the preparative SEC system, and was corrected for by the mandatory rinse with NaOH and DI water during each preparative SEC. The humps in the tail elute 18-25 minutes apart, which is close to the 20 interval between the injection of NaOH and DI water.

The graphical representation for the statistical analysis of all 70 chromatograms is shown in Figure 4.2. Generally, all 70 chromatograms have the same shape and size with slight variations in absorbance. Overall, significant absorbance was first detected at a retention time of 19.25 ± 0.75 minutes. The void volume of the preparative SEC column is evacuated at ~ 18.7 minutes, or 37.5 ml of eluent. The leading edge of the main peak and the shoulder that eluted between 19 and 21 minutes are probably the very largest MW solutes that migrate through the column at the rate of the exclusion volume. The peak maximum is at 34 ± 0.75 minutes and the trailing edge of the main peak at 48 ± 1 minutes.

The variations of absorbance are probably caused by the development of non-steady baselines between consecutive elutions. During the course of the working day, three or four elutions of SRNOM were often completed consecutively. It was observed that the zero-baseline was the most stable for the first elution of the day and became increasingly unstable with the second, third, and fourth runs of the day. The initial run of each day began after a 1-hour rinse and purge of the column with DI water, NaOH, and the carbonate mobile phase. The latter runs did not have a rinse and purge regimen

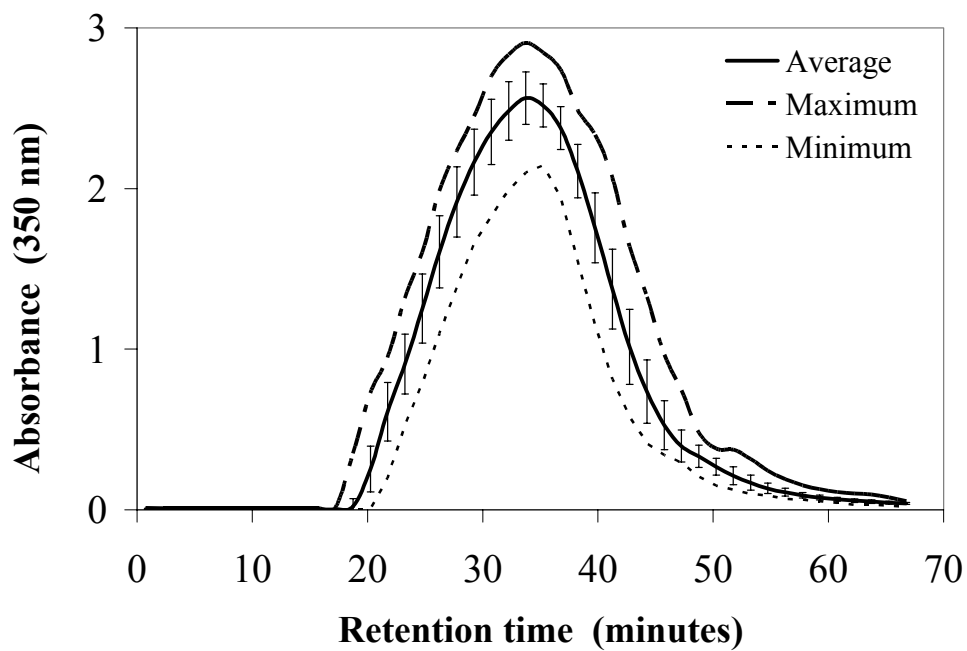


Figure 4.2. The minimum, maximum, and average chromatograms for 70 elutions of 4 g L⁻¹ SRNOM on the preparative SEC system.

beforehand, other than the column rinse 0.1 M NaOH and DI water. It is probable that small, perhaps negligible, amounts of residual NOM were still eluting from the column long after the effects of the NaOH and DI water rinses had passed. Although the baseline became slightly irregular with column usage during the course of the day, data for each elution were plotted and the resulting chromatograms were individually divided into areas, and the fractions for that individual elution curve were designated. The spectrophotometer was always zeroed before beginning each run. Therefore, the offset of peak-heights between consecutive runs should have had no effect on the division of the SRNOM into the seven fractions based on areas of absorbance.

The pH of each test tube in the fraction collector was measured for the last four SEC elutions performed on April 17, 18, and 19, 2001 (Figure 4.3). The pH of the eluting SRNOM-mobile phase from the point of sample injection until 45 minutes retention time is 9.16 ± 0.02 . At a retention time of approximately 45-48 minutes, the pH of the eluent increases to 9.21 ± 0.01 , followed by a sharp decrease to pH 9.01 (± 0.01) at a retention time of 51-52 minutes. The pH quickly recovers to pH 9.14 ± 0.01 at a retention time of 54 minutes and remains near pH 9.14 for the next 20 minutes.

The trailing shoulder on the low MW side of the main peak (see Figure 4.1) tends to occur between the retention times of 45-52 minutes. The organic matter eluting at those times were eventually included into Fraction 6. It is suspicious that the spike in pH and the trailing shoulder occurred at the same retention time, which also coincides to 102-104 ml of eluent having passed through the column, because the total volume of the column is calculated to be 105 cm³.

Figure 4.3 is very reminiscent of Figure 1 in Müller *et al.* (2000) and Figure 2a in

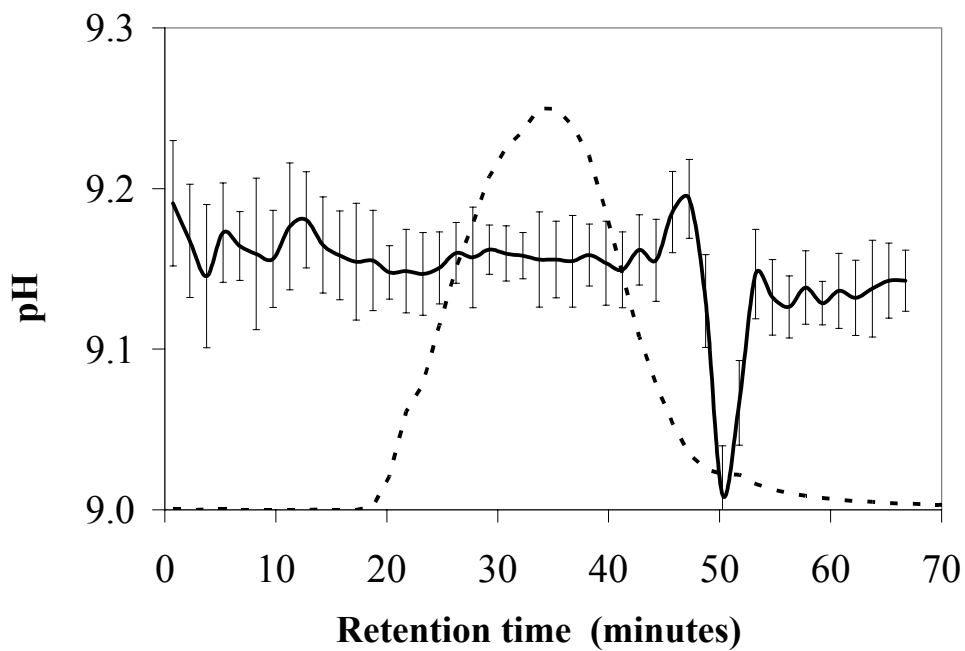


Figure 4.3. pH of the eluent during preparative SEC. The solid black line is the average pH of the last four elutions of the SRNOM on the preparative SEC column that was completed on April 17, 18, and 19, 2001. The dashed line is the outline of the average chromatograms for the same samples.

Müller and Frimmel (2002), where a very sharp trough in conductivity was observed at the total column volume of their HPSEC systems. Barth (1987) described this in terms of “ion inclusion”—an enrichment of ions in the mobile phase that preferentially partition into pore spaces with the smaller, charged solutes to maintain charge balance in the mobile phase. When the smaller, charged solutes diffuse out of the pore space into the main flow of the column, this ion-enriched volume travels in concert with them, creating a conductivity spike. Müller and Frimmel (2002) and Swift (1999) referred to this phenomenon as a “salt peak” and considered it as an artifact. This zone would have prevented NOM solutes from diffusing into pore spaces—solute would not have separated by size or MW, but would have been entrained within the zone. Müller and Frimmel (2002) advised that organic matter that eluted in the “salt peak” was not representative of the composition of the NOM and should not be considered.

In this work, the concentration of SRNOM fractionated by preparative SEC was ~500 times greater than the NOM concentrations used by Müller and Frimmel (2002) and Specht and Frimmel (2000) in their HPSEC systems. Care was taken to prepare the SRNOM to have the same background ionic strength and pH as the mobile phase. Yet the overall shape of the preparative-SEC chromatograms of the SRNOM very closely resembled the absorbance-based HPSEC chromatograms obtained by other researchers on isolates from the Suwannee River at significantly lower concentrations and smaller injection volumes. If all of the carboxyl groups and half of the phenolic groups across the entire MW spectrum of the SRNOM were assumed to be ionized at pH 9.1 (~ 6 mmol/g) (Ritchie and Perdue, 2003), the estimated contribution of organic charge at the point of injection would have slightly increased the ionic strength of the mobile phase by

~0.012 (equation 4.1).

$$(4.1) \quad \Delta I \approx \frac{1}{2} \left(\frac{0.006eq}{gram} \times \frac{4.0g}{L} \right) = 0.012$$

ΔI would diminish rapidly as the injected SRNOM plug dispersed and moved through the preparative SEC column. It is unlikely that any significant gradients of ionic strength or pH would have developed once the plug dispersed. Fraction 6 has the narrowest SEC chromatogram (see Figures 4.6 and 4.7), and its peak retention was between those of Fractions 5 and 7. Fraction 6 also had reasonable M_n and M_w values when compared to the six other fractions. If a “salt-peak” phenomenon had indeed developed, its effect on the preparative SEC in this work was minimal.

4.1.2 Division of fractions.

Each preparative SEC chromatogram (absorbance vs. retention time) was printed onto grid paper. The total area of squares contained under the absorbance curve of each chromatogram between 0 to 140 minutes of retention time was counted. The main peak of each chromatogram was then divided into approximately equal areas of absorbance between fractions 1-6. Fraction 7 contained the area under the absorbance curve for the tail after the main peak. It was assumed that Fraction 7 contained the fraction of the NOM with the smallest MWs and organic materials that were previous sorbed onto the resin then released by NaOH and DI water. The percent areas of Fractions 1-7, based on the areas of absorbance, were calculated using equation 4.2,

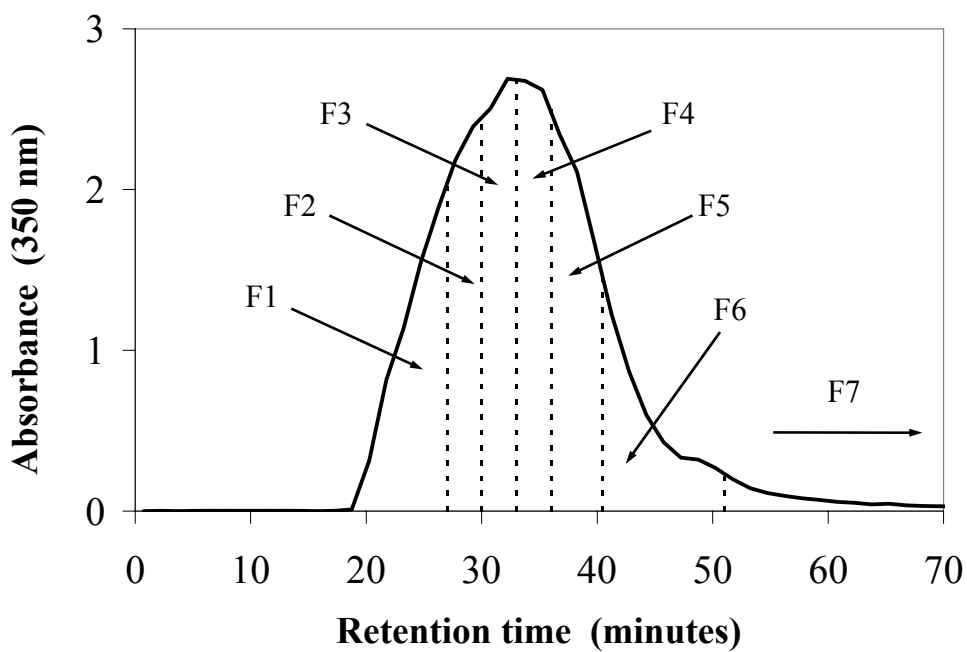


Figure 4.4. The division of the preparative SEC chromatogram for the SRNOM, performed on February 19, 2001. The chromatogram was divided into six areas of approximately equal absorbance at 350 nm—Fractions 1-6. Fraction 7 contained all organic material that eluted from the column after the total column volume.

Table 4.1. The division of the preparative SEC chromatogram for the SRNOM elution performed on February 19, 2001 (see Figure 4.4).

	Test tube numbers	Retention times (min)	Volume per fraction (ml)	% Area by absorbance
Fraction 1	11-19	16.5-30.0	27.0	16.2
Fraction 2	20-21	30.0-33.0	6.0	12.7
Fraction 3	22-23	33.0-36.0	6.0	14.2
Fraction 4	24-25	36.0-39.0	6.0	14.7
Fraction 5	26-28	39.0-43.5	9.0	14.0
Fraction 6	29-34	43.5-52.5	18.0	15.2
Fraction 7	35 to end	52.5-140	>150	13.0

$$(4.2) \quad \%Area_{Fi} = 100 \times \frac{Area_{Fi}}{\sum Area_{F1-F7}}$$

where $Area_{Fi}$ is the area of the i th fraction and $\sum Area_{F1-F7}$ is the sum of areas for Fractions 1-7. The division of the preparative SEC chromatogram for February 19, 2001 is shown in Figure 4.4 and the corresponding allocation of liquid in the collected test tubes is shown in Table 4.1. All 70 chromatograms and the corresponding eluent in the test tubes were divided into their respective seven fractions. All like fractions were then combined into the same polyethylene container for further processing.

4.1.3 Recovery and yield of the fractions.

A total of 1.034 grams of Suwannee NOM was separated over the course of 70 preparative SEC elutions. The overall recoveries of the total masses and total carbon in each of the fractions are shown in Table 4.2. The total recovered mass of Fractions 1-7 is 1.035 grams of material. The sum of the masses of the seven fractions more or less equal the total mass of the SRNOM input. However, the fractions contain significant inorganic ash (mostly sodium) in addition to the organic matter. According to the carbon mass-balance, approximately 504 mg of carbon is contained within the initial 1.034 grams of SRNOM. According to the elemental analysis of Fractions 1-7, a total of 474 mg of carbon was recovered after the preparative SEC, which is 94% of the carbon in the SRNOM that was fractionated.

The factors that caused the observed loss of 6% of the carbon cannot be identified, except for a spill of Fraction 4 liquid during the desalting step. It may be the case that the observed loss of 6% reflects an even greater loss of SRNOM that was

Table 4.2. The final recoveries of the % area by absorbance, total mass, and total carbon for Fractions 1-7 after the completion of the 70 separations of the SRNOM by preparative SEC.

	Final Recoveries				
	% Area	Mass (mg)	TOC (mg)	% Mass	% TOC
Fraction 1	16.3 ± 2.6	106.4	49.7	10.3	10.5
Fraction 2	13.8 ± 1.8	80.6	39.2	7.8	8.3
Fraction 3	15.2 ± 1.5	98.9	49.8	9.6	10.5
Fraction 4	15.6 ± 1.2	125.3	62.7	12.1	13.2
Fraction 5	13.3 ± 2.5	150.3	70.1	14.5	14.8
Fraction 6	13.8 ± 1.6	217.0	107.7	21.0	22.7
Fraction 7	12.0 ± 0.9	256.8	95.0	24.8	20.0
Sum F1-F7		1035	474.2		

partially offset by some contaminating source of carbon. It is assumed, however, that contamination was negligible.

The percent organic carbon that was recovered in Fractions 1-7 is different from recoveries that were predicted from their respected areas of absorbance. The percent recovered carbon tends to increase in the order from Fraction 1 to Fraction 6. Detection by absorbance at 350 nm, used as a proxy for the concentration of organic matter, over-predicted the carbon in Fractions 1, 2, and 3, while under-predicting the carbon in Fractions 6 and 7. Fraction 7 contains approximately 20% of the total recovered carbon, which is greatly disproportional to its rather small area of absorbance, when compared to the other fractions.

4.2 Determination of Molecular Weights by SEC.

4.2.1 Calibration of SEC system.

The retention times of the peak absorbance and TOC values at pH 6.8 and the peak absorbance values at pH 9.3 for the five standard compounds were very reproducible, with standard deviations of ± 10 , ± 15 and ± 5 seconds, respectively (Figure 4.5). Although SEC was performed in two different columns under different pH conditions at two different flow rates, the relative retention times of the calibration standards are nearly identical. This suggests that there are no significant physicochemical differences in Superdex-30TM resin at the two different pHs. The closeness of the corresponding retention times for the standard compounds (low standard deviations) indicates that tandem absorbance and online-TOC detection could

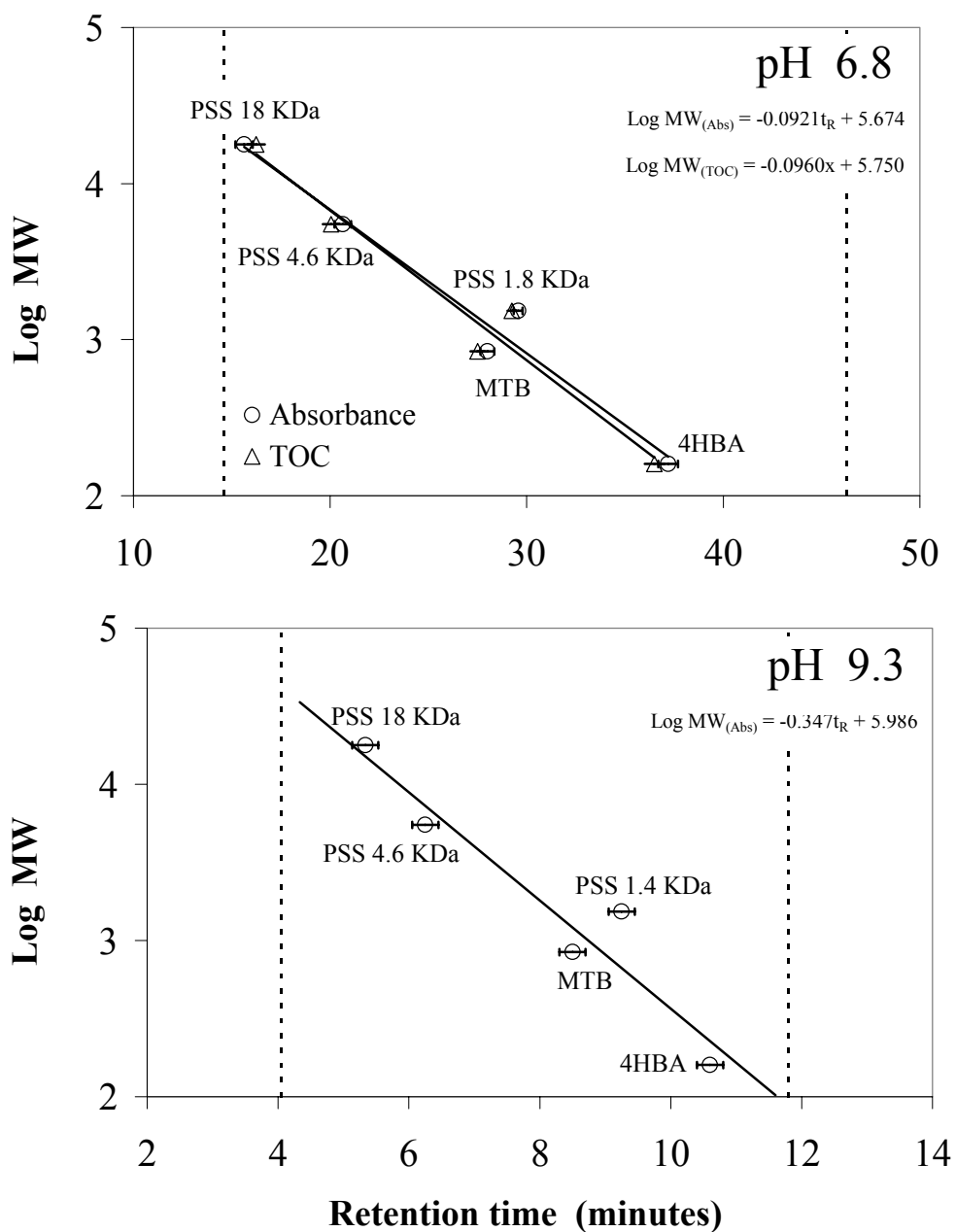


Figure 4.5. The calibration curves for the SEC system for the determination of the molecular weights at pH 6.8 and pH 9.3. The dashed vertical lines represent the retention times of the void volume and total column volume. PSS are the polystyrene sulfonate salt standards. MTB and 4HBA are the methylthymol blue dye and 4-hydroxybenzoic acid.

consistently measure the mass concentrations of solutes eluting from the SEC column with little variation between the two detection methods. The slight offset between the peak absorbance and TOC retention times at pH 6.8 may be due to the uncertainty in the ~ 4.5 minute lag between the real-time detection of absorbance and the online-TOC analysis of the same aliquot of sample. Online-TOC detection could not be used at pH 9.3 due to the overwhelming concentration of carbonate in the mobile phase.

The most notable nuance of the calibration standards is the superposition of the smallest PSS standard and the MTB, where the MTB eluted from the column ~ 70 seconds earlier at pH 6.8 and ~ 30 seconds earlier at pH 9.3 than the PSS standard. No explanation can be offered for this phenomenon, except that the smallest PSS standard may have an unusual tendency to sorb to or strongly interact with the SuperdexTM-30 resin. Similar observations of the lower MW PSS standards that deviated from their “predicted” retention times with respect to the higher MW PSS standards using HPSEC methods were seen by Perminova *et al.* (1998), Pelekani *et al.* (1999), Zanardi-Lambardo *et al.* (2001), O’Loughlin and Chin (2001), and discussed by Zhou *et al.* (2000).

All of the calibration standards eluted from the columns between their respective void volumes and total column volumes. If the calibration curves for UV absorbance and TOC detection are accurate, then the ranges of MW values that should be “ideally” separated by MW are ~22,300–20 D at pH 6.8 and ~23,200–140 Da at pH 9.3. The range for MW separation as stated by Amersham Pharmacia Biotech for the Superdex-30TM is ~ 30,000 - 300 D. It is unlikely that NOM contains an appreciable quantity of any solute with a MW lower than 60-100 Da. For example, the smallest aromatic strong UV-absorbing compound is benzene (MW = 78 Da). Lignins or other substituted aromatic

compounds must have MWs greater than benzoic acid or benzaldehyde (MW = 122 and 106 Da). Additionally, lignin derived phenols tend to be in very low quantity in NOM samples, on average ~1% of the total NOM (Perdue and Ritchie, 2003). Thus solutes with retention times greater than 42-43 minutes (< 60-65 Da) at pH 6.8 and 11.75 minutes (140 Da) at pH 9.3 are considered to be suspect because of possible non-ideal interactions with the stationary phase.

4.2.2 Absorbance and online-TOC chromatograms.

The UV absorbance and online-TOC chromatograms (pH 6.8) and absorbance chromatograms (pH 9.3) for the SRNOM and Fractions 1-7 at pH 6.8 and 9.3 are shown in Figures 4.6 and 4.7. The absorbance and TOC chromatograms at pH 6.8 more or less track each other and have similar topographic details (humps, shoulders, and small ridges) at the same retention times. The absorbance chromatograms are slightly smoother than the TOC chromatograms. This is due to the frequency of the detection intervals (15 seconds for absorbance and 3-7 seconds for TOC).

After the completion of the SEC, it was determined that the Sievers 800 Turbo TOC analyzer had a systematic baseline error that was caused by the NaCl used as the ionic strength adjuster. The Sievers TOC analyzer could not effectively detect very small concentrations of TOC ($< 0.04 \text{ mgC L}^{-1}$) in the presence of high chloride concentrations. Sievers instruments use wet oxidation/acidification for the determination of TOC and total inorganic carbon (TIC). The acidification of the mobile phase by concentrated phosphoric acid will induce the Cl^- to volatilize as HCl vapor. HCl vapor in the instrument will cause an overprediction of inorganic carbon concentration and an

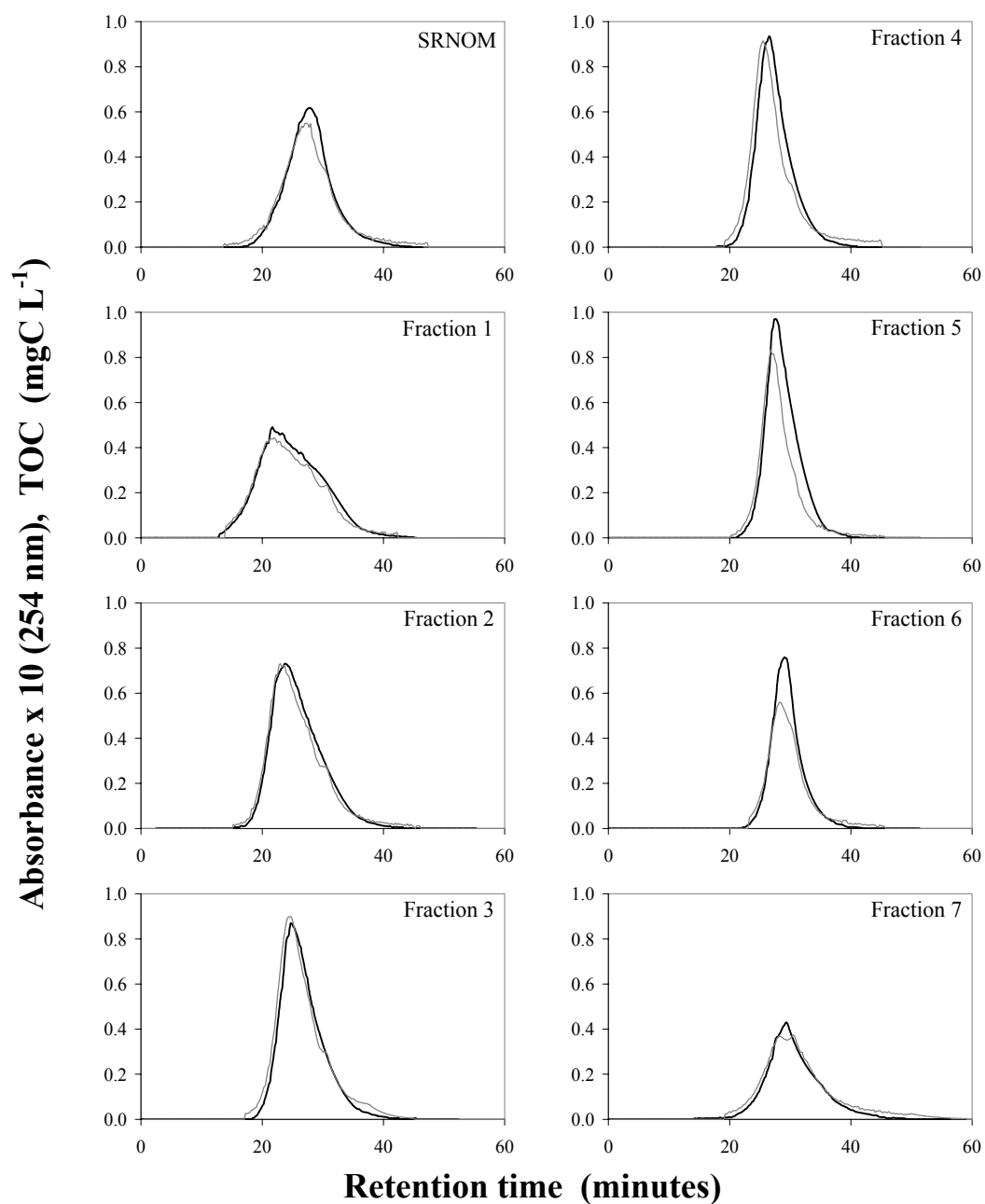


Figure 4.6. The absorbance (thin gray line) and online-TOC chromatograms (black lines) for the SRNOM and Fractions 1-7 as determined by SEC at pH 6.8. The absorbance values in the absorbance chromatograms were multiplied by 10 for better resolution.

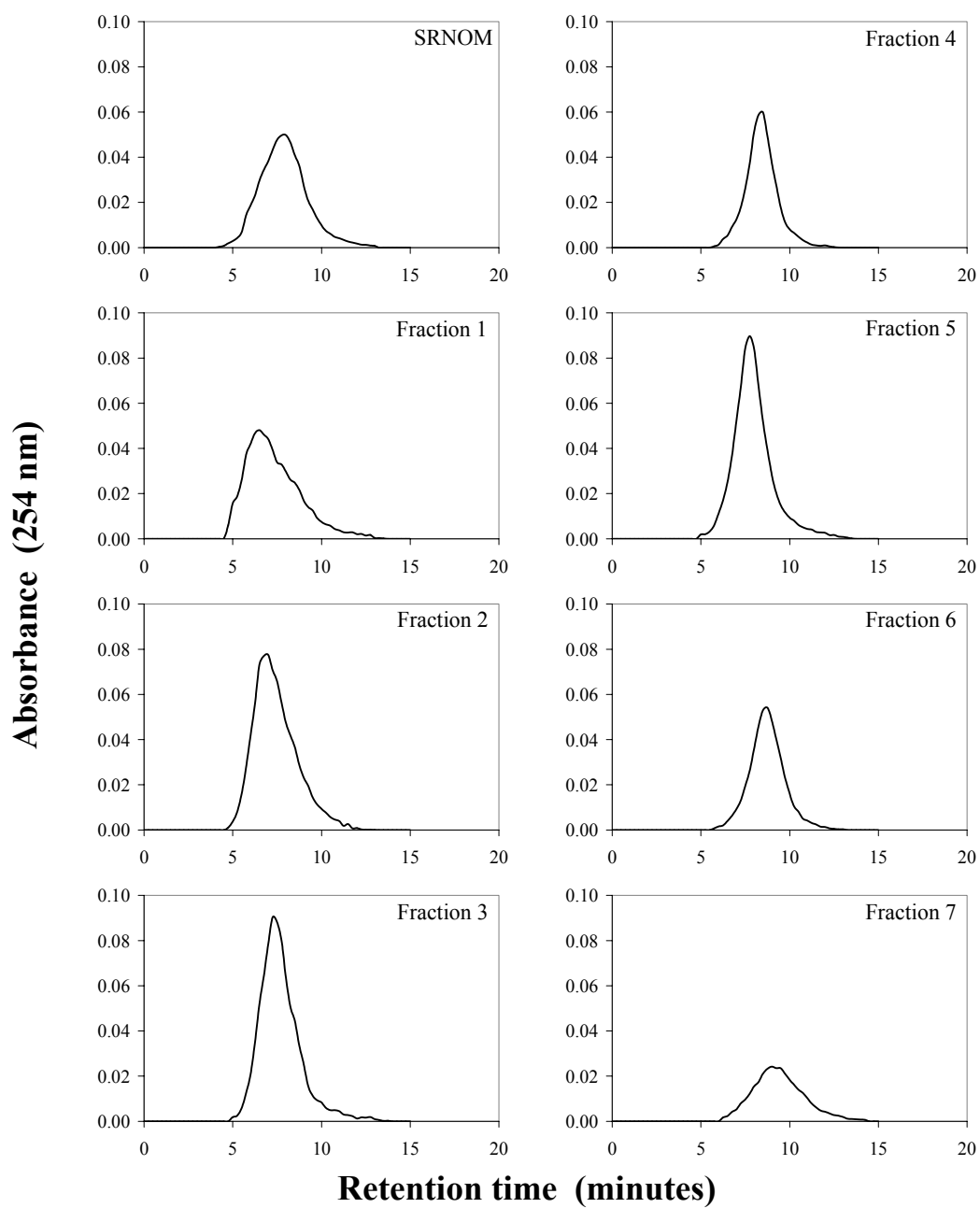


Figure 4.7. The absorbance chromatograms for the SRNOM and Fractions 1-7 as determined by SEC at pH 9.3.

underprediction of TOC. These very small TOC concentrations would have occurred at the extreme high MW values (log MW ~ 4.34 to ~ 4.1) and low MW values (log MW ~ 1.7 to ~ 2.0). The mass of organic matter in these extreme MWs is considered to be very small. Cabaniss *et al.* (2000) and Kudryavtsev *et al.* (2000) treat the tailing at the extreme ends of HPSEC chromatograms as insignificant and often discard those data points. Regardless of this after-the-fact discovery, the agreement between retention times for absorbance and TOC detection were good.

There is an offset between the absorbance and TOC chromatograms at pH 6.8 for the SRNOM and Fractions 3-6, in which the absorbance chromatograms were slightly shifted to shorter retention times than the TOC chromatograms. The time intervals between the peak absorbance and peak TOC values for those samples are 45 to 90 seconds, exceeding the predicted error in retention times of 10-20 seconds for the standard calibration compounds. The offset between tandem absorbance and online-TOC chromatograms was also observed by Huber *et al.* (1990), Müller *et al.* (2000), Her *et al.* (2002), and Perminova *et al.* (2003) for various unfractionated aquatic and terrestrial NOM samples. In those studies, TOC chromatograms were shifted to longer retention times than absorbance chromatograms, thus absorbance detection predicted greater MWs than the online-TOC detection method.

All chromatograms for Fraction 1 are moderately skewed to shorter retention times (or higher MW) with significant tailing. The chromatograms become progressively more pseudo-Gaussian in shape, smoother, and narrower in the order from Fraction 2 to 6. The chromatograms for Fraction 7 are more irregular and flatter than Fractions 2-6, but more symmetrical than Fraction 1. The absorbance maxima for chromatograms at pH

6.8 for the SRNOM and Fractions 1-6 are just slightly greater than those at pH 9.3. The absorbance maximum for Fraction 7's absorbance chromatogram at pH 6.8 is 33% greater than at pH 9.3. The solutions of Fraction 7 were prepared at the same concentration of 15 mgC L⁻¹ TOC, though in different background matrices. The injected volumes were scaled proportionately to the different column sizes used at the different pHs. Fraction 7 obviously absorbed light differently at pH 9.3 than at pH 6.8. This would explain the significant difference between the % area of absorbance and TOC recovery for Fraction 7 during the preparative SEC fractionation (Table 4.2).

The most profound information gained from inspection of Figures 4.6 and 4.7 is that there is significant overlap of the MW ranges between Fractions 1-7 regardless of the pH at which the separations were performed or the method of detection. No single fraction contains a unique range of MWs that is not shared by another fraction. Therefore, the preparative SEC method used in this research did not adequately separate the SRNOM into discrete "slices" with a unique range of MWs. Instead, seven broad segments of a MW continuum were created.

Egeberg and Alberts (2003) and Müller *et al.* (2000) conducted a similar fractionation work on other NOM samples by HPSEC, then verified the MW distributions of their fractions by HPSEC. The retention times of the chromatograms of their MW fractions also overlapped forming a continuum of MWs, but not as significantly as observed in this work. Pelekani *et al.* (1999) and especially Perminova *et al.* (1998) discuss the non-ideal physicochemical processes, in addition to MW or size, that affect the separation of organic acids by HPSEC. Faults in this work, other than the non-ideal interactions of solutes with the SEC column, can only be speculated.

On one hand, the divisions of the preparative SEC chromatograms into Fractions 1-7 were consistent for all 70 separations. The main body of the preparative SEC chromatograms (divided into Fractions 1-6) eluted from the SEC column between the retention times of the void volume and the total column volume. The shapes of the preparative SEC chromatograms closely resemble those for other Suwannee River isolates as determined by HPSEC. On the other hand, Fractions 1-7 underwent a large change in pH during the desalting (from pH ~ 9.2 to pH ~ 3.5), followed by freeze-drying to powder form. It is uncertain if the desalting and freeze-drying had adversely affected the MWs of the fractions.

With the exception of Egeberg and Alberts (2003) and Müller *et al.* (2000), this author could not cite any literature sources in which the researchers verified that HPSEC reliably separated their NOM samples by MW other than relying on the retention times of their HPSEC chromatograms relative to their system's calibration curves.

4.2.3 The mode MW.

The mode MW values for the absorbance (at pH 6.8 and 9.3) and TOC chromatograms (at pH 6.8) decreased from Fraction 1 to Fraction 7—the order of collection during the preparative SEC (Figure 4.8, top graph). Qualitatively, the significant differences between the decreasing mode MWs in order from Fraction 1 to Fraction 7 indicated the preparative SEC had fractionated the SRNOM by size, though the overlap of chromatograms show that the separation was not clean. If the logs of the mode MWs for Fractions 1-6 (the six fractions that composed the main hump of the preparative SEC chromatograms) at pH 9.3 are plotted against their respective mid-point

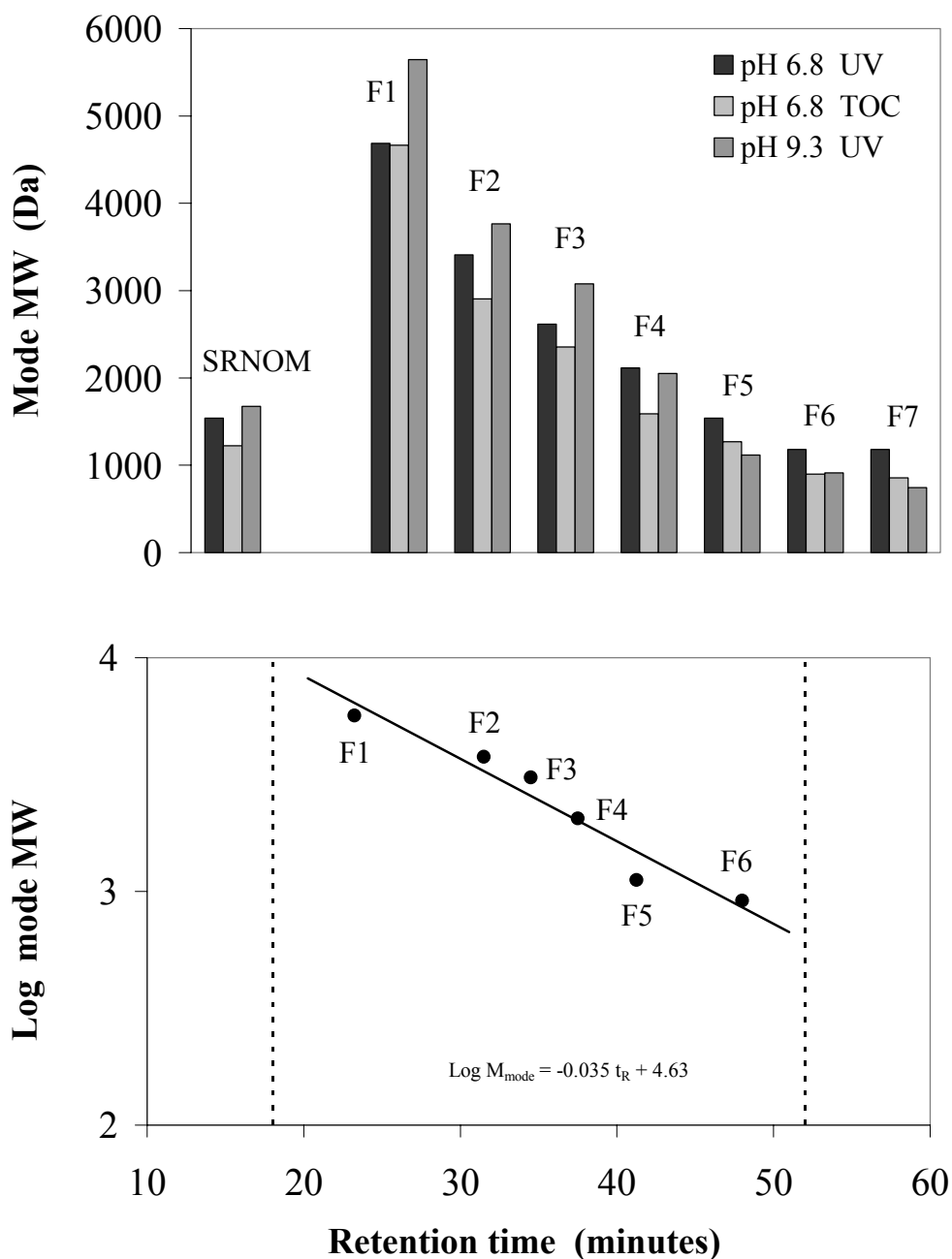


Figure 4.8. The mode MWs for the SRNOM and Fractions 1-7 at pH 6.8 and 9.3 (top graph). The correlation between mode MWs at pH 9.3 for Fractions 1-6 and their respective “midpoint” retention times during the fractionation of the SRNOM by preparative SEC (bottom graph). The dashed vertical lines represent the retention times of the void volume and the total column volume for the column used in the preparative SEC.

retention times during the preparative SEC (Table 4.1), there is a well-correlated linear trend ($R^2 = 0.940$) (Figure 4.8, bottom graph).

If the linear trend between midpoint retention time and the log of the mode MWs for Fractions 1-6 is used as crude proxy for the calibration curve of the preparative SEC column, the predicted MW range that was separated during the preparative SEC was 11,030 to 530 Da. It is unlikely that using mode MWs is a valid proxy for calibration, however, the mode MWs do give a fair indication of the overall separation of the SRNOM solutes by size during the preparative SEC based on UV absorbance detection at 350 nm.

4.2.4 The 3-Gaussian (3-G) model.

The optimal parameters to generate the best-fit 3-G models for the absorbance (pH 6.8 and 9.3) and the TOC chromatograms (pH 6.8) are shown in Table 4.3. The goodness of fit of the 3-G models compared to the experimental absorbance and TOC chromatograms for Fractions 1 and 7 is shown in Figure 4.9. Overall, the 3-G models are excellent fits ($R^2 > 0.999$) to the experimental data and adequately replicated the shapes of the absorbance and TOC chromatograms, though the 3-G model curves are slightly smoother than the experimental chromatograms.

4.2.5 Average MWs and ranges of MWs.

Values for the number-average (M_n) and weight-average (M_w) molecular weights, as well as the range of MWs in the SRNOM and Fractions 1-7 are shown in Table 4.4. Values of M_w decrease in order from Fraction 1 to Fraction 7—the order in which the

Table 4.3. The parameters for the three-Gaussian model (3-G) for absorbance and TOC chromatograms.

	Gaussian 1			Gaussian 2			Gaussian 3		
	μ_1	σ_1	A_1	μ_2	σ_2	A_2	μ_3	σ_3	A_3
Absorbance pH 6.8									
SRNOM	3.222	0.391	0.027	3.165	0.226	0.013	2.500	0.700	0.007
Fraction 1	3.698	0.290	0.029	3.074	0.291	0.017	2.500	0.700	0.005
Fraction 2	3.583	0.171	0.018	3.267	0.345	0.037	2.500	0.700	0.006
Fraction 3	3.433	0.162	0.023	3.194	0.355	0.036	2.500	0.700	0.005
Fraction 4	3.330	0.136	0.019	3.198	0.299	0.027	2.500	0.700	0.008
Fraction 5	3.205	0.110	0.011	3.113	0.248	0.027	2.500	0.415	0.003
Fraction 6	3.109	0.066	0.001	3.023	0.219	0.027	2.500	0.422	0.005
Fraction 7	3.120	0.066	0.001	2.979	0.320	0.024	2.500	0.658	0.013
Online-TOC pH 6.8									
SRNOM	3.157	0.334	0.386	3.049	0.149	0.056	2.544	0.441	0.056
Fraction 1	3.642	0.316	0.336	2.970	0.337	0.203	2.500	0.580	0.028
Fraction 2	3.529	0.203	0.256	3.144	0.328	0.338	2.504	0.349	0.039
Fraction 3	3.380	0.181	0.249	3.116	0.316	0.324	2.500	0.377	0.034
Fraction 4	3.248	0.149	0.192	3.086	0.287	0.332	2.500	0.322	0.026
Fraction 5	3.127	0.122	0.143	2.976	0.258	0.360	2.604	0.375	0.041
Fraction 6	2.987	0.105	0.045	2.981	0.203	0.288	2.570	0.259	0.058
Fraction 7	2.995	0.150	0.057	2.893	0.362	0.201	2.500	0.548	0.093
Absorbance pH 9.3									
SRNOM	3.642	0.263	0.013	3.136	0.281	0.027	2.850	0.577	0.015
Fraction 1	3.741	0.275	0.028	3.174	0.339	0.019	2.629	0.595	0.009
Fraction 2	3.613	0.215	0.018	3.255	0.339	0.033	2.690	0.437	0.009
Fraction 3	3.467	0.215	0.018	3.273	0.324	0.049	2.527	0.576	0.007
Fraction 4	3.466	0.219	0.001	3.234	0.281	0.055	2.564	0.551	0.010
Fraction 5	3.547	0.161	0.003	3.021	0.218	0.031	2.579	0.330	0.006
Fraction 6	2.923	0.343	0.025	2.892	0.181	0.009	2.688	0.528	0.007
Fraction 7	2.922	0.352	0.007	2.741	0.220	0.002	2.545	0.535	0.019

μ : mean log MW. σ : standard deviation. A: relative area for Gaussian distributions.

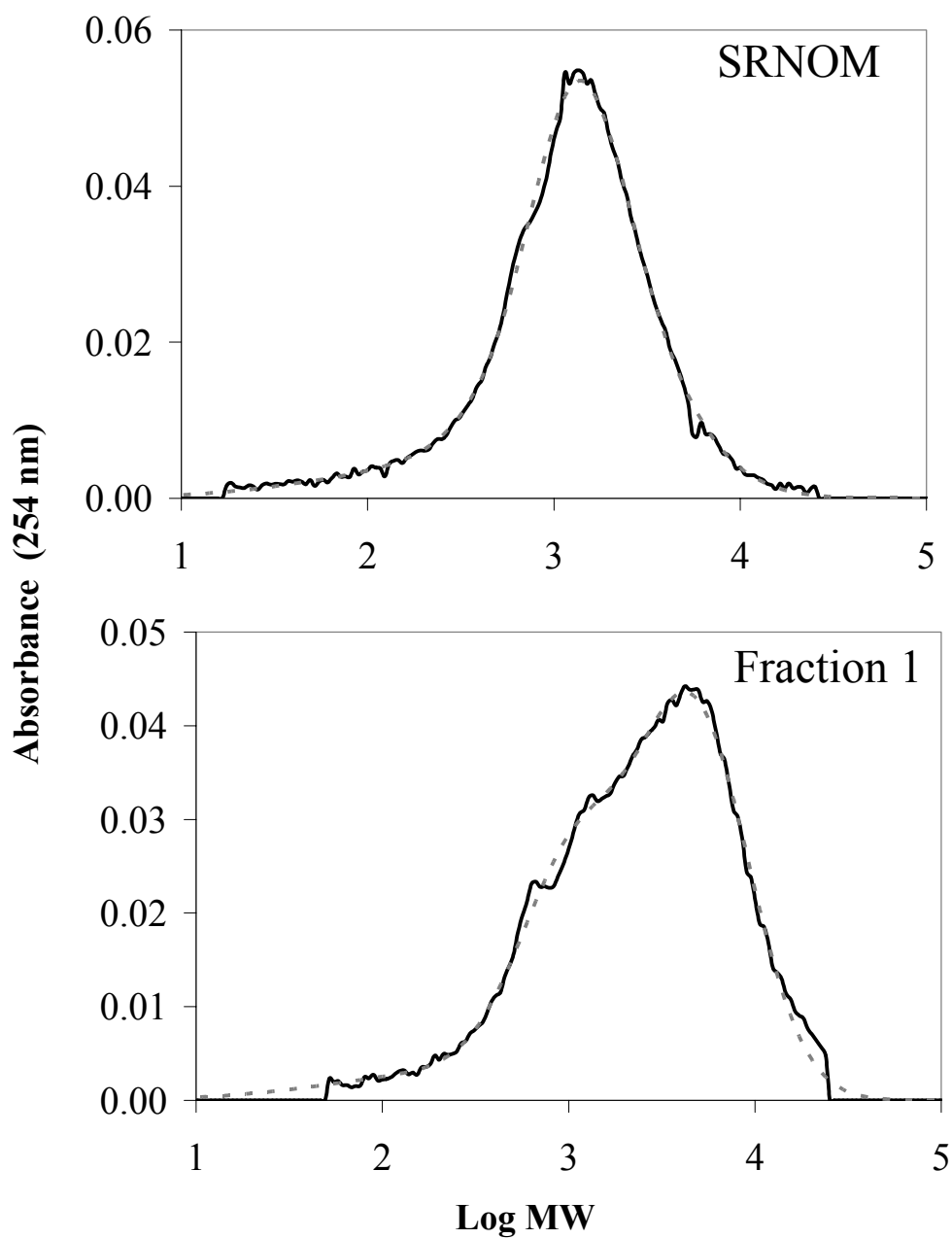


Figure 4.9. The best-fit 3-G models (dashed lines) for the SRNOM and Fraction 1 are superimposed on the absorbance chromatograms (solid black line) as determined by SEC at pH 6.8.

fractions were collected during the preparative SEC. Values of M_n also decrease in the same order, with the exception of Fraction 1 at pH 9.3, which was calculated to be ~230 and 200 Da less than M_n for Fraction 2 and Fraction 3. The absorbance chromatogram for Fraction 1 at pH 9.3 (Figure 4.7) has more tailing at longer retention times than the absorbance and TOC chromatograms for Fraction 1 at pH 6.8 (Figure 4.6), which would bias M_n to lower MW.

The values of M_w for the absorbance chromatograms at pH 6.8 are ~10 to 20% (~200 to 400 D) greater than M_w for the TOC chromatograms. The values of M_n for absorbance chromatograms at pH 6.8 are also larger than M_n for the TOC chromatograms. M_n and M_w for the absorbance chromatograms are 3 to 18% greater than M_n and M_w for the TOC chromatograms, but overall were very close. If the M_w and M_n for the TOC chromatograms are plotted against those for the absorbance chromatograms at pH 6.8, both M_w and M_n were strongly correlated ($R^2 = 0.992$ and 0.905). The differences between the average MW values are attributed to the different equations for the absorbance and TOC calibration curves. Additionally, the peaks of the absorbance chromatograms are positioned at shorter retention times (45 to 90 seconds) than the corresponding peak TOC. The exact effect of the TOC baseline error or the offset of time between the tandem absorbance and TOC detection on the calculation of M_w and M_n is unknown.

If M_w and M_n for the absorbance chromatograms at pH 9.3 are plotted against those for the absorbance chromatograms at pH 6.8, M_w is strongly correlated ($R^2 = 0.954$), but M_n is weakly correlated ($R^2 = 0.750$). The M_w values for Fractions 1-4 at pH 9.3 are greater than those at pH 6.8, but M_w values for Fractions 5-7 at pH 6.8 are greater

Table 4.4. The number-average (M_n) and weight-average (M_w) molecular weights, and the minimum and maximum MWs for the SRNOM and Fractions 1-7 as determined by semi-analytical SEC at pH 6.8 and pH 9.3. Average MWs have units of g mol^{-1} . Polydispersity (P) is calculated as M_w/M_n . Minimum and maximum MWs have units of Daltons.

	Absorbance pH 6.8			Online-TOC pH 6.8			Absorbance pH 9.3		
	M_n	M_w	P	M_n	M_w	P	M_n	M_w	P
SRNOM	815	2119	2.38	846	1742	2.06	969	2683	2.77
Fraction 1	1529	4198	2.74	1243	3774	3.04	1248	4575	3.67
Fraction 2	1329	2962	2.23	1227	2623	2.14	1474	3507	2.38
Fraction 3	1193	2401	2.01	1156	2072	1.79	1448	2751	1.90
Fraction 4	1179	1844	1.56	1066	1623	1.52	1059	2080	1.96
Fraction 5	1099	1538	1.40	830	1217	1.47	847	1369	1.62
Fraction 6	727	1124	1.55	694	991	1.43	627	1094	1.74
Fraction 7	519	1229	2.37	465	996	2.14	376	907	2.41

	Absorbance pH 6.8		Online-TOC pH 6.8		Absorbance pH 9.3	
	Min	Max	Min	Max	Min	Max
SRNOM	60	21,200	60	20,800	86	21,690
Fraction 1	60	23,260	60	21,980	86	21,700
Fraction 2	60	18,580	71	18,970	86	17,770
Fraction 3	60	12,160	78	14,930	102	14,550
Fraction 4	78	8,390	78	10,330	91	9,750
Fraction 5	90	6,100	102	7,410	91	6,540
Fraction 6	60	4,190	78	4,760	86	5,720
Fraction 7	60	8,600	60	11,120	91	4,687

than those at pH 9.3. The same trend is seen for M_n , with the exception of Fraction 1 and Fraction 3 whose values at pH 9.3 were calculated to be 280 Da less and 250 Da greater than those at pH 6.8, respectively. Overall, M_w and M_n at pH 9.3 are within $\pm 3\%$ to 25% of M_w and M_n at pH 6.8.

The polydispersities (P) for MWs generally decrease from Fraction 1-6, with polydispersities for Fraction 7 being larger and most comparable to the polydispersities of Fraction 2. Fraction 1 has the most asymmetrical chromatograms, widest distributions of MWs, and largest values of P. Fractions 5 and 6, the samples with the lowest polydispersities, have chromatograms that are the most symmetrical and have the narrowest distributions of MWs. The SRNOM has values of M_w and M_n that are very similar to those for Fraction 5. The polydispersities of the SRNOM, however, are more comparable to those for Fractions 2 and 7, samples that have a relatively wide distribution of MWs.

As previously stated, Fractions 1-7 contain a continuum of overlapping MWs at both pH 6.8 and 9.3. The ranges of MWs contained in Fractions 1-7 are shown in Table 4.4. Pelekani *et al.* (1999) and Assemi *et al.* (2004) also reported a continuum of overlapping MWs for their fractionated soil humic acid. Those researchers first fractionated their soil humic acids by sequential-stage ultrafiltration (UF), then verified the MWs of their fractions by flow field-flow fractionation (FFFF).

The ranges of MWs for Fractions 1-7 are within the range of MWs for the SRNOM. The maximum MWs, just like average MWs and the mode MW, decrease in order from Fraction 1 to Fraction 6 (at pH 6.8 for absorbance and online-TOC detection) and decrease from Fraction 1 to Fraction 7 at pH 9.3. This indicates that solutes at the

points of division of the preparative SEC chromatograms were more-or-less eluting through the preparative SEC column based on their size. Due to the overlap of the MWs between Fractions 1-7, this author suspects that the majority of solutes of all MWs and sizes in the SRNOM had minor non-ideal interactions with the Superdex-30 resin from the point of injection to the final elution of organic matter to be included in Fraction 6 at the retention time of the total column volume. The fact that Fraction 7 is predicted to have greater maximum MWs than Fractions 4-6 indicates that the organic matter that was flushed off of the resin with NaOH during the cleaning step should have been in Fractions 1, 2, or 3, or all three, based on their ranges of MWs.

Due to the extensive tailing at the lower MW side of the SEC chromatograms, the minimum MWs correspond to the retention times of the column volume of the SEC columns. The lowest MWs, as predicted by the calibration curve for absorbance and TOC detection, are 60 and 140 Da respectively. Because the chromatograms for the SRNOM and Fractions 1-7 have tailing that extends to the lowest MW limit, a small portion of solutes in each sample either strongly sorb to the resin by hydrophobic interactions (Perminova *et al.*, 1998) or are being retarded from migrating through the column by ionic-repulsive forces (Barth, 1987). Both phenomenon increase the retention times of organic solutes on the SEC column.

4.2.6 Literature values of M_n and M_w .

The M_n and M_w values for Fractions 1-7 at pH 6.8—the pH most common for performing MW measurements on NOM (Janos, 2003)—were compared to literature reports of M_n and M_w for other, well characterized Suwannee River isolates (Table 4.5).

Table 4.5. The average MWs for the Suwannee River fulvic acid (SRFA), humic acid (SRHA), and other Suwannee River NOM samples (SRNOM) as reported in the literature. Average MWs have units of g mol⁻¹.

	M_n	M_w	Method of analysis
IHSS std. SRFA^a	840	-	Vapor pressure osmometry
IHSS std. SRFA^a	829	-	Vapor pressure osmometry
IHSS std. SRFA^b	1360	2310	High pressure SEC
IHSS std. SRFA^c	1400	1700	High pressure SEC
IHSS std. SRFA^d	1790	2430	High pressure SEC
IHSS std. SRFA^e	1260	2170	High pressure SEC
IHSS std. SRFA^f	-	2310	High pressure SEC
IHSS std. SRFA^g	980		Flow field-flow fractionation
IHSS std. SRFA^h	1150	1910	Flow field-flow fractionation
IHSS std. SRFAⁱ	1119	1372	Flow field-flow fractionation
IHSS std. SRFA^j	1160	1240	Flow field-flow fractionation
IHSS std. SRFA^k	-	1460	UV-scanning ultracentrifugation
IHSS std. SRFA^l	-	1532	Ultrafiltration
IHSS std. SRHA^f	-	3320	High pressure SEC
IHSS std. SRHA^m	-	2600	High pressure SEC
IHSS std. SRHA^h	1580	4390	Flow field-flow fractionation
IHSS std. SRHAⁱ	2247	3157	Flow field-flow fractionation
IHSS std. SRHA^j	1320	2029	Flow field-flow fractionation
IHSS std. SRHA^k	-	4260	UV-scanning ultracentrifugation
IHSS std. SRHA^l	-	2748	Ultrafiltration
SRNOM^b	1330	2190	High pressure SEC
SRNOM^d	1440	2200	High pressure SEC
Mean SRFA	835 ± 8	-	Colligative methods
Mean SRFA	1277 ± 247	1843 ± 440	Non-colligative methods
Mean SRHA	1716 ± 478	3224 ± 851	Non-colligative methods
Mean SRNOM	1385 ± 78	2195 ± 7	Non-colligative methods

References: ^a Aiken and Malcolm (1987); ^b Chin *et al.* (1994); ^c Chin and Gschwend (1991); ^d Everett *et al.* (1999); ^e Maurice *et al.* (2001); ^f Westerhoff *et al.* (1999); ^g Schimpf and Petteys (1997); ^h Beckett *et al.* (1987); ⁱ Dycus *et al.* (1995); ^j Benedetti *et al.* (2002); ^k Reid *et al.* (1990); ^l Austin *et al.* (2001); ^m Croue *et al.* (1999). SRNOM samples for references b and d were collected independently by those researchers.

Values of M_w for Fractions 1-3 are in the range of M_w reported for the Suwannee River humic acid (SRHA). Values of M_w for Fractions 4 and 5 are most similar to the Suwannee River fulvic acid (SRFA). Values of M_w for Fractions 6 and 7 are slightly lower than M_w reported for any Suwannee River sample. The values of M_n for Fractions 1-3 are comparable to reported values of M_n for the SRFA as determined by HPSEC and flow field-flow fractionation (FFFF). The values of M_n for Fractions 4-6 are most comparable to M_n values for SRFA by vapor pressure osmometry (VPO)—a colligative method. Fractions 7 has a M_n value that is lower than any reported M_n for any Suwannee River sample.

Based on comparison of the average MWs of Fractions 1-7 with other Suwannee River isolates, it could be generalized that Fraction 1 is most similar to the SRHA, Fractions 2 and 3 have MW properties similar to both the SRHA and SRFA, and Fractions 4 and 5 are most similar to the SRFA. Fractions 6 and 7 may be similar to SRFA, but their average MWs do not correspond well to any reported Suwannee River samples.

4.2.7 Reconstructing chromatograms of the SRNOM.

The integrity of the preparative SEC process need to be tested. This is done by reconstructing the absorbance and TOC chromatograms for the SRNOM from the weighted-sums of the chromatograms for Fractions 1-7. First, the 3-G model chromatographs for Fractions 1-7 were plotted as absorbance vs. log MW and TOC vs. log MW. The absorbance chromatograms at pH 6.8 and pH 9.3 were weighted to their respective % average areas of absorbance as the criteria for division during the

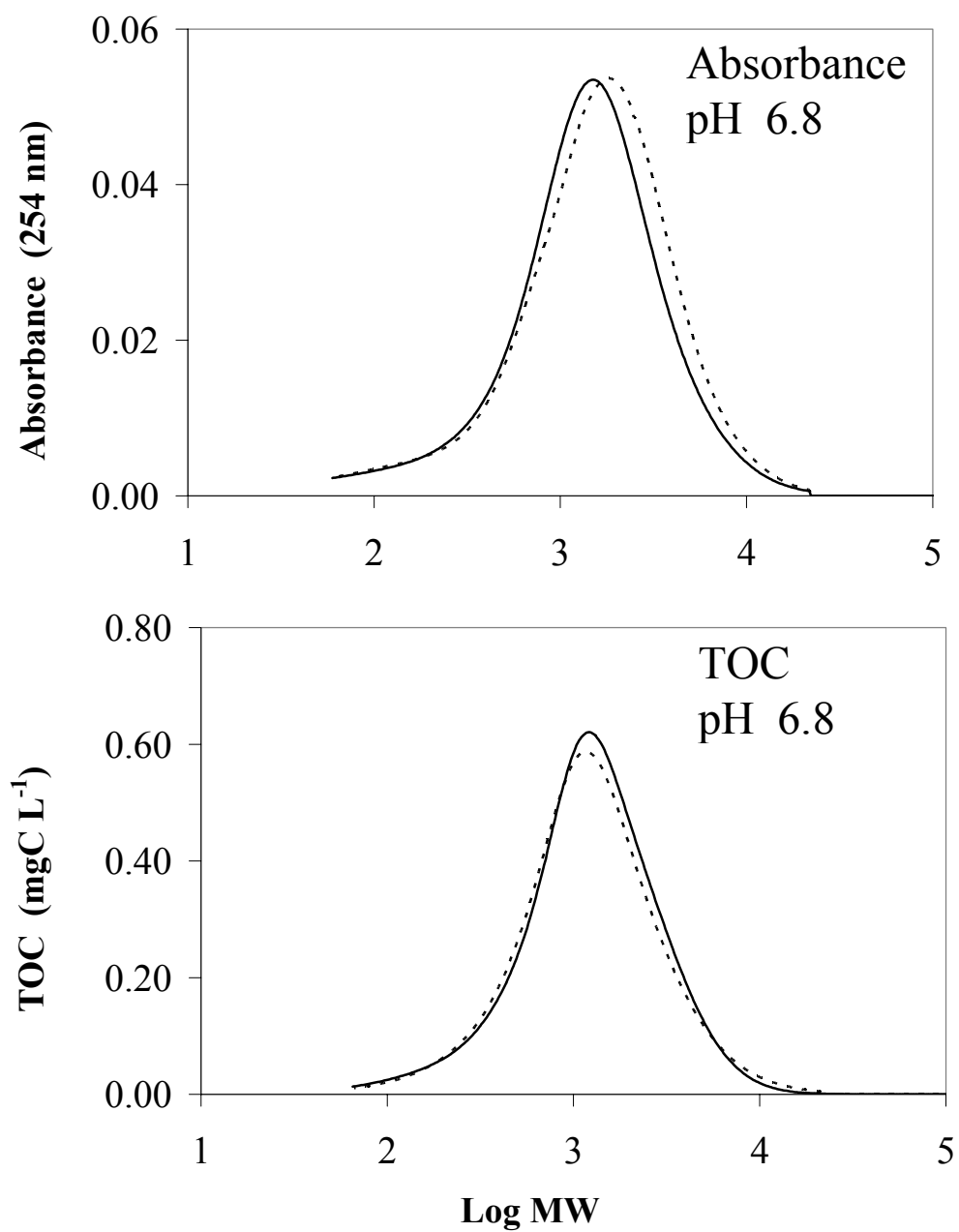


Figure 4.10. The absorbance and online-TOC chromatograms for the SRNOM (solid lines) at pH 6.8 compared to the reconstructed absorbance and online-TOC chromatograms (dashed lines) that were created from the weighted sums of chromatograms for Fractions 1-7.

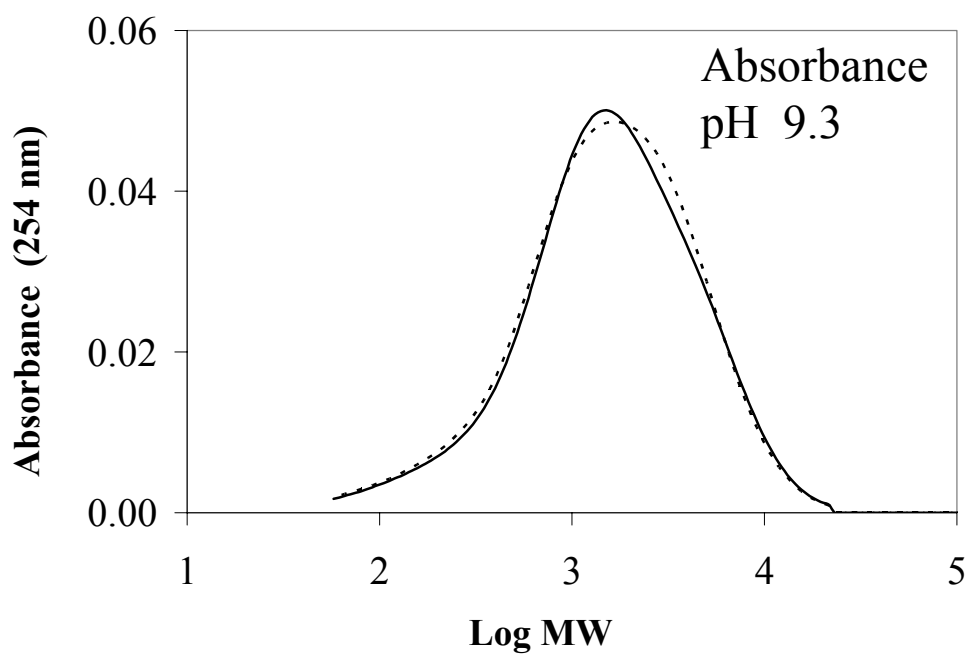


Figure 4.11. The absorbance chromatogram for the SRNOM (solid line) at pH 9.3 compared to the reconstructed absorbance chromatogram (dashed line) that was created from the weighted sums of absorbance chromatograms for Fractions 1-7.

preparative SEC fractionation (Table 4.2). The online-TOC chromatograms were weighted to their respective % carbon recovered from the preparative SEC (Table 4.2). The weighted chromatograms were then added together to form the reconstructed chromatograms. The comparisons of the reconstructed absorbance and TOC chromatograms with those for the SRNOM are shown in Figures 4.10 and 4.11.

The overall agreements between the reconstructed absorbance (pH 6.8) and TOC chromatograms and the chromatograms for the SRNOM are very good (Figure 4.10). The reconstructed absorbance chromatogram at pH 6.8 is slightly offset to higher log MWs. Conversely, the reconstructed TOC chromatogram for Fractions 1-7 is slightly shifted to lower log MW than the SRNOM chromatogram. The reconstructed absorbance and TOC chromatograms cover the same log MW range as their respective SRNOM chromatograms. The reconstructed absorbance chromatogram and the chromatogram for the SRNOM at pH 9.3 are almost identical (Figure 4.11), in spite of Fraction 7 having significantly lower absorbance at pH 9.3. The very good agreement between the reconstructed absorbance and TOC chromatograms and those for the SNROM indicates that the processing after fractionation did not significantly alter the fractions and that the impact of the 6% loss of carbon was minimal.

4.3 Elemental Analysis.

4.3.1 Elemental composition.

The raw data for elemental analysis as reported by Huffman Laboratory are shown in Table 4.6. Fractions 1-6 are more-or-less similar in elemental composition,

Table 4.6. The raw elemental composition for the SRNOM and Fractions 1-7 as reported by Huffman Laboratory (Golden, Colorado) in June, 2001.

	Raw elemental composition ^b				
	% C	% H	% N	% Ash	% H ₂ O ^c
SRNOM^a	48.80	3.90	1.02	7.00	10.00
Fraction 1	46.71	4.32	1.89	12.53	1.75
Fraction 2	48.61	3.94	1.33	8.13	4.84
Fraction 3	50.37	3.76	1.08	6.01	2.47
Fraction 4	50.07	3.76	1.04	4.64	4.06
Fraction 5	49.63	3.91	0.88	3.13	1.63
Fraction 6	46.62	4.02	1.17	12.40	0.39
Fraction 7	37.01	3.95	2.04	25.78	3.34

^aElemental composition reported by Huffman Laboratories in July 1999.

^bElemental and ash data reported as % dry weight (g/g).

^c%H₂O is the % weight due to moisture removed from sample before elemental analysis.

Table 4.7. The inorganic ions in the ash portion of each sample.

	Inorganic ions in ash ^a						SO ₄
	Na	K	Mg	Ca	Fe	Si	
SRNOM	90.7	-	-	-	750	717	-
Fraction 1	27.3	-	-	-	1539	364	223
Fraction 2	35.5	-	-	-	850	879	387
Fraction 3	51.2	-	-	-	1352	1109	1289
Fraction 4	51.5	-	-	-	-	1309	-
Fraction 5	54.6	-	-	-	-	367	-
Fraction 6	22.2	-	-	-	-	1556	344
Fraction 7	15.2	-	-	-	-	324	140

^aInorganic ions reported as C:ion ratios (mole:mole).

containing between 46.7 and 50.3% carbon, 3.8 to 4.3% hydrogen, and 0.9 to 1.9% nitrogen by dry weight. Fraction 7 contained much less carbon at 37.0% and had the highest nitrogen and ash content. The suspiciously high nitrogen content for Fraction 7, and perhaps for Fraction 1, prompted an analysis for total free amino acids (TFAA) by the Ninhydrin method (Moore and Stein, 1954; Yemm and Cocking, 1955). There was no conclusive evidence for TFAAs in any of the samples. The possibility remains that the large quantity of nitrogen in Fraction 7 may be in intact peptides or proteins from a contaminating biological source that can only be analytically detected by hydrolyzing the samples. Samples could not be spared to test this hypothesis.

All seven fractions, especially Fractions 6 and 7, contain significant amounts of inorganic ash, ranging from 3.1 to 25.8 by dry weight. The composition of the ash is shown in Table 4.7. Na^+ is the dominant component of the inorganic ash, even though the cation exchange resin removed 99.1 to 99.6% of the total Na^+ from the mobile phase in the liquid samples prior to their freeze-drying. There is no measurable quantities of the cations K^+ , Ca^{2+} , and Mg^{2+} . Fractions 1, 2, and 3 and the SRNOM contained trace amounts of Fe^{3+} . Trace quantities of silica are found in all of the samples. Sulfate is a significant ion in Fractions 1, 2, 6, and 7, which would have a very large impact on the acid-base chemistry of those fractions. Considering that the SRNOM had only a trace amount of sulfate, the relatively large quantities of sulfate in Fractions 1, 2, 6, and 7 can not be explained.

4.3.2 The elemental compositions of dry, ash-free samples.

The elemental compositions of the fractions were normalized to percents C, H, N,

Table 4.8. Elemental analyses on a dry, ash-free basis.

	Elemental composition ^a				Mole ratio		
	% C	% H	% N	% O ^b	H/C	N/C	O/C
SRNOM	52.47	4.19	1.10	42.70	0.952	0.018	0.611
Fraction 1	53.40	4.94	2.16	39.50	1.102	0.035	0.555
Fraction 2	52.91	4.29	1.45	41.35	0.966	0.024	0.587
Fraction 3	53.59	4.00	1.15	42.47	0.889	0.018	0.595
Fraction 4	52.51	3.93	1.09	40.86	0.892	0.018	0.584
Fraction 5	51.23	4.04	0.91	42.07	0.940	0.015	0.616
Fraction 6	53.22	4.59	1.33	43.82	1.028	0.021	0.618
Fraction 7	49.86	5.32	2.75	43.53	1.272	0.047	0.655

^aElemental compositions reported as %weight (g/g) on a dry, ash-free basis.

^bOxygen content calculated as $\%O = 100 - (\%C + \%H + \%N)$.

Table 4.9. The mass yield (g) and % mass yield of the organic forms of carbon, hydrogen, nitrogen, and oxygen that were recovered in Fractions 1-7 compared to those in the SRNOM separated during the preparative SEC.

	Carbon		Hydrogen		Nitrogen		Oxygen	
	Mass	%	Mass	%	Mass	%	Mass	%
SRNOM^a	0.504	100	0.0402	100	0.0106	100	0.410	100
Sum F1-F7^b	0.474	94.1	0.0409	101.5	0.0144	135.9	0.385	93.8
Fraction 1	0.050	9.9	0.0046	11.4	0.0020	19.0	0.037	9.0
Fraction 2	0.039	7.8	0.0032	7.9	0.0011	10.2	0.031	7.5
Fraction 3	0.050	9.9	0.0037	9.2	0.0011	10.1	0.040	9.6
Fraction 4	0.063	12.4	0.0047	11.7	0.0013	12.3	0.049	11.9
Fraction 5	0.070	13.9	0.0060	15.0	0.0018	16.6	0.058	14.1
Fraction 6	0.108	21.4	0.0085	21.1	0.0019	18.1	0.088	21.6
Fraction 7	0.095	18.8	0.0101	25.2	0.0052	49.6	0.083	20.2

and O, based on their dry, ash-free masses (Table 4.8)—the conventional method of reporting elemental data for NOM. There is little variation for %C and %H between Fractions 1-6, ranging from 51.2-53.6% and 3.93-4.94% by dry ash-free weight. The %O ranged from 39.5-43.8%. Fraction 7 had a slightly smaller %C and slightly larger %H than the other six fractions at 49.9% and 5.32%, respectively. With the exception of Fraction 7, the %N content tends to decrease in order Fraction 1 to Fraction 5, perhaps linking %N as a function of MW. The %N in Fraction 6 was ~30% greater than that in Fraction 5. According to Huber and Frimmel (1994) and Huber and Frimmel (1996), the organic compounds that elute from SEC columns at longer retention times—approaching the retention time of the total column volume—tend to be enriched with lipids, amino acids, and phenols. Fraction 6 is composed of NOM that eluted from the preparative SEC column at the retention time corresponding to the total column volume. It is probable that Fraction 6 contains the natural assemblage of low MW amine or amide containing solutes that Huber and coworkers observed.

The total mass balances of each organic element (C, H, N, and O) in Fractions 1-7 were compared to those in the SRNOM that was fractionated during the preparative SEC. Mass balances are based on the recoveries of carbon and the total mass of Fractions 1-7 (Table 4.2) with their dry, ash-free elemental compositions reported in Table 4.8. The mass and %mass yields for the elemental data are shown in Table 4.9.

A total of 504 mg C, 4.02 mg H, 1.06 mg N, and 410 mg O (O + S) in the SRNOM was fractionated during the preparative SEC. The sum of the organic elements for Fractions 1-7 yielded 474 mg C (-5.9 %), 4.09 mg H (+ 1.5 %), 1.44 mg N (+ 35.9 %), and 385 mg O (- 6.2 %). There was a net loss of 6% carbon and 6% oxygen and net

increase of 1.5% hydrogen and 36% nitrogen during the preparative SEC and the subsequent desalting and freeze-drying of the samples. Fraction 7 contains approximately one-third of the total recovered nitrogen, 0.52 mg of the 1.44 mg N, supporting the theory of biological contamination.

4.3.3 Literature reports of elemental data.

The elemental compositions for Fractions 1-7 (Table 4.8) were compared to literature reports of the elemental composition (Table 4.10) of the other, well-characterized Suwannee River samples. Fractions 1-7 had %C, %H, and %O that were within the ranges for both the FAs and HAs. The %N for Fractions 2, 3, 4, 5, and 6 were in better agreement with the % N for SRHA and SRNOM samples than for the SRFA. The %N for Fractions 1 and 7 was greater than all literature reports of %N for the Suwannee River samples. Overall, there was no clear indication if any of the fractions could be described as more “fulvic acid-like” or “humic acid-like” based on elemental data.

4.3.4 Elemental data and MW.

Various correlations between the elemental data and the average MWs for Fractions 1-6 were examined. Fraction 7 is considered an outlier, due to its large %N and very high ash content. The only substantial correlation between elemental data and the M_w is for the O/C values (Figure 4.12), where O/C increased with decreasing M_w for Fractions 1-6. This is an indication that quantities of oxygenated functional groups, such as carboxyl groups, should be inversely proportional to the average MW of the sample.

Table 4.10. The elemental data for the Suwannee River fulvic acid (FA), humic acid (HA), and NOM as reported in the literature.

	% C	% H	% N	% O	H/C	N/C	O/C
IHSS std. SRFA^a	52.4	4.31	0.72	42.2	0.980	0.012	0.605
IHSS std. SRFA^b	53.8	4.29	0.68	40.5	0.950	0.011	0.565
IHSS std. SRFA^c	53.8	4.30	0.70	41.0	0.952	0.011	0.572
IHSS std. SRFA^d	51.3	4.32	0.56	43.8	1.004	0.009	0.641
IHSS std. SRFA^e	53.2	4.07	0.76	43.2	0.912	0.012	0.610
SRFA^f	46.0	4.11	0.59	49.1	1.065	0.011	0.801
IHSS std. SRHA^a	52.6	4.40	1.19	42.5	0.997	0.019	0.607
IHSS std. SRHA^b	54.2	4.14	1.21	39.0	0.910	0.019	0.540
IHSS std. SRHA^c	54.2	4.10	1.20	39.8	0.901	0.019	0.551
IHSS std. SRHA^e	53.5	4.24	0.69	41.3	0.944	0.011	0.580
SRHA^f	50.6	4.50	1.62	43.0	1.060	0.027	0.638
IHSS SRNOM^a	52.5	4.19	1.10	42.7	0.951	0.018	0.611
SRNOM^g	49.2	4.45	0.80	45.6	1.078	0.014	0.696
SRNOM^g	48.8	4.44	0.90	45.9	1.084	0.016	0.706
Mean SRFA	51.8 ± 3.0	4.2 ± 0.7	0.67 ± 0.1	43.3 ± 3.1	0.98 ± 0.05	0.01 ± 0.00	0.63 ± 0.09
Mean SRHA	53.0 ± 1.5	4.3 ± 0.2	1.2 ± 0.3	41.1 ± 1.7	0.96 ± 0.07	0.02 ± 0.01	0.58 ± 0.04
Mean SRNOM	50.2 ± 2.0	4.4 ± 0.2	0.93 ± 0.2	44.7 ± 1.8	1.04 ± 0.08	0.02 ± 0.00	0.67 ± 0.05

References: ^aIHSS standard collection, Huffman Laboratory 1996, 1999. ^bIHSS standard collection, Huffman Laboratory 1984. ^cDavis *et al.* (1999). ^dGauthier *et al.* (1987). ^eSenesi *et al.* (1989). ^fSuwannee River samples collected independently by Ma *et al.* (2001). ^gSuwannee River samples collected by Serkiz and Perdue (1990).

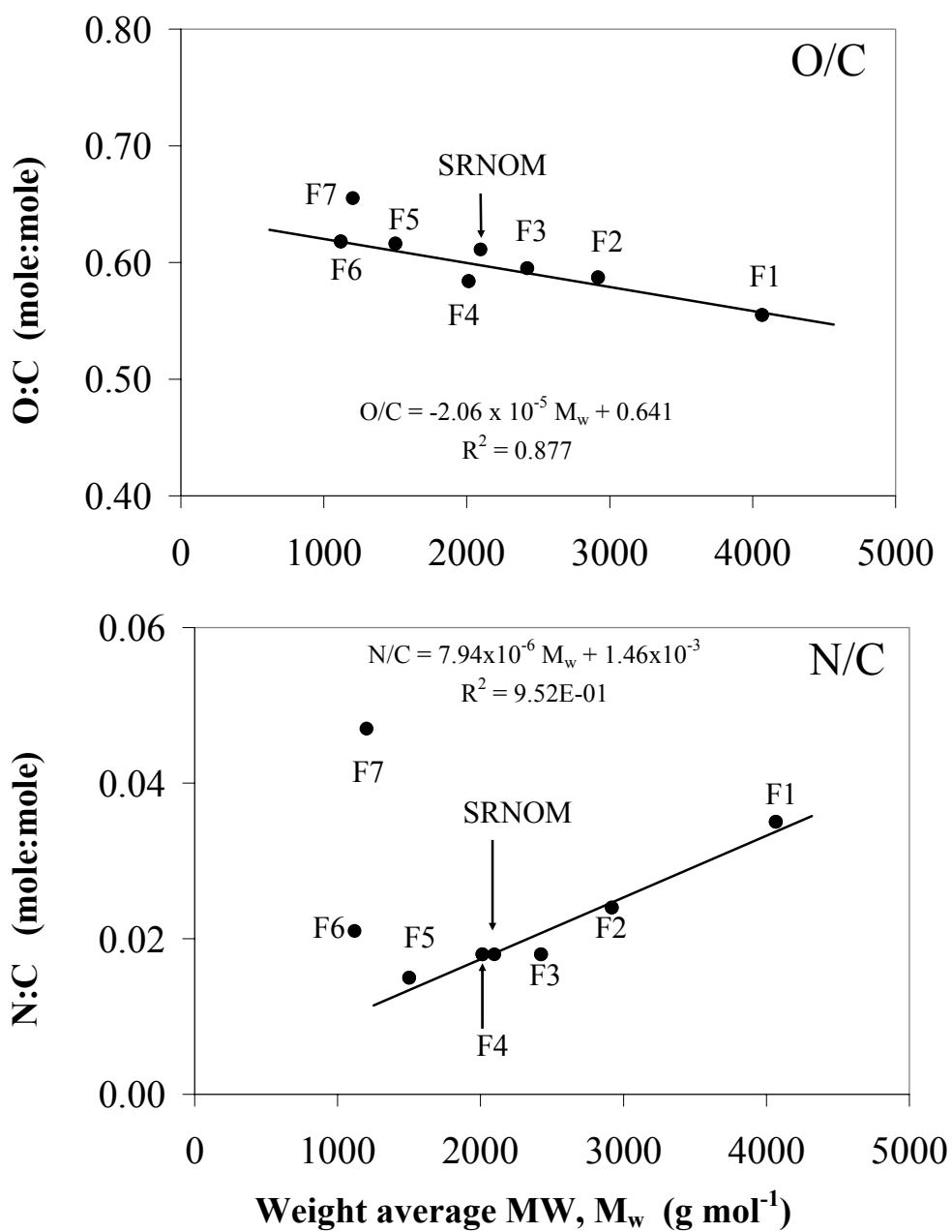


Figure 4.12. The O/C and N/C ratios for the SRNOM and Fractions 1-7 as a function of their weight-average (M_w) MWs. The linear trend line for O/C was fit through data for Fractions 1-6. The linear trend line for N/C was fit through data for Fractions 1-5.

There was a strong correlation between N/C and M_w for Fractions 1-5, where N/C increased with increasing M_w (Figure 4.12). Fractions 6 and 7 are outliers.

4.4 UV-Visible Spectroscopy.

4.4.1 The absorbance of UV-visible light.

The UV-visible spectra for the SRNOM and Fractions 1-7 are shown in Figure 4.13. The maximum absorbances for the samples at pH 6.8 are at 210 nm. The maximum absorbances at pH 9.3 are at 220 nm. The intensity of absorbances at both pHs decreases pseudo-exponentially from 220 nm to the maximum wavelength of 720 nm. The absorbance profiles at pH 6.8 are almost identical to the absorbance profiles at pH 9.3 for the SRNOM and Fractions 1-6 between 230 and 720 nm. The absorbance profile for Fraction 7 at pH 6.8 is approximately 25-30% greater than those at pH 9.3 between 230 and 720 nm. Fraction 7 absorbs UV and visible light more strongly at pH 6.8, even though Fraction 7 was in the same concentration at pH 6.8 and pH 9.3. Approximately 25-30% of the organic matter in Fraction 7 was invisible to the UV detector at pH 9.2 during the preparative SEC, giving the impression that the small % area of absorbance for Fraction 7 (Table 4.2) was proportional to a small quantity of organic matter.

Fraction 2 has the greatest absorbance values at all wavelengths at both pHs, and absorbance values at all wavelengths decrease in the order from Fraction 2 to Fraction 6, the weakest light-absorbing fraction. Fraction 1, the fraction with the largest average MW values, has absorbance values slightly smaller than Fractions 2 and 3 between 200 and 600 nm. The absorbance values for Fraction 7 at pH 6.8 tend to be comparable to

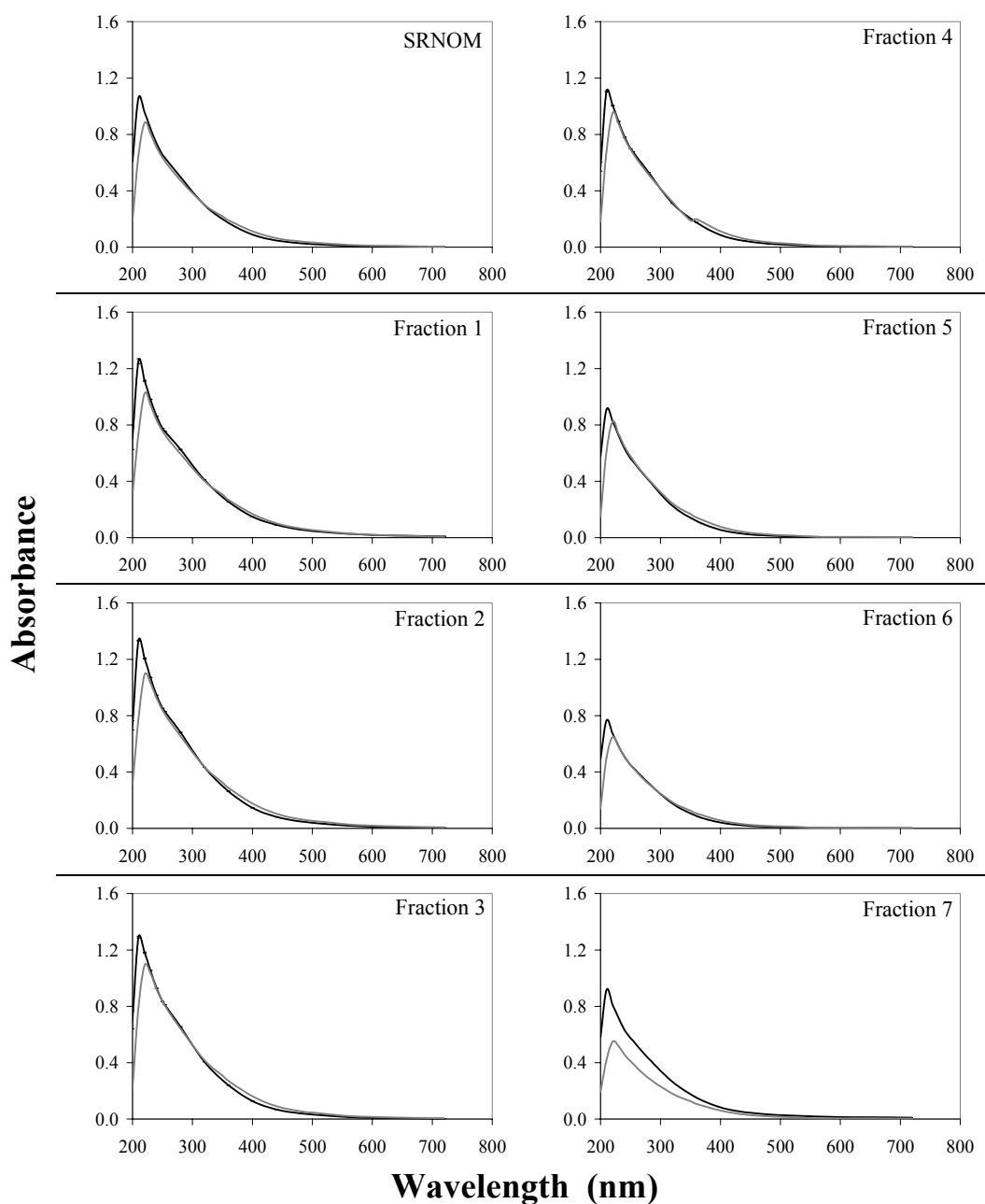


Figure 4.13. The UV-visible absorbance profiles for the SRNOM and Fractions 1-7 as determined at pH 6.8 (solid black line) and pH 9.3 (thin gray line). The working solution of each sample was prepared at 15 mgC L⁻¹ with 0.1 ionic strength.

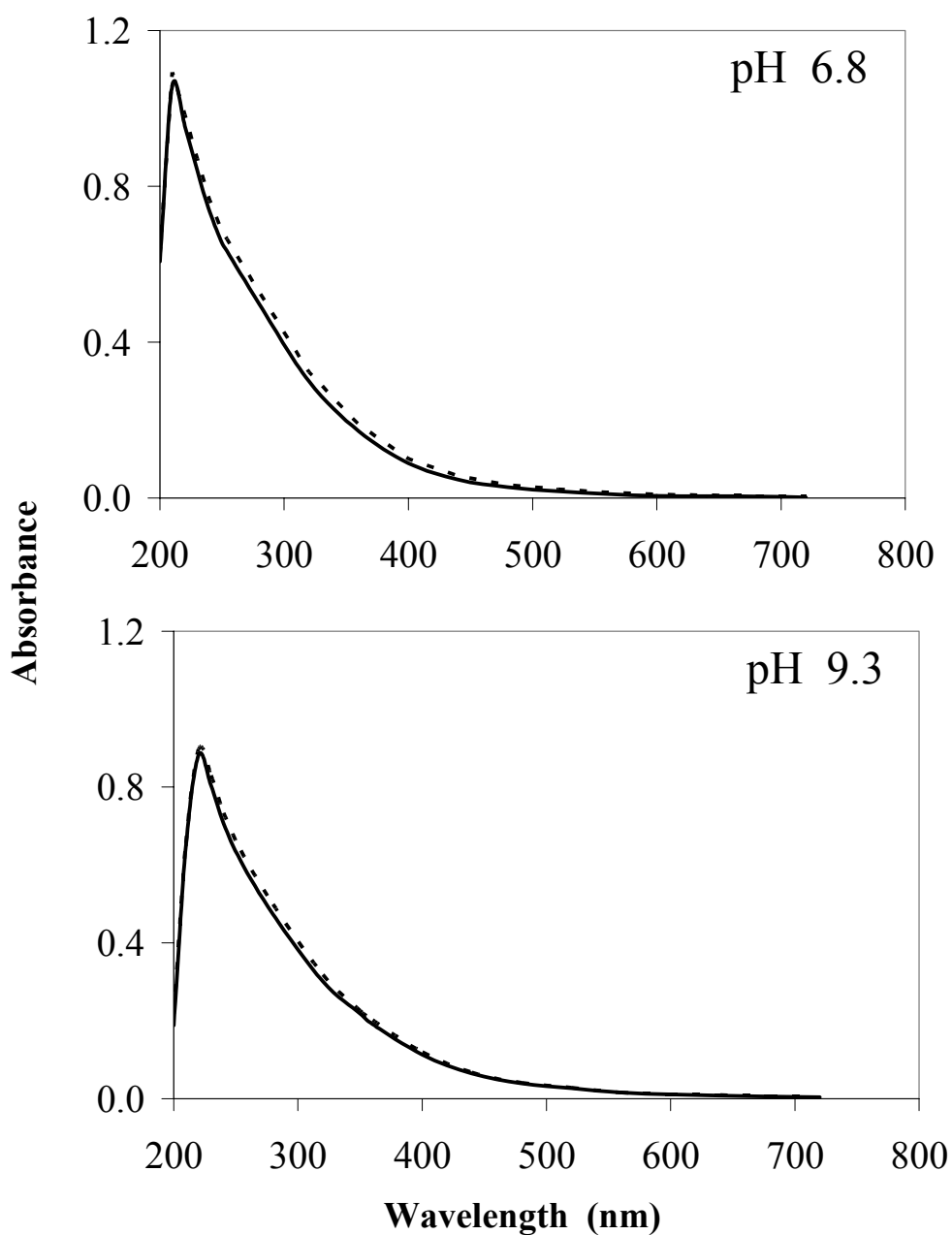


Figure 4.14. The UV-visible absorbance profiles for the SRNOM sample (solid lines) at pH 6.8 and 9.3 compared to the reconstructed absorbance profile (dashed lines) that were created from the weighted sums of absorbance profiles for Fractions 1-7.

Fraction 5, but greater than those for Fraction 6. The SRNOM sample has absorbance values between absorbance values for Fractions 4 and 5.

4.4.2 Reconstructing the UV-visible spectrum of the SRNOM.

The second opportunity to validate the effectiveness and integrity of the preparative SEC fractionation is to reconstruct the UV-visible absorbance profile for the SRNOM from the weighted sums of the UV-visible absorbance profiles for Fractions 1-7. First, the absorbances at each wavelength (200-700 nm) for Fractions 1-7 were weighted according to their % areas of absorbance (Table 4.2), then added together to form the reconstructed absorbance profiles. The reconstructed profiles at pH 6.8 and 9.3 were compared to their respective UV-visible profiles for the SRNOM (Figure 4.14).

The reconstructed absorbance values between 230 and 560 nm at both pHs are just slightly greater than those of the SRNOM. However, the agreements between the absorbance spectrum for the SRNOM and the reconstructed UV-visible absorbance spectrum for Fractions 1-7 are excellent, meaning that the chromophoric compounds in Fractions 1-7 were conserved during the preparative SEC fractionation and the subsequent processing of the fractions.

4.4.3 Specific UV absorptivity (SUVA) and E_4/E_6 values.

The SUVA (254 nm) and E_4/E_6 values for the SRNOM and Fractions 1-7 at pH 6.8 and 9.3 are shown in Table 4.11. Fraction 2 has the greatest SUVA values at pH 6.8 and 9.3. SUVAs decrease from Fraction 2 to Fraction 6 at pH 6.8, and decrease from Fraction 2 to Fraction 7 at pH 9.3. The SUVA value for Fraction 7 at pH 6.8 was larger

Table 4.11. The specific UV absorptivity (SUVA) at 254 nm ($\text{L gC}^{-1} \text{ cm}^{-1}$) and the E_4/E_6 values for the SRNOM and Fractions 1-7 at pH 6.8 and pH 9.3.

	pH 6.8		pH 9.3	
	SUVA	E_4/E_6	SUVA	E_4/E_6
SRNOM	42.28 ± 0.06	9.9 ± 0.9	40.70 ± 0.06	8.2 ± 0.5
Fraction 1	50.23 ± 0.09	6.2 ± 0.4	48.68 ± 0.07	6.7 ± 0.2
Fraction 2	55.25 ± 0.08	9.9 ± 0.3	54.06 ± 0.08	7.7 ± 0.4
Fraction 3	54.05 ± 0.04	10.9 ± 0.3	53.67 ± 0.04	8.5 ± 0.4
Fraction 4	45.15 ± 0.05	12.0 ± 1.0	44.43 ± 0.03	8.6 ± 0.2
Fraction 5	36.12 ± 0.02	10.6 ± 1.2	36.84 ± 0.02	7.1 ± 0.6
Fraction 6	28.90 ± 0.06	7.7 ± 1.3	28.07 ± 0.02	6.3 ± 0.5
Fraction 7	37.03 ± 0.14	3.8 ± 0.2	26.21 ± 0.14	6.2 ± 0.2

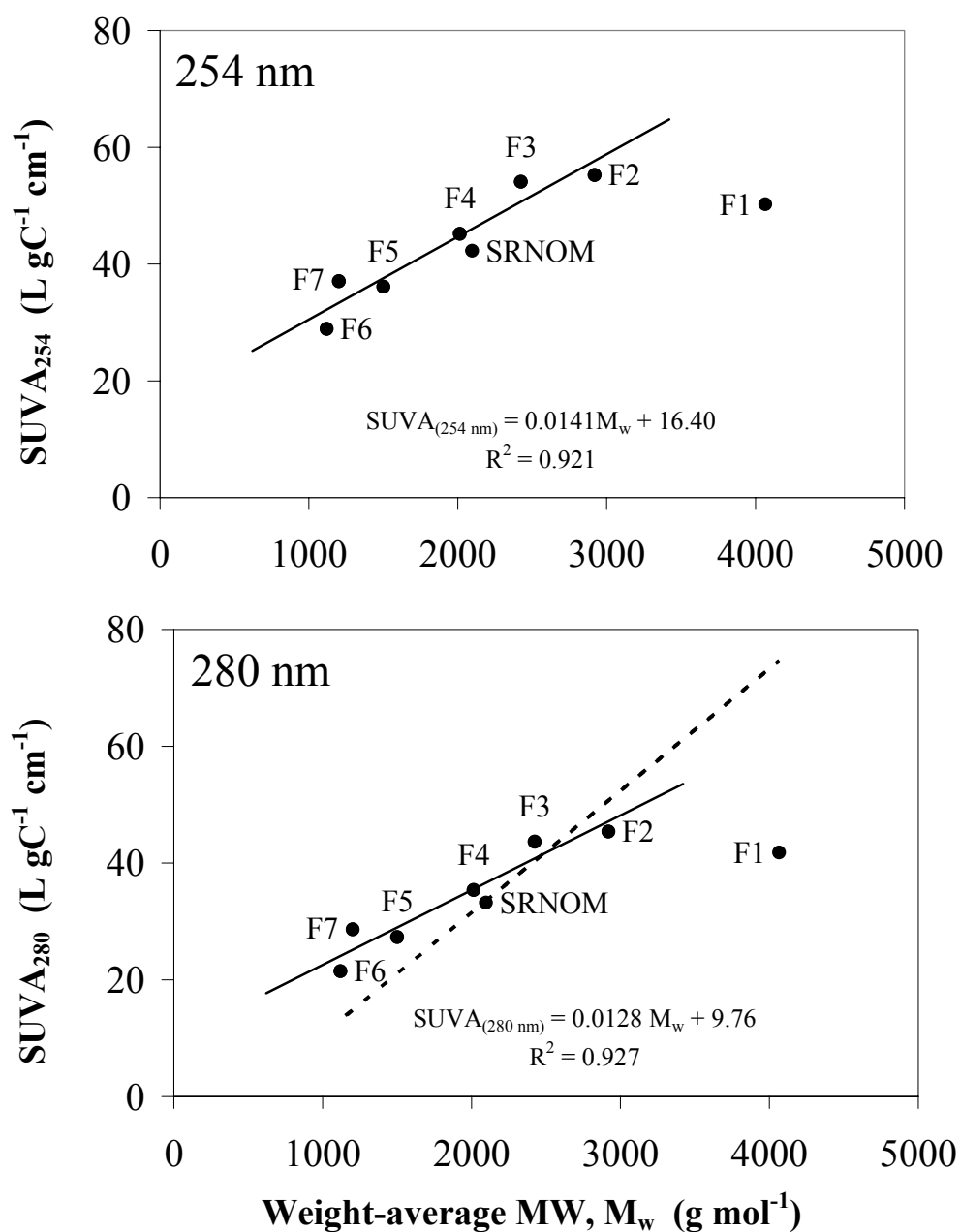


Figure 4.15. The specific UV absorptivity (SUVA) at 254 nm and 280 nm for the SRNOM and Fractions 1-7 as a function of weight-average (M_w) MWs. The linear trend lines were fit through data for Fractions 2-7. The dashed line is the empirical relationship between SUVA at 280 nm and M_w as observed by Chin *et al.* (1994).

than that of Fraction 6, but comparable to that of Fraction 5. Generally, SUVA values at pH 9.3 are almost equal to SUVA values at pH 6.8, except for Fraction 7 because that fraction absorbs less UV light at the higher pH. The SUVA values for the SRNOM are comparable to those of Fraction 4.

Stevenson (1994) stated that the absorbance of UV light tends to be directly proportional to the MW of NOM. The correlation between the average MWs and the SUVA values for the samples at pH 6.8 for 254 nm (the standard wavelength) and 280 nm (Chin *et al.*, 1994) are shown in Figure 4.15. SUVA values at both 254 and 280 nm are equally well-correlated to the M_w values for Fractions 2-7. Fraction 1 is considered an outlier and is not included in the trend. The empirical relationship between SUVA at 280 and M_w from Chin *et al.* (1994) does not hold true for Fractions 1-7, but Chin *et al.*'s (1994) equation (equation 3.10) does plot through the SUVA value for the SRNOM. Chin *et al.* (1994) analyzed whole, unfractionated fulvic acids and aquatic NOM samples. It may be the case that their relationship does not apply to samples that are fractioned by MW.

Fraction 4 had the largest E_4/E_6 values at pH 6.8 and 9.3, with E_4/E_6 values decreasing from Fraction 3 to 1 and from Fraction 5 to 7. According to the references in section 3.5.3, E_4/E_6 is inversely proportional to the quantity of aromatic and pi-bonded structures in NOM. This would indicate, at least as a qualitative observation, that aromatic and pi-bond functionalities for the SRNOM were enriched in solutes having the highest and lowest MWs (Fractions 1 and 7) and are relatively depleted in the medium MWs (Fractions 3-5). There is no correlation between E_4/E_6 and M_w . However, values of E_4/E_6 have linear inverse-correlations to the N/C and H/C ratios of Fractions 1-7

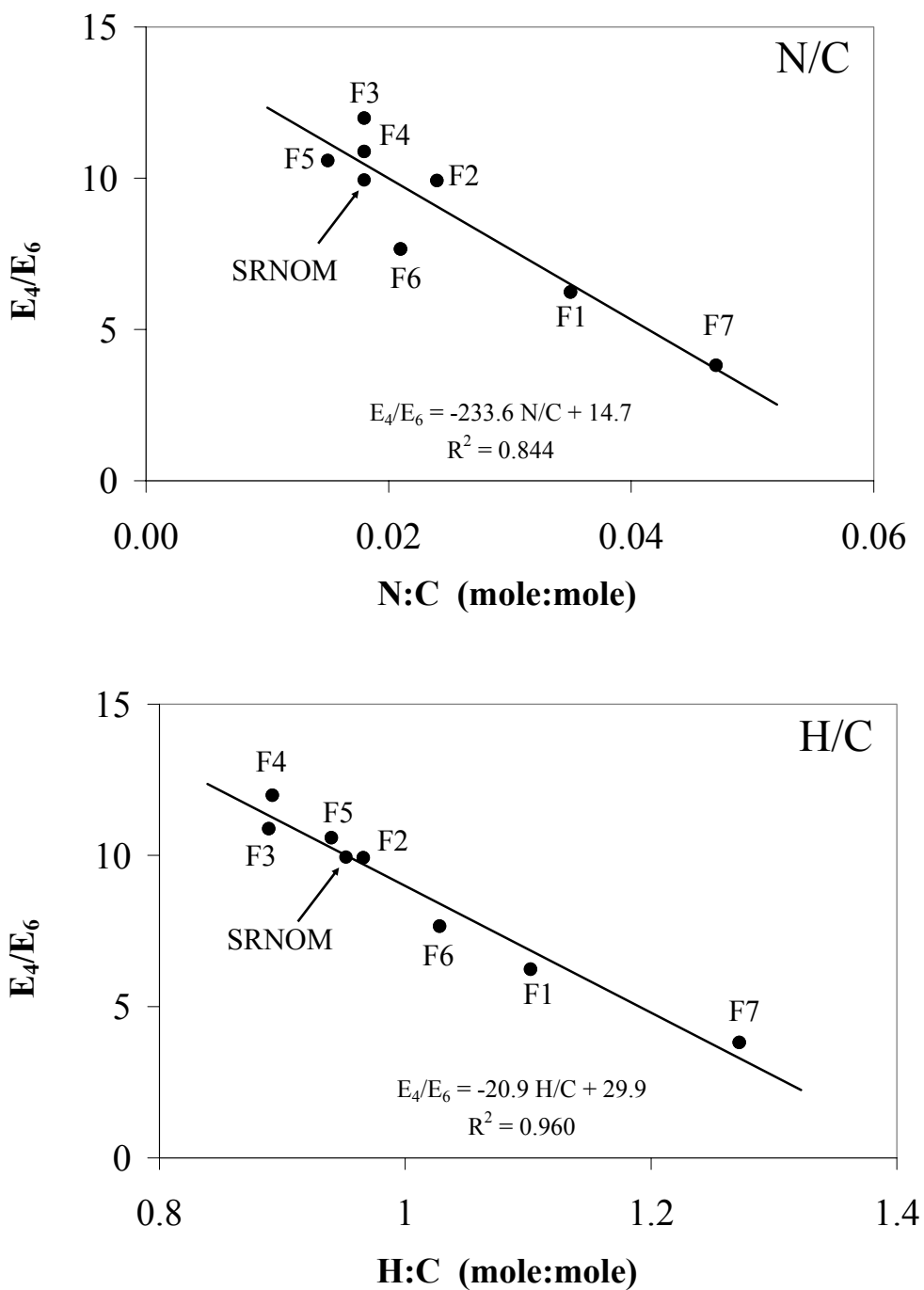


Figure 4.16. The E_4/E_6 values for the SRNOM and Fractions 1-7 as a function of their N/C and H/C ratios (mol/mol). The linear trend lines were fit through data for Fractions 1-7.

Table 4.12. The specific UV absorptivity (SUVA) at 254 nm ($\text{L gC}^{-1} \text{ cm}^{-1}$) and the E_4/E_6 values for the IHSS standard collection and other soil FAs and HAs as reported in the literature.

	SUVA	E_4/E_6		SUVA	E_4/E_6
IHSS std. SRFA ^a	38.1	23.5	IHSS std. Soil FA ^a	48.8	14.0
IHSS ref. SRFA ^a	41.8	21.8	IHSS std. Soil FA ^c	47	-
IHSS std. SRFA ^b	31.1	-	IHSS std. Soil HA ^a	58.8	5.7
IHSS std. SRFA ^c	35	-	IHSS std. Soil HA ^c	73	-
IHSS ref. SRFA ^c	40	-	IHSS std. Peat FA ^a	64.7	18.2
IHSS std. SRHA ^a	65.1	10.8	IHSS std. Peat FA ^c	57	-
IHSS ref. SRHA ^a	68.7	11.7	IHSS std. Peat HA ^a	81.0	5.4
IHSS std. SRHA ^b	35.6	-	IHSS std. Peat HA ^c	70	-
IHSS std. SRHA ^c	59	-	IHSS std. Leonardite HA ^a	91.4	4.9
IHSS ref. SRNOM ^c	36	-	IHSS std. Leonardite HA ^c	70	-
IHSS ref. Nordic FA ^a	46.7	18.8	IHSS ref. SH Soil HA ^c	44	-
IHSS ref. Nordic FA ^b	38.8	-			
IHSS ref. Nordic FA ^c	45	-	Soil FAs ^d	-	17.3
IHSS ref. Nordic HA ^a	43.8	12.8	Soil FAs ^e	-	8.7
IHSS ref. Nordic HA ^b	34.1	-	Soil HAs ^e	-	5.6
IHSS ref. Nordic HA ^c	53	-	Soil HAs ^f	-	3.1
	SUVA	E_4/E_6			
Mean SRFA	37.2 ± 4.2	22.7 ± 1.2			
Mean SRHAs	57.2 ± 14.9	11.3 ± 0.6			
Mean SRNOM	36	-			
Mean Nordic FA	43.5 ± 4.2	18.8			
Mean Nordic HA	43.6 ± 9.5	12.8			
Terrestrial FAs	54.4 ± 8.1	15.5 ± 3.7			
Terrestrial HAs	69.7 ± 15.2	3.4 ± 1.0			

References: ^aSenesi *et al.* (1989); ^bPeuravuori and Pihlaja (1997); ^cAlberts and Tokacs (2004); ^dBaes and Bloom (1990) (3 FAs); ^eChen *et al.* (1977) (1 FA and 1 HA--average of 4 measurements); ^fOrlov (1966) (17 HAs). Terrestrial samples included the IHSS soil, peat, leonardite, and Summit Hill (SH) soil and the other soil samples.

(Figure 4.16).

4.4.4 Literature values of SUVA and E_4/E_6 .

A small dataset of SUVA and E_4/E_6 values reported in the literature (Table 4.12) were compared to SUVA and E_4/E_6 values at pH 6.8 for Fractions 1-7. It was necessary to include SUVA and E_4/E_6 values for terrestrial FAs and HAs and other aquatic samples because literature reports for the Suwannee River samples are very limited. The SUVA values for Fractions 1-3 are most comparable to those for SRHA and terrestrial FAs. SUVA values for Fractions 4, 5, and 7 are comparable to those for the SRFA and Nordic FA and HA. Fraction 7's E_4/E_6 value is the same as the average of terrestrial HAs (from soil, peat, and ligneous coal). Based on average MWs and spectroscopic analyses, Fractions 1-3 are probably enriched in chromophoric solutes common to aquatic humic acids, Fractions 4 and 5 are enriched in chromophoric solutes common to aquatic fulvic acids, and Fraction 7 is spectroscopically similar to terrestrial humic acids.

4.5 Acid-base Chemistry by Direct Titrations.

4.5.1 Comparison of forward and reverse titration curves.

The sequential forward-reverse-forward-reverse-forward titration curves for the mixture of seven simple organic acids (SOA), when titrated under the same experimental conditions as Fractions 1-7 and the SRNOM, show no evidence of hysteresis (Figure 4.17). All five titration curves, plotted as the standard titration curves (Q_{pH} vs. pH) overlap. There was neither an observed drift in pH above pH 10.5 nor any generation of

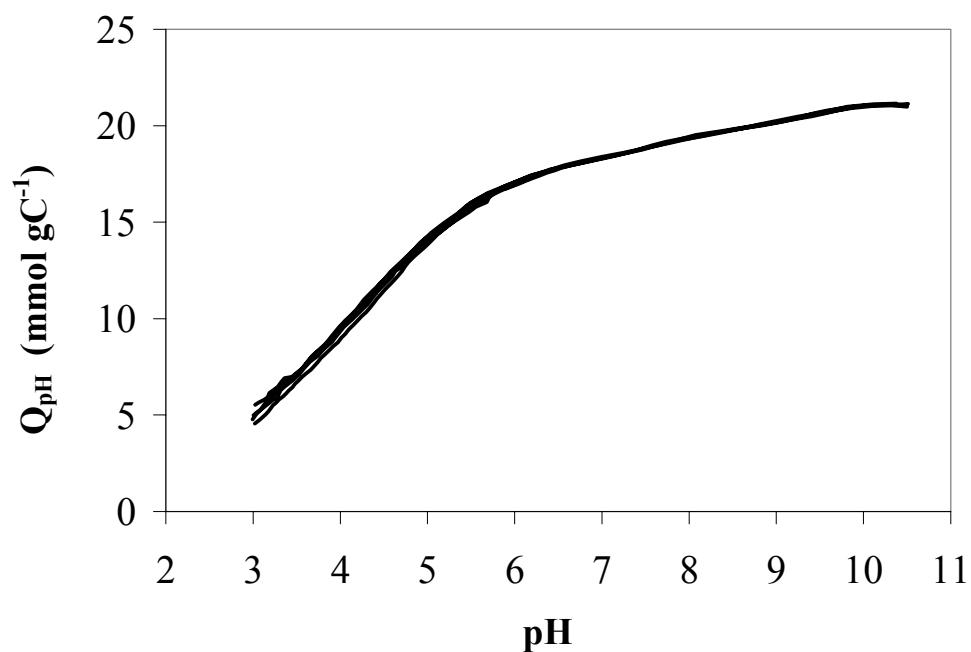


Figure 4.17. The standard forward and reverse titration curves for a mixture of seven simple organic acids (SOA). One 10-ml aliquot of SOAs was sequentially titrated forward (3 times) with NaOH and backward (2 times) with HCl, with 30-minute intervals between each titration.

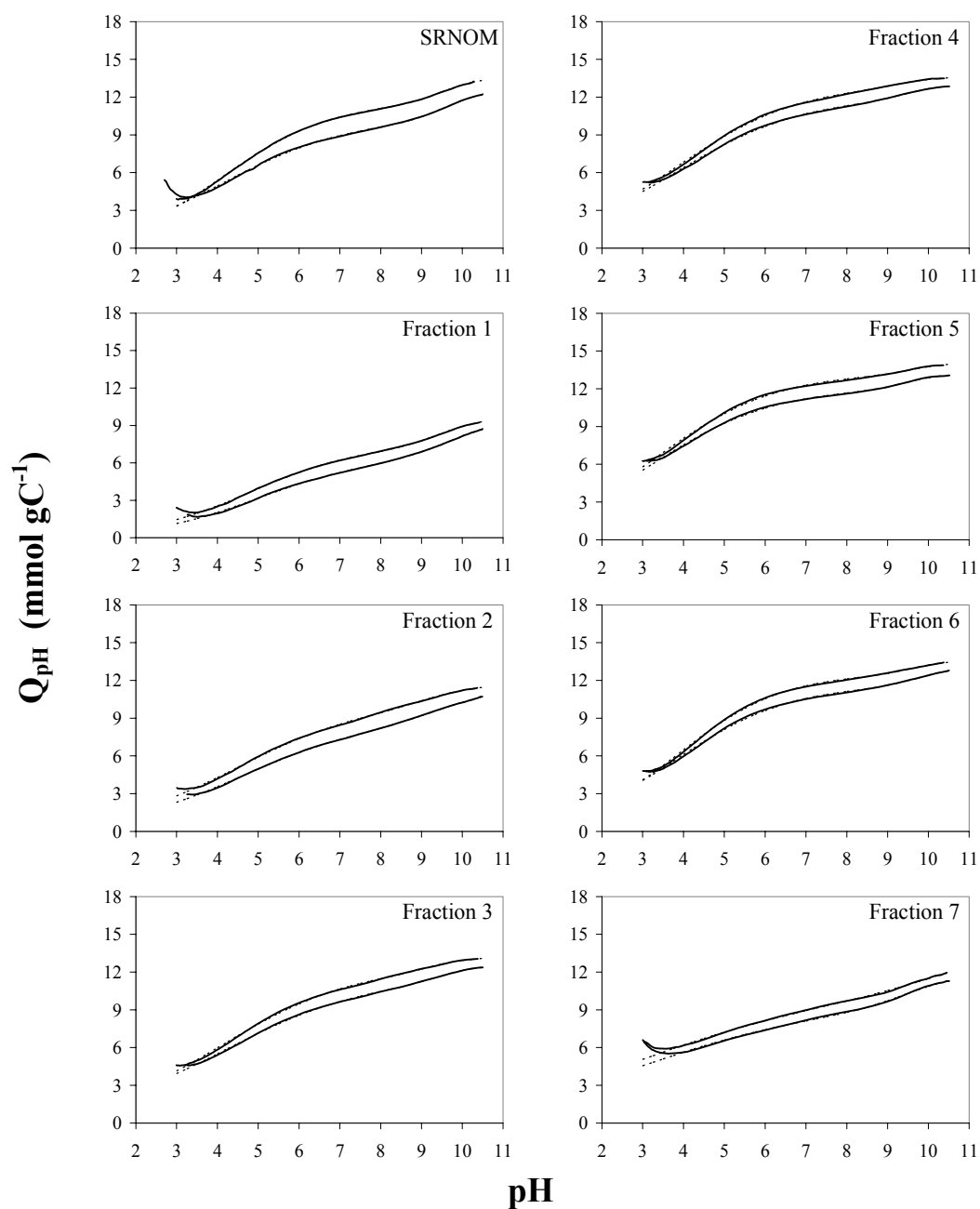


Figure 4.18. The forward (lower) and reverse (upper) titration curves for the SRNOM and Fractions 1-7. The modified Henderson-Hasselbalch (H-H) models for the forward and reverse titrations (dashed lines) are superimposed over the titration curves (solid black lines).

additional acidity (increase in Q_{pH}) during the 30-minute interval after the completion of each forward titration. The contribution of each acid in the SOA cannot be distinguished or identified from the titration curves. The overlap of all ionizing acid groups causes the titration curves to lack inflection points or distinct topographic signatures of the individual acids.

The forward and reverse standard titration curves for the SRNOM and Fractions 1-7 are shown in Figure 4.18. All of the titration curves are relatively featureless and lacked distinct inflection points. The charge density, Q_{pH} (mmol gC^{-1}), for the forward and reverse titration curves increases with increasing pH, indicating that more acidic functional groups become ionized with increasing pH. Most of the titration curves have slight “curling” phenomenon at pHs < 3.2 , an unexplainable artifact inherent to most direct titrations of natural organic substances (Sposito *et al.*, 1977; Marshall *et al.*, 1995; Robertson and Leckie, 1999; Ritchie and Perdue, 2003). Hysteresis is observed for all samples, with the reverse titration curves always having a greater Q_{pH} at all pHs than the forward titration curves.

The forward titration curves have a large increase in Q_{pH} between pH ~ 3.2 and pH ~ 6.0 , a relatively gradual increasing in Q_{pH} between pH ~ 6.0 and ~ 9.0 , and a slight upturn in Q_{pH} between pH ~ 9.5 and 10.5. Reverse titration curves are steeper than the forward titration curves below pH 6.0—indicating that more acid groups with apparent pK_{a} values less than 6.0 (e.g. carboxyl groups) were reprotonated in the reverse titration than were initially ionized during the forward titration (Davis and Mott, 1981; Paxeus and Wedborg, 1985; Marshall *et al.* 1995). Forward and reverse titration curves for the same sample tend to be nearly parallel, but vertically offset, at pHs > 6.0 —suggesting that

there was little change in Q_{pH} in the pH range where phenolic acids would ionize. Additionally, the reverse titration curves approached convergence with the forward titration curves near pH ~3.0. This author supports the hypothesis of base-catalyzed ester hydrolysis as the source of the apparent new acidity in reverse titration curves (Bowles *et al.* 1989; Antweiler, 1991). Because titration curves for the SRNOM and Fractions 1-7 are affected by hysteresis, it is evident that each fraction contains some portion of the SRNOM's ester content. Therefore, esters are distributed over the entire range of MWs.

4.5.2 Reconstructing the titration curves of the SRNOM.

The third opportunity to validate the effectiveness and integrity of the preparative SEC fractionation is to reconstruct the forward and reverse titration curves for the SRNOM from the titration curves of Fractions 1-7 (Figure 4.19). The value of Q_{pH} for Fractions 1-7 at each pH was weighted according to the respective % carbon recoveries during the preparative SEC (Table 4.2), and then summed to form the reconstructed titration curve. The reconstructed titration curves closely matched the titration curves for the SRNOM (Figure 4.19). The reconstructed titration curve predicts slightly greater Q_{pH} values than the SRNOM titration curve below pH 9 for the forward titrations and below pH 5 for the reverse titrations. The fact that the reconstructed titration curves of Fractions 1-7 are very close to the titration curves of the SRNOM indicates that the concentrations of all inorganic ions in the ash are accounted for correctly, and that the acidic functional groups in Fractions 1-7 were conserved during the preparative SEC fractionation and subsequent processing.

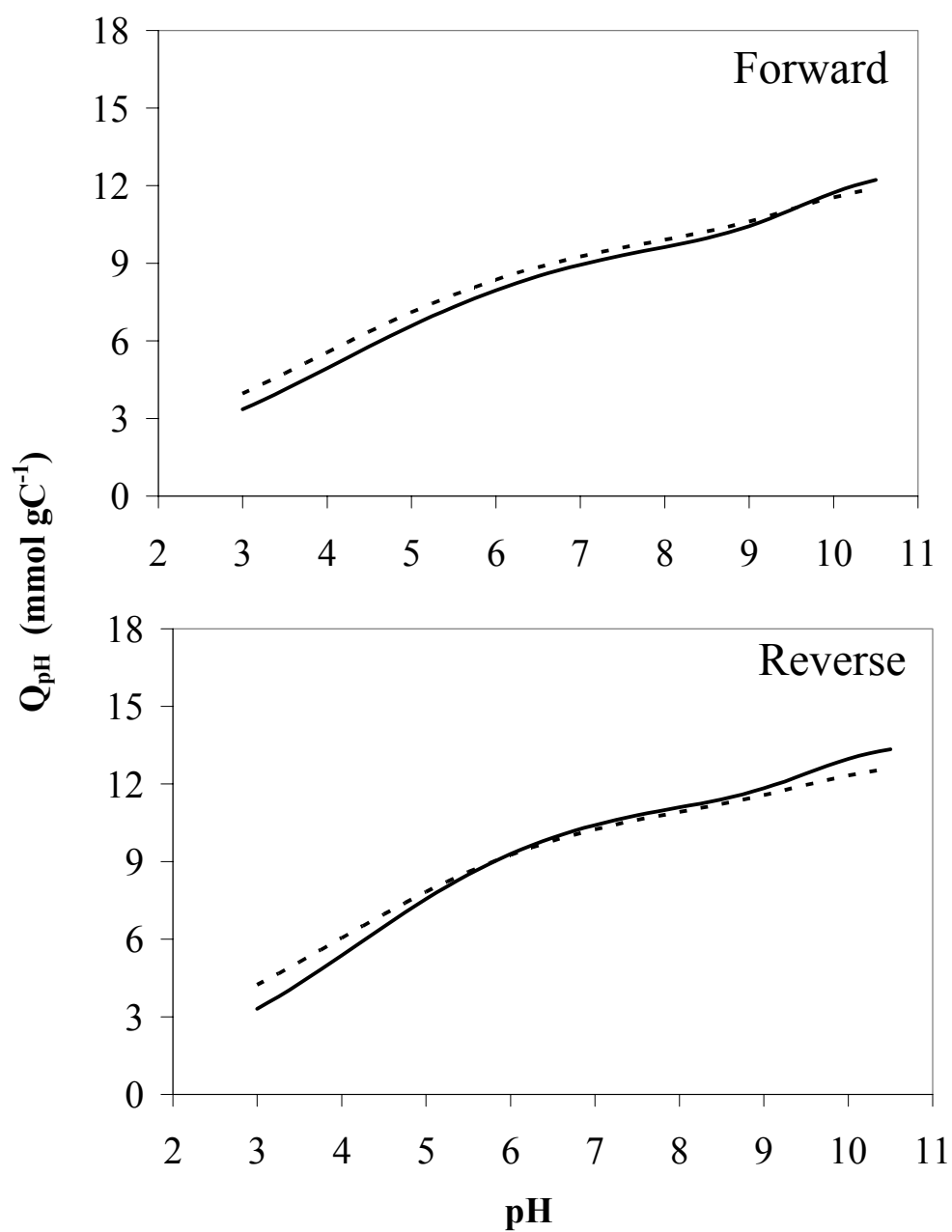


Figure 4.19. The forward and reverse titration curves for the SRNOM sample (solid line) compared to the reconstructed titration curves (dashed lines) that were created from the weighted sums of forward and reverse titration curves for Fractions 1-7.

4.5.3 The modified Henderson-Hasselbalch (H-H) model parameters.

The modified Henderson-Hasselbalch (H-H) model was fitted to the forward and reverse titration curves for the SRNOM, Fractions 1-7, and the SOA sample. The “best-fit” estimates of carboxyl and phenolic contents (Q_1 and Q_2), mean proton-binding constants ($\log K_1$ and $\log K_2$), and width parameters for proton-binding (n_1 and n_2) are reported in Table 4.13. The values of Q_1 and Q_2 for the samples, estimated using the pH method, are also shown in Table 4.13.

Because no hysteresis is observed for the SOA sample, all of the H-H model parameters are nearly identical for the sequential forward and reverse titrations. For the SRNOM and Fractions 1-6, values of Q_1 for reverse titrations are larger than values of Q_1 for forward titrations, indicating a net increase of carboxyl groups during the 30-minute interval between forward and reverse titrations. Conversely, values of Q_2 for reverse titrations are smaller than values of Q_2 for forward titrations, indicating a net decrease in phenolic content during the 30-minute interval. Values of Q_1 for forward and reverse titrations increase in order from Fraction 1 to Fraction 5, with Fraction 6 being comparable to Fraction 3. Values of Q_2 for forward and reverse titrations decrease in order from Fraction 1 to Fraction 4, with Fractions 5 and 6 having values of Q_2 comparable to Fraction 3. This indicates that the concentrations of carboxyl and phenolic group are influenced by the MWs of the samples.

For the SRNOM and Fractions 1-6, the mean $\log K_1$ and mean $\log K_2$ values for the forward titrations are slightly greater, by approximately 0.1 to 0.2 log units, than for the reverse titrations. This indicates that, overall, both carboxyl and phenolic acid groups in the SRNOM and Fractions 1-6 “appear” to be more acidic in the reverse titrations—or

Table 4.13. The estimates of acid functional groups by pH-cutoff method and the Henderson-Hasselbalch (H-H) model parameters for the SRNOM, Fractions 1-7, and the mixture of seven simple organic acids (SOA).

	pH Estimates			Modified Henderson-Hasselbalch Model					
	Q ₁ ^a	Q ₂ ^b	Q ₁ /Q ₂	Q ₁ ^c	Log K ₁ ^d	n ₁ ^e	Q ₂ ^c	Log K ₂ ^d	n ₂ ^e
Forward Titrations									
SRNOM	9.63	4.20	2.29	10.31	4.02	3.54	2.46	9.53	1.17
Fraction 1	5.97	4.32	1.38	6.24	4.86	3.02	3.52	9.66	1.71
Fraction 2	8.21	4.12	1.99	8.70	4.47	3.56	2.78	9.39	1.82
Fraction 3	10.46	3.34	3.13	11.60	4.07	4.05	1.19	9.31	1.02
Fraction 4	11.31	2.70	4.19	12.03	3.70	3.58	1.08	9.33	1.00
Fraction 5	11.66	2.43	4.80	12.09	3.15	3.40	1.17	9.34	1.00
Fraction 6	11.12	2.61	4.26	11.64	3.76	3.16	1.44	9.63	1.04
Fraction 7	8.79	4.14	2.12	9.35	3.00	5.00	2.88	9.42	1.72
Reverse Titrations									
SRNOM	11.10	3.74	2.97	11.61	4.09	2.99	2.08	9.44	1.11
Fraction 1	6.93	3.96	1.75	7.33	4.70	2.99	2.48	9.41	1.38
Fraction 2	9.44	3.50	2.70	10.08	4.36	3.56	1.81	9.04	1.64
Fraction 3	11.47	2.92	3.93	12.47	4.03	3.74	0.90	9.06	1.00
Fraction 4	12.30	2.21	5.57	13.05	3.76	3.45	0.69	9.19	1.00
Fraction 5	12.78	1.95	6.55	13.29	3.27	3.33	0.85	9.49	1.00
Fraction 6	12.12	2.22	5.46	12.57	3.82	2.91	1.06	9.51	1.00
Fraction 7	9.71	3.54	2.74	9.50	2.69	5.00	10.00	12.31	4.63
Simple Organic Acids (SOA)									
Forward 1	19.32	3.22	6.00	19.14	4.00	2.18	2.19	8.76	1.62
Reverse 1	19.29	3.32	5.81	19.21	3.94	2.24	2.05	8.74	1.40
Forward 2	19.29	3.35	5.76	19.32	3.92	2.29	1.90	8.78	1.25
Reverse 2	19.28	3.44	5.60	19.36	3.90	2.28	1.86	8.79	1.13
Forward 3	19.27	3.49	5.52	19.04	3.87	2.17	2.44	8.83	1.58
Average	19.29	3.36	5.74	19.21	3.93	2.23	2.09	8.78	1.40
S.D.	0.02	0.11	0.19	0.13	0.05	0.06	0.23	0.03	0.21

^aCarboxyl contents estimated as the total charge at pH 8.0 (mmol gC⁻¹).

^bPhenolic contents estimated as the two times the difference in charge between pH 8.0 and pH 10.0 (mmol gC⁻¹).

^cBest fit concentrations of carboxyl and phenolic groups (mmol gC⁻¹).

^dThe mean log K values for proton binding of carboxyl and phenolic groups.

^eWidth parameter to describe the distribution of mean log K values.

will ionize at a lower pH—than the assemblage of carboxyl groups and phenolic groups present in the forward titrations.

The values of mean $\log K_1$ and mean $\log K_2$ values for the SRNOM and Fractions 1-7 are within ranges of reported pK_{as} for carboxyl and phenolic for the suite of IHSS standard and reference fulvic and humic acids (Ritchie and Perdue, 2003). Fractions 1-3 have values of mean $\log K_1$ that are comparable to the IHSS aquatic and terrestrial humic acids. Fractions 4 and 6 have values of mean $\log K_1$ that are comparable to IHSS aquatic and terrestrial fulvic acids. Mean $\log K_1$ values for Fraction 5 are lower than those for the fulvic acids. The values of mean $\log K_2$ for Fractions 1-6 tend to be comparable to the reported mean $\log K_2$ values for the IHSS samples, but no clear comparison between the IHSS fulvic and humic acids and the samples in this study.

The n_1 values (width parameter for mean $\log K_1$) are large, between 3.0 and 4.9, compared to n_2 values (width parameter for mean $\log K_2$), which are smaller and range from 1.0 and 1.8. Larger values of n indicate a greater distribution of non-identical acid functional groups that will ionize over a very wide range of pH centered at mean $\log K$. The larger n_1 values in the SRNOM and Fractions 1-7 indicate that there is a large distribution of carboxyl groups on a large diversity of solutes. The smaller values of n_2 mean that there is little diversity between phenolic groups, and that the phenols will ionize in a more narrow range of pH. If n_2 equals 1.00—as did for Fractions 3-6, samples with relatively large carboxyl concentrations and smaller phenolic concentrations—then all phenolic groups in those samples are considered to be on identical solutes.

The assignment of a 1.00 value for n_2 may be an artifact to the model. Direct titrations were performed to the maximum pH of 10.5. Phenolic groups readily ionize

between pH ~7-8 and ~12. It may be the case that a significant portion of the total phenolic concentration (aside from the additional carboxyl groups formed from ester hydrolysis in the alkaline pH range) is not titrated. The H-H model can only replicate and interpret the available data, thus the H-H model may incorrectly represent the phenolic concentrations, values of mean log K_2 , and n_2 . This is the nature of modeling.

The “best-fit” H-H parameters for the phenolic content for Fraction 7’s reverse titration are unusual, even though the carboxyl parameters appear to be reasonable when compared to those of Fractions 1-6. The reverse titration curve for Fraction 7 is very similar to that of Fraction 2 above pH 7, and in theory, the phenolic parameters (Q_2 , mean log K_2 , and n_2) should be similar to those for Fraction 2. The Solver tool freely fit the H-H model to the titration data and generated the most optimal parameters to replicate the titration curve. If any one of the parameters in the H-H model for Fraction 7 were fixed to a “reasonable” value—for example, fixing $Q_2 = 2.00 \text{ mmol gC}^{-1}$ or mean log $K_2 = 9.40$ —the H-H model most likely would generate values for the parameters that are comparable to the other Fractions, but at the integrity of the five other parameters.

4.5.4 pH method for Q_1 and Q_2 .

Values of Q_1 and Q_2 that were estimated by the pH method are reported in Table 4.13. Because no hysteresis was observed for the SOA mixture, the values of Q_1 and Q_2 are nearly identical for the forward and reverse titrations. The Q_1 values for the forward and reverse titrations increase in order from Fraction 1 to Fraction 5. The Q_2 values for the forward and reverse titrations decrease from Fraction 1 to Fraction 5. Fraction 6 has Q_1 and Q_2 values similar to those for Fraction 4. Q_1 and Q_2 values for Fraction 7 tend to

be similar to those for Fraction 2.

The values of Q_1 and Q_2 , estimated by the pH method, for the forward and reverse titrations were plotted against their respective values of M_w (Figures 4.20 and 4.21). Q_1 values are inversely correlated and Q_2 values are directly correlated to M_w for Fractions 1-6 for both the forward and reverse titrations. Fraction 7 is an outlier in both instances. Ritchie and Perdue (2003) reported the concentrations of the acidic functional groups for the suite of IHSS standard and reference fulvic and humic acids. Dycus *et al.* (1995) analyzed the same suite of IHSS samples for their average MWs by flow field-flow fractionation. The concentrations of carboxyl groups in those samples were larger for fulvic acids which had the smallest average MWs. The terrestrial IHSS humic acids, the samples with the largest average MWs, had the smallest carboxyl concentrations. Fraction 1, the fraction with the largest MWs, has the largest phenolic concentration. Fraction 6, has the lowest values of Q_2 . This indicates that abundances of aromatic structures decrease as the MWs of organic solutes in NOM decreases, supporting the generalities made by Stevenson (1994).

If the values of Q_1 and Q_2 for the pH method are compared with values of Q_1 and Q_2 estimated by the H-H model, the pH method predicts Q_1 to be approximately 6% lower and Q_2 to be approximately 1.2 to 2 times greater than those for the H-H model. This discrepancy between the pH method and the H-H method was observed by Ritchie and Perdue (2003) for the 14 IHSS standard and reference FAs, HAs, and NOM. The H-H model, like any model, can only interpret and model titration data up to pH ~10.5, the upper limit of the forward titration. The pH method may give better estimates of phenolic group concentrations than the H-H model because the pH method assumes that 50% of

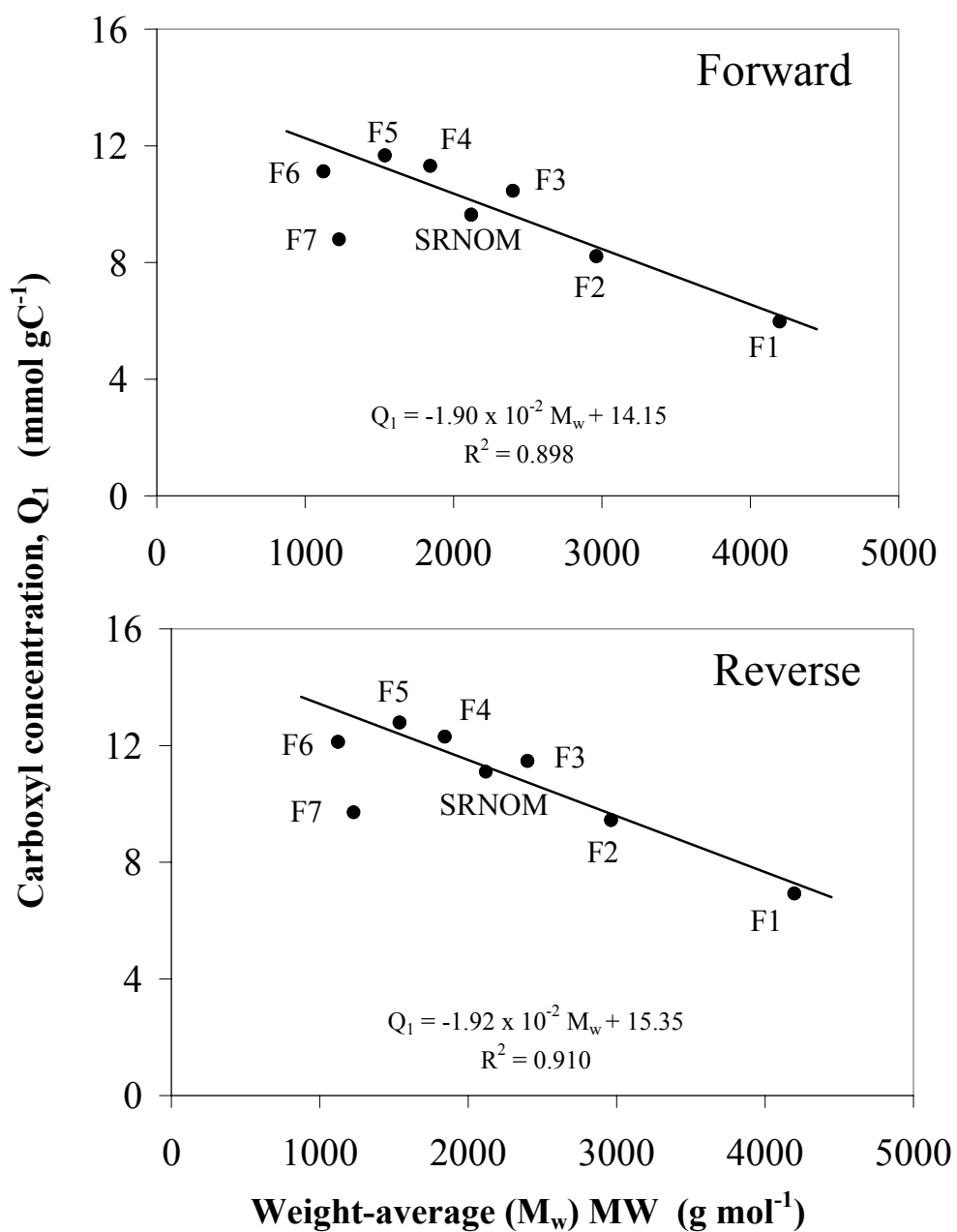


Figure 4.20. The carboxyl concentrations (pH method) for forward and reverse titrations for the SRNOM and Fractions 1-7 with respect to their weight-average MWs (M_w). The linear trend lines for all graphs are for Fractions 1-6.

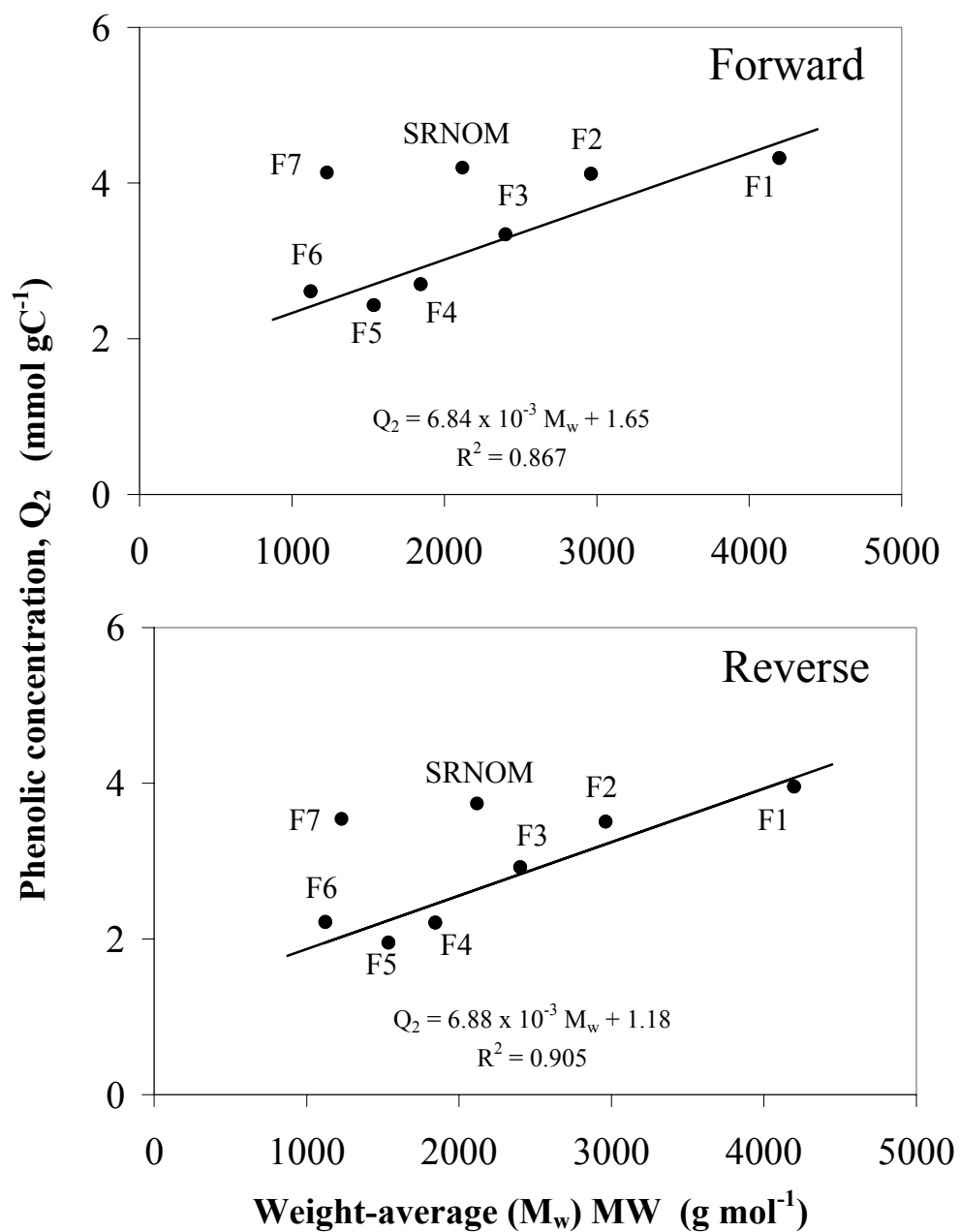


Figure 4.21. The phenolic concentrations (pH method) for forward and reverse titrations for the SRNOM and Fractions 1-7 with respect to their weight-average MWs (M_w). The linear trend lines for all graphs are for Fractions 1-6.

the total phenolic groups will ionize between pH 10 and 12.

Carboxyl groups dominate the overall acid-base chemistry of the samples for both forward and reverse titrations of the SRNOM and Fractions 1-7, with Q_1 always being larger than Q_2 . Q_1/Q_2 ranges from 1.4 to 4.8 for the forward titrations and 1.8 to 6.6 for the reverse titrations (Table 4.13). Q_1/Q_2 is always greater for the reverse titrations than for the forward titrations because reverse titrations have greater Q_1 and smaller Q_2 than the forward titrations. Q_1/Q_2 for the forward and reverse titrations increase in order from Fraction 1 to Fraction 5. Q_1/Q_2 values for Fraction 6 are very similar to that of Fraction 4, and Q_1/Q_2 values for Fraction 7 are most similar to the SRNOM.

Ritchie and Perdue (2003) criticized the the 2:1 carboxyl-to-phenolic ratio in Models V and VI (Tipping and Hurley, 1992; Tipping, 1998), stating that the vast majority of reported carboxyl and phenolic concentrations—as determined by direct titrations—for aquatic fulvic acids, terrestrial fulvic acids, and aquatic humic acids have Q_1/Q_2 values > 2 . With the exception of Fraction 2, the MW fractions in this work do not conform to the 2:1 ratio. Therefore, the concentrations of acidic functional groups in the majority of unfractionated natural organic samples (Ritchie and Perdue, 2003) and six of the seven MW fractions of the SRNOM cannot be accurately described by Models V and VI.

4.5.5 The consequences of hysteresis.

The downward drift in pH was not monitored during the 30-minute interval between the completion of the forward titration and the beginning of the reverse titrations of the SRNOM and Fractions 1-7. According to Table 4.14, the net change in pH during

Table 4.14. The downward drift in pH and differences in acidic functional group concentrations for the SRNOM and Fractions 1-7 caused by hysteresis.

	Maximum pH ^a			Acidic functional groups ^b		
	Forward	Reverse	ΔpH	ΔQ_1	ΔQ_2	ΔQ_{TOT}
SRNOM	10.500	10.281	- 0.219	+ 1.47	- 0.46	+ 1.01
Fraction 1	10.496	10.416	- 0.080	+ 0.96	- 0.36	+ 0.60
Fraction 2	10.492	10.366	- 0.126	+ 1.23	- 0.62	+ 0.61
Fraction 3	10.506	10.377	- 0.129	+ 1.01	- 0.42	+ 0.59
Fraction 4	10.514	10.385	- 0.129	+ 0.99	- 0.49	+ 0.50
Fraction 5	10.519	10.367	- 0.152	+ 1.12	- 0.48	+ 0.64
Fraction 6	10.507	10.374	- 0.133	+ 1.00	- 0.39	+ 0.61
Fraction 7	10.511	10.439	- 0.072	+ 0.92	- 0.60	+ 0.32

^aSamples were titrated with base (forward titration) to maximum pH 10.5. Maximum pH for reverse titration was recorded 30 minutes after completion of forward titration.

^bCarboxyl (Q_1) and phenolic (Q_2) concentrations are based on pH method. Q_{TOT} is total acidity = $Q_1 + Q_2$. (mmol gC⁻¹).

the 30-minute interval was from pH 10.5 to pH 10.28-10.44. Antweiler (1991) observed that the initial downward drift in pH is fast, and the rate of downward drift in pH of NOM solutions at alkaline pHs is time dependent. Plots of pH drift vs. time is a pseudo-exponential decay function that approaches an asymptotic lower pH limit, due to the complete hydrolysis of the available pool of esters after 12 to 48 hours of exposure at alkaline pH conditions.

If the exposure time of the SRNOM and Fractions 1-7 to alkaline pHs after the completion of the forward titration were increased—for example, 60 minutes or 24 hours—the initial pH of the reverse titration would be significantly lower than 10.28-10.44. This would yield even greater calculated values of Q_{pH} for the reverse titrations. Because base-catalyzed ester hydrolysis is assumed to be the mechanism driving the observed hysteresis, the estimated concentrations of carboxyl groups would be even greater than those reported for the reverse titrations in Table 4.13 if the time interval was longer than 30 minutes.

The net changes in Q_1 , Q_2 , and Q_{TOT} (total acidity = $Q_1 + Q_2$) between the forward and reverse titrations are shown in Table 4.14. The SRNOM had the greatest drift in pH and the greatest increase in Q_1 during the 30-minute interval. The net increases in Q_1 and Q_{TOT} for Fractions 1-7 are very similar, indicating that the possible esters from the SRNOM are more-or-less uniformly distributed in the fractions and across all ranges of MWs. For all samples, the Q_1 and Q_{TOT} have a net increase, and Q_2 has a net decrease. The net increase in Q_1 is greater than for Q_{TOT} , which is offset by the net decrease in Q_2 . This strongly indicates that new carboxyl groups were not only formed during the 30-minute interval at alkaline pH, but also during the forward titration above pH 7-8. The

new carboxyl groups that formed above pH 7-8 during the forward titration were modeled and estimated to be part of the phenolic content because they were observed to ionize in the phenolic acidity range. During the reverse titration, these additional carboxyl groups would not be pH reactive at high pHs because carboxyl groups gain protons at much lower pHs (probably 3-5). Thus, they would be modeled and estimated to be part of the carboxyl content of the reverse titration. The slightly lower mean $\log K_1$ values for the reverse titrations indicate, at least qualitatively, that the new carboxyl groups formed from hydrolyzed esters are more acidic than the original pool of carboxyl groups that were titrated in the forward titration before the observed hysteresis.

4.5.6 Literature reports of acidic functional groups.

The concentrations of acidic functional groups for the SRNOM and Fractions 1-7 were compared with literature reports of carboxyl and phenolic for other Suwannee River samples (Table 4.15). The reports of titration data for the IHSS-SRFA significantly outnumber all other reports of titration data for all commercially available FAs, HAs, and NOM samples, including the Fluka and Aldrich HAs. It should be noted that Tipping (1998) and Gustafsson (2001) used their respective Model VI and Stockholm model to estimate Q_1 and Q_2 for the IHSS-SRFA sample that was originally titrated by Ephraim *et al.* (1986). The Ephraim *et al.* (1986) titration data was also modeled by deWit *et al.* (1993) with the first-generation NICA model and by Milne *et al.* (2001) with the NICA-Donnan model. One titration dataset is represented five different times in Table 4.15, with its acidic functional groups determined by five different empirical models. Each model gives a different result. This author believes that the mandatory 2:1 carboxyl-to-

Table 4.15. The concentrations of acidic functional groups (mmol gC⁻¹) for the Suwannee River fulvic acid(s) and humic acid(s) that were determined by direct titration methods as reported in the literature.

	Carboxyl	Phenolic	Method
IHSS std. SRFA^a	11.63	2.29	pH method
IHSS std. SRFA^b	11.45	2.88	pH method
IHSS std. SRFA^c	11.44	4.00	pH method
IHSS std. SRFA^d	10.70	N/A	Second derivative, pH method
IHSS std. SRFA^e	10.66	N/A	NICA model
IHSS std. SRFA^f	10.58	3.55	NICA-Donnan model
IHSS std. SRFA^f	10.22	5.87	NICA-Donnan model
IHSS std. SRFA^f	9.00	3.55	NICA-Donnan model
IHSS std. SRFA^g	9.34	4.77	pH method
IHSS std. SRFA^h	8.94	3.83	Stockholm model
IHSS std. SRFAⁱ	8.09	2.71	unknown
IHSS std. SRFA^j	5.46	2.73	Model V, VI
SRFA^k	6.90	2.97	pH method
IHSS std. SRHA^b	9.61	4.25	pH method
IHSS std. SRHA^c	8.96	4.39	pH method
SRHA^k	7.22	3.10	pH method
Mean SRFA	9.57 ± 1.9	3.56 ± 1.0	
Mean SRHA	8.60 ± 1.2	3.91 ± 0.7	

References: ^aBowles *et al.* (1989); ^bRitchie and Perdue (2003); ^cSteelink *et al.* (1983); ^dSantos *et al.* (1999); ^edeWit *et al.* (1993); ^fMilne *et al.* (2001); ^gMachesky (1993); ^hGustafsson (2001); ⁱEphraim *et al.* (1986); ^jTipping (1998); ^kMa *et al.* (2001).

phenolic ratio in Models V and VI (Tipping and Hurley, 1992; Tipping, 1998) wrongfully characterizes the concentrations of acidic functional groups.

Only three direct titrations of the Suwannee River HA are found in the literature, and their values of Q_1 and Q_2 were all estimated by the pH method. Additionally, all reports of titration data in Table 4.15 are estimated from forward titrations—no reverse titrations were performed. Therefore, Q_1 and Q_2 for the forward titrations of Fractions 1-7 were compared to values for the SRFA and SRHA that were determined by the pH method only. Fractions 3-6 have Q_1 values that are in the range of Q_1 for the SRFA. Fractions 2 and 7 had Q_1 values that are in the range of those for the SRHA, with Fraction 1 having a Q_1 value approximately 18% lower than the lowest reported Q_1 for SRHA. Fractions 1, 2, and 7 have values of Q_2 that were comparable to the SRHA, while Fractions 3-6 have Q_2 values comparable to the SRFA.

4.6 Capillary Electrophoresis.

The charge-to-size distributions of the SRNOM and Fractions 1-7 were characterized by capillary electrophoresis (CE). The experimental CE work was performed under the direction of Prof. Dr. Philippe Schmitt-Kopplin at the GSF Forschungszentrum für Umwelt und Gesundheit (GSF Research Center for Environment and Health). This author has consulted with Prof. Dr. Schmitt-Kopplin on numerous occasions and will, if necessary, paraphrase his statements within this section.

4.6.1 Overview of CE electropherograms.

A subset of six of the baseline-corrected CE electropherograms for the SRNOM

and Fractions 1-7 are shown in Figures 4.22-4.29. There were 15 to 22 electrophoretic separations performed on each of the samples over the pH range of 3.0 to 11.4. Discussions of electropherograms not shown in Figures 4.22-4.29 will be made when warranted.

The subset of six electropherograms for each sample (Figures 4.22-4.29) was chosen for three reasons. First, the pHs of those electrophoretic separations are common to all samples, allowing for immediate visual comparison between electropherograms of different samples at approximately the same pH. Secondly, those electropherograms are excellent examples of every shape, size, and distribution of all electropherograms in this work. And lastly, the pHs of those separations represent “key” points in the acid-base chemistry of the samples. The pH range of 3.8-4.1 is near the mean $\log K_1$ values for the samples (Table 4.13)—40-50% of carboxyl groups and zero phenolic groups are ionized. pH 7.6-7.9 is near the endpoint of carboxyl group ionization and near the beginning of phenolic group ionization— > 95% of carboxyl groups and < 10% of phenolic groups are ionized. pH 9.0-9.3 is very near the mean $\log K_2$ values for the samples (Table 4.13)— 40-50% of phenolic groups and 100% of carboxyl groups are ionized. pH 10.4-10.6 is near pH 10.5, the highest pH for the direct titrations— >90 % of phenolic groups and 100% of carboxyl groups are ionized. The pH ranges of 4.7-4.9 and 6.2-6.4 are intermediate pHs for the ionization of carboxyl groups. Electrophoretic separations at pH < 7 were buffered by acetic acid/ Na^+ -acetate carrier solutions. Electrophoretic separations at pH > 7 were buffered by $\text{NaHCO}_3/\text{Na}_2\text{CO}_3$ carrier solutions.

At pHs < 4.0, electropherograms are generally confined to lower negative μ_{eff} , centered between -0.005 and $-0.01 \text{ cm}^2 \text{ V}^{-1} \text{ min}^{-1}$. Their shapes tend to be parabolic

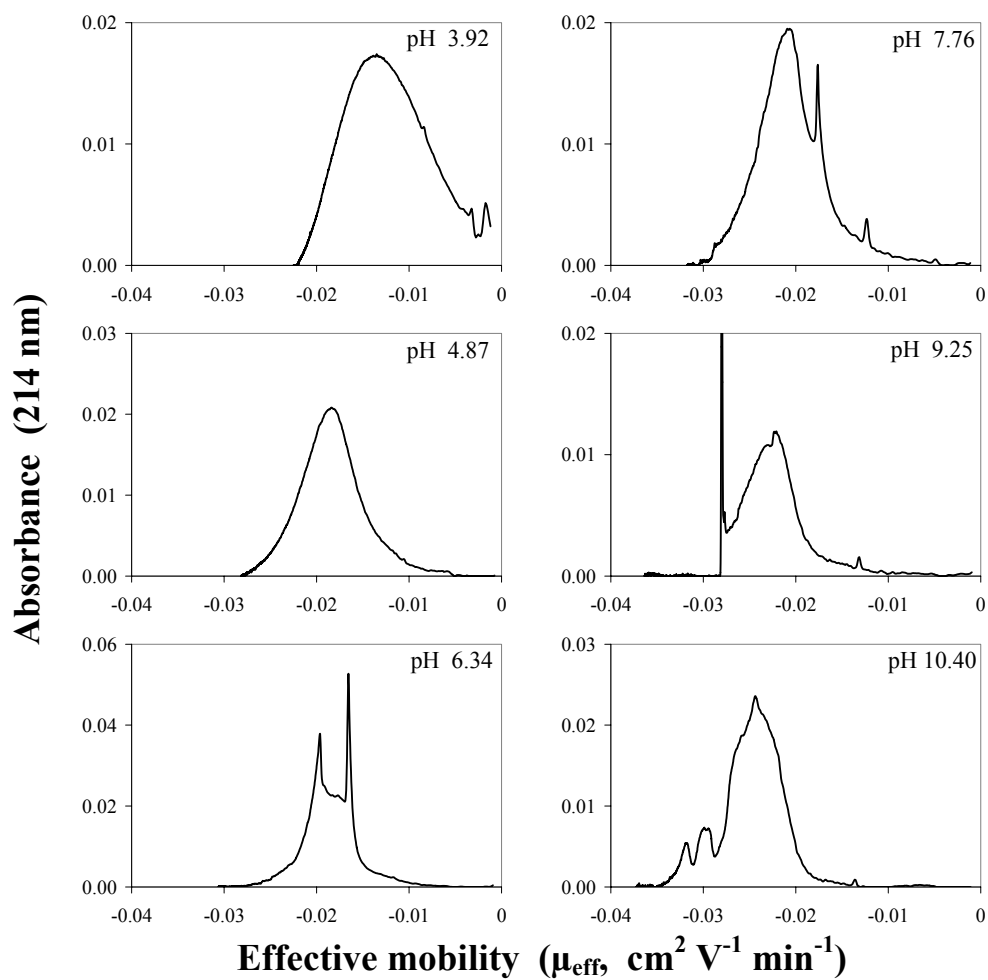


Figure 4.22. A subset of six capillary electropherograms for the SRNOM.

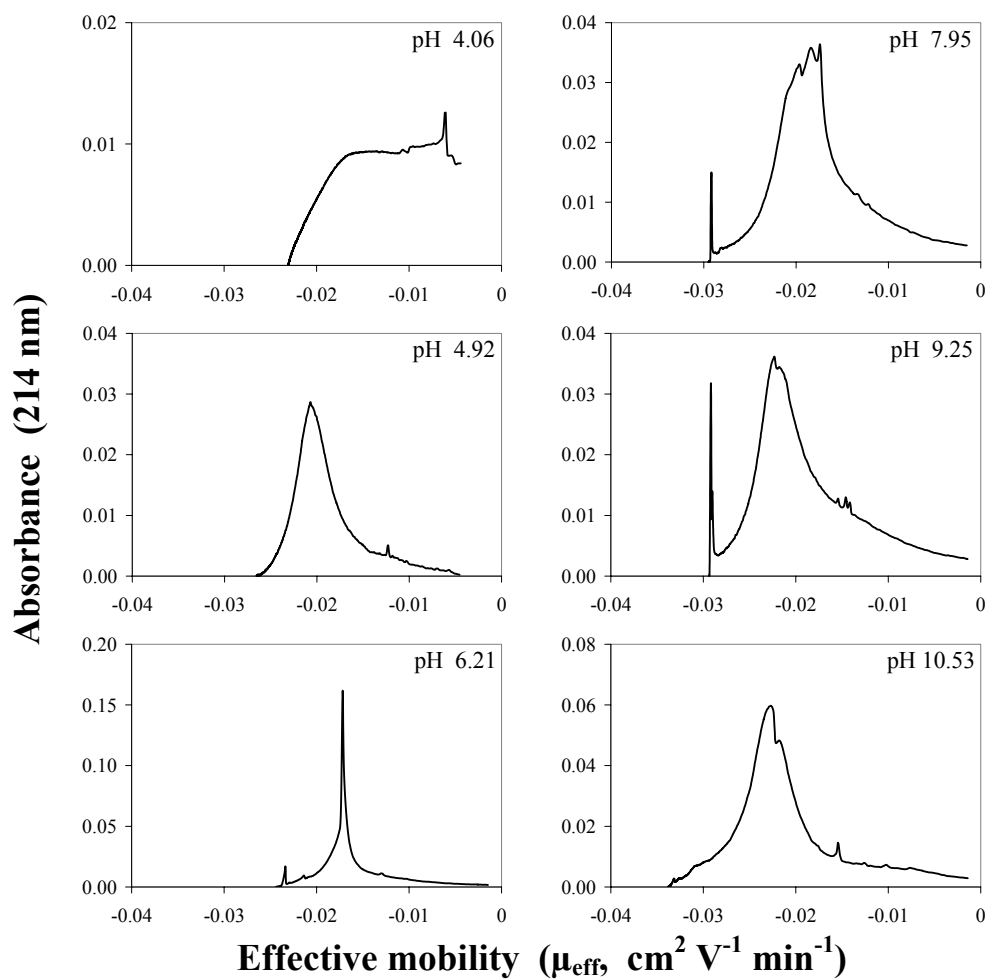


Figure 4.23. The subset of six capillary electropherograms for Fraction 1.

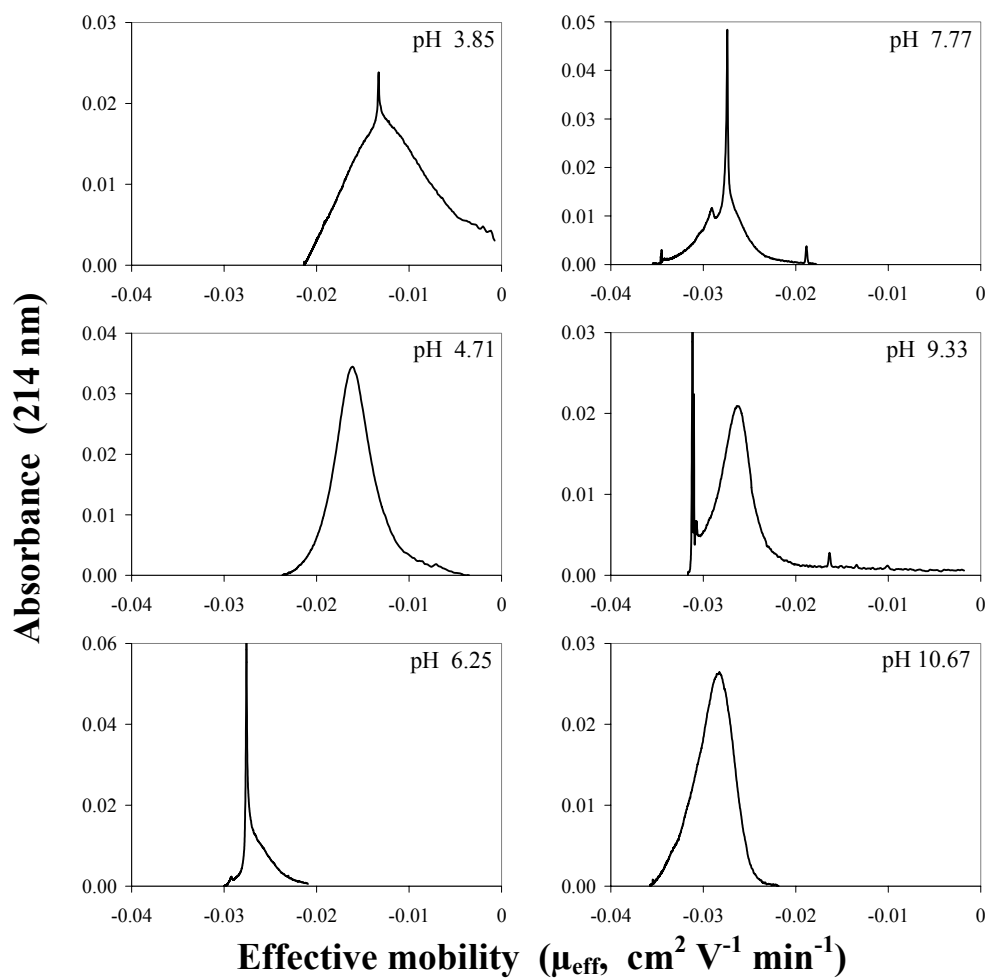


Figure 4.24. The subset of six capillary electropherograms for Fraction 2.

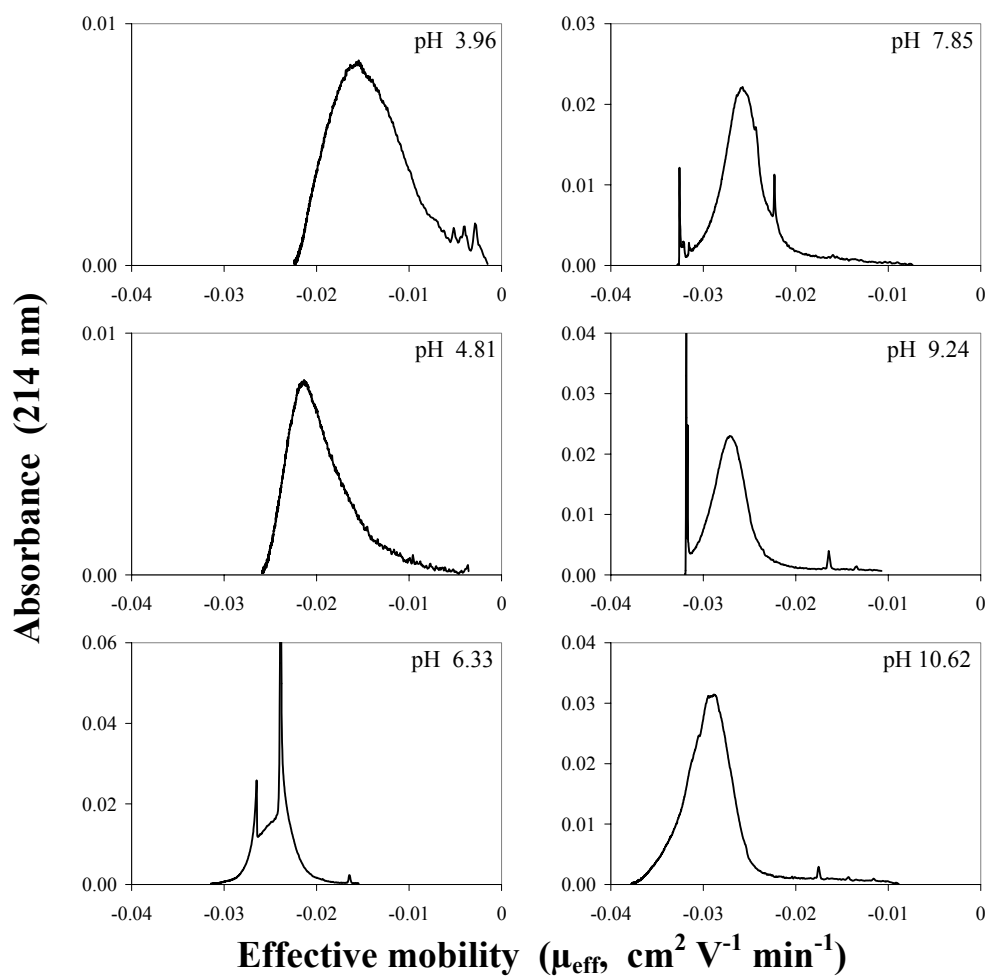


Figure 4.25. The subset of six capillary electropherograms for Fraction 3.

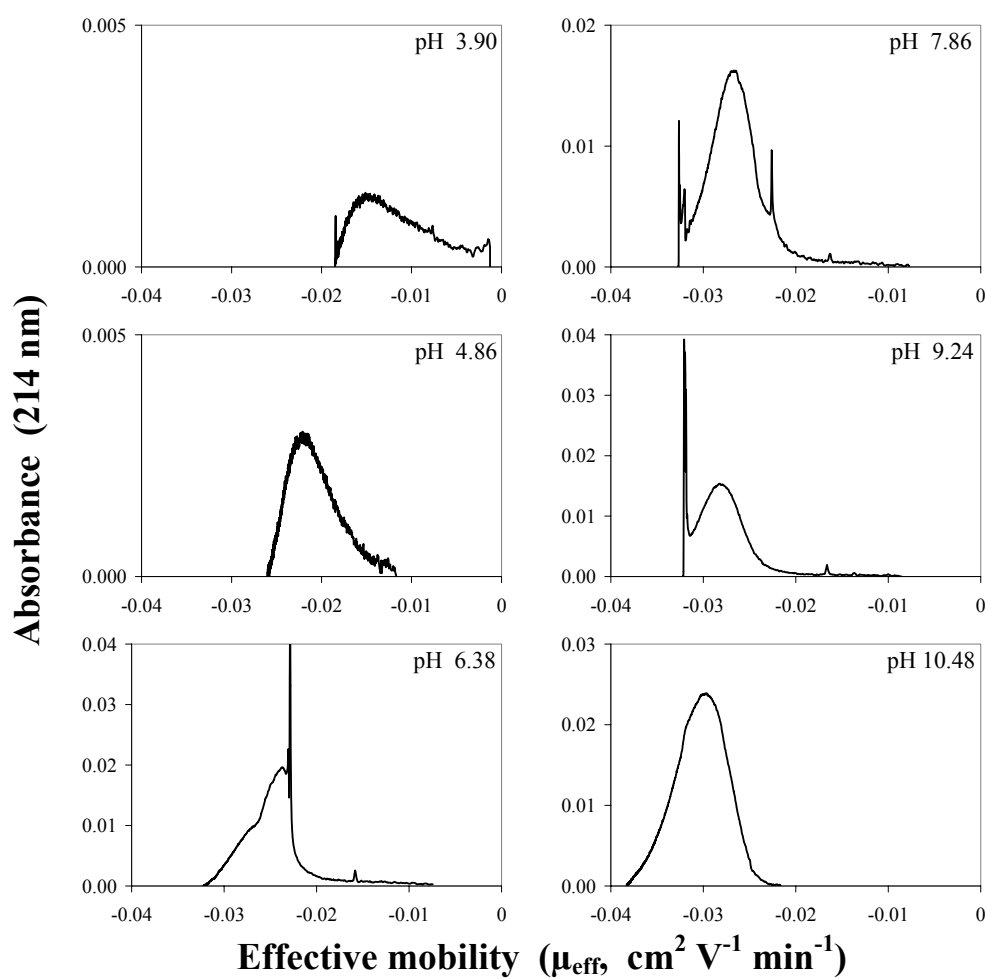


Figure 4.26. The subset of six capillary electropherograms for Fraction 4.

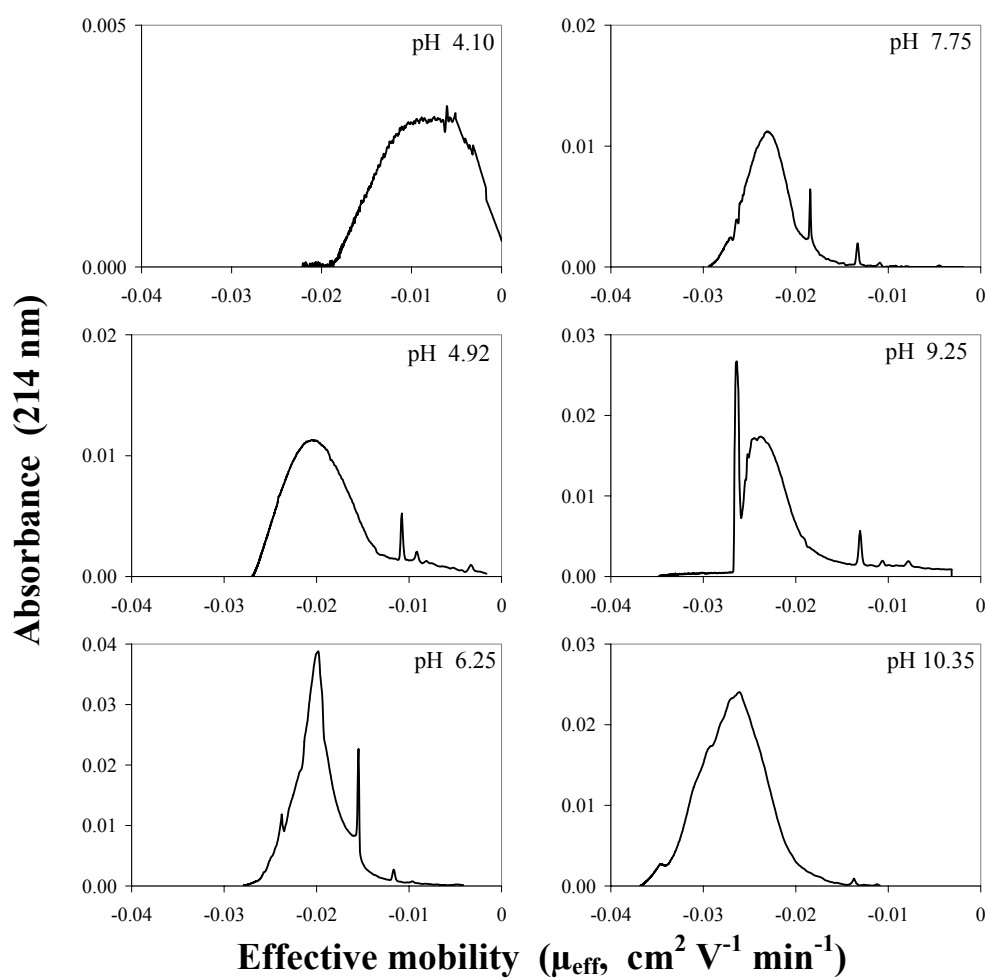


Figure 4.27. The subset of six capillary electropherograms for Fraction 5.

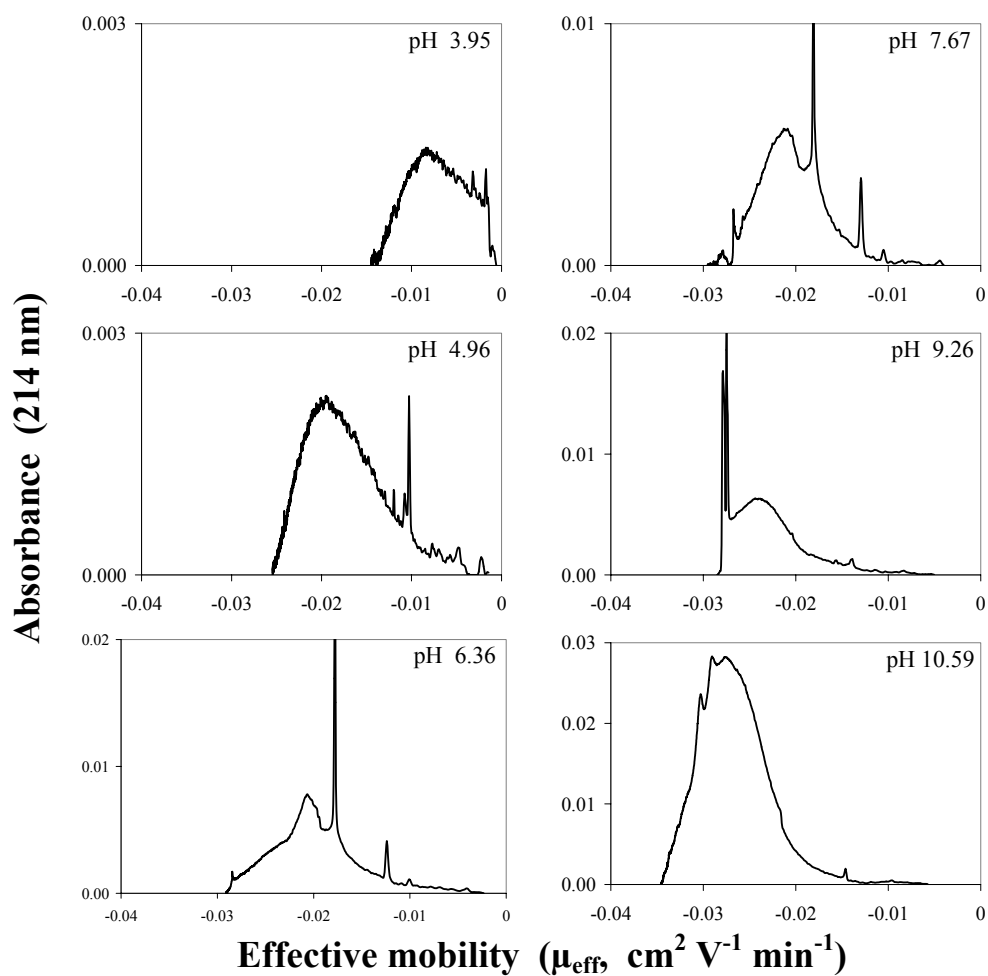


Figure 4.28. The subset of six capillary electropherograms for Fraction 6.

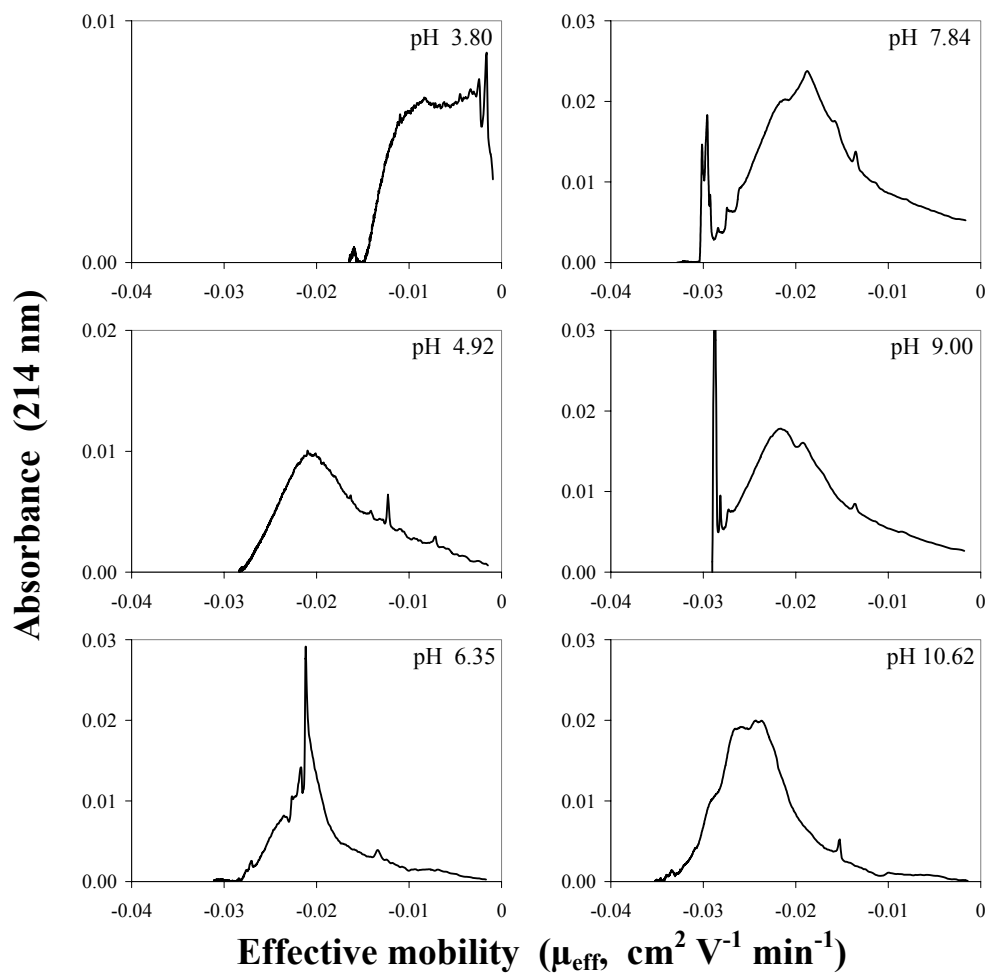


Figure 4.29. The subset of six capillary electropherograms for Fraction 7.

(Figure 4.22: pH 3.92) or semi-parabolic (Figure 4.29: pH 3.80). In most cases, a significant portion of the electropherograms is about to zero mobility, implying that solutes with μ_{eff} nearest to the zero mobility either have very large MWs with very few ionized carboxyl groups, or they are small to medium MW solutes on which the first carboxyl group is partially ionized ($0 < z < -1$), or both.

Electropherograms at pH 4.7-4.9 are translated to greater (more negative) μ_{eff} , centered between -0.017 and $-0.022 \text{ cm}^2 \text{ V}^{-1} \text{ min}^{-1}$. Their shapes tend to be more symmetrical and Gaussian-like (Figure 4.24: pH 4.71), with minor to moderate tailing toward the lower μ_{eff} side of the electropherograms (Figure 4.25: pH 4.81). The electropherograms for Fractions 2-6 at pH 4.7-4.9 have no contact with the zero mobility, implying that most solutes in those samples have a greater negative charge due to more ionized carboxyl groups.

Additionally, “fingerprint” peaks in the tailing and on the low μ_{eff} mobility side of electropherogram are often first seen in the pH 4.7-4.9 range. These fingerprints peaks remain stationary at a single value of μ_{eff} in the electropherograms between pH 4.7 to pH 9-10, even though the bulk electropherogram translates to greater negative mobility with increases in pH. For example, a well-defined fingerprint peak is at $-0.0120 \text{ cm}^2 \text{ V}^{-1} \text{ min}^{-1}$ in the pH 4.92, 6.25, 7.75, and 9.25 electropherograms for Fraction 5 (Figure 4.27). Fingerprint peaks may slightly increase or decrease in height or width, but generally remain at the same μ_{eff} .

Schmitt-Kopplin *et al.* (1998b) attributed fingerprint peaks to polysubstituted aromatic acids derived from the degradation of lignin. The development of these

fingerprint peaks in the pH 4.7-4.9 range would indicate that at least one carboxyl group is substituted on the benzene ring (e.g. vanillic acid) or on an aliphatic side chain connected to the benzene ring (e.g. ferulic acid). The observation that these peaks tend not to translate to greater μ_{eff} with an increase in above pH ~ 4.7 means that the pK_a of the carboxyl group on these acids is ≤ 4.0 . It is probable that these compounds were already ionized at pHs < 4.0 , but their signals were overwhelmed by bulk of the electropherogram centered at the lower μ_{eff} . The phenolic group (if one is present) would not ionize until pH is greater than pH 9.

A significant number of CE electropherograms in the pH 5.0-6.5 range appear to be Lorentzian-like distributions—one very large spike (Figure 4.23: pH 6.21)—or contained a suspiciously large peak near the center of the electropherogram that was significantly taller than the main body of the electropherogram (Figure 4.26: pH 6.38). These electropherograms are very reminiscent of electropherograms of NOM in Garrison *et al.* (1995), Schmitt-Kopplin *et al.* (1998b), Schmitt-Kopplin *et al.* (1998c), and Schmitt-Kopplin *et al.* (1999a) that were buffered by borate salts at pH 8.5-9.0. Schmitt-Kopplin and colleagues (1998c) attributed those peaks to organic-borate esterification. It is unclear if acetate in this pH range forms esters with the NOM. Schmitt-Kopplin and colleagues have not discussed this possibility.

If acetate does not readily form esters with NOM solutes, then the other plausible explanation is that the bulk of organic matter in those samples had become one cohesive system peak—a peak formed from the non-ideal redistribution of sample within the sample zone due to contrasting conductivities, mobilities, or pHs between the sample zone and the carrier solution. Each sample was prepared by dissolving 1 mg into 1 ml of

0.1 M NaOH in order to ensure complete dissolution of the sample. The sample was injected into the capillary, probably at pH 12-12.5, surrounded by the carrier solution of different pH. De Nobili and Chen (1999) advise that samples to be analyzed by HPSEC and SEC should be prepared at the same ionic strength, pH, and background matrix as the mobile phase. Prof. Dr. Schmitt-Kopplin stated (in personal communication) that the differences in pH would rapidly dissipate as the sample and carrier solution mix and migrate under the influence of the electric field. This author suspects that system peak formation is due to the potential pH gradient at the moving boundary between the sample zone and the carrier solution.

Neglecting the possible system peaks, the translation of electropherograms to greater negative mobilities between pH 4.7-4.9 and pH 6.2-6.4 is smaller than the translation of mobilities between pH 3.8-4.1 and pH 4.7-4.9. This would suggest that there is little change in the distribution of $\frac{z}{MW^{2/3}}$ in the samples between pH 4.7-4.9 and 6.2-6.4. The shift of mobilities for electropherograms between pH 6.2-6.4 and pH 7.6-7.9 is even less, if any shift was even observed. If the bulk of solutes in the samples had achieved sufficiently large enough values of $\frac{z}{MW^{2/3}}$ by pH 5 (relative to their MW distributions), then the ionization of an additional 1 or 2 carboxyl groups per solute of a small portion of sample is relatively inconsequential to the cumulative $\frac{z}{MW^{2/3}}$ distribution already established by pH 5.

The shapes of electropherograms at pH > 7 tend to be near-Gaussian with 1 to 3 fingerprint peaks and 1 or 2 suspected system peaks. For example, the electropherogram for Fraction 5 at pH 9.25 (Figure 4.27) has three fingerprint peaks (-0.0080, -0.0110, and

-0.0135 cm² V⁻¹ min⁻¹) and one possible system peak at -0.0255 cm² V⁻¹ min⁻¹. Most electropherograms in the pH 7.5 to 10.0 range have a very large system peak that abruptly truncates the high mobility side of the electropherogram (Figure 4.25: pH 7.85 and 9.24). Those system peaks at high mobility are attributed to a migrating ionic strength boundary (Schmitt-Kopplin and Junkers, 2003), where the ionic strength in the high mobility side of the sample zone is significantly greater than the carrier solution. The electropherograms have a very gradual translation to greater negative mobilities from pH 7.6-7.8 to pH 9.0-9.3 and from pH 9.0-9.3 to pH 10.4-10.6, due to the ionization of phenolic groups. However, the overall shape and width of the electropherograms at pH 9.0-9.3 and pH 10.4-10.6 are not significantly different from electropherograms at pH 7.6-7.8.

The ionization of phenolic groups would only increase the cumulative $\frac{z}{MW^{2/3}}$ of solutes by a relatively small amount compared to the ionization of carboxyl groups because phenolic groups are less abundant. The fact that the width and shapes of the electropherograms did not change as the pH of the separations was increased would result from phenolic groups being on solutes that already had a minimum of one ionized carboxyl group. If phenolic groups were only on solutes that did not contain carboxyl groups, new fingerprint peaks and shoulders would develop at the lower μ_{eff} side of the “humic hump” at pHs > 9. This was not seen for any of the samples.

The SRNOM had two unusual shoulders develop on the high mobility side of its distribution at pH 10.40 (Figure 4.22), the origin of which is unknown. The electropherogram for Fraction 7 at pH 9.84 (not shown) had similar shoulders, but at different mobilities than the SRNOM. Neither the pH 9.64 and 11.25 electropherograms

(not shown) for the SRNOM nor the pH 9.00 and 10.62 electropherograms for Fraction 7 contained those unusual shoulders.

4.6.2 Comparison of electropherograms between samples.

Generally, Fractions 1, 2, and 7 were the most susceptible samples for the formation of the Lorentzian-like electropherograms (see example in Figure 4.23, pH 6.21). Fractions 1 and 2 had six each, and Fraction 7 had five. Fractions 3-6 had only one electropherogram each that tended to be Lorentzian-like in shape. Fractions 3-6 were more susceptible to developing the very tall, thinner spikes just on the low mobility side of the “humic hump” maximum (see example in Figure 4.26, pH 6.38).

All fractions have electropherograms that contain fingerprint peaks at the low mobility side of the humic hump and in the tailing. These peaks occurred at the same μ_{eff} in the different samples and remained at that μ_{eff} between pH ~4.5 and 9.5. The two most distinguishable fingerprint peaks that all seven fractions have in common are at μ_{eff} of -0.0120 to -0.0130 and -0.0140 to -0.0150 cm² V⁻¹ min⁻¹. Electropherograms for Fractions 5-7 have two additional fingerprint peaks at -0.0100 to -0.0110 and -0.0070 to -0.0080 cm² V⁻¹ min⁻¹. The latter peaks, although present, are not as cleanly developed in electropherograms for Fractions 1-4 as they are in electropherograms for Fractions 5-7. The ubiquitous presence of fingerprint peaks in the electropherograms suggests small compounds (that strongly absorb UV light) were not separated by size during the preparative SEC fractionation, even though there is a well-defined decreasing trend in MW from Fraction 1 to Fraction 6 as indicated by the mode and average MWs. Fingerprint peaks are generally not present in electropherograms above pH 10.0,

suggesting that they indeed have at least one phenol group undergoing ionization at alkaline pHs. Therefore, the small acids that appear as fingerprint peaks in electropherograms have a minimum of one carboxyl and one phenolic group.

Excluding the Lorentzian-like electropherograms, electropherograms for Fractions 1 and 7 at pHs < 10 generally have moderate to significant tailing on the low mobility size of their electropherograms that contacts the zero mobility. Fraction 1 has the lowest concentration of carboxyl groups (Q_1) and the largest average MWs—low density of ionized carboxylic acids distributed over solutes with large MWs would give very low values of $z/MW^{2/3}$. Fraction 7 has the smallest average MWs and the third smallest value of Q_1 —the small size of solutes limits the maximum number of carboxyl groups per solute to only a few at most, giving relatively small values of $z/MW^{2/3}$. Electropherograms for Fractions 2-6 have no contact with the zero mobility at pHs > 4 and have very minor tailing on the low mobility side of the electropherograms. Q_{pH} for Fractions 3-6 nearly double between pH 3 and pH 5 (Figure 4.18), distributing a large charge density over their pools of solutes with smaller MWs.

4.6.3 Peak effective mobilities (μ_p).

Peak effective mobility (μ_p) was used as a proxy for the center position, or mean μ_{eff} , of electropherograms on the effective mobility scale at different pHs. The values of μ_p for the SRNOM and Fractions 1-7 (Appendix Tables A.1-A.8) were first plotted against their respective pHs (Figure 4.30), forming their electrophoretic titration curves (Glück *et al.*, 1996). The electrophoretic titration curves for Fractions 1-7 tend to

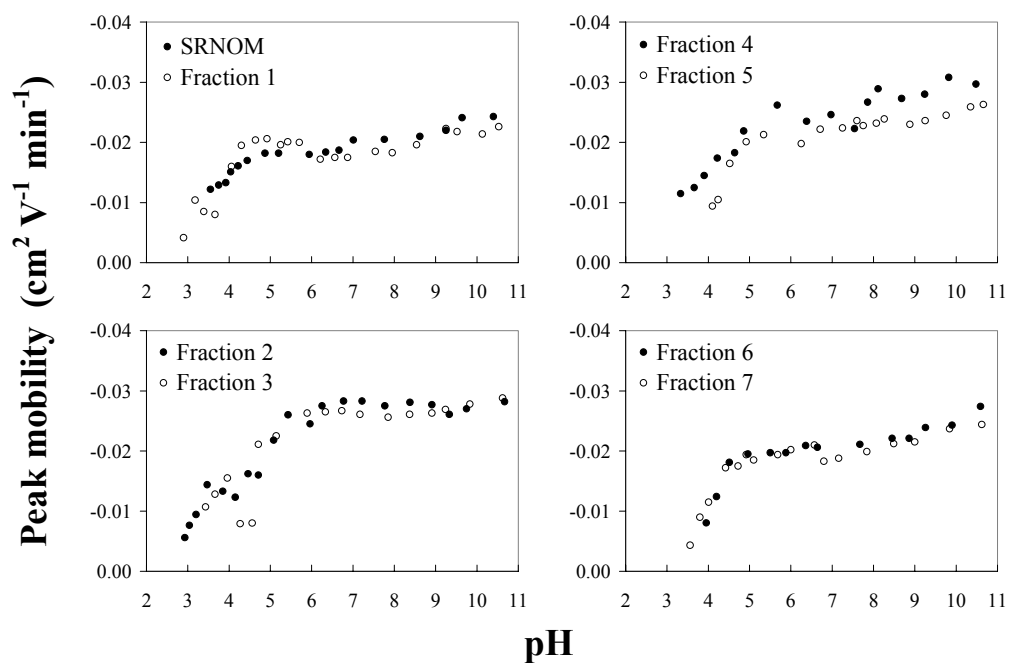


Figure 4.30. The peak effective mobilities (μ_p) for the SRNOM and Fractions 1-7 as a function of increasing pH

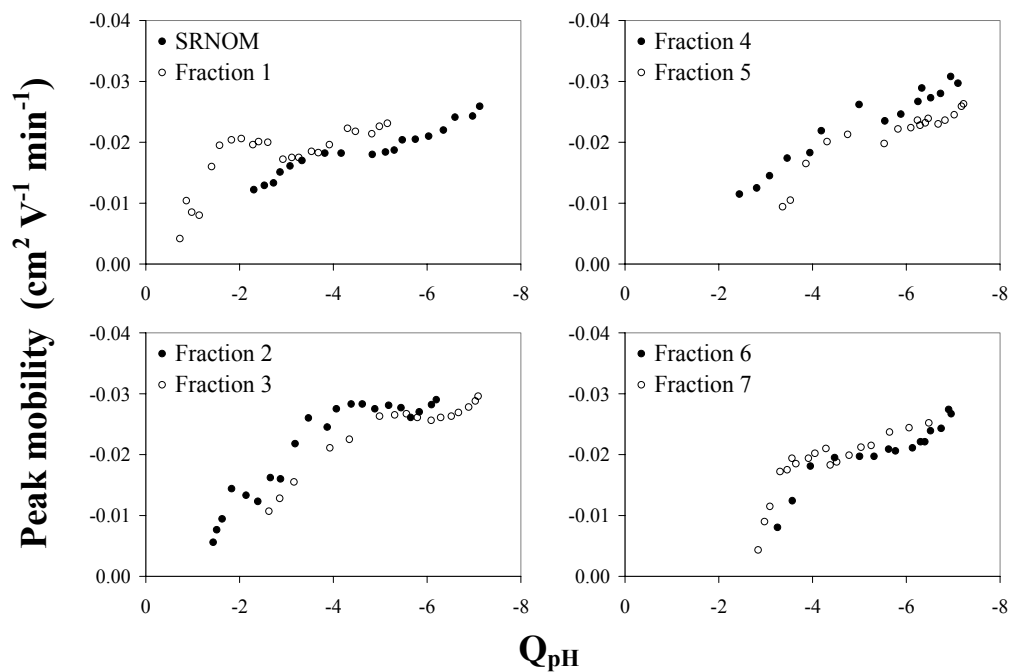


Figure 4.31. The peak effective mobilities (μ_p) for the SRNOM and Fractions 1-7 as a function of increasing charge density (Q_{pH}). Q_{pH} was calculated using the modified Henderson-Hasselbalch (H-H) model for reverse titrations.

resemble the titration curves shown in Figures 4.18, but with some minor irregularities in the pH 5.0-6.5 range, due to suspicious phenomena in those electropherograms. The electrophoretic titration curves for Fractions 1-7 have a very large increase in μ_p between the lowest pH (pH 3-4) and pH 5-5.5. μ_p becomes relatively invariant between pH 6.0 and 7.5, at which point μ_p very gradually translates to more negative μ_{eff} up to the maximum pH 11.2-11.4. Q_{pH} , as determined by direct titrations, is a continuously increasing function. Generally, standard titration curves of NOM do not have any segments in which Q_{pH} does not increase with increasing pH, although the pH 6-8 region of titration curves is generally much flatter than the regions below pH 6 or above pH 8.

Peak mobilities for the SRNOM and Fractions 1-7 were plotted against their respective values of Q_{pH} , calculated using the H-H models for reverse titrations, to compare μ_p with the accumulation of the total charge in the samples (Figure 4.31). The H-H models for the reverse titrations were preferentially used for this comparison because the samples for CE were prepared at alkaline pH in 0.1 M NaOH. The hydrolysis of esters in the CE samples would have probably generated a greater quantity of new carboxyl groups than the 30-minute interval at pH 10.5 for the titration work. Nonetheless, values of Q_{pH} derived from the H-H models for the reverse titration curves are best for comparing the total charge of the samples to their CE distributions.

When μ_p is plotted against Q_{pH} for the SRNOM and Fractions 1-3, three distinct segments for each plot become evident. The plot for Fraction 3 is used as an illustrative example. The values of μ_p for Fraction 3 significantly increase between Q_{pH} of -2.2 and -5.0 meq g⁻¹—the whole sample is accumulating charge (number of ionized carboxyl groups increases) and the bulk of Fraction 3's solutes are gaining higher charges (number

of ionized carboxyl groups per solute increases). Between Q_{pH} of -5.0 to -6.1 meq g⁻¹, values of μ_p are relatively invariant— μ_p oscillates between -0.0261 and -0.0267 cm² V⁻¹ min⁻¹ (-0.0265 ± 0.0003)—even though Fraction 3 is still accumulating charge. At Q_{pH} of -5.0, 81% of the total carboxyl group concentration in Fraction 3 ($Q_1 = 6.15$ mmol g⁻¹) is ionized. The ionization of the remaining 19% of carboxyl groups in Fraction 3 have no real effect on μ_p . Between Q_{pH} of -6.1 and -7.1, values of μ_p increase from -0.0265 to -0.0296 cm² V⁻¹ min⁻¹, due to the ionization of phenolic groups.

The inflection in the shape of μ_p vs. Q_{pH} curves, from steeply increasing to horizontal, for Fractions 2-7 generally occurs at the point where 75% ± 5 of carboxyl groups have become ionized. The change in Fraction 1's plot occurs when only 49% of its carboxyl groups become ionized. For μ_p to remain invariant while the samples continue to accumulate charge, the bulk average $\frac{z}{MW^{2/3}}$ of the sample must remain relatively constant. Therefore, the remaining 25% ± 5 of carboxyl groups are more likely to be on solutes with MWs greater than the average MW of the sample.

As the phenolic groups begin to ionize at pHs > 9, μ_p increases with increasing Q_{pH} , as well as the entire electropherogram translates to greater mobilities. If phenol-bearing solutes had no carboxyl groups, the signal for those solutes would appear as new fingerprint peaks at low μ_{eff} or change the electropherogram into a bi-modal distribution. This would cause μ_p to become lower with increasing Q_{pH} , which was not the case for any of the samples.

Chapter 5.

A PROBABILISTIC APPROACH FOR CHARACTERIZING THE DISTRIBUTION OF CHARGE IN NOM

The results presented in Chapter 4 for the MW distributions, acid-base chemistry, and capillary electrophoresis will be used in Chapter 5 formulate the probabilistic model for the distribution of charge in natural organic matter. The range of MWs of solutes and their relative [mass or molar] concentrations in a sample will be described by size-exclusion chromatography. The range and distribution of the charge-to-size of solutes will be described by capillary electrophoresis. The bulk charge-to-mass and concentrations of ionized acidic groups in a sample will be described by direct titrations.

5.1 Molecular weight, Electrophoresis, and Titration data.

5.1.1 Probability of molecular weight, $P(\text{MW})$.

The MW distributions for the SRNOM and Fractions 1-7 were determined by a semi-analytical, low-pressure SEC method at pH 6.8 and 9.3. There were slight differences between the MW distributions and the average MWs at pH 6.8 (absorbance and online-TOC) and at pH 9.3 (absorbance). In spite of these observed differences, the MW distribution for the pH 6.8 absorbance chromatograms are used in the Charge Distribution Model because the majority of HPSEC analyses of NOM are performed under those experimental conditions (Janos, 2003). It is assumed that the MW distributions for the SRNOM and Fractions 1-7 as determined at pH 6.8 with absorbance

detection do not change with pH.

The absorbance chromatograms in their original form (absorbance vs. retention time) were based on detection at 15 second intervals and contained, depending on the sample, 180 to 230 data points. The x-axis of each absorbance chromatogram was then transformed from the time scale to the log MW scale according to the calibration curve. The 3-G models (Table 4.3) are used to exactly replicate the absorbance chromatograms (absorbance vs. log MW). The benefit of the 3-G model is that the x-axis is uniformly scaled using very small intervals of log MW that improve the resolution of the MW distributions. Because absorbance was the method of detection during SEC, 3-G models for the SRNOM and Fractions 1-7 are models of mass distributions.

The 3-G models are continuous functions because they are the summation of three overlapping Gaussian distributions. Therefore, it was necessary to reasonably define the uppermost and lowermost limits for the 3-G models. The 3-G model for each sample was first normalized to its respective peak maximum, where the maximum = 1.00. The MW range for the 3-G model was then defined at the largest and smallest values of log MW values where the 3-G model had values of 0.01, or 1% of the maximum peak height. Any value of the 3-G model that was ≤ 0.0099 was filtered to equal zero.

The MW distributions for the SRNOM and Fractions 1-7 in the Charge Distribution Model are characterized by their respective mole distributions of MWs, calculated from the 3-G models using equations 3.3, 3.4, and 3.5. The entire range of MWs that is modeled by the 3-G model for this work is between log MW 4.350 (22,390 Da) and 1.780 (60 Da)—the log MWs corresponding to the void volume and total volume of the SEC column used at pH 6.8. That log MW range is divided into 0.005 log

increments, giving 515 discrete values of log MW.

The probability of any discrete value of MW ($P(MW_i)$) in the sample is defined as the mole fraction of all solutes with the discrete value of MW_i (equation 5.1).

$$(5.1) \quad P(MW_i) = \frac{n_i}{\sum_i n_i} = \frac{n_i}{\sum_i \left(m_i / MW_i \right)}$$

If any MW is outside the filtered range of log MWs for the 3-G model, $P(MW)$ for that $MW = 0$.

The mass (from the 3-G model) and mole distributions ($P(MW)$) for the SRNOM are shown in the top graph of Figure 5.1. Unlike the mass distribution, the mole distribution of MWs for the SRNOM (and for Fractions 1-7, not shown) is nearly bimodal, due to the tailing at the low log MW (longer retention time) side of the chromatogram. If SEC chromatograms are symmetrical and lacked tailing, the mass and mole distributions of MW would be identical in shape and in size, but mole distributions would be translated to lower MWs (Cabaniss *et al.*, 2000). Cabaniss *et al.* (2000) suggested that the tailing at the very high and very low log MWs was insignificant—less than 10% of the total HPSEC chromatogram peak area—and should be discarded. Cabaniss *et al.* (2000) also suggested that most HPSEC chromatograms of NOM could be well replicated by a single Gaussian function. A single Gaussian function could not replicate the chromatograms in this work—especially for Fractions 1, 2, and 7 because of their asymmetry and topography. This author considers the tailing at the lower log MW regions of the SEC chromatograms to be an important part of that sample that should be

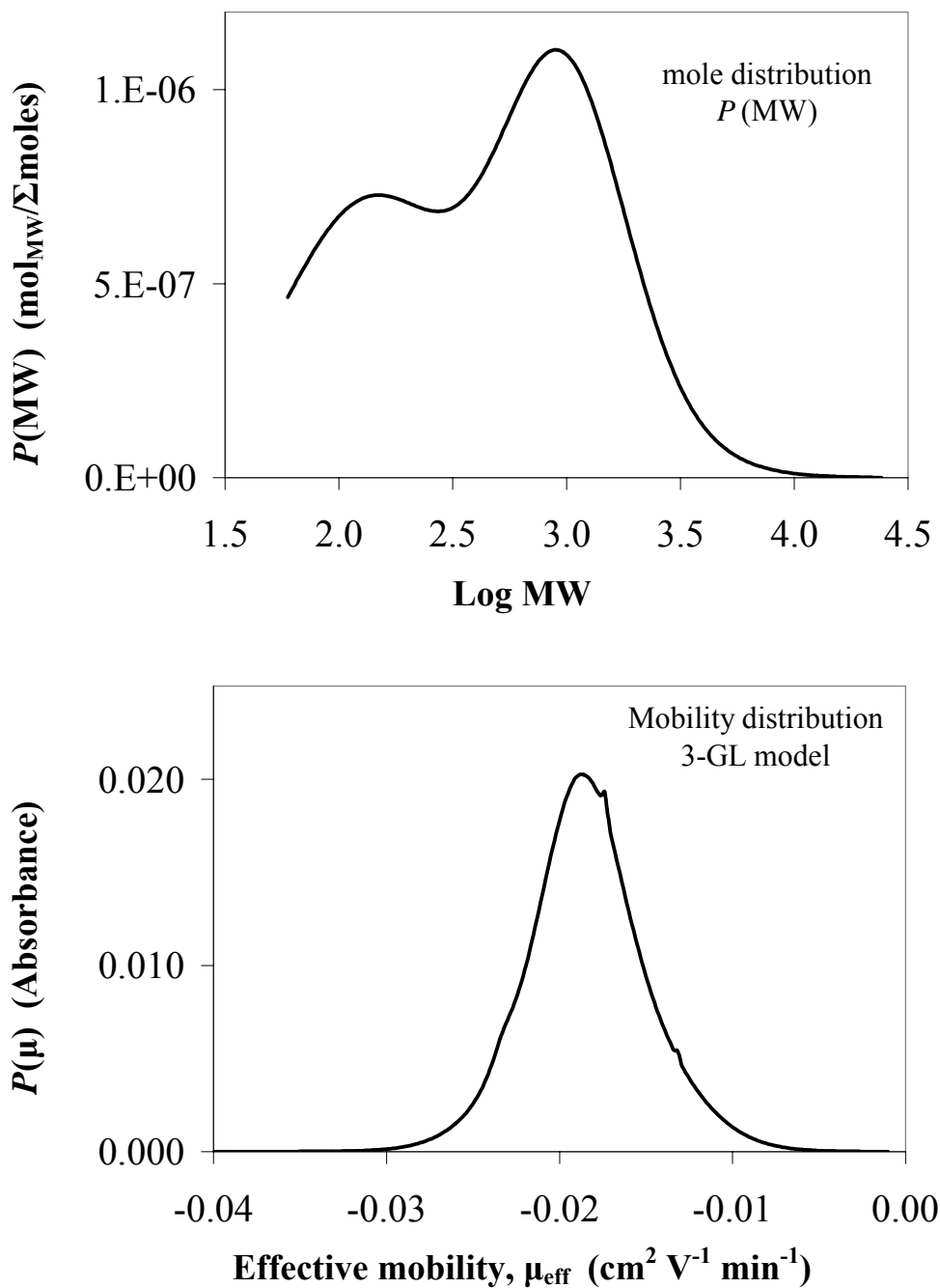


Figure 5.1. $P(\text{MW})$ is the probability of MWs based on the mole distribution of MWs derived from the 3-G model for the SRNOM. $P(\mu)$ is the probability of effective mobilities (μ_{eff}) as derived from the 3-GL model for the electropherogram of the SRNOM at pH 4.87.

included in the 3-G models, even though the tailing will ultimately bias the mole distribution (to an unknown degree) toward lower MWs.

5.1.2 Probability of effective mobility, $P(\mu)$.

The CE electropherograms in this work are based on UV detection at 0.5 to 1 second intervals. After the transformation of the retention time scale to the effective mobility scale, electropherograms contain 1000 to 2500 data points. The CE electropherograms are replicated using the 3-Gaussian-3-Lorentzian (3-GL) model (equation 3.18) between μ_{eff} of -0.0010 and -0.0400 cm² V⁻¹ min⁻¹. The 3-GL model allow for all CE datasets (on the effective mobility scale) to be uniformly scaled and reduce the number of data points without losing the detail of the electropherograms.

The 3-GL models are continuous functions because they are the summation of six overlapping distributions. Therefore, it is necessary to reasonably define the uppermost and lowermost limits for each of the 3-GL models. The 3-GL model for each sample at a given pH was first normalized to its respective peak maximum, where the maximum = 1.00. The μ_{eff} range for the 3-G model was then defined at the largest and smallest values of μ_{eff} where the 3-GL model had values of 0.03, or 3% of the maximum peak height. Any value of the 3-GL model that was ≤ 0.0299 was filtered to equal zero. For this work, the 0.0001 mobility interval is used between -0.001 and -0.0400 cm² V⁻¹ min⁻¹, giving 391 discrete values of μ_{eff} .

A mole distribution cannot be calculated from an electrophoretic distribution because a single value of μ_{eff} contains from one to dozens of different solutes of

different MWs with different charges (z). However, all solutes at a discrete value of μ_{eff} have the identical value of $z/MW^{2/3}$. Likewise, solutes with a common value of MW may have multiple “allowed” charges that correspond to multiple values of μ_{eff} in the electropherogram. Therefore, the probability of any discrete value of μ_{eff} ($P(\mu)$) is simply equal to its UV absorbance as modeled by the 3-GL model. The $P(\mu)$ distribution for the SRNOM at pH 4.87 is shown in Figure 5.1.

5.1.3 Charge density (Q_{pH}) and the charge-to-mass ratio.

The acid-base chemistry of the SRNOM and Fractions 1-7 was characterized by direct titrations between pH 3.0 and 10.5. At each pH during a titration, Q_{pH} (mmol gC^{-1}) was calculated, and the resulting titration curves were modeled using the modified Henderson-Hasselbalch (H-H) model. The H-H model is a continuous function and allows for the accurate calculation of Q_{pH} for a sample at any pH between pH 3 and 10.5.

Q_{pH} is technically negative because NOM is a mixture of organic acids and their negatively-charged conjugate bases. By convention, Q_{pH} is reported as its absolute value in units of mmol gC^{-1} in Chapter 4. From this point forward, Q_{pH} will be discussed as a negative quantity with the units $eq\ g^{-1}$. Equation 5.2 transforms Q_{pH} from mmol gC^{-1} to $eq\ g^{-1}$,

$$(5.2) \quad Q_{pH}(eq\ g^{-1}) = Q_{pH}(mmol\ gC^{-1}) \times \left(\frac{\%C}{100} \right) \times \frac{1\ eq}{1000\ mmol}$$

where %C is the percent carbon by weight on a dry, ash-free basis (Table 4.8). The

electrophoretic separations of the SRNOM and Fractions 1-7 were performed at 15-22 different pH steps between pH 3.0 and 11.4. The H-H models for reverse titrations are to calculate Q_{pH} (negative and in units of eq g⁻¹) of each sample at those pHs.

5.1.4 The conservation of mass and charge.

The integrated areas under an absorbance chromatogram and a CE electropherogram (at a given pH) represent the total mass (and total moles) of solutes in the sample, and are assumed to be equal. The range of MWs in the mole MW distribution is limited to those contained within the filtered 3-G model. All values of MW within that range have a $P(MW) > 0$. All values of MW that fall outside that range have a $P(MW) = 0$. If $P(MW)$ equals zero for a given value of MW, then that MW cannot exist in any CE electropherogram at any pH for that sample. Therefore, the filtered 3-G model restricts the range of possible MWs in all electropherograms for that sample.

The range of μ_{eff} in a CE electropherogram at a given pH is limited to those within the filtered 3-GL model. All values of μ_{eff} within the limits of the filtered 3-GL model have a $P(\mu) > 0$. All values of μ_{eff} that fall outside that range have a $P(\mu) = 0$. If $P(\mu)$ equals zero for a given value of μ_{eff} , then any combination of charge (z) and MW that will generate that value μ_{eff} cannot exist, even if $P(MW) > 0$ for that particular MW. The restricted ranges of MWs and μ_{eff} result in a restricted range of possible z for all solutes in the sample at a given pH. Electrophoretic separations were performed at 15-22 different pHs for each sample, resulting in 15-22 different distributions of μ_{eff} , 3-GL

models, and values of Q_{pH} that are evaluated individually. The mole MW distribution (and 3-G model) for a given sample is assumed to be invariant with pH.

The value of Q_{pH} (eq g⁻¹) is the total charge density and is equal to the total charge accrued by the total mass of sample at a given pH. The total mass of sample in Q_{pH} is equal to the total mass represented by the MW chromatogram and CE electropherogram. This means that total moles of solutes in the mole MW distribution, the CE electropherogram, and in Q_{pH} are equal. Additionally, the MWs of solutes represented by Q_{pH} are the same MWs that were defined by the filtered 3-G model.

Therefore, the weighted-sums of all combinations of allowed z and MW (restricted by the filtered 3-G and 3-GL models) for all solutes in a sample at a given pH must be consistent with Q_{pH} .

The equation for the conservation of charge is written as

$$(5.3) \quad Q_{pH} = \frac{\sum_i n_i \frac{z_i}{MW_i}}{\sum_i n_i} = \sum_i \left(P(MW_i) \frac{z_i}{MW_i} \right)$$

where n_i and z_i (eq mol⁻¹) are the number of moles and the charge (s) of solutes with MW_i (g mol⁻¹).

Offord (1966), later tested by Rickard *et al.* (1991), established the relationship between μ_i , z , and MW to be Offord's equation (equation 2.8). This equation was the best empirical fit relating solute size to μ_i for their suites of large polypeptide molecules with low polydispersity. Schmitt-Kopplin used Offord's equation (substituting μ_{eff} for

μ_i) to characterize effective mobilities for 66 small aliphatic and aromatic acids (MWs from 60-400 Da) that were individually separated by CE at three different pHs (5.0, 9.0, and 11.4). All values of z for the allowed combinations of MW and μ_{eff} are calculated with equation 5.4, the modified Offord's equation.

$$(5.4) \quad z = \frac{\mu_{eff} (MW)^{2/3}}{k_{pH}}$$

Each specific combination of allowed MW and μ_{eff} will generate one value of z . The variable k_{pH} in equation 5.4 is defined as the conditional Offord's constant. k_{pH} is designated as an adjustable fitting parameter that forces all calculated values of z from every probable combination of MW and μ_{eff} , in accordance with equation 5.3, to equal Q_{pH} . Although it is unlikely that all solutes in NOM are spheres, the 2/3 coefficient is applied to all MWs in all samples.

The probability of a value of z ($P(z)$) for a specific combination of allowed MW and μ_{eff} is equal to the product of their probabilities (equation 5.5).

$$(5.5) \quad P(z) = P(MW) \times P(\mu)$$

$P(z)$ will differ depending on the various combinations of MW and μ_{eff} . For the example shown in Table 5.1, the most probable charge for a solute in the SRNOM with MW = 1000 Da at pH 4.87 is -4.2. The least probable charge for a solute in the SRNOM

Table 5.1. The probabilities of MWs ($P(\text{MW})$), effective mobilities ($P(\mu)$), and the charges ($P(z)$) of solutes for the SRNOM at pH 4.87.

MW	$P(\text{MW})$	μ_{eff}	$P(\mu)$	z	$P(z)$
1000	1.09×10^{-6}	-0.0150	9.42×10^{-3}	-3.3	1.03×10^{-8}
1000	1.09×10^{-6}	-0.0160	1.29×10^{-2}	-3.5	1.41×10^{-8}
1000	1.09×10^{-6}	-0.0170	1.69×10^{-2}	-3.7	1.84×10^{-8}
1000	1.09×10^{-6}	-0.0180	1.97×10^{-2}	-4.0	2.15×10^{-8}
1000	1.09×10^{-6}	-0.0190	2.01×10^{-2}	-4.2	2.19×10^{-8}
1000	1.09×10^{-6}	-0.0200	1.78×10^{-2}	-4.4	1.94×10^{-8}
500	8.61×10^{-7}	-0.0180	1.97×10^{-2}	-2.5	1.70×10^{-8}
750	1.08×10^{-6}	-0.0180	1.97×10^{-2}	-3.3	2.13×10^{-8}
1500	8.50×10^{-7}	-0.0180	1.97×10^{-2}	-5.2	1.67×10^{-8}
2000	5.75×10^{-7}	-0.0180	1.97×10^{-2}	-6.3	1.13×10^{-8}
3000	2.71×10^{-7}	-0.0180	1.97×10^{-2}	-8.2	5.34×10^{-9}
4000	1.32×10^{-7}	-0.0180	1.97×10^{-2}	-10.0	2.60×10^{-9}
5000	7.32×10^{-8}	-0.0180	1.97×10^{-2}	-11.6	1.44×10^{-9}

with MW = 1000 Da at pH 4.87 is -3.3. In reality, the actual probability of a specific combination of z , MW, and μ_{eff} may grossly differ from the predictions of made by equation 5.5. It may be the case that a specific combination of z , MW, and μ_{eff} —where $(P(MW) > 0)$ and $\mu_{eff} (P(\mu) > 0)$ —may not even exist.

5.2 The Charge Distribution Model (CDM).

The determination of the most probable distribution of charge in the SRNOM and Fractions 1-7 was performed using the Charge Distribution Model (CDM). The CDM was designed as an optimized double-matrix format in Microsoft Excel.

5.2.1 Input data.

The Charge Distribution Model (as constructed in Excel) requires three sets of input data: the 3-G model for the MW distribution, the 3-GL model for an electrophoretic separation, and Q_{pH} for the pH at which the electrophoretic separation was performed. Values of k_{pH} will be independently solved for using the solver tool.

5.2.2 z-matrix.

The z -matrix is the matrix of all possible values of z that will be generated from all allowed combinations of MW and μ_{eff} . The schematic representation of the z -matrix is shown in Table 5.2. The x -vector of the z -matrix is the values of μ_{eff} evenly divided between -0.0010 and -0.0400 $\text{cm}^2 \text{V}^{-1} \text{min}^{-1}$ at 0.0001 unit increments, and will contain 391 elements. The y -vector of the z -matrix is the values of MW evenly divided between log MW 4.350 and 1.780 (22,300 and 60 Da) at 0.005 log unit increments, and will

Table 5.2. Schematic representation of the z-matrix.

$z = \frac{1}{k_{pH}} \mu_{eff} MW^{\frac{2}{3}}$		$\mu_{eff} \text{ (-0.001 to -0.0400)}$				
		μ_{eff_1}	μ_{eff_2}	μ_{eff_3}	μ_{eff_4}	$\mu_{eff_{max}}$
MW (log 4.350 to 1.780)	MW ₁	$z_{(1,1)}$	$z_{(1,2)}$	$z_{(1,3)}$	$z_{(1,4)}$	$z_{(1,max)}$
	MW ₂	$z_{(2,1)}$	$z_{(2,2)}$	$z_{(2,3)}$	$z_{(2,4)}$	$z_{(2,max)}$
	MW ₃	$z_{(3,1)}$	$z_{(3,2)}$	$z_{(3,3)}$	$z_{(3,4)}$	$z_{(3,max)}$
	MW ₄	$z_{(4,1)}$	$z_{(4,2)}$	$z_{(4,3)}$	$z_{(4,4)}$	$z_{(4,max)}$
	MW _{max}	$z_{(max,1)}$	$z_{(max,2)}$	$z_{(max,3)}$	$z_{(max,4)}$	$z_{(max, max)}$

contain 515 elements. The values of z (eq mol^{-1}) that would correspond to all combinations of MW_i and $\mu_{\text{eff}j}$ are calculated using equation 5.6 (with the most optimal value of k_{pH} according to procedure in section 5.2.4). The maximum possible number of z values that will be generated in the z -matrix is 201,365.

NOM is a very complex mixture of organic acids with a very wide distribution of MWs. Electropherograms of NOM are formed from coalescence of thousands of narrow peaks that represent the $z/\text{MW}^{2/3}$ for thousands individual acids. At any given pH, all of the acids will have charges between 0 to upwards of -60 (Bartschat *et al.*, 1992). Because the CDM will solve for the most probable values of z , integer and fraction values of z were expected to be generated considering all 201,365 combinations of MW and μ_{eff} . All fractional values of z were rounded to the nearest 0.5 unit within the z -matrix. Due to the complexity of NOM, it is expected that at any given pH a large portion of acidic functional groups on NOM solutes are in rapid equilibrium between their protonated acids (H_XA) and their conjugate bases (H_{X-1}A^-),



that is controlled by the pH of the carrier solution and the pK_{a} s of the acidic functional groups. The calculated half-integer values of z are considered as the partial ionization of acidic functional groups.

5.2.3 P-matrix.

The P-matrix is the matrix of $P(z)$ for all values of z that were generated in the z -

Table 5.3 Schematic representation of the P-matrix.

$P(z) = P(MW) \times P(\mu)$		$P(\mu)$				
		$P(\mu_1)$	$P(\mu_2)$	$P(\mu_3)$	$P(\mu_4)$	$P(\mu_{\max})$
$P(MW)$	$P(MW_1)$	$P_{(1,1)}$	$P_{(1,2)}$	$P_{(1,3)}$	$P_{(1,4)}$	$P_{(1, \max)}$
	$P(MW_2)$	$P_{(2,1)}$	$P_{(2,2)}$	$P_{(2,3)}$	$P_{(2,4)}$	$P_{(2, \max)}$
	$P(MW_3)$	$P_{(3,1)}$	$P_{(3,2)}$	$P_{(3,3)}$	$P_{(3,4)}$	$P_{(3, \max)}$
	$P(MW_4)$	$P_{(4,1)}$	$P_{(4,2)}$	$P_{(4,3)}$	$P_{(4,4)}$	$P_{(4, \max)}$
	$P(MW_{\max})$	$P_{(\max,1)}$	$P_{(\max,2)}$	$P_{(\max,3)}$	$P_{(\max,4)}$	$P_{(\max, \max)}$

matrix. The schematic representation of the P-matrix is shown in Table 5.3. The x-vector of the P-matrix is the probability of all values of μ_{eff} ($P(\mu)$)—as modeled by the filtered 3-GL model, between -0.0010 and -0.0400 $\text{cm}^2 \text{V}^{-1} \text{min}^{-1}$ at 0.0001 unit increments, and will contain 391 elements. The y-vector of the P-matrix is the probability of all values of MW ($P(\text{MW})$)—the mole distribution of MWs derived from the filtered 3-G model—between log MW 4.350 and 1.780 at 0.005 log unit increments, and will contain 515 elements. $P(z)$ for each combination of MW_i and $\mu_{eff,j}$ is calculated using equation 5.5.

Any value of $P(\text{MW})$ or $P(\mu)$ that equals zero (outside the range of the filtered 3-G or 3-GL model) will automatically result in $P(z) = 0$ for z of that specific combination of MW and μ_{eff} . An additional boundary condition was applied to the P-matrix. The z/MW of acetic acid ($z = -1$; $\text{MW} = 60 \text{ Da}$) was arbitrarily set as the maximum charge-to-mass value that may exist. A carboxyl group ($-\text{COOH}$) has a MW of 45 Da. By forcing the minimum z/MW to be 60, all carboxyl groups are forced to be attached to a minimum of one $-\text{CH}_2-$ unit ($\text{MW} = 14$), preventing the prediction of unrealistic structures such as $\text{C}(\text{COOH})_4$. All values of z in the z -matrix that will produce a z/MW smaller than $-1/60$ will have a corresponding $P(z) = P(\text{MW}) \times P(\mu)$ for that combination of MW and μ_{eff} . $P(z)$ will be automatically filtered to equal zero if a value of z is calculated (using equation 5.4) that violates the $-1/60$ z/MW boundary condition even if both $P(\text{MW})$ and $P(\mu) > 0$. For example, the singly-charged ion of oxalic acid ($-1/90$) may exist; the doubly-charged ion of oxalic acid ($-2/90$) is in violation of the $-1/60$ boundary condition and $P(z)$ will be filtered to equal zero.

5.2.4 Optimization of k_{pH} .

The Solver tool was used to target the most optimal value of k_{pH} that would force all values of z in the z -matrix (equation 5.4) to conform to the charge conservation equation (equation 5.3).

5.3 Results of the Charge Distribution Model.

5.3.1 Optimized values of k_{pH} .

The optimal values of k_{pH} were solved for in the CDM so that charge conservation was maintained between Q_{pH} , the MW distribution, the electropherogram, and values of z in the z -matrix. The optimized values of k_{pH} for each sample (Tables A.1-A.8) are plotted against their respective pHs in Figure 5.2. Values of k_{pH} at $pH > 7$ are markedly different than k_{pH} at $pH < 7$ in each sample. k_{pH} is erratic below pH 4. k_{pH} sharply increases between pH 4 and 5-6, decreases between pH 6-7, then becomes more-or-less constant at $pHs > 7$.

The graphs of k_{pH} vs. pH for Fractions 3-7 in Figure 5.2 remarkably resemble the plot of electroosmotic flow (EOF) velocity vs. pH shown in Figure 2 of Garrison *et al.* (1995). If the data points for k_{pH} below pH 4 for the SRNOM and Fractions 1 and 2 were discarded, those samples will have the similar trend. According to Garrison *et al.* (1995), the inner walls of fused silica capillaries, like those used in this work, have points of zero charge (PZC) between pH 3-5. EOF is retarded at $pHs < 4$. EOF significantly increases between pH 4-6 (as more silanol groups become negatively charged) and reaches its maximum around pH 6. Above pH 7, the EOF is lower than the maximum but remains constant thereafter with increasing pH.

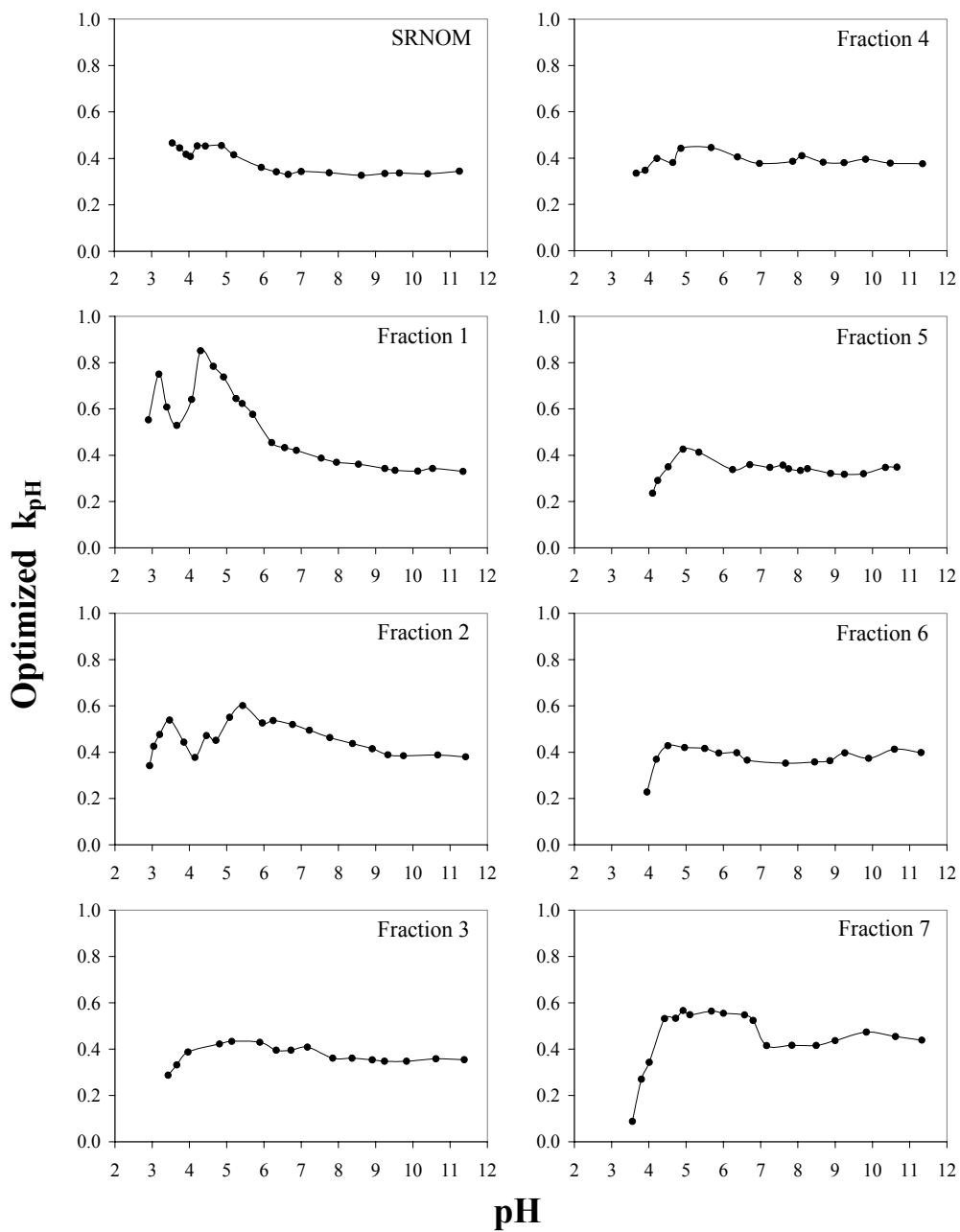


Figure 5.2. The optimized values of k_{pH} for the SRNOM and Fractions 1-7 as a function of pH.

Although the electropherograms for the SRNOM and Fractions 1-7 were very diverse, the similarities between Figure 5.2 and Figure 2 in Garrison *et al.* (1995) suggests that the separation efficiency of the samples in this work is strongly dependent on the EOF velocity. The variation between the optimized values of k_{pH} for the SRNOM and Fractions 1-7 is attributed to differences in MWs and Q_{pH} for the samples.

5.3.2 Charge distribution histograms.

The CDM allowed for the generation of all probable charges (z) from -0.5 to an unconstrained maximum value of z (rounded to the nearest half-integer) from all combinations of MW (3-G model), μ_{eff} (3-GL model), Q_{pH} (modified H-H model), and the optimized values of k_{pH} . The values of z in the z -matrix, their corresponding values of $P(z)$ in the P -matrix, and the MWs in the y -vector—corresponding to z and $P(z)$ —were first sorted by $P(z)$ in ascending order. All combinations of z , $P(z)$, and MW in which $P(z) = 0$ were removed from the sorted data. For a given set of 201,365 possible outcomes, approximately 20-40% of $P(z)$ equaled zero. The remaining data were sorted by z in ascending order. For a single value of z , its values of $P(z)$ were plotted against $\log MW$, forming a charge distribution histogram.

A charge distribution histogram represents a single charge (z), an integer or half-integer value. Half-integer values of z are treated as the charge from partially ionized acidic functional groups due to the rapid equilibrium between the protonated acidic functional group and its ionized form. The range of MWs under a single charge distribution histogram is the most probable range of MWs that are allowed to have that charge at a given pH, $P(z) > 0$. The CDM forbids all MWs outside of the MW range

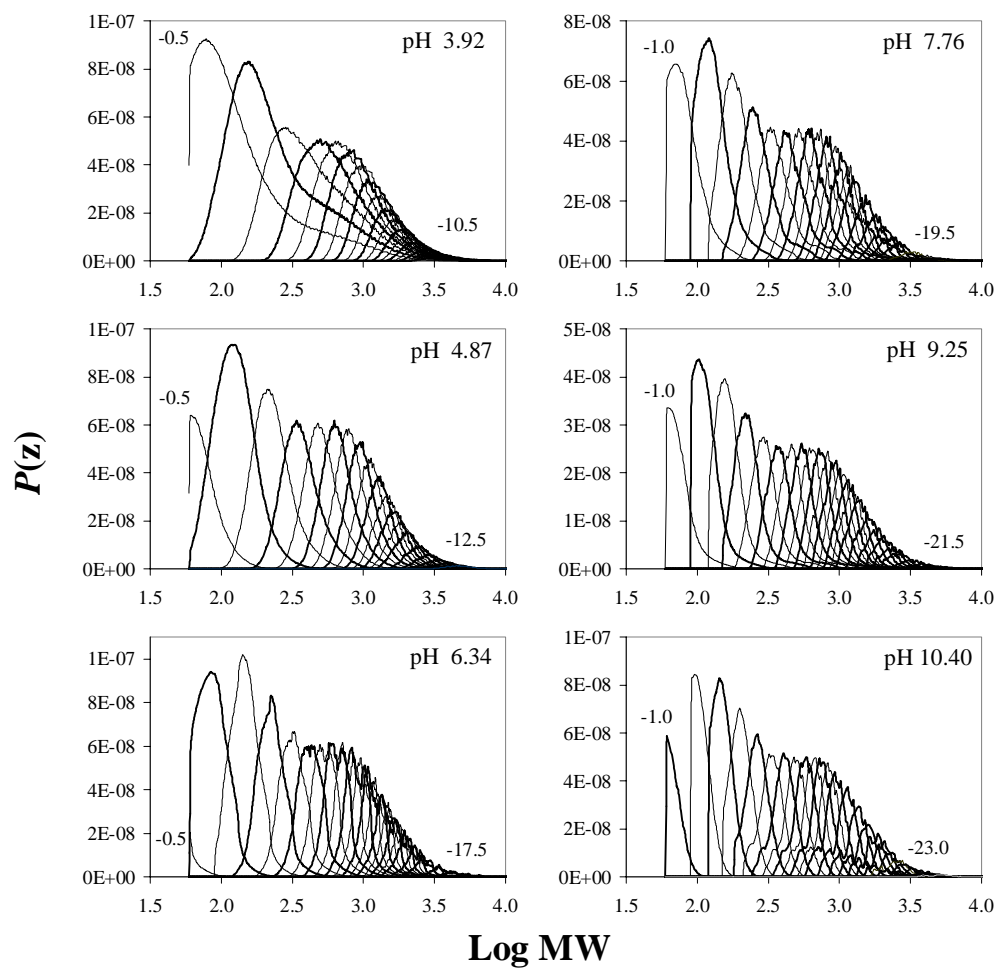


Figure 5.3. The subset of charge distribution histograms for the SRNOM.

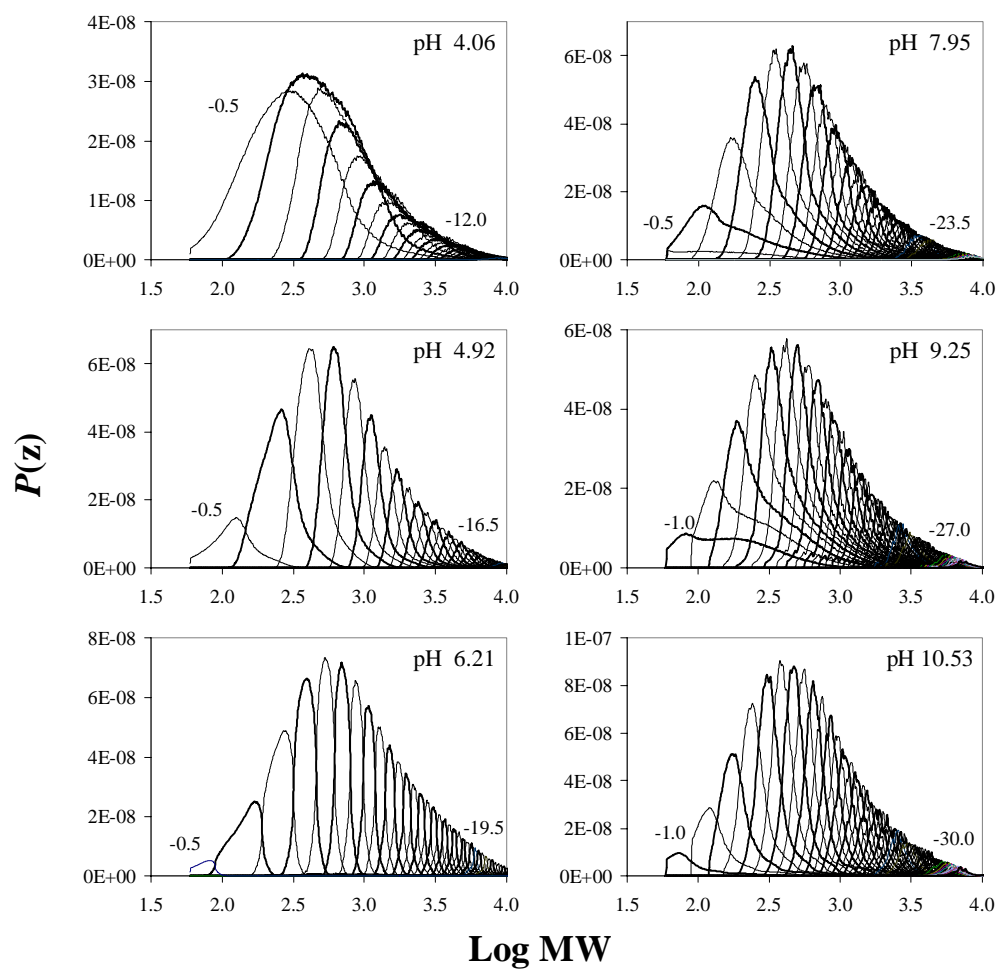


Figure 5.4. The subset of charge distribution histograms for Fraction 1.

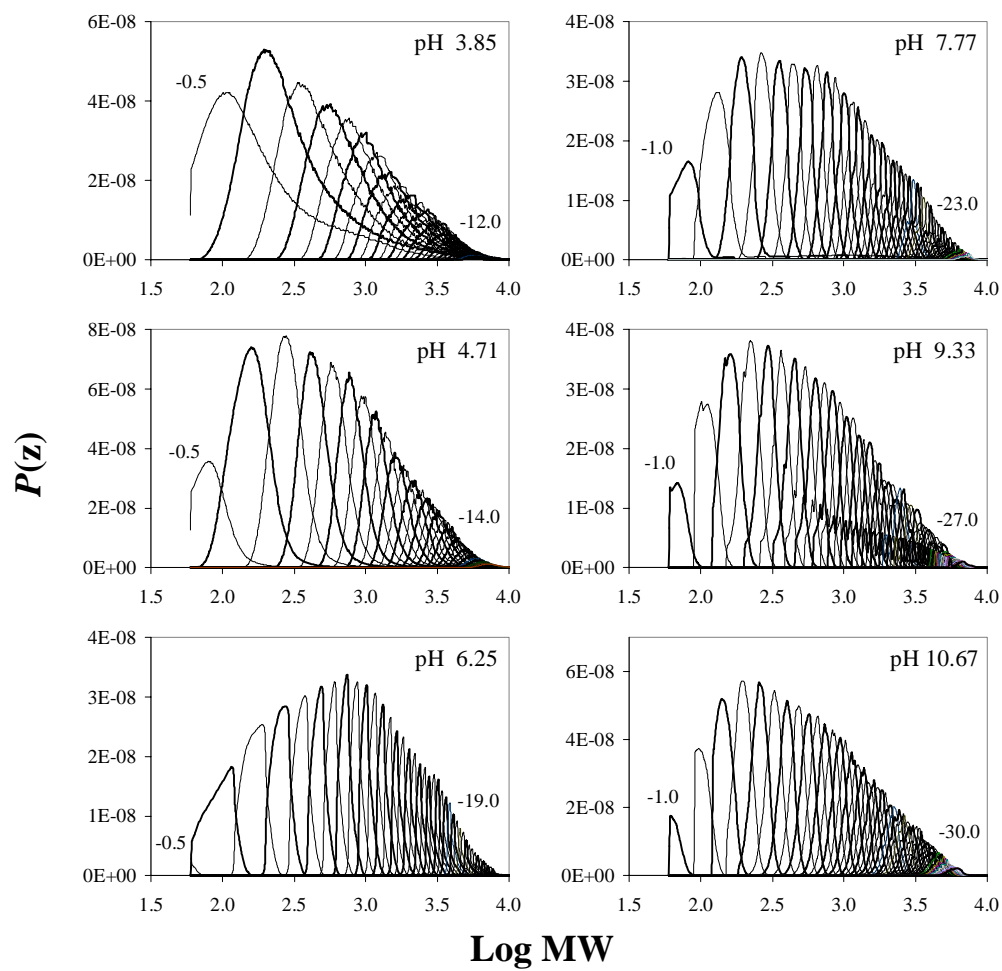


Figure 5.5. The subset of charge distribution histograms for Fraction 2.

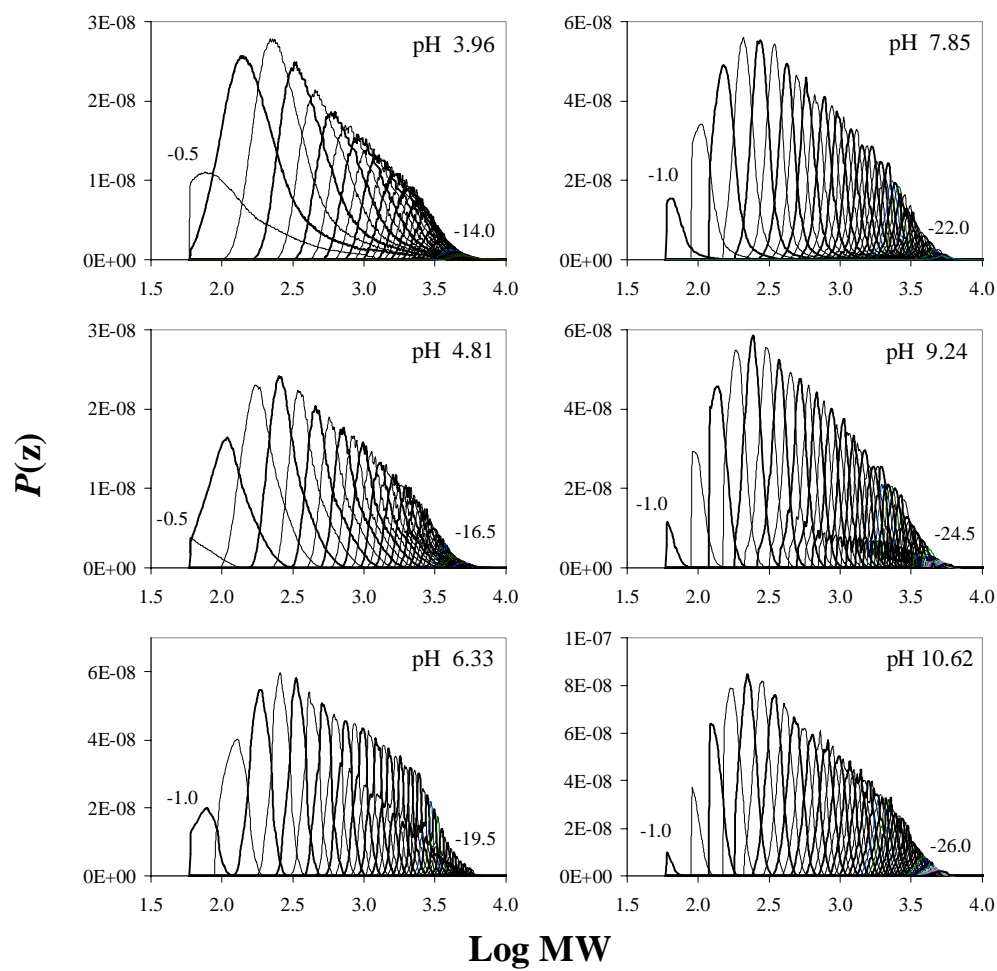
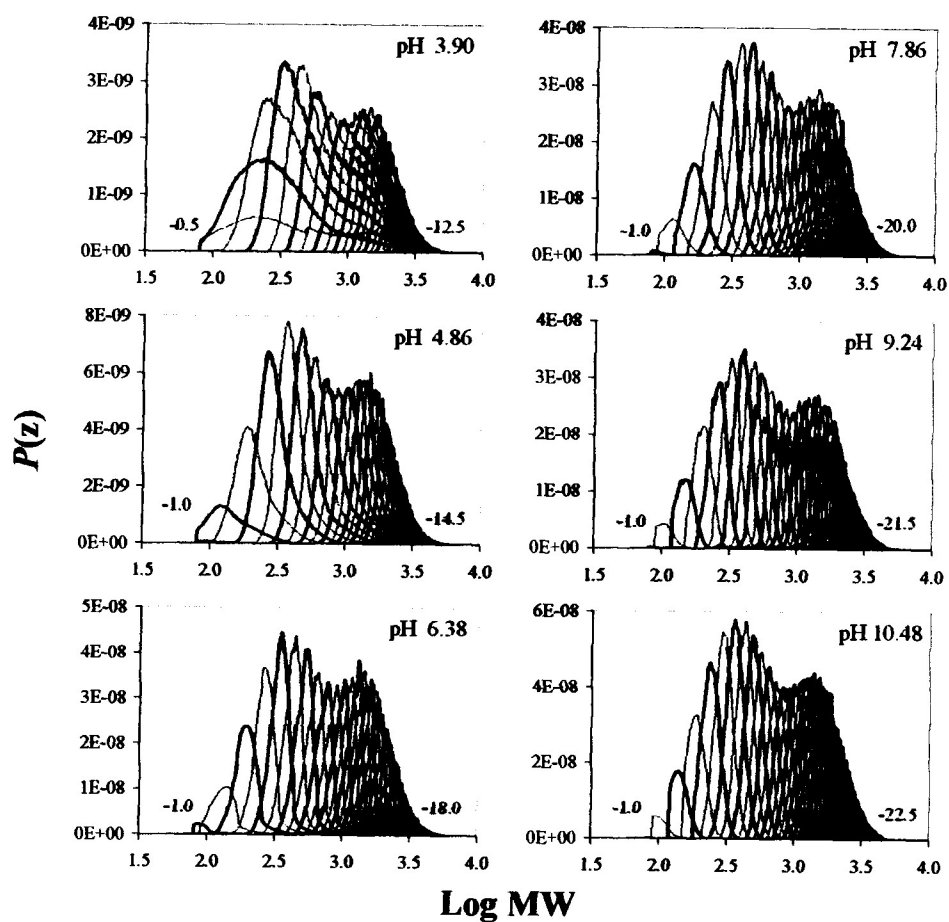


Figure 5.6. The subset of charge distribution histograms for Fraction 3.



Fraction 5.7. The subset of charge distribution histograms for Fraction 4.

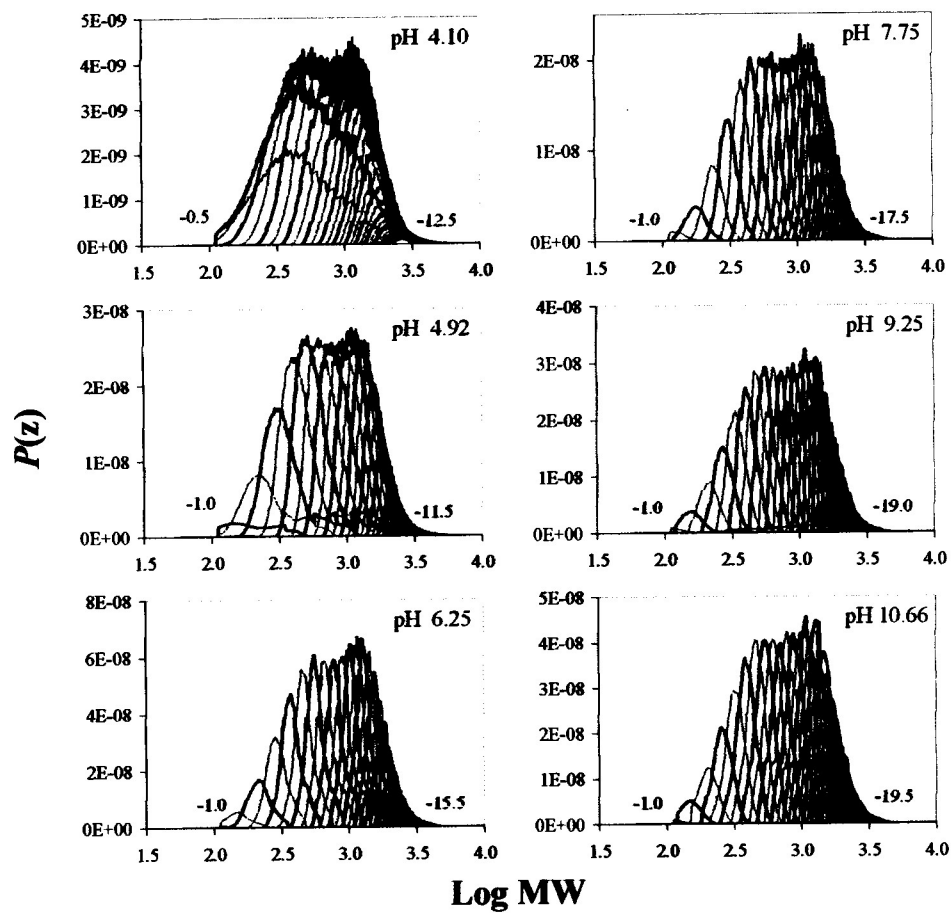


Figure 5.8. The subset of charge distribution histograms for Fraction 5.

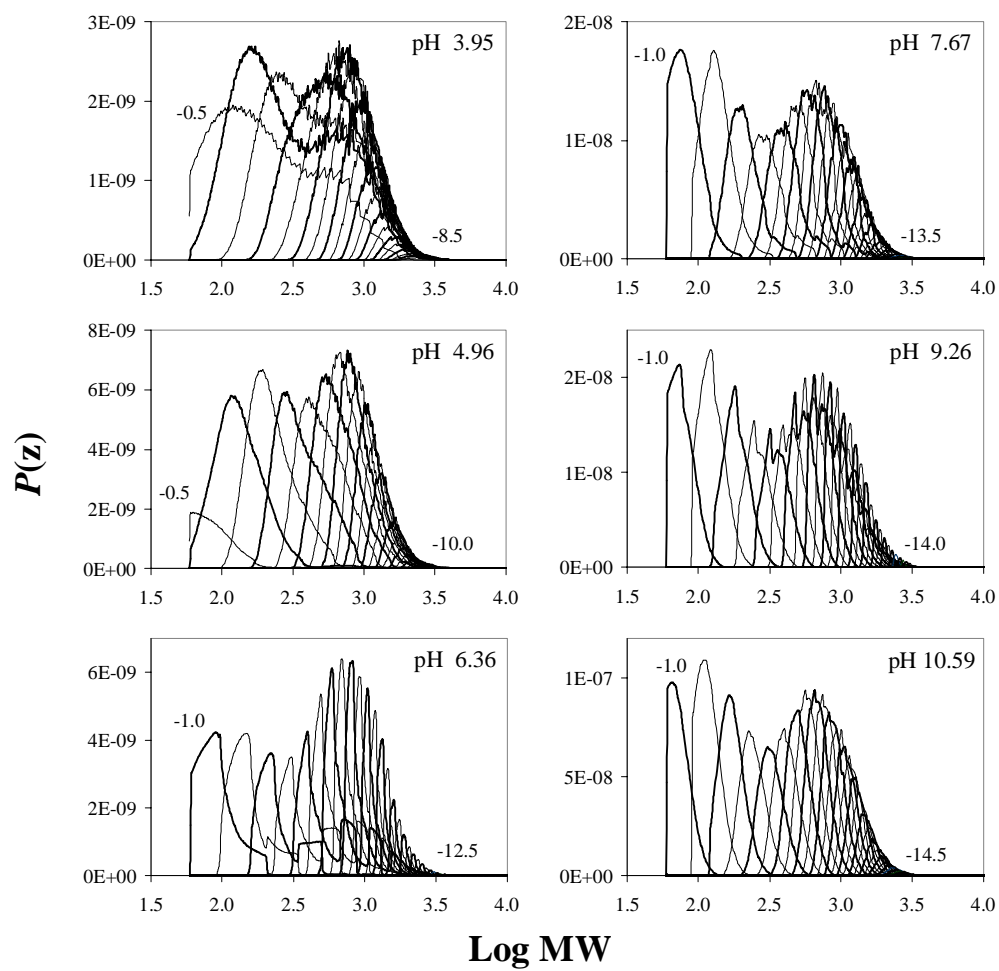


Figure 5.9. The subset of charge distribution histograms in Fraction 6.

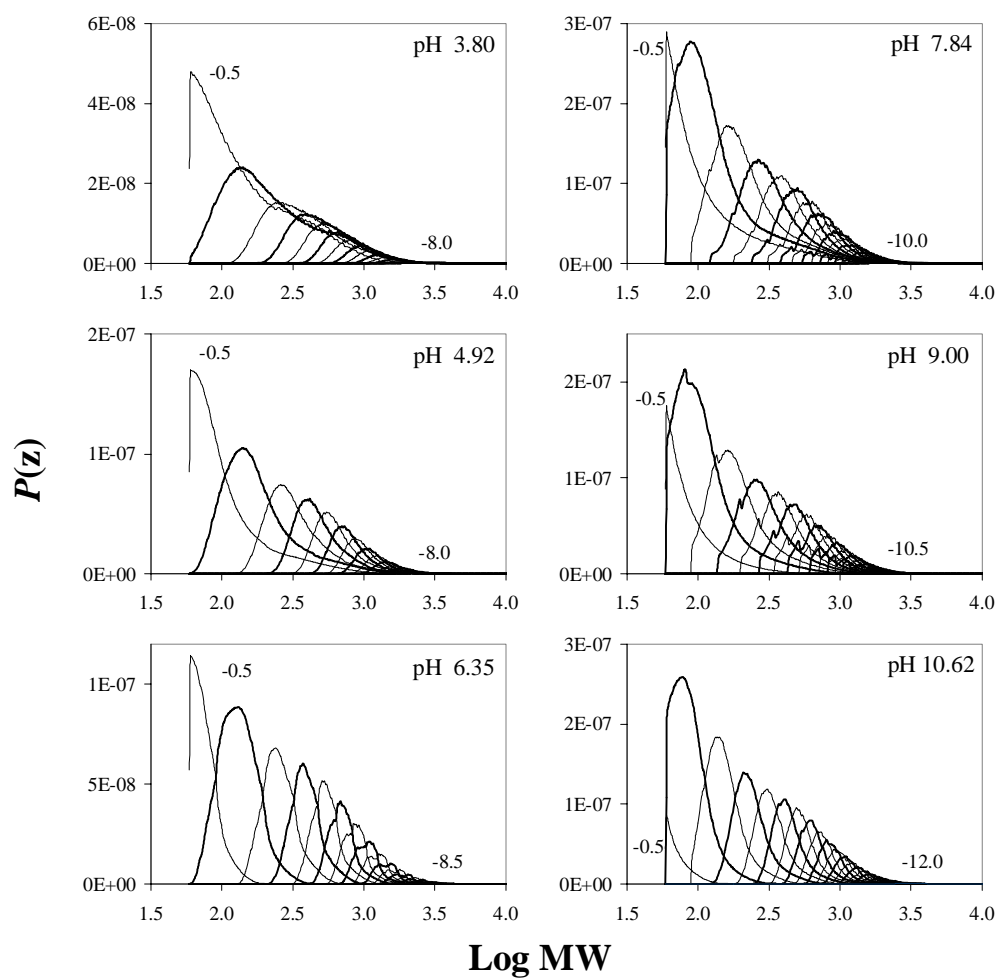


Figure 5.10. The subset of charge distribution histograms for Fraction 7.

under a charge distribution histogram from having that charge at that pH, $P(z) = 0$, for one of three reasons. That combination of z and MW (1) violates the $-1/60$ boundary condition, (2) cannot generate a value of $k_{pH} \frac{z}{(MW)^{2/3}}$ that is within the electropherogram, or (3) cannot conform to the conservation of charge with Q_{pH} .

A set of charge distribution histograms was created for all values of z from -0.5 (or the minimum) to the maximum z for each pH. Charge distribution histograms were created for all 15-22 analyses for the SRNOM and Fractions 1-7. For brevity, the charge distribution histograms ($P(z)$ vs. $\log MW$) for the subset of analyses for the SRNOM and Fractions 1-7 (see discussion in section 4.7.1) are shown in Figures 5.3-5.10. Figures 5.3-5.10 contain all histograms for all values of z between the most probable minimum and maximum charges as predicted by the CDM at each pH.

The shapes of charge distribution histograms are influenced by the shape and topography of their respective electropherograms. If electropherograms are symmetrical and pseudo-Gaussian in shape, histograms will be smooth and symmetrical (Figure 5.3: pH 4.87; Figure 5.5: pH 4.71). If electropherograms are Lorentzian-like, histograms will resemble very narrow oblique-like peaks (Figure 5.4: pH 6.21; Figure 5.5: pH 6.25). If electropherograms have significant tailing toward lower negative mobilities, histograms will have tailing at the higher $\log MW$ side (Figure 5.4: pH 7.95; Figure 5.8: pH 4.92). If electropherograms have a very large system peak or shoulder, histograms will have a prominent shoulder or spike to the low MW side of the histogram (Figure 5.9: pH 9.26; Figure 5.10: pH 9.00). If electropherograms have smaller system peaks or numerous fingerprint peaks, histograms will have a saw-tooth pattern near the crest of the histogram (Figure 5.8: pH 4.92).

Table 5.4. The most probable ranges of MWs contained within the charge distribution histograms for integer charges (z) between -1.0 and -10.0 for the SRNOM (Figure 5.3).

z	MWs					
	pH 3.92	pH 4.87	pH 6.34	pH 7.76	pH 9.25	pH 10.40
-1.0	75-4955	60-500	60-112	60-260	60-205	60-115
-2.0	195-6095	160-1215	120-590	120-645	120-500	120-270
-3.0	380-6530	315-2020	232-1025	185-1120	185-880	185-475
-4.0	605-7080	505-2885	365-1530	295-1660	290-1300	280-670
-5.0	860-7585	715-3675	525-2040	415-2190	410-1740	330-965
-6.0	1150-7850	945-4365	690-2570	555-2725	535-2190	440-1260
-7.0	1460-8220	1200-4965	880-3090	700-3200	685-2570	560-1590
-8.0	1800-8610	1495-5500	1085-3590	860-3630	840-3020	685-1910
-9.0	2190-8800	1800-6095	1305-4075	1035-4120	1010-3350	820-2240
-10.0	2600-9000	2140-6685	1550-4465	1230-4625	1190-3935	965-2600

Charge distribution histograms are not static. They will change in shape, in size, and in their ranges of MWs with changes in pH because Q_{pH} and electropherograms are different at different pHs. Solutes in NOM may only increase in charge (increased degree of ionization) or remain at the same charge with an increase in pH. The CDM allows for the possibility of all MWs to increase their charges with increasing pH. Because the MW distribution is assumed to be invariant with pH, charge distribution histograms will shift to lower MWs and contain narrower ranges of MWs with increases in pH. Simultaneously, new larger charge will become probable at the higher MWs. The limitation of the CDM is that it cannot predict what fraction of solutes will gain charge or remain at same charge with increasing pH—the CDM only predicts the most probable outcome.

For example, the ranges of MWs covered by the -1.0 to -10.0 charge distribution histograms for the SRNOM at the six pHs (in Figure 5.3) are shown in Table 5.4. At pH 3.92, the charge distribution histograms have the widest ranges of MWs of the pHs shown. The ranges of MWs, the minimum MW, and the maximum MW under each charge distribution histogram become progressively smaller as pH is increased from pH 3.80 to pH 10.40. The CDM restricts the MW ranges for smaller charges more than for larger charges. At pH 3.80, the CDM predicts that solutes with MWs of 75-4955 Da have probabilities of having a -1.0 charge. At pH 4.92, the CDM predicts that solutes with MWs of 60-500 Da may have a -1.0 charge—the solutes with MWs 501-4955 are forbidden to have a -1.0 charge at pH 4.92 ($P(z) = 0$). Solute at pH 4.92 with MWs > 501 Da must have charges of -1.5 or greater. By pH 10.40, the CDM predicts that only MWs of 60-115 may have a -1.0 charge—60 Da is the lowest permitted MW for the -

1/60 boundary condition, and 115 Da is the largest MW with a -1.0 charge that will generate a value of μ_{eff} that is present on the pH 10.40 electropherogram.

Charge distribution histograms of different charges will overlap. The CDM often predicts that a single value of MW will have probabilities of having multiple charges, though not necessarily with equal probability. For example, the CDM predicts that a solute in the SRNOM with a MW of 229 Da ($\log MW = 2.36$) has equal probability of having a -1.0 and -2.0 charge at pH 4.87, but has 2.5 times greater probability of having a -1.5 charge (Figure 5.3: pH 4.87). A solute with a MW of 750 Da ($\log MW = 2.88$) at pH 4.87 is allowed to have charges between -2.0 and -5.0, with -3.0 and -3.5 charges having the highest and equal probabilities. The -5.0 charge is the least probable charge because it has the lowest value of $P(z)$ for 750 Da.

The CDM only predicts the most probable charges for solutes with a discrete value of MW. In reality, those solutes may have only one, two, or all of the charges predicted by the CDM.

5.3.2 Mole distribution histograms.

Mass and charge must be conserved between the MW distribution, the electrophoretic distribution, and Q_{pH} . $P(MW)$ in the CDM was based on the mole distribution of MW, which represents 100% of the total number of moles of solutes in the sample. $P(\mu)$ in the CDM was based on the absorbance of the electropherograms (reproduced by the 3-GL model)—a mole distribution could not be determined for electropherograms because a single value of μ_{eff} may contain from one to dozens of different solutes of different MWs and values of z . The total number of moles of solutes

within an electropherogram, however, must equal the number of moles in the MW distribution. To remain consistent, all probable values of z across all 201,365 combinations of MW and μ_{eff} , solved for in the z -matrix and forced to conform with Q_{pH} , are distributed over the total number of moles of solutes in the sample. In theory, the integrated area represented under a charge distribution histogram ($P(z)$ vs. $\log MW$) is equal to the mole fraction of all solutes in the sample that have that unique charge at that pH.

Each charge distribution histogram was first integrated to determine its area (A_{z_i}), then all areas for all charge distribution histograms at that single pH were summed. The mole percent of all solutes in the sample that have a unique charge ($\%n_z$) was calculated using equation 5.7.

$$(5.7) \quad \%n_{z_i} = 100 \times \frac{A_{z_i}}{\sum_{i=-0.5}^{z_{max}} A_{z_i}}$$

Mole distribution histograms are created by plotting $\%n_z$ vs. z , and show the % mole abundances of solutes that have the most probable values of z at a single pH. Mole distribution histograms allow for immediate comparison between the charge distributions of the same sample at different pHs or between different samples at the same pH. Mole distribution histograms were created for all 15-22 analyses for each of the samples in this work. The subset of six mole distribution histograms for the SRNOM and Fractions 1-7 are shown in Figures 5.11-5.18.

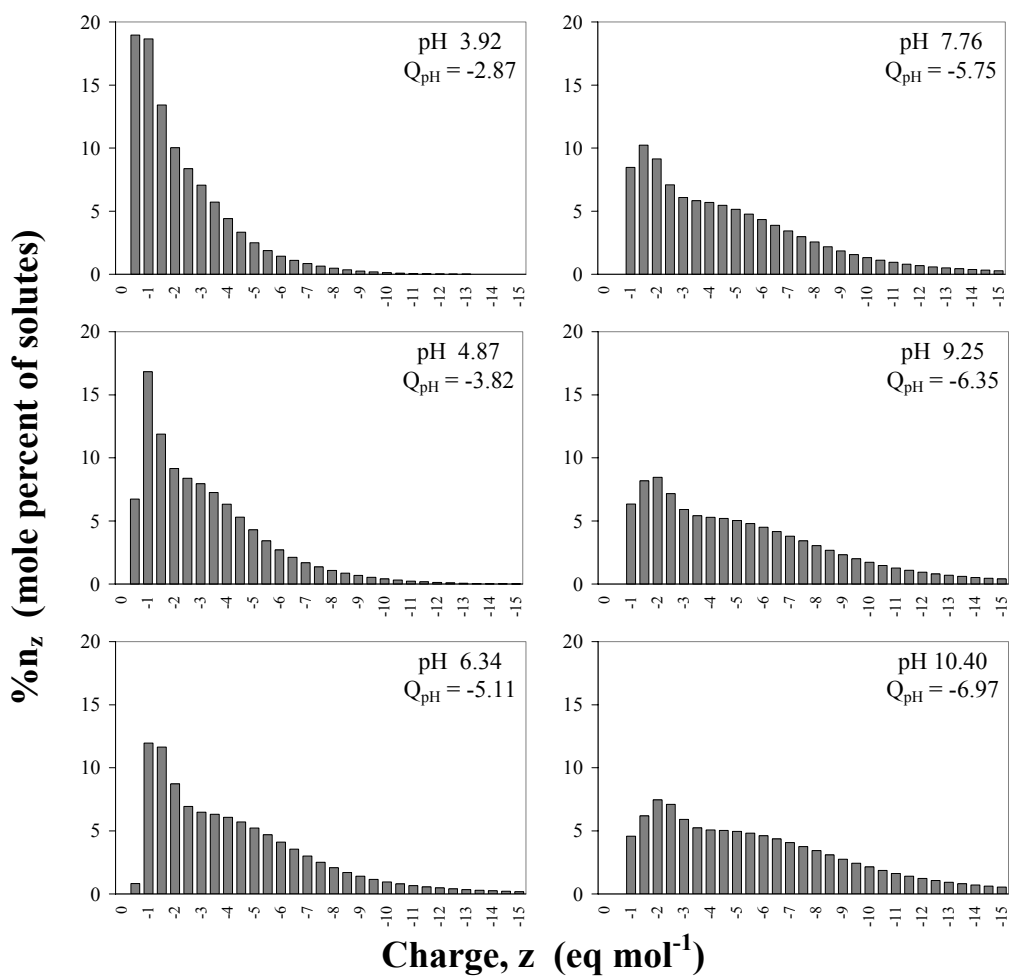


Figure 5.11. The subset of mole distribution histograms for the SRNOM.

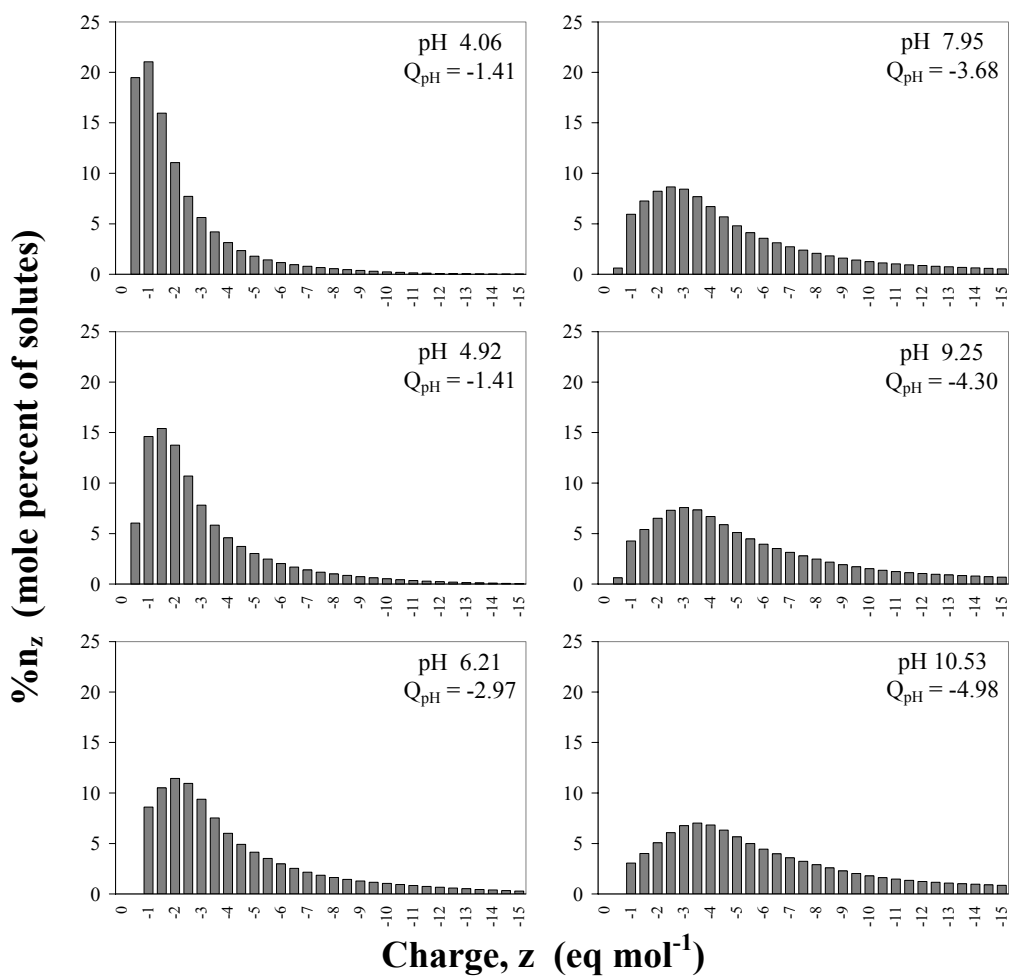


Figure 5.12. The subset of mole distribution histograms for Fraction 1.

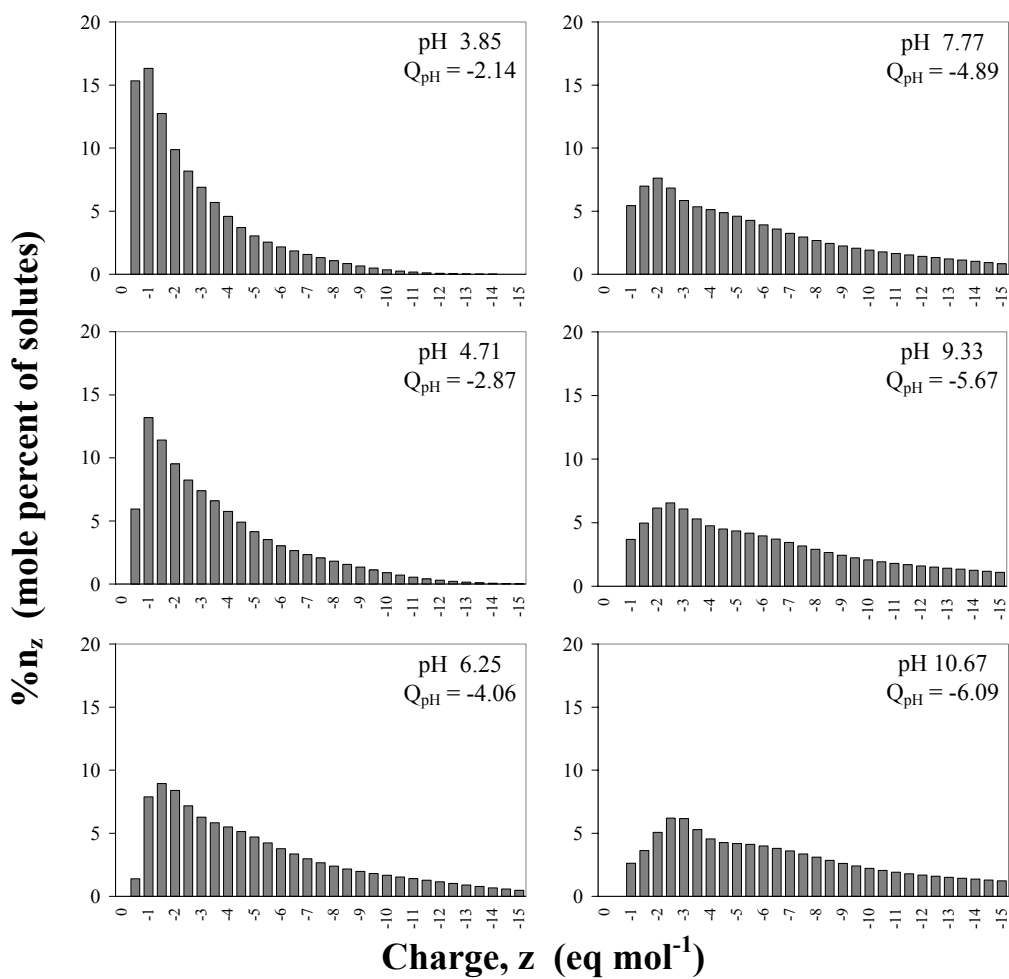


Figure 5.13. The subset of mole distribution histograms for Fraction 2.

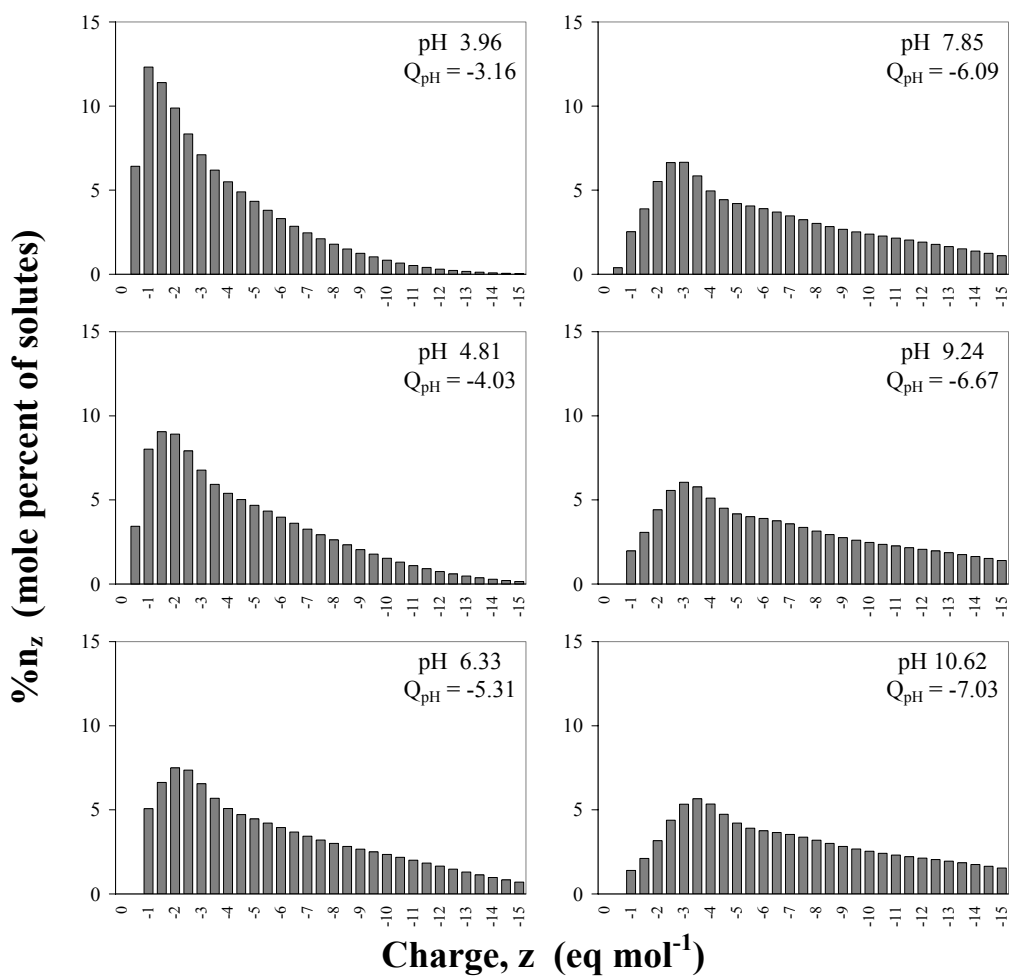


Figure 5.14. The subset of mole distribution histograms for Fraction 3.

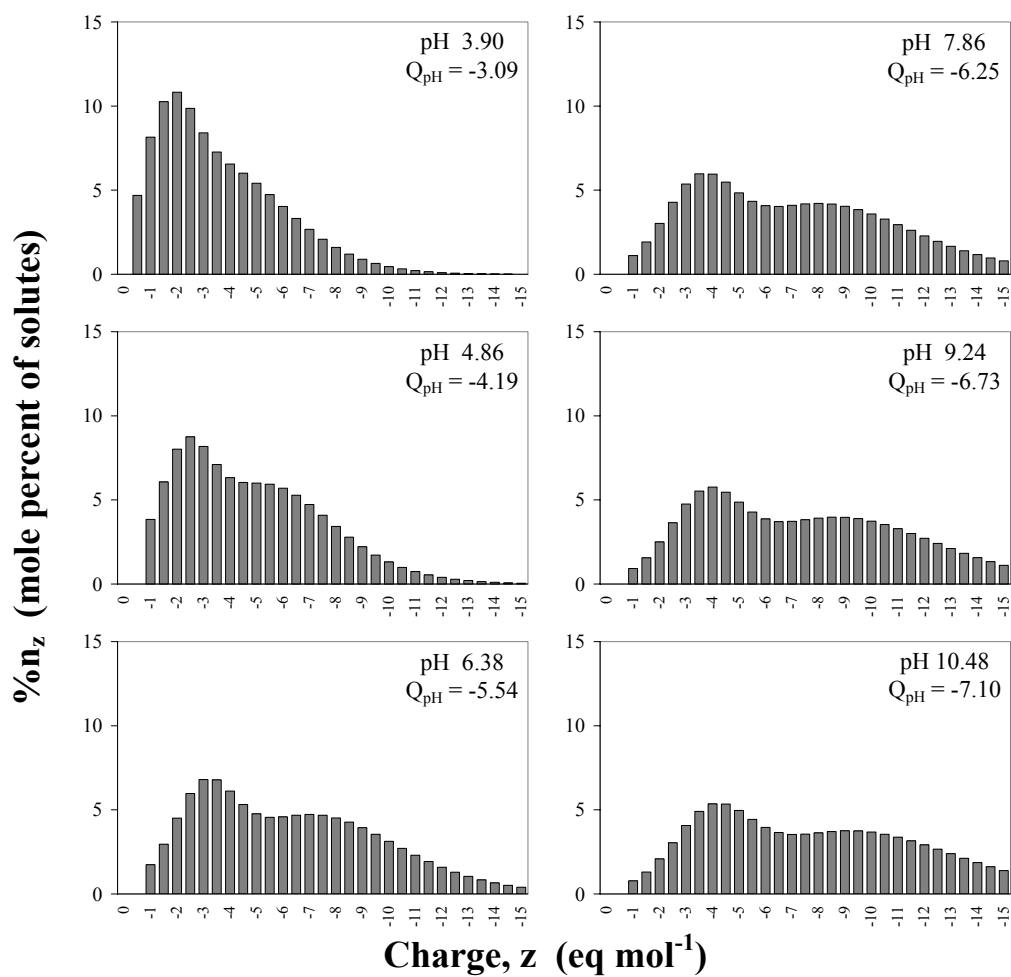


Figure 5.15. The subset of mole distribution histograms for Fraction 4.

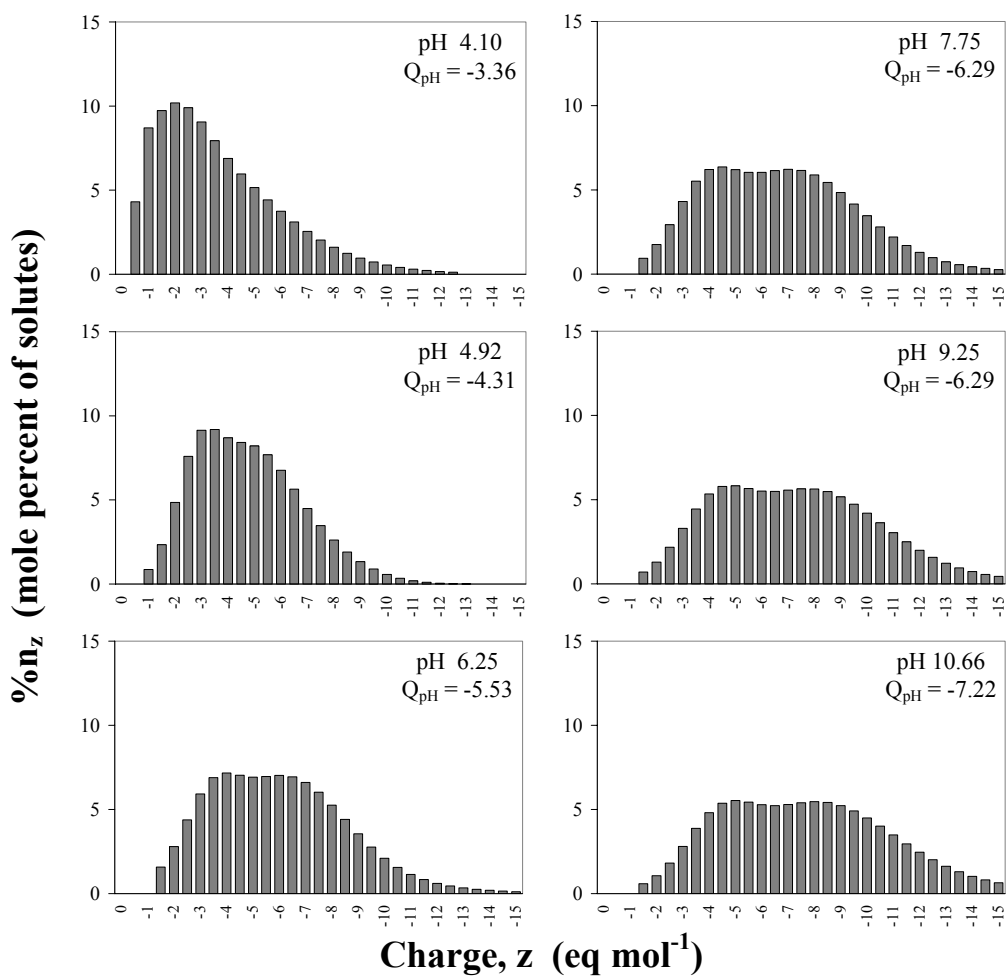


Figure 5.16. The subset of mole distribution histograms for Fraction 5.

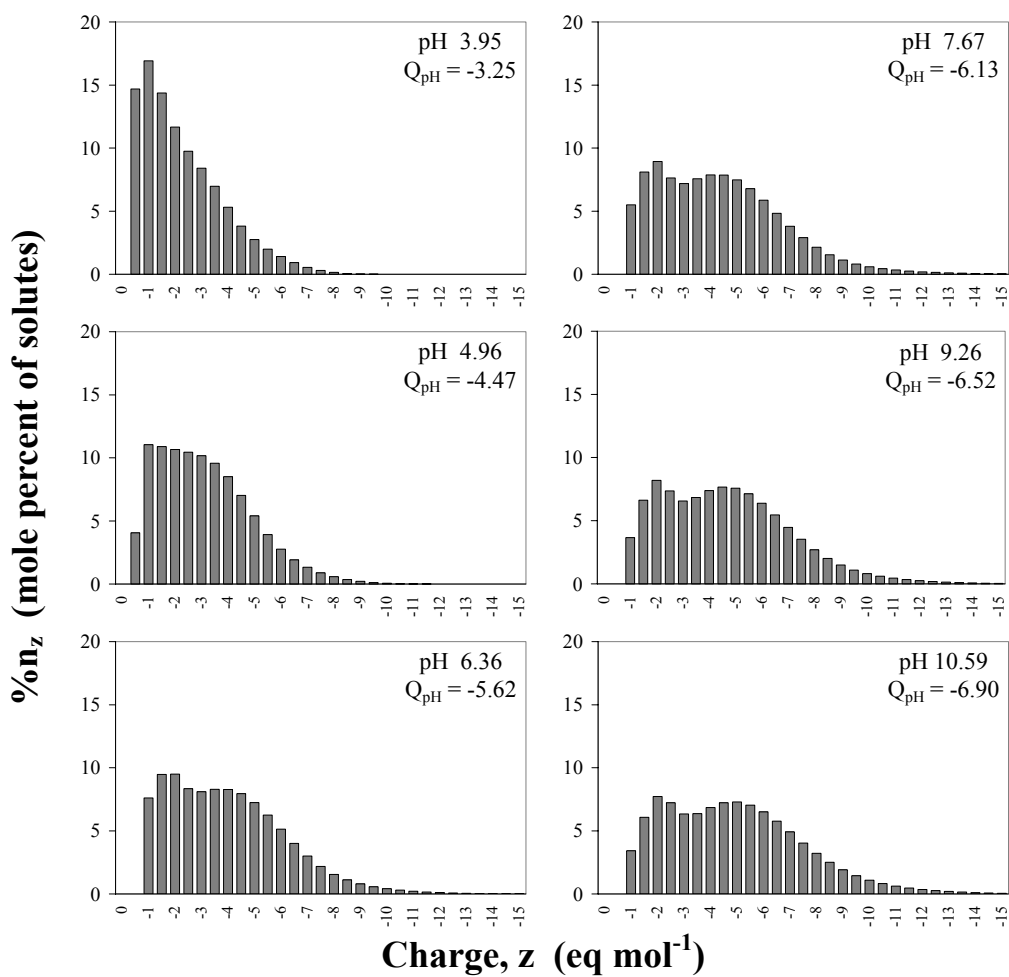


Figure 5.17. The subset of mole distribution histograms for Fraction 6.

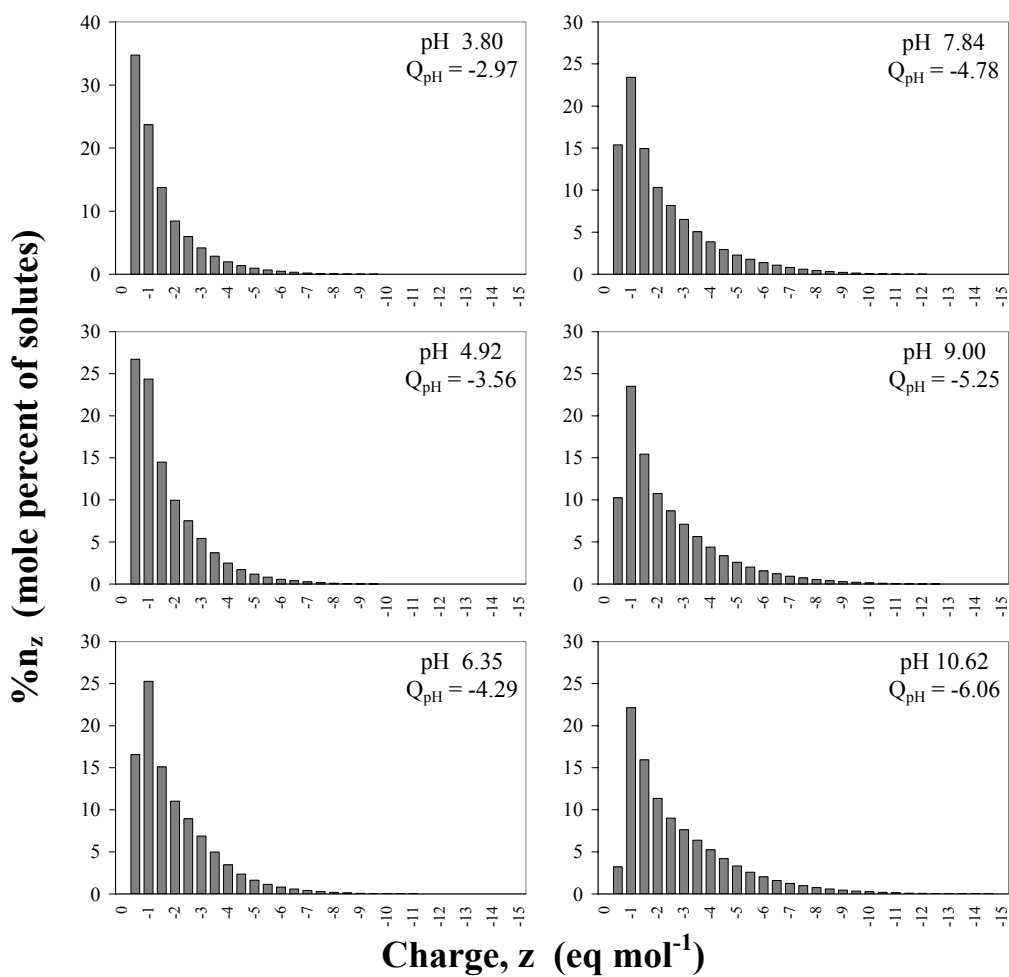


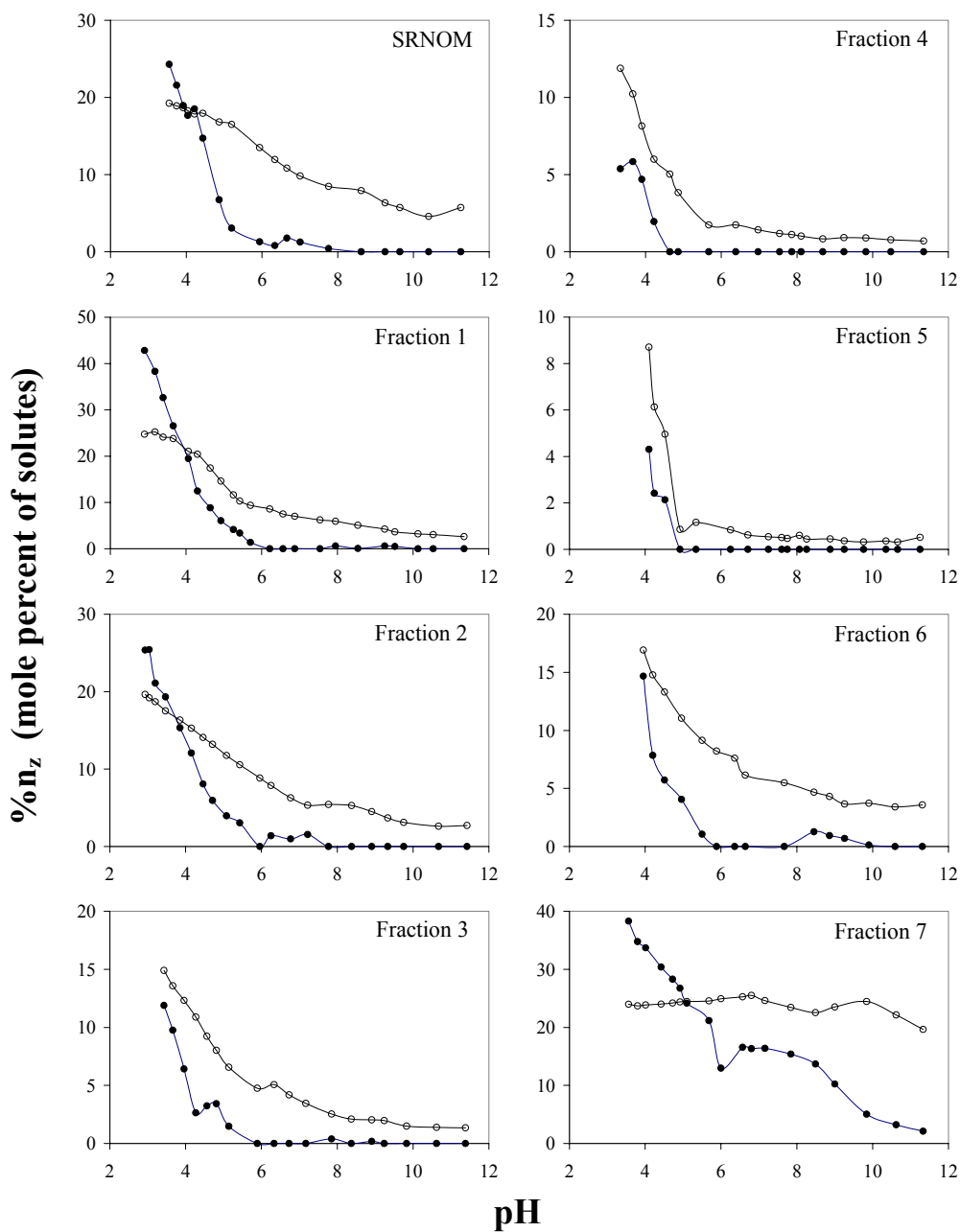
Figure 5.18. The subset of mole distribution histograms for Fraction 7.

5.4 The most probable distribution of charge.

5.4.1 Minimum probable charges.

Minimum probable charges for the SRNOM and Fractions 1-7 are strongly influenced by the lower-most mobility of the electropherograms. Electropherograms that are in close proximity to the zero effective mobility require very low values of z (-0.5, -1.0, and -1.5). At pH 3.8-4.1, electropherograms for the SRNOM and Fractions 1-7 have contact with the zero mobility and have relatively low values of μ_{eff} (Figures 4.22-4.29). Charge distribution histograms for -0.5 and -1.0 are the most ubiquitous for all samples at pH 3.8-4.1 (Figures 5.3-5.10) and for all analyses at pHs < 4.0 (not shown). The CDM predicts that almost every MW between 60 and 4000 Da for the SRNOM and Fractions 1-7 have some probability of having -0.5 and/or -1.0 charges. The -1.0 charge is generally the most abundant or second-most abundant charge at pH 3.8-4.1 (Figures 5.11-5.18). The CDM predicts that 34.8 and 23.7% of solutes in Fraction 7 (the fraction with the smallest MWs) will have a -0.5 and -1.0 charge (Figure 5.18). In contrast, the CDM predicts that only 4.3 and 8.7% of solutes in Fraction 5 (the most acidic sample) will have -0.5 and -1.0 charges (Figure 5.16).

As electropherograms are translated away from the zero effective mobility at higher pHs, the lowest values of z become less probable and lower in mole abundance, because greater values of z are required to generate the greater negative μ_{eff} within the electropherograms. By pH 4.7-4.9, electropherograms for the SRNOM and Fractions 2-6 have no contact with the zero mobility. Electropherograms for Fractions 1 and 7 have minimal contact with the zero mobility. Additionally, values of Q_{pH} at pH 4.7-4.9 tend to be 1.5 to 2 times greater than Q_{pH} at pH 3.8-4.1. The CDM predicts that charge



● -0.5; ○ -1.0

Figure 5.19. The %molar abundances of solutes in the SRNOM and Fractions 1-7 that have -0.5 and -1.0 charges.

distribution histograms for -0.5 and -1.0 are the ones most affected by the change in pH—much narrower ranges of probable MWs (see example in Table 5.3) and smaller areas. With the exception of Fraction 7, the %n_z for the -0.5 and -1.0 were much lower at pH 4.7-4.9 than at pH 3.8-4.1. For example, mole percents of solutes with -0.5 and -1.0 charges for Fraction 1 decreased from 19.5 and 21.0% to 6.0 and 14.6% between pH 4.06 and pH 4.92 (Figure 5.12). The CDM predicted that Fractions 4 and 5 (the most acidic samples with the greatest carboxyl concentrations) had zero probability of having solutes with a -0.5 charge at pH 4.7-4.9, making -1.0 their minimum probable charge at pHs > 5 (Figures 5.15 and 5.16). By pH 6.2-6.4, the CDM predicts that %n_z for the -0.5 charge for the other samples is either very small or is zero. With the exception of Fraction 7, -1.0 is the minimum probable charge at pHs > 7.

The values of %n_z for the -0.5 and -1.0 charge (for all data) were plotted as a function of pH (Figure 5.19). Values of %n_z for the -0.5 charge (solid circles) for the SRNOM and Fractions 1-6 generally decrease from their maximum values at pH 3-4 to zero, depending on the sample, between pH 5 and 7, making -1.0 the minimum probable charge for the SRNOM and Fractions 1-6 at pHs > 7. Because the SRNOM and Fractions 1-6 have zero probability of having a -0.5 charge above pH 7, this means that there are no monoprotic phenolic acids in those samples. All monoprotic acids must be carboxylic acids, and phenolic groups in those samples must be on solutes that have a minimum of one carboxyl group. The -0.5 charge for Fraction 7 linearly decreases with increasing pH, but never reaches zero below pH 11.4. All electropherograms for Fraction 7 at all pHs have some degree of contact with the zero mobility. Low effective mobilities coupled with very low MWs would force the CDM to predict that a -0.5 charge must be

present. If the very large nitrogen content in Fraction 7 is due to proteinaceous material from a biological contaminant, then the acid-base chemistry of the alkaline pHs could be partly due to amine groups—zwitterions (R-COO^- and R-NH_3^+) going to a full -1.0 charge with the releases of the amine acidic hydrogen in the pH 9-10.5 range.

The CDM predicts that all samples will have solutes with a -1.0 charge (open circles) at all pHs (Figure 5.19). With the exception of Fraction 7, $\%n_z$ for the -1.0 charge decreases with increasing pH and approaches an “asymptotic” minimum at high pH. The -1.0 charge for Fractions 4 and 5 (the most acidic samples) reaches their respective asymptotic minimums by pH 8. This would indicate that phenolic groups in Fractions 4 and 5 must be on solutes that have a minimum of two carboxyl groups, and all mono- and diprotic acids in Fractions 4 and 5 are carboxylic acids.

The $\%n_z$ for the -1.0 charge for Fraction 7 never approaches an asymptotic limit, but appears to be at steady state between pH 3.5 and 10.0—the quantity of solutes that complete their ionization from -0.5 to -1.0 equals the quantity of solutes that ionize from -1.0 to -2.0 at the next increase in pH.

5.4.2 Maximum probable charges.

The maximum probable charges on solutes in the SRNOM and Fractions 1-7 are influenced more by the samples' mole distributions of MW (the filtered 3-G model) and Q_{pH} than by their electropherograms. Bartschat *et al.* (1992) stated that 5-25% of the masses of humic substances are solutes with MWs greater than 10,000 Da, and have the potential to accumulate charges > -60 . In this work, approximately 0.3-8.2% of the total masses of the SRNOM and Fractions 1-3 are solutes with MWs $\geq 10,000$ Da. Fractions

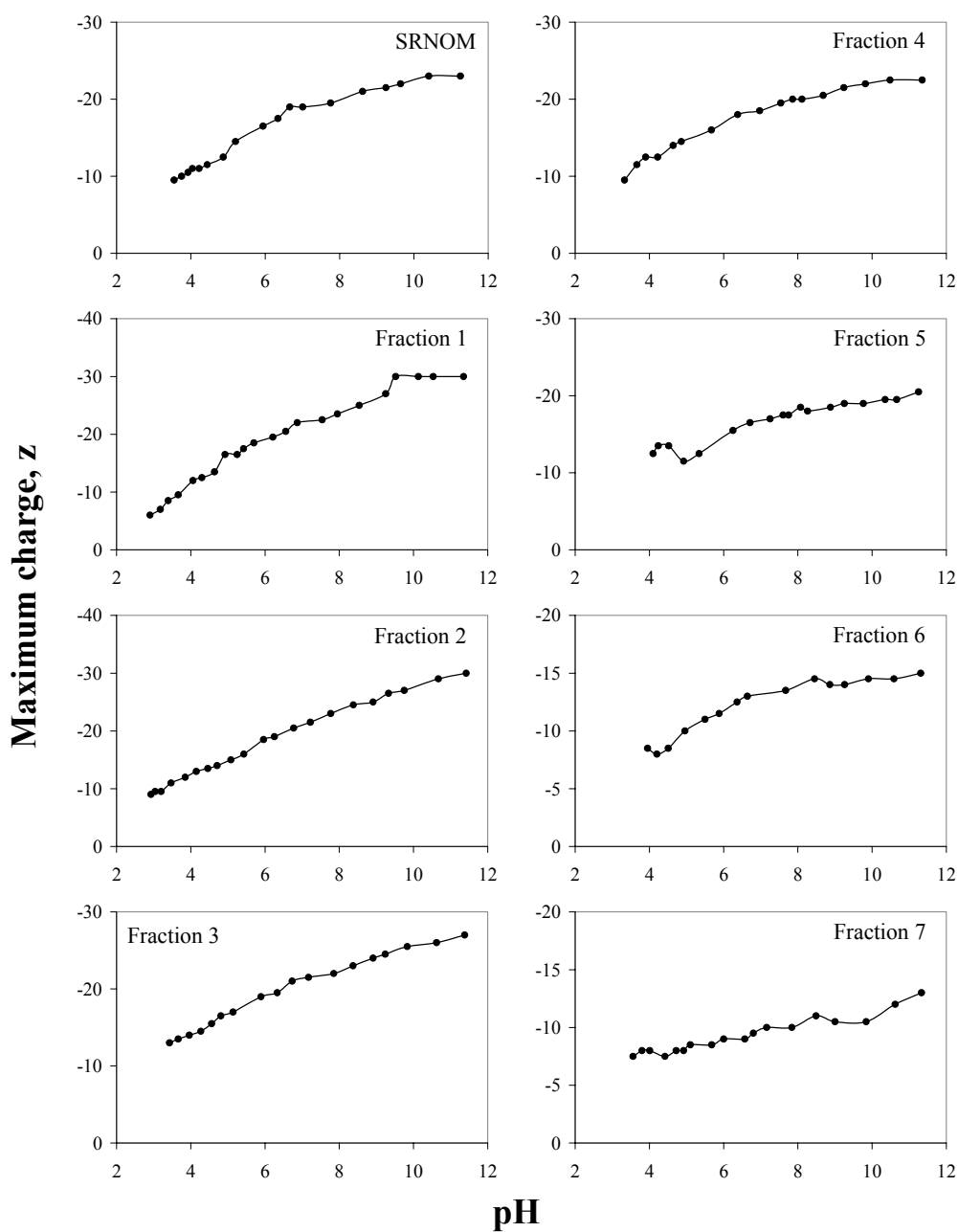


Figure 5.20. The maximum probable charges in the SRNOM and Fractions 1-7.

4-7 have no solutes with MWs > 10,000 Da—their respective maximum MWs are 8390, 6100, 4190, and 8600 Da. On a mole basis, approximately 0.01-0.7 % of solutes in the SRNOM and Fractions 1-3 have MWs > 10,000 Da, which means that $P(\text{MW})$ for solutes greater than 10,000 approaches zero or equals zero. The overall contributions of $\frac{z}{\text{MW}^{2/3}}$ for solutes with MWs > 10,000 (if present) to the electropherograms are insignificant compared to those with MWs < 10,000 Da.

Additionally, Q_{pH} , Q_1 and Q_{TOT} (carboxyl + phenolic) are inversely proportional to the average MWs for Fractions 1-6. It is expected that samples that contain the largest MWs (Fractions 1 and 2) will have the largest probable charges overall, but cannot have extremely large charges that are proportional to their largest MWs because of low Q_{pH} . Conversely, samples that are the most acidic (Fractions 4-6) cannot generate very large charges proportional to their large values of Q_{pH} because of their relatively smaller MWs.

The charge distribution histograms for the maximum charge for each sample (shown in Figures 5.3-5.11) represent less than ~ 0.03% of the total combined area of all histograms at that pH. The peak heights ($P(z)$) for the maximum charge histograms range between 0.1 and 0.3% of the peak height for the histograms of the most abundant charge. The CDM predicts that maximum charges for the samples increase with increasing pH because Q_{pH} increases and electropherograms are translated to greater negative mobilities.

The maximum probable charges (predicted by the CDM) for the SRNOM and Fractions 1-7 (for all data) were plotted against pH (Figure 5.20). The maximum probable charges for the SRNOM and Fractions 1-3 linearly increase between their respective minimum pHs (pH 3-4) and their maximum pHs (pH 11.2-11.4). In contrast,

the maximum possible charges for Fractions 4-6 linearly increase with increasing pH between their minimum pHs (pH 3-4) and pH 6, but appear to approach an asymptotic maximum limit as pH is increased from 6 to 11.2-11.4. This indicates, on a qualitative level, that solutes in Fractions 4-6 are approaching saturation with ionized carboxyl groups by pH 6-7. The concentrations of carboxyl groups (Q_1) for Fractions 4-6 are 5.5 to 6.5 times greater than the concentrations of phenolic groups (Q_2) (Table 4.13), thus the ionization of phenolic groups between pH 8 and 12 would have the most effect on the maximum charge if only the largest solutes were predicted to have phenolic groups.

Fractions 1 and 2 have the largest maximum charges of all samples at pH 11.2-11.4 ($z = -30$) even though Fraction 1 has average MWs that are 25% greater and Q_{pH} that is 20% less than those of Fraction 2. Fraction 7 (the sample with the smallest average MWs) has the smallest maximum charge ($z = -13.0$) at pH 11.2-11.4, even though Q_{pH} for Fraction 7 at pH 11.2-11.4 is 5% greater than Q_{pH} for Fraction 2. Maximum charges for Fraction 1 are limited by Fraction 1's small values of Q_{pH} , and maximum charges for Fraction 7 are limited by Fraction 7's small MWs.

5.4.2 The most probable distribution of carboxyl groups.

It is commonly assumed that only carboxylic acids ionize below pH 8.0 and only phenolic acids ionize above pH 8.0 (Bowles et al., 1989; Ritchie and Perdue, 2003). Electrophoretic separations were performed at pH 7.6-7.9 for the SRNOM and Fractions 1-7, from which the most probable distribution of charge was determined. Therefore, the distribution of carboxyl groups in the samples (assuming that pH 8.0 is the absolute endpoint for carboxyl group ionization) can be closely approximated from the mole

distribution histograms for pH 7.6-7.9. Charges on solutes, as predicted by the CDM, may be fractions (due to the rapid localized equilibria between the protonated acid and its conjugate base as controlled by pH and pK_a). Acid functional groups, however, must be integer values—half of a carboxyl group or half of a phenol cannot exist. For example, if the CDM predicts that a solute has a -2.5 charge, that solute will be treated as a triprotic acid (at that pH) with two fully ionized acid groups and one partially ionized acid group. At higher pH, the CDM may predict that same solute to carry a higher charge at a higher pH, like -3.5 or -4.5, at which point that solute will be treated as a tetraprotic or pentaprotic acid. It will be assumed that all half-integer values of z at pH 7.6-7.9 are partially ionized carboxyl groups that will reach its total ionization at pH 8.0.

First, all half-integer values of z were rounded to the next higher integer value of z (-0.5 rounded to -1.0, -1.5 rounded to -2.0, etc...). The $\%n_z$ values of the half-integer charge distribution histograms, rounded to the next higher integer, were then added to the $\%n_z$ values of the already present next higher integer. The resulting $\%n$ values (consistent as integer values) are now the distribution of carboxyl groups within the sample, and are plotted as $\%n$ (mole percent of sample) vs. n_{COOH} (number of carboxylic acid groups per solute) (Figure 5.21).

The distributions of carboxyl groups in the SRNOM, Fractions 1-3 are asymmetrical, with > 50% of solutes containing 1-5 carboxyl groups per solute. The relative abundances of solutes with 6 or more carboxyl groups decreases exponentially to up 20-25 carboxyl groups on the solutes with the largest MWs. Less than 6% of solutes the SRNOM and Fractions 1-3 have 15 or more carboxyl groups, however, ~16% of the total number of carboxyl groups are on solutes with 15 or more carboxyl groups. Gregor

et al. (1955) and Sutheimer *et al.* (1995) showed that titration curves of polyacrylic acids (PAA), with 40 to 100 carboxyl groups per molecule, are linear between pH 4 and 7. Even though Fractions 1 and 2 do not have solutes with more than 25 carboxyl groups, their titration curves (Figure 4.18) tend to be the most linear between pH 4 and 7. Carboxyl groups in Fractions 1 and 2 tend to be weakly acidic, with $\log K_1$ values of 4.7 and 4.4 (Table 4.13) which are more analogous to proton-binding constants for carboxyl groups in terrestrial HAs (Ritchie and Perdue, 2003) and not aquatic HAs or FAs. Sutheimer *et al.* (1995) experimentally verified that average pK_a s for polyacrylic acids, with MWs of 1000 to 5000 Da, range between 4.0 and 4.5. This may suggest that the highly carboxylated solutes (15-25 groups per solute) of larger MWs may behave like synthetic organic polymers—very similar carboxyl groups nearly evenly spaced along flexible organic solutes—adding the linear appearance to their titration curves in the carboxyl region. The titration curves for the largest MW fractions of humic acids isolated that were fractionated by sequential stage UF in the works of Christl and Kretzschmar (2001) and Tombácz (1999) are the flattest of their respective samples.

Conversely, Fractions 4 and 5—the most carboxyl rich samples—are dominated by solutes that have 4-10 carboxyl groups, and are nearly depleted in solutes that are predicted to have one and two carboxyl groups. Fraction 6 is nearly depleted in solutes with only one carboxyl group, and < 5% of solutes have 10 or more carboxyl groups. The titration curves for Fractions 4-6 have a more distinct curvature in the pH 5-7 range, where carboxyl group ionization is nearly complete, and a very steep region between pH 3-5. Carboxyl groups in Fractions 4-6 are more acidic than carboxyl groups in Fractions 1 and 2 based on their mean $\log K_1$ values in Table 4.13. Although Fractions 4-6 have

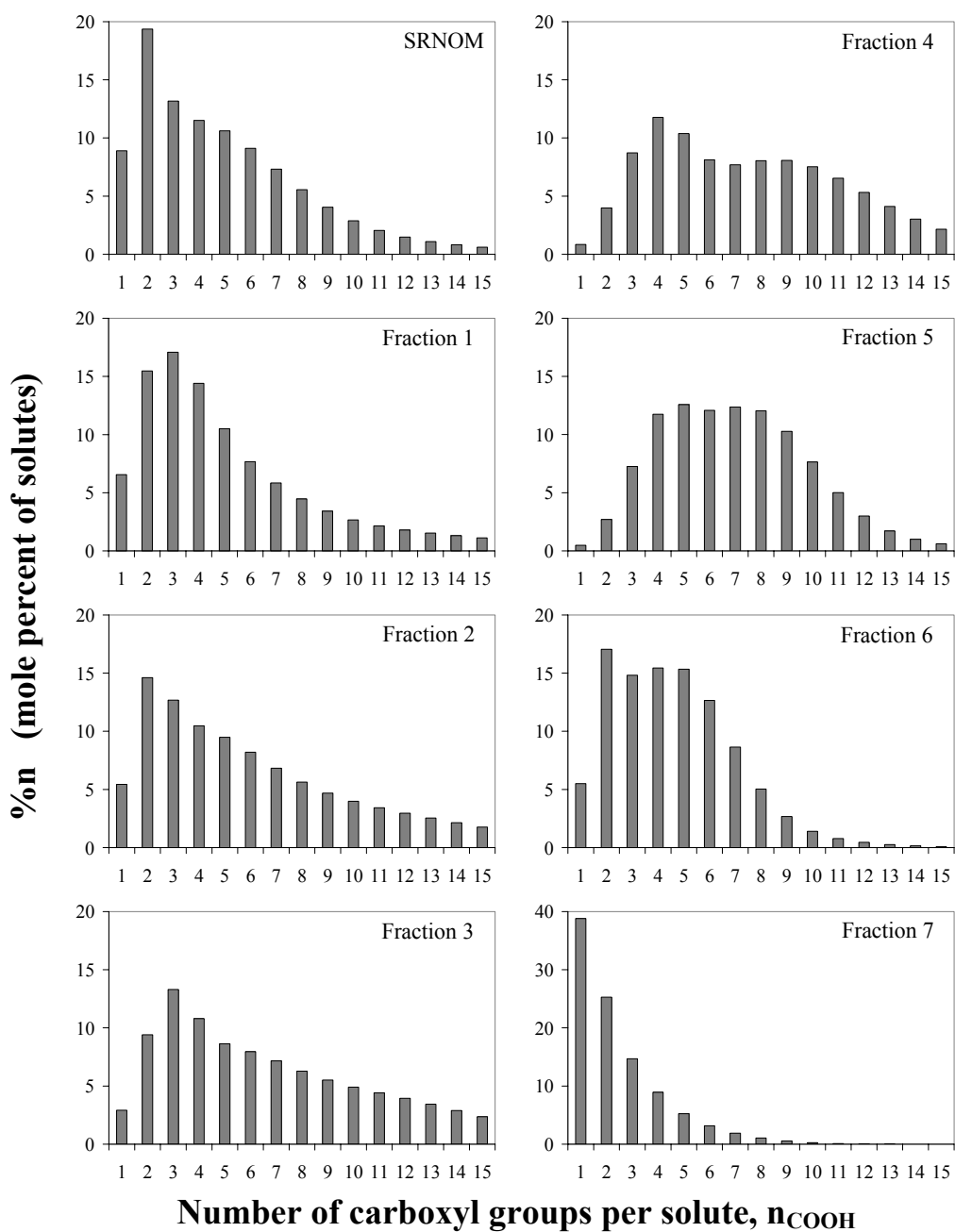


Figure 5.21. The most probable distribution of solutes with carboxylic acid groups in the SRNOM and Fractions 1-7.

the most narrow and symmetrical distributions of MWs (Figures 4.6 and 4.7), those samples probably have the most diverse assemblage of solutes containing carboxyl groups.

5.4.4 The most probable distribution of phenolic groups.

It is commonly assumed that only phenolic acid groups will ionize above pH 8.0. By pH 12.0, 100% of all acidic functional groups (carboxyl and phenolic) in NOM will be ionized (Bowles et al., 1989; Ritchie and Perdue, 2003). Electrophoretic separations were performed at pH 11.2-11.4 for the SRNOM and Fractions 1-7, from which the most probable distribution of charge was determined. The most probable distribution of carboxyl groups in the SRNOM and Fractions 1-7 (as discussed in section 5.4.3 and shown in Figure 5.21) will be the same at pH 11.2-11.4 as it was at pH 7.6-7.9—solute with seven carboxyl groups, for example, will still have seven carboxyl groups at pH 11.2-11.4. The resulting distribution of total acidic functional groups by pH 11.2-11.4 is, first-and-foremost, the underlying distribution of the carboxyl groups with the cumulative addition of phenolic groups.

First, all half-integer values of z at pH 11.2-11.4 were rounded to the next higher integer value of z (-0.5 rounded to -1.0, -1.5 rounded to -2.0, etc...). The $\%n_z$ values of the half-integer charge distribution histograms, rounded to the next higher integer, were then added to the $\%n_z$ values of the already present next higher integer. The resulting $\%n$ values (consistent as integer values) are now the distribution of all acidic functional groups within the sample, and are plotted as $\%n$ (mole percent of sample) vs. n_{TOT} (number of acidic functional groups per solute) (Figure 5.22).

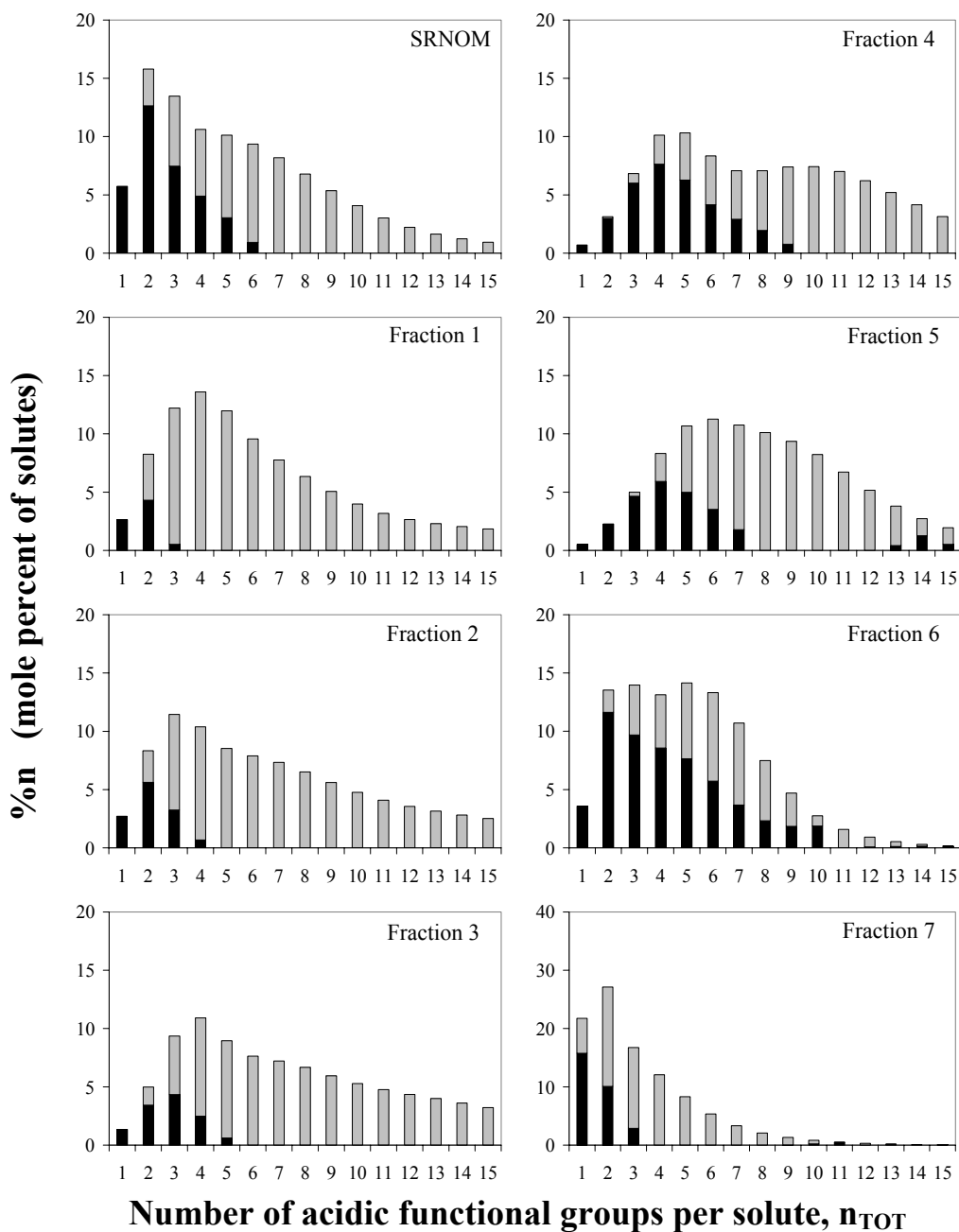


Figure 5.22. The most probable distribution of total acidic functional groups in the SRNOM and Fractions 1-7. Black bars represent the % of solutes with only carboxyl groups. Gray bars represent the % of solutes with carboxyl and ≥ 1 phenolic groups.

The change (+/-) of the heights of bars between those in Figure 5.21 (% solutes with n number of carboxyl groups) and Figure 5.22 reflects the redistribution of solutes due to the addition of phenolic groups. If solutes with five carboxyl groups, for example, were to have phenolic groups, then those solutes could possibly be represented in Figure 5.22 as $n_{TOT} = 5$ (5 carboxyls, 0 phenolic), $n_{TOT} = 6$ (5 carboxyls, 1 phenolic), and $n_{TOT} = 7$ (5 carboxyls, 2 phenolics). The most probable outcome is two classes of solutes: solutes with only carboxyl groups, and solutes with carboxyl and phenol groups. The exact distribution of phenolic groups on solutes cannot be absolutely determined, however, will be approximated according to the chain calculation scheme in the Appendix.

All monoprotic acids for the SRNOM and Fractions 1-6 are predicted to be carboxylic acids. Fraction 7 is the only sample that is predicted to have solutes with only one carboxyl group (no phenolic groups) and one phenolic group (no carboxyl groups). It is suspected, however, that the phenolic acidity is attributed to amine groups. All diprotic acids in Fractions 4 and 5, and the majority of diprotic acids in Fractions 2, 3, and 6, are dicarboxylic acids. Greater than 90% of solutes in Fractions 1-3 have carboxyl and phenolic groups. Fractions 1-3 have the fewest solutes with only carboxyl groups, due to those samples having large phenolic concentrations. Approximately 30% of the solutes in Fractions 4 and 5 (the most acidic samples), and 55% of solutes in Fraction 6, have the probability of having only carboxyl groups and no phenolic groups primarily due to their large carboxyl concentrations and low phenolic concentrations.

Overall, solutes with greater than 5-7 acidic functional groups are predicted to have both phenolic and carboxyl groups with very few to no solutes that have only

carboxyl groups. It is predicted, although unlikely, that Fraction 6 will have solutes with 10 carboxyl groups and zero phenolic groups. The exact ratios of carboxyl-to-phenolic groups per solute cannot be absolutely known, however, it is assumed that the number of carboxyl groups will be significantly greater than phenolic groups on the same solute.

Chapter 6

APPLICATION OF THE MOST PROBABLE

DISTRIBUTION OF CHARGE

6.1 Accurate calculations of ionic strength at high NOM concentrations.

$\sum_i z_i [Org^{z_i}]$ is defined as the total charge contribution of NOM to an aqueous solution at a given pH. $\sum_i z_i [Org^{z_i}]$ (eq L⁻¹) is calculated as the difference between the normal concentrations of the known cations and anions in aqueous solution using equation 1.2, and is equal to the the sum of the molar concentrations of NOM solutes across all charges at a given pH (equation 1.3). Direct titration methods are only able to determine the total contribution of charge by the NOM to the solution, and cannot determine the molar concentrations of the organic acids in the NOM nor their respective charges.

The simultaneous evaluation of direct titration data, electrophoresis data, and MW data by the Charge Distribution Model has probabilistically estimated every variable (z and $\sum_i [Org_i^{z_i}]$) on the right side of equation 1.3. All values of z on the right side of equation 1.3 are the most probable charges of solutes in the NOM (in half-integer increments) at a given pH. All values of $\sum_i [Org_i^{z_i}]$ are equal to the molar concentrations of solutes with those respective charges based on the mole % of solutes ($\%n_{z_i}$) from the mole distribution histograms.

The total molar concentration of NOM solutes (mol L^{-1}) in solution is equal to the dilution-corrected mass concentration of NOM (g L^{-1}) divided by the number-average MW, M_n (g mol^{-1}) (equation 6.1).

$$(6.1) \quad \sum_i [\text{Org}_i^{z_i}] = \frac{[\text{NOM}]}{M_n}$$

The molar concentration of solutes in the NOM sample with the unique value of z_i , $[\text{Org}_{n_{z_i}}^{z_i}]$, is calculated as

$$(6.2) \quad [\text{Org}_{n_{z_i}}^{z_i}] = \frac{\%n_{z_i}}{100} \times \frac{[\text{NOM}]}{M_n}$$

where $\%n_{z_i}$ is the mole percent of solutes with the unique charge z_i (eq mol^{-1}) at a given pH and $[\text{NOM}]$ is the dilution corrected concentration of NOM (g L^{-1}).

If equations 1.3 and 6.2 are combined, the rigorous calculation of total organic charge for a NOM sample in aqueous solution (eq L^{-1}) at a given pH is

$$(6.3) \quad \sum_i z_i [\text{Org}_i^{z_i}] = -0.5 [\text{Org}_{n_{-0.5}}^{-0.5}] - 1.0 [\text{Org}_{n_{-1.0}}^{-1.0}] - 1.5 [\text{Org}_{n_{-1.5}}^{-1.5}] \dots - z_{\max} [\text{Org}_{n_{\max}}^{z_{\max}}]$$

and the corresponding charge density (Q_{pH} , eq g^{-1}) is

$$(6.4) \quad Q_{pH} = \frac{\sum_i z_i [Org_i^{z_i}]}{[NOM]} = \frac{-0.5[Org_{n-0.5}^{-0.5}] - 1.0[Org_{n-1.0}^{-1.0}] - 1.5[Org_{n-1.5}^{-1.5}] \dots - z_{\max}[Org_{n_{\max}}^{z_{\max}}]}{[NOM]}$$

In laboratory experiments, direct titrations or metal-binding titrations are often performed on NOM solutions with concentrations of 1:1 background electrolytes ranging from 10^{-3} to 10^{-1} M. A stable ionic strength over the duration of a direct titration allows for the same activity coefficient that calculates concentrations for H^+ and OH^- from their respective activities using the Davies equation (equation 3.14) or the extended Debye-Hückel equation (Stumm and Morgan, 1996). The base or acid titrant is typically prepared at the same concentration as the background electrolyte to minimize the perturbation of ionic strength by the addition of the titrant to the bulk solution being titrated. The dilution-corrected concentrations of the additional strong base cations (Na^+ or K^+ from NaOH or KOH) or strong acid anions (Cl^- or NO_3^- from HCl or HNO_3) from the titrant, and the changes in $[H^+]$ and $[OH^-]$ concentrations are usually accounted for by most models or calculation schemes.

This work has shown that the charges of solutes, and the abundances of solutes with increasingly higher charges, increase with increasing pH. The charge contributions of the very concentrated solutions of NOM (100 mg L^{-1} to 2 g L^{-1}) that are required for accurate titrations in the laboratory, however, are often ignored (Marshall *et al.*, 1995), even though the total charge contribution of the NOM triples or quadruples during a titration from pH 3 to pH 11.

The accurate ionic strength of an NOM solution at each pH during a titration can now be very closely approximated, using equation 6.5, because the CDM has predicted the most probable distribution of charge (z) and the molar quantities of NOM solutes with

each charge are known.

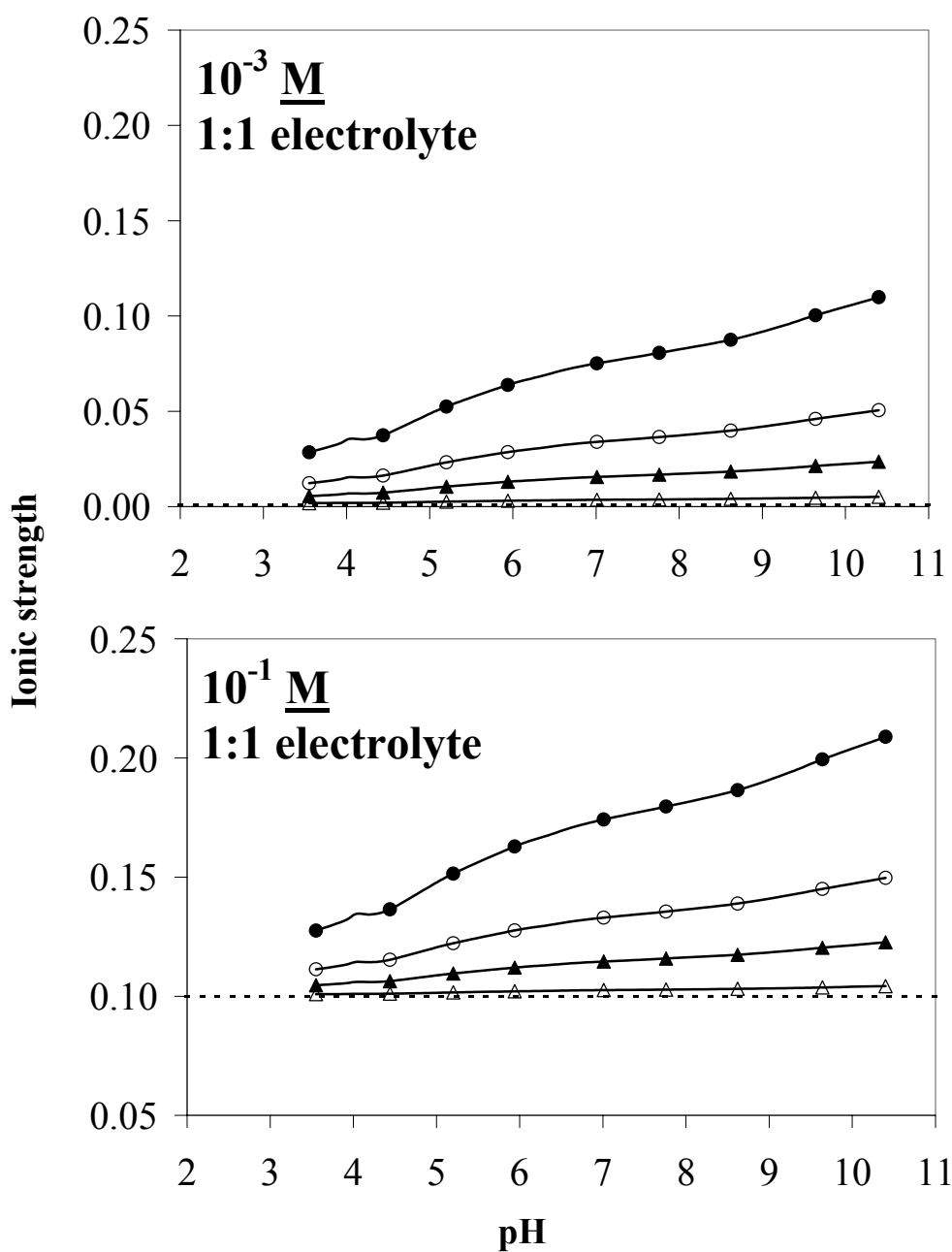
$$(6.5) \quad I = \frac{1}{2} \left([H^+] + \sum m^2 [Cations^{m+}] + [OH^-] + \sum n^2 [Anions^{n-}] + \right. \\ \left. (-0.5)^2 [Org_{n-0.5}^{-0.5}] + (-1.0)^2 [Org_{n-1.0}^{-1.0}] + (-1.5)^2 [Org_{n-1.5}^{-1.5}] \dots + (z_{max})^2 [Org_{n_{max}}^{z_{max}}] \right)$$

The effect of concentrated dissolved NOM on the ionic strength of aqueous solutions was tested using the most probable distribution of charge. The accurate ionic strengths are calculated for solutions containing four different concentrations of SRNOM (100, 500, 1000, and 2000 mg L⁻¹) in two different concentrations of 1:1 background electrolyte (10⁻³ and 0.10 M) over the pH range of 3.55 to 10.40—the 20 data points at which electrophoresis was performed. Values of *z* and %*n_z* for the SRNOM at the 20 pHs were determined by the Charge Distribution Model. A subset of *z* and %*n_z* data are reported in Table 6.1. The molar concentrations of SRNOM in solution is calculated using equation 6.1 (*M_n* = 815 g mol⁻¹, Table 4.4). Activity corrections for H⁺ and OH⁻ are iteratively solved for according to the procedure in section 3.6.2 using equations 3.14 and 3.15. Although the ionic strength is not expected to exceed 0.5, the activity coefficient corrections for H⁺ and OH⁻ using the Davies equation (equation 3.14) is valid up to maximum ionic strengths of ~0.5 (Stumm and Morgan, 1996). The resulting ionic strengths of the solutions are plotted against pH (Figure 6.1).

The actual ionic strengths of the solutions based on the different concentrations of SRNOM are always greater than the ionic strengths predicted by the concentration of the 1:1 background electrolyte (dashed line)—the greater the concentration of SRNOM, the greater the deviation from the assumed ionic strength to greater ionic strength. The ionic

Table 6.1. The mole percent of solutes ($\%n_z$) that have charge states (z) between -0.5 and -15.0 in the SRNOM (as shown in molar distribution histograms in Figure 5.11).

z	$\%n_z$					
	pH 3.92	pH 4.87	pH 6.34	pH 7.76	pH 9.25	pH 10.40
-0.5	19.1	6.9	0.9	0.7	0.0	0.0
-1.0	18.7	16.8	12.0	8.5	6.3	4.6
-1.5	13.4	11.9	11.6	10.2	8.2	6.2
-2.0	10.0	9.2	8.7	9.1	8.5	7.5
-2.5	8.4	8.4	6.9	7.1	7.2	7.1
-3.0	7.1	7.9	6.5	6.1	5.9	5.9
-3.5	5.7	7.3	6.3	5.8	5.4	5.2
-4.0	4.4	6.3	6.1	5.7	5.3	5.1
-4.5	3.3	5.3	5.7	5.5	5.2	5.0
-5.0	2.5	4.3	5.2	5.1	5.0	5.0
-5.5	1.9	3.4	4.7	4.8	4.8	4.8
-6.0	1.4	2.7	4.1	4.3	4.5	4.6
-6.5	1.1	2.1	3.5	3.9	4.2	4.4
-7.0	0.8	1.7	3.0	3.4	3.8	4.1
-7.5	0.6	1.3	2.5	3.0	3.4	3.8
-8.0	0.5	1.1	2.1	2.6	3.0	3.4
-8.5	0.4	0.9	1.7	2.2	2.7	3.1
-9.0	0.3	0.7	1.4	1.9	2.3	2.8
-9.5	0.2	0.5	1.2	1.6	2.0	2.4
-10.0	0.1	0.4	0.9	1.3	1.7	2.1
-10.5	0.1	0.3	0.8	1.1	1.5	1.9
-11.0	0.0	0.2	0.7	0.9	1.3	1.6
-11.5	0.0	0.2	0.6	0.8	1.1	1.4
-12.0	0.0	0.1	0.5	0.7	0.9	1.2
-12.5	0.0	0.1	0.4	0.6	0.8	1.1
-13.0	0.0	0.0	0.3	0.5	0.7	0.9
-13.5	0.0	0.0	0.3	0.4	0.6	0.8
-14.0	0.0	0.0	0.3	0.4	0.5	0.7
-14.5	0.0	0.0	0.2	0.3	0.5	0.6
-15.0	0.0	0.0	0.2	0.3	0.4	0.5
> -15	0.0	0.0	0.1	1.2	2.1	2.8



● 2000 mg L⁻¹; ○ 1000 mg L⁻¹; ▲ 500 mg L⁻¹; △ 100 mg L⁻¹.

Figure 6.1. The effect of the SRNOM at four different concentrations on the ionic strength of aqueous solutions prepared in 10^{-3} and 10^{-1} M 1:1 background electrolyte at 25 °C. The horizontal dashed line represents the concentration of the 1:1 background electrolyte.

strengths at each concentration increased with increasing pH due to the increasing concentrations of solutes with greater z and the z^2 term in the ionic strength equation.

If the SRNOM is neglected, γ for H^+ and OH^- is ~ 0.968 for the 10^{-3} M 1:1 electrolyte solution. If the SRNOM is considered (at 2000 mg L^{-1}) in the 10^{-3} 1:1 electrolyte, the initial ionic strength of the solution at pH 3.55 is 0.029, or 29 times greater than the predicted ionic strength if SRNOM is neglected. By pH 10.4, the same solution has an ionic strength of 0.110, or 110 times greater than predicted by the background electrolyte concentration alone. The activity coefficients (γ) for H^+ and OH^- will range from ~ 0.852 at pH 3.5 to ~ 0.776 at pH 10.4.

The effect of the non-static ionic strength during the course of a pH titration (between pH 3 and 11) is lessened by performing titrations in solutions of 0.1 M background salts with the more dilute concentrations of NOM, like the 100 mg L^{-1} . The ionic strength of the 10^{-1} M 1:1 electrolyte solution with 100 mg L^{-1} SRNOM increases from 0.101 to 0.106 between pH 3.55 and 10.4, with γ ranging from 0.781 to 0.778. These are very minor deviations from $I = 0.100$ and $\gamma = 0.782$ if the SRNOM is neglected.

The conventional calculation of $\sum_i z_i [Org^{z_i}]$, and the corresponding values of Q_{pH} , is by the electroneutrality equation (equation 1.2). The accurate ionic strength of the aqueous solution is directly impacted by the concentration of NOM, especially at high concentrations. However, only H^+ and OH^- in equation 1.2 are directly affected by ionic strength. $\sum_i z_i [Org^{z_i}]$ is strongly dependent on $[H^+]$ at low pHs (3-5) and $[OH^-]$ at high pHs (9-11) because those are the dominant inorganic cations and anions in the bulk solution. Strong anions and cations, such as those from the base titrant (Na^+ or K^+ from

NaOH and KOH), are insensitive to changes in pH or ionic strength. At neutral pHs (5-9), $\sum_i z_i [Org^{z_i}]$ is directly proportional to the dilution-corrected molar concentrations of Na^+ or K^+ because $[H^+]$ and $[OH^-]$ are very small. As a result, the ionic strength corrections of $\{H^+\}$ and $\{OH^-\}$ to their respective molar concentrations in the bulk solution in the presence of NOM is only effective at low pH and high pH. The underprediction of ionic strength underpredicts $[H^+]$ and $[OH^-]$, which will underpredict $\sum_i z_i [Org^{z_i}]$ at low pH and overpredict $\sum_i z_i [Org^{z_i}]$ at high pH. Those corrections have little or no effect on the calculation of $\sum_i z_i [Org^{z_i}]$ by equation 1.2 in the neutral pHs and the overall appearance of titration curves are not significantly different except at the very high and low pHs. The vertical offset of titration curves at different ionic strengths (where Q_{pH} across all pHs is greater at higher ionic strengths) probably cannot be reconciled even by the ionic strength corrections alone. Electrostatic parameters, such as those described by Benedetti *et al.* (1996) and Christensen *et al.* (1998) for the NICA-Donnan model, are used to conform titration curves at different ionic strengths into a single “master curve”.

6.2 Treatment of Ionic Strength by the Major Proton-binding Models.

The details of the Models V and VI (Tipping and Hurley, 1992; Tipping, 1998) and the NICA-Donnan (Non-ideal competitive absorption) model (Kinniburgh *et al.*, 1996; Benedetti *et al.*, 1996; Milne *et al.*, 2001) are described elsewhere. The use of ionic strength in those models will be briefly discussed in perspective to the findings in this work.

6.2.1 Model V and model VI.

Model V and Model VI incorporate the effect of ionic strength on the interpretation of titration data into two calculations: (1) the calculation of the Donnan volume, and (2) the calculation of intrinsic proton (or metal) binding constants.

Unlike the H-H model used in this work, Models V and VI invoke an electrostatic diffuse layer, or Donnan volume (V_D), around all NOM solutes that forces the ionized acidic functional groups in NOM to be in electroneutrality with an enrichment of H^+ or cations inside that Donnan volume and not with the bulk solution. The Donnan volume (V_D) is calculated using equation 6.6, assuming that all solutes in NOM have a spherical geometry and the same MW (equal to M_n).

$$(6.6) \quad V_D = \frac{4\pi}{3} \times \frac{M_n}{N_A} \times \left(\left(r + \frac{1}{\kappa} \right)^3 - r^3 \right)$$

M_n	number-average MW (g mol^{-1})
N_A	Avogadro's number (mol^{-1})
K	Debye-Hückel parameter (m^{-1})
r	radius of the average NOM solute (m)

The Debye-Hückel parameter, κ (m^{-1}), in equation 6.6 is calculated using equation 6.7,

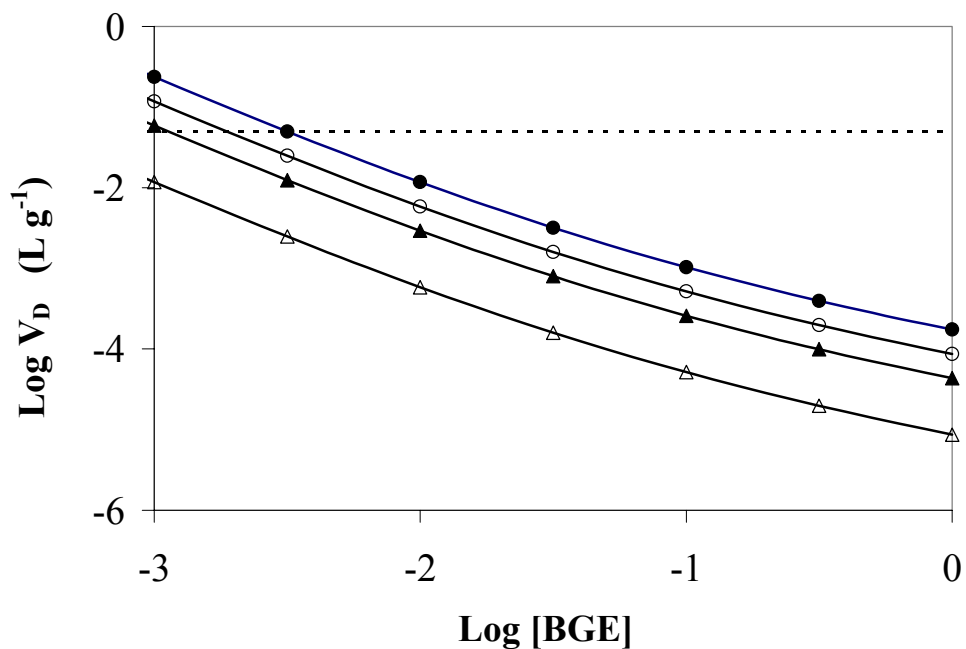
$$(6.7) \quad \kappa = \sqrt{\frac{8\pi N_A e^2}{\epsilon k T}} \times \sqrt{I} \approx 3.29 \times 10^9 \sqrt{I}$$

e	elementary charge of the electron (C)
N_A	Avogadro's number (mol^{-1})
ϵ	dielectric constant of water ($\text{C}^2 \text{ J}^{-1} \text{ m}^{-1}$)
k	Boltzmann's constant (J K^{-1})
T	temperature (K)
I	ionic strength of the solvent

where κ is directly proportional to the square root of the ionic strength—as the ionic strength of the aqueous solution increases, the size of κ increases. The calculation of κ holds true for 1:1 background electrolytes that are in much greater concentration than other charged solutes in the bulk solution. Because κ is inversely proportional to V_D (equation 6.6), V_D decreases with increasing ionic strength. The size of V_D is important in Tipping's models because all calculations of Z (equivalent to Q_{pH} in this work) for the NOM at each pH in the titration rely the partitioning of H^+ and cations into V_D to maintain charge balance with the negatively-charged acidic functional groups on the NOM.

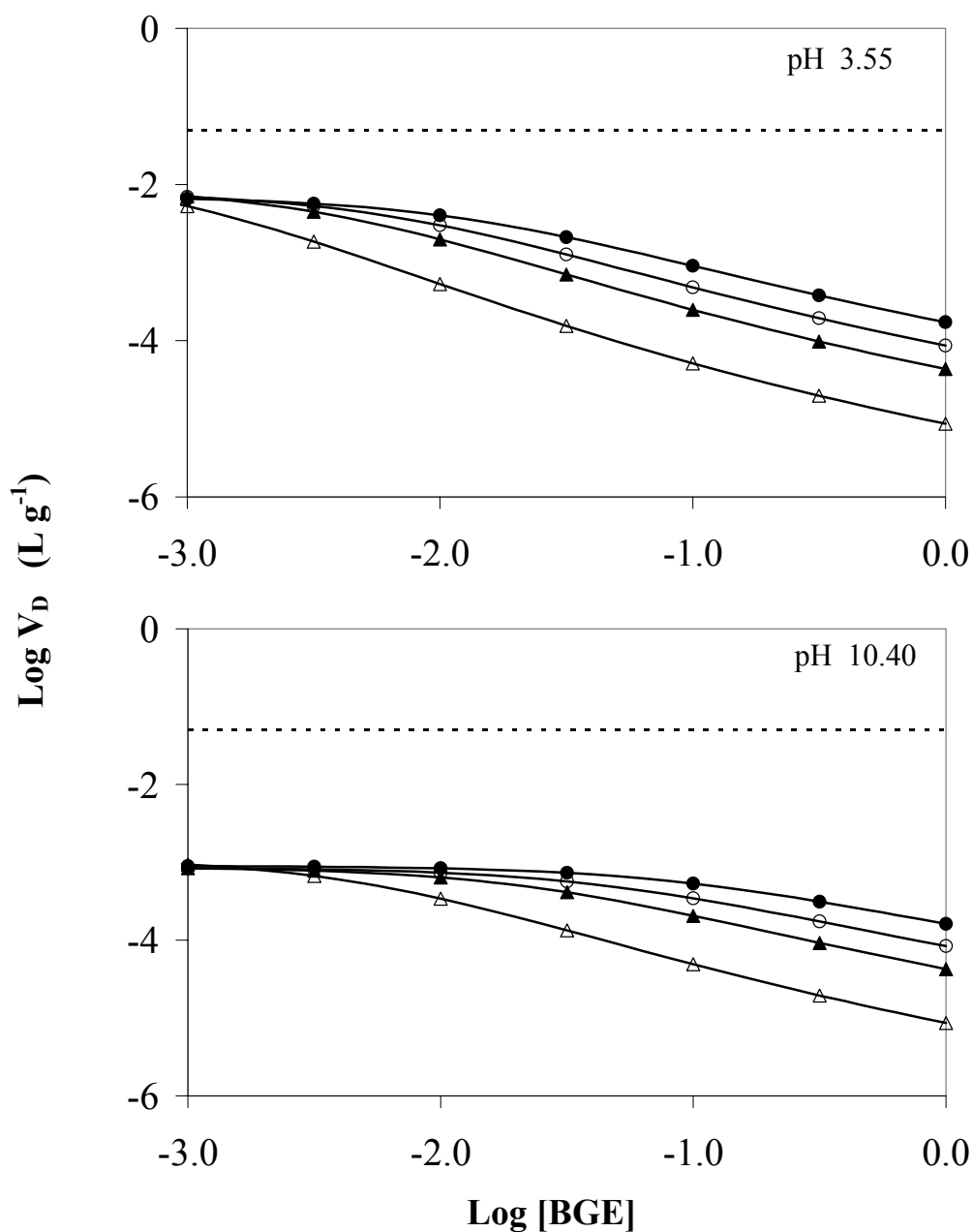
Tipping and Hurley (1992) and Tipping (1998) modeled titration data that were conducted by others at multiple ionic strengths, ranging from 10^{-3} to 1.0. If the contribution of the NOM to the ionic strength is neglected (as is the case in Model V and Model VI), the assumed V_D of solutions containing 2000, 1000, 500, and 100 mg L^{-1} SRNOM over a continuum of ionic strengths ranging from 10^{-3} to 1.0 is shown in Figure 6.2.

At low ionic strengths, $< \sim 10^{-2.5}$ to 10^{-3} , the calculated Donnan volume for a solution containing a high concentration of NOM may exceed the total volume of the solution. The dashed horizontal line at $\log I = -1.3$ in Figure 6.2 represents the constrained uppermost limit for the Donnan volume, 20% of the total solution volume (Tipping, 1994). Any calculation of V_D that exceeds this limit is automatically constrained by Models V and VI to equal 20%. The $\log V_D$ - $\log I$ plot in Figure 6.2 shows that greater concentrations of NOM in solution will produce greater values of V_D



● 2000 mg L⁻¹; ○ 1000 mg L⁻¹; ▲ 500 mg L⁻¹; △ 100 mg L⁻¹.

Figure 6.2. The effect of ionic strength on the calculation of the Donnan volume (V_D) used in Models V and VI (Tipping and Hurley, 1992; Tipping, 1998) over a continuum of 1:1 background electrolyte concentrations [BGE]. The effect of NOM on the calculation of ionic strength is neglected. The horizontal dashed line represents the uppermost limit allowed for the Donnan volume in Models V and VI at 20% of the total solution volume. $M_n = 1500$ (for a fulvic acid). $r = 0.8$ nm.



● 2000 mg L⁻¹; ○ 1000 mg L⁻¹; ▲ 500 mg L⁻¹; △ 100 mg L⁻¹.

Figure 6.3. The effect of the SRNOM (at pH 3.55 and pH 10.40) on the calculation of the Donnan volume (V_D) used in Models V and VI (Tipping and Hurley, 1992; Tipping, 1998) over a continuum of 1:1 background electrolyte concentrations [BGE]. The horizontal dashed line represents the uppermost limit allowed for the Donnan volume in Models V and VI at 20% of the total solution volume. $M_n = 1500 \text{ g mol}^{-1}$ (for a fulvic acid), $r = 0.8 \text{ nm}$.

for all possible ionic strengths between 10^{-3} to 1.0. Solutions at low ionic strength and high NOM concentrations (neglecting the contribution of NOM to the ionic strength) will have the largest values of V_D , and are predicted to contain a greater enrichment of H^+ or cations than their presence in the bulk solution. As a consequence, the calculated Z of the NOM at any pH—assuming electroneutrality between the NOM and the larger enrichment of cations in V_D —would be greater than if the NOM was in equilibrium and electroneutrality with bulk solution. V_D is the smallest at the highest ionic strengths and lowest concentration of SRNOM, and would contain a smaller enrichment of counterions. Thus the calculation of Z of the NOM at a given pH would approach Z if NOM were in equilibrium and electroneutrality with the bulk solution.

As discussed in section 6.1, the contribution of high concentrations of SRNOM to the accurate ionic strength of the aqueous solution deviates from the ionic strength predicted from the concentration of the 1:1 background electrolyte. Even at 100 mg L^{-1} , the SRNOM contributes significant charge to aqueous solutions and increase the ionic strength of the solution. The effect of the SRNOM on the calculation of V_D is shown in Figure 6.3, using equation 6.5 and data for z and $\%n$ shown in Table 6.1.

The plots in Figure 6.3 are strikingly different than the plot shown in Figure 6.2. At pH 3.55—a pH near the beginning of a titration where values of z are low—the charge contribution of the SRNOM to the ionic strength, over the whole ionic strength range, is great enough that V_D , even at the lowest concentrations of 1:1 electrolyte, never exceed 1% ($\log V_D = -2$) of the total solution volume. At pH 10.40—a pH near the end of a titration where values of z are large—values of V_D are predicted to be less than $\sim 0.1\%$ of the solution volume. The calculation of V_D in the presence of concentrated NOM (using

equations 6.6 and 6.7) is not pH-independent.

Model V and Model VI also incorporate ionic strength into the estimation of “intrinsic” proton (and metal) binding constants. The dissociation of a proton from one acidic functional group on the NOM will yield the thermodynamic equilibrium expression

$$(6.8) \quad K_H(Z) = \frac{[R^{z-1}][H^+]}{[HR^z]} = K_H \exp(2wZ)$$

where HR^z and R^{z-1} are the protonated acidic functional group and its conjugate base, $K_H(Z)$ is the charge-dependent dissociation constant, and K_H is the intrinsic dissociation constant. $K_H(Z)$ is the observed dissociation constant for that acid group when ionic strength and other electrostatic factors are considered. K_H is the true thermodynamic equilibrium constant for that single acidic functional group when at infinite dilution and not in the presence of other ionic species. The term $\exp(2wZ)$ on the right side of equation 6.8 is the electrostatic interaction factor that contains a parameter for ionic strength (w) and the charge of the NOM solute (Z), both of which influence the deprotonation equilibria of that acid group.

The ionic strength correction term, w , in Models V and VI is calculated as

$$(6.9) \quad w = P \times \log I$$

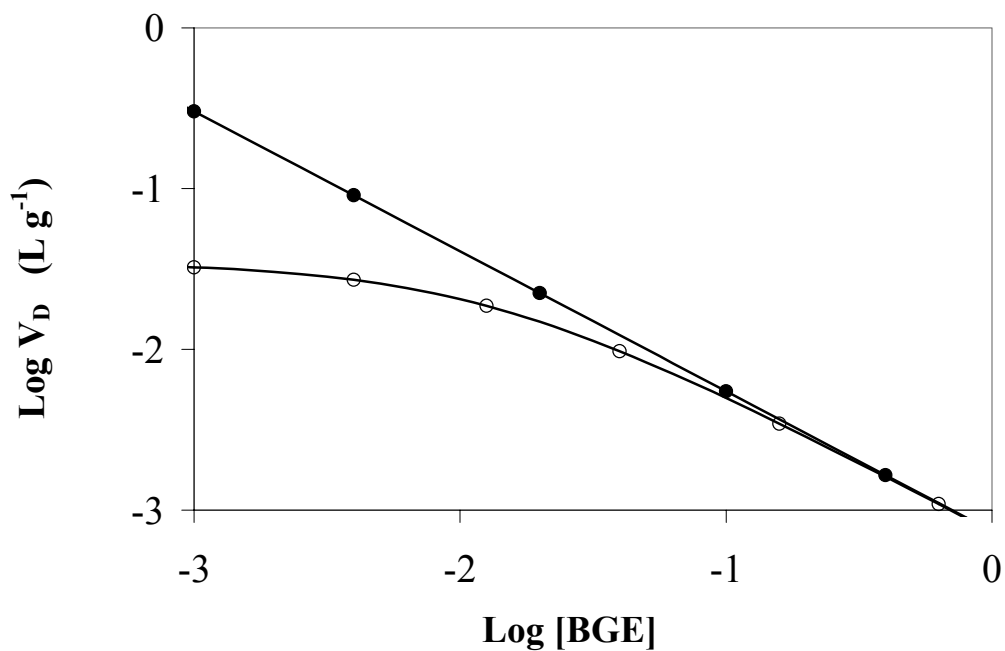
where P is an empirical constant and I is the ionic strength of the bulk solution. The constant P is a fitting parameter inside Models V and VI that adjust w so that the models

adequately fit data and generate acceptable estimates of carboxyl and phenolic concentrations (2:1) and mean proton-binding constants. One “best fit” value of P is fitted to the entire set of titration data. Ionic strength is calculated from the concentration of the background electrolyte. Because P and I are considered invariant with pH over the entire pH range of the titration, w is invariant. Therefore the only changing parameter in equation 6.8 as a function of pH is Z , the charge of the NOM solutes.

If a carboxyl group in NOM has K_H of $10^{-4.5}$, and the solute has a Z of -3.0 meq mol^{-1} in 0.001 M background electrolyte at pH 4.0 (neglecting NOM in the calculation of ionic strength), the value of $K_H(Z)$ for that carboxyl group would be $10^{-5.27}$ ($P = -99$ for the Suwannee River fulvic acid (Tipping, 1998)). That carboxyl group, according to equation 6.8, should be 50% ionized at pH 5.27. If the charge contribution of 1000 mg L^{-1} SRNOM at pH 4 were included in the calculation of the ionic strength with the 0.001 molar background electrolyte, I equals 0.0130 and the resulting $K_H(Z)$ (assuming Z and P are the same) is $10^{-4.98}$. In the higher ionic strength due to the NOM, that acid is 50% deprotonated at pH 4.98, ~ 0.3 pH units lower than if NOM is neglected. This calculation is only valid at that pH for that value of Z . Both ionic strength and Z increase as a function of pH, resulting in a different $K_H(Z)$ for that acid group at the next higher pH.

6.2.2 NICA-Donnan model.

The NICA-Donnan model (Kinniburgh *et al.*, 1996; Benedetti *et al.*, 1996; Milne *et al.*, 2001) is an electrostatic model that incorporates ionic strength into the calculation of a Donnan volume (V_D) around NOM solutes using the strictly empirical relationship



-
- Neglecting the contribution of SRNOM to ionic strength.
 - Includes the contribution of the SRNOM at 1000 mg L⁻¹ at pH 4.0 to the ionic strength.
-

Figure 6.4. The effect of the Suwannee River NOM on the calculation of the Donnan volume (V_D) used in the NICA-Donnan model (Kinniburgh *et al.*, 1996; Benedetti *et al.*, 1996; Milne *et al.*, 2001) for a continuum of 1:1 background electrolyte concentrations [BGE]. The empirical constant b is set to 0.87 (Milne *et al.*, 2001).

$$(6.10) \quad \log V_D = b(1 - \log I) - 1$$

where b is an adjustable empirical constant that is used to “best fit” the model to the titration data. Like Models V and VI, the NOM solutes are assumed to be surrounded by V_D in which association-dissociation equilibria occur and electroneutrality is maintained by an enrichment of H^+ and cations. I and V_D are assumed to be invariant with pH. The ranges of V_D for the continuum of ionic strengths for a solution with 1000 mg L^{-1} SRNOM (neglecting and including the contribution of the SRNOM to the ionic strength at pH 4.0) are shown in Figure 6.4. The constant b is set to 0.87 (determined for the Suwannee River fulvic acid (Milne *et al.*, 2001)).

The contribution of the SRNOM to the ionic strength at pH 4 will compress V_D to a significantly smaller volume than V_D predicted by the concentration of the 1:1 background electrolyte. The resulting smaller V_D will yield smaller calculations of larger apparent mean proton and metal binding affinities (noted as \tilde{K}) that are closer to their predicted mean intrinsic proton and metal binding affinities. Milne *et al.* (2001) report values of mean $\log \tilde{K}_{H1}$ (proton-binding affinities for carboxyl groups) for 25 fulvic acids and 22 humic acids that range from 2.00 to 3.80 (average = 2.65) for fulvic and 1.99 to 3.90 (average = 2.66) for humic acids. Milne *et al.*'s (2001) mean $\log \tilde{K}_{H2}$ (proton-binding affinities for phenolic groups) for the same 25 fulvic and 23 humic acids range from 7.19 to 10.91 (average = 8.60) for fulvic and 6.06 to 10.06 (average = 7.98) for humic acids. These estimates are significantly lower than those reported in Ritchie and Perdue (2003) who modeled the titrations of 14 IHSS standard and reference samples with the H-H model, a non-electrostatic model. Mean $\log K_1$ and $\log K_2$ values for the

IHSS samples range between 3.5-4.5 and 9.2-10.6 respectively, which are more in line with the known pK_a s of small organic carboxylic and phenolic acids (Perdue *et al.*, 1984; Perdue, 1985).

This author does not have enough experience using Models V and VI and the NICA-Donnan model to unequivocally know how the correction of ionic strength by accounting for NOM in those models will ultimately change their interpretations of titration data.

6.3 The Complexity of NOM and the Distribution of Charge.

Bartschat *et al.* (1992) treated NOM as a complex mixture with the possibility of some solutes having large, polymer-like characteristics—MWs > 10,000 Da with the potential to have 60 or greater acidic functional groups per solute. Although the CDM predicts that the maximum charges for the SRNOM and Fractions 1-7 never exceed -30 for the fractions with the greatest MWs (at very high pHs), the diversity of MWs (~60 to ~22,000 Da) and the predicted distribution of charge (-0.5 to -30) in the SRNOM would allow for potentially thousands of different combinations of H^+ -NOM and metal-NOM interactions.

In Model VI, Tipping (1998) allows for only eight monodentate sites—four carboxyl and four phenolic—to which H^+ and metals may bind. From those eight sites, Tipping (1998) statistically determined that there are 36 and 120 probable bidentate and tridentate metal-binding sites using all combinations of carboxy-carboxyl and carboxyl-phenolic groups. For simplicity, Model VI assumes that all NOM solutes have the same

MW and the same charge at a given pH, and that the carboxyl-to-phenolic concentration ratio is 2:1. The NICA-Donnan model assumes that the total charge of the NOM is spread uniformly across all solutes in the NOM (Milne *et al.*, 2001) and that metal-NOM interactions are not site-specific. Researchers using lanthanide ion-probe spectroscopy (Dobbs *et al.* 1989; Grimm *et al.*, 1991) could only model the competitive binding of europium-III (Eu^{3+}) and copper-II (Cu^{2+}) ions to the Suwannee River fulvic acid with the competitive Gaussian distribution model if the average charge of the fulvic acid was fixed to -2.8 over the entire range of pH (Grimm *et al.*, 1991). Ritchie and Perdue (2003) and Bowles *et al.* (1989) independently determined that the Suwannee River fulvic acid has 6.0 mmol g^{-1} of carboxyl groups, and the ionization of those carboxyl groups between pH 3 and 8 would yield average charges from -2.2 meq g^{-1} at pH 3 to -6.0 meq g^{-1} at pH 8. (Ritchie and Perdue, 2003).

This work (and the works of Schmitt-Kopplin and colleagues, De Nobili and colleagues, and Perminova and colleagues) has shown that there is a large diversity of MWs (by HPSEC and SEC) and charge in NOM at any given pH (by capillary electrophoresis). If NOM only contained solutes that all have the same MW and charge, then the resulting electropherograms for NOM would be a slender spike at one effective mobility instead of a broad Gaussian-like distribution. Although the aforementioned models use unrealistic physicochemical assumptions in their computational schemes, they fit titration and metal-binding data very well. The Henderson-Hasselbalch (H-H) model used in this work is not perfect either, but serves its purpose of fitting to titration data and providing reasonable estimates of proton-binding parameters. A fourth or fifth-degree polynomial will exactly reproduce direct titration data as well as the models. It may be

unrealistic that any model could ever be designed to account for the diversity of MWs and the distribution of charges in NOM. Any accurate interpretation of NOM by a model should consider the NOM's complexity.

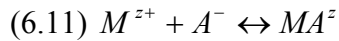
6.4 Considerations of the Most Probable Distribution of Charge.

Titration in this work was performed at $\sim 200 \text{ mg L}^{-1}$ of purified sample in 0.1 M NaNO_3 at 25°C . The concentrations of NOM in natural surface waters range from 1 to 10 mg L^{-1} (Thurman, 1985), 10 to 200 times lower than concentrations of NOM used in laboratory experiments. Typical concentrations of the major ions in freshwater systems are also very low, ranging from 3×10^{-5} to $2 \times 10^{-3} \text{ mol L}^{-1}$ (Stumm and Morgan, 1996), which would give the natural waters very low ionic strengths. If the titration in this work were performed under those conditions, the calculations of Q_{pH} , Q_1 and Q_2 , and mean $\log K_1$ and $\log K_2$ would be different. Titrations performed at very low ionic strengths will yield lower estimates of Q_{pH} across all pHs of the titration (Khalaf *et al.*, 1975; Ephraim *et al.*, 1996; Christensen *et al.*, 1998). Because Q_{pH} is a function of the ionic strength at which the titration was performed (due to the calculations of $[\text{H}^+]$ and $[\text{OH}^-]$ from their respective activities), the most probable distribution of charge in the SRNOM from this work may only be valid at high ionic strengths, and may not be absolutely applicable to real environmental conditions—low NOM and low ionic strengths.

For example, the most common laboratory method of measuring the stability of metal-NOM complexes is by ion selective electrode (ISE) detection (Buffle *et al.*, 1977; Brady and Pagenkopf, 1978; Cabaniss and Shuman, 1988a; Cabaniss and Shuman,

1988b; Li *et al.*, 1998). An ISE detects the activities of free (uncomplexed) metal cations in the bulk aqueous solution. Free metals (M^{z+}) simultaneously compete with other free metals and H^+ for ionized acidic functional groups on the NOM. Additionally, OH^- , CO_3^{2-} , and other inorganic ligands will complex with the free metal. Because ISE is an electrochemical method, the accurate detection of $\{M^{z+}\}$ in bulk solution and knowledge of the ionic strength is necessary to determine the total concentration of free metal, the total concentrations of the metal-inorganic ligand complexes, and the total concentration of metal bound to the NOM. Because concentrated NOM affects the ionic strength of aqueous solutions, the detection of $\{M^{z+}\}$ by the ISE may be compromised by incorrectly assuming the ionic strength is controlled by the 1:1 background electrolyte only.

The thermodynamic equilibria of binding between M^{z+} and NOM is driven by the activities of both species and by pH. Metal binding by NOM may be discussed as a simple metal-ligand complexation reaction (equation 6.11)



where the metal binds to an ionized acidic functional group. The other scenario is the cation exchange where the hydrogen on the acidic functional group is displaced by the metal (equation 6.12).



The thermodynamic mass action equations for these reactions require the

knowledge of the concentrations of the free metal and NOM, the charge of the metal and NOM, and the appropriate activity coefficients to correct activities to concentrations. NOM contains thousands of solutes that will simultaneously have charges from -0.5 to a maximum of -30.0. Appropriate activity coefficients for NOM are not available.

Because of the diversity of carboxyl groups on NOM, thousands of different carboxyl groups may have significantly different affinities to bind metals, some more strongly than others. The stoichiometry of the metal-binding reactions is also unknown. Individual NOM solutes, depending on their size and the proximity of acidic functional groups may bind one, two, or three metal ions. Additionally, two small NOM solutes may simultaneously bind to the same di- or trivalent cation.

An additional complication arises that the Davies equation can only estimate activity coefficients for ions with $z < \pm 5$ (Stumm and Morgan, 1996). If, for argument's sake, the Davies equation could estimate activity coefficients for ions with $z > \pm 5$, the activity of those solutes approaches zero at very high ionic strengths. The extremely low activities of those solutes will result in very low reactivity, even though those solutes may have acidic sites that are stronger binding sites than smaller charged NOM solutes. ISE experiments conducted at high ionic strengths would favor the formation of metal-NOM complexes for the NOM solutes with the lowest charges, and disallow metal complexes for the highly-charged NOM solutes.

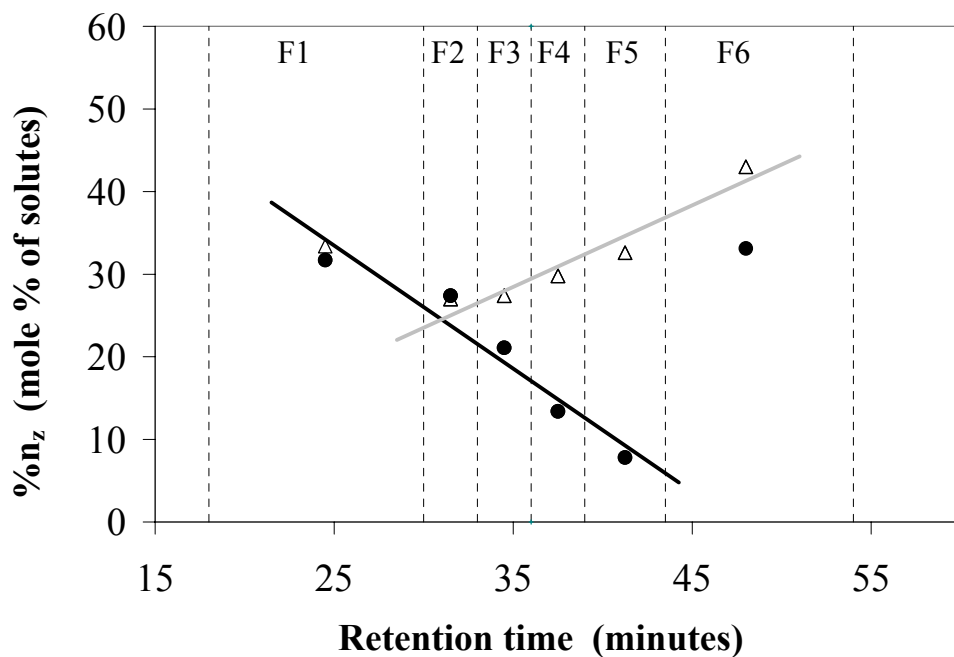
If the same NOM and free metal were to be characterized at their natural concentrations (1-10 mg L⁻¹ and μ M) in surface waters of low ionic strengths, the binding of that metal to the NOM would probably be significantly different (assuming that competing reactions from inorganic anions are negligible). At low ionic strengths,

activity of an ion approaches its molar concentration. The activities of the NOM solutes with higher charges will be significantly larger than in the laboratory experiment. In the natural water, the solutes with z between -5.0 and -10.0 could possibly be the dominant NOM solutes that bind that metal whereas they were negligible at the higher ionic strength. This is an area to be explored by future research.

6.5 The Most Probable Distribution of Charge and SEC.

The SRNOM was fractionated into Fractions 1-7 using low-pressure preparative SEC. The best experimental protocol for conducting good SEC work for NOM samples was followed (De Nobili *et al.*, 1999; Chin *et al.*, 1994; and Zhou *et al.*; 2000). Although the mode, M_n , and M_w decrease from Fraction 1 to Fraction 7, no single fraction contains a unique range of MWs that is not shared by other Fractions. Perminova *et al.* (1998) and Pelekani *et al.* (1999) contend that charge-to-mass ratios and hydrophobicity (K_{ow}) are factors, in addition to MW, that affect the retention times of model organic solutes during SEC separations. The observations made by Perminova *et al.* (1998) and Pelekani *et al.* (1999) about charges of organic solutes were tested by examining various relationships between the most probable distribution of charge for Fractions 1-7 and their respective retention times on the preparative SEC column during fractionation.

Charges and their corresponding mole percents of solutes in Fractions 1-6 were grouped together (i.e. -0.5 to -3.0, -3.5 to -6.0) into “charge classes”. The total mole percents of each class of charges (as determined by the CDM for data at pH 9.0-9.3, the pH at which the preparative SEC was performed) were then plotted against the midpoint retention times of Fractions 1-6 during the preparative fractionation (calculated from data



-
- Mole percent of solutes with charges between -0.5 to -3.0.
 - Δ Mole percent of solutes with charges between -3.5 to -6.0.
-

Figure 6.5. The qualitative comparison of the distribution of charge in Fractions 1-6 with respect to their retention times during fractionation by preparative SEC.

in Table 4.1). Only two qualitative relationships between the distribution of charge and the retention times of Fractions 1-6 on the SEC column are possible (Figure 6.5).

The retention time of Fractions 1-6 could be due their populations of solutes with the lowest charges ($z = -0.5$ to -3.0) or intermediate charges ($z = -3.5$ to -6.0), or a combination of both. The abundances of solutes with lowest charge for Fractions 1-5 are inversely correlated with increasing retention time. If hydrophobic interactions between solutes and the stationary phase is the predominant process that increases the retention times of solutes, then the trend, in theory should be reversed—the abundances of solutes with low charge would increase with increasing pH.

The abundances of the intermediate charges ($z = -3.5$ to -6.0) increase with longer retention times on the SEC column for Fractions 2-6. Larger charges on solutes would enhance ion-ion repulsive forces between NOM solutes and possibly lead to ion-inclusion phenomenon (Barth, 1987). Ion-inclusion would result if highly-charged solutes diffuse into poor spaces or cavities within the stationary phase and become “trapped” in those cavities by electrostatic repulsion from other highly-charged solutes entrained in the mobile phase. Those solutes cannot diffuse out of the cavities until the concentrations of the other highly-charged solutes had passed. For this to occur, there must be an extreme concentration or ionic strength gradient above the buffering capacity of the mobile phase caused by the sample within the column. This may partially explain the spike in pH observed in Figure 4.3 and the spikes in conductivity in the works of Müller *et al.* (2000) and Müller and Frimmel (2002).

In this work, the carboxyl concentrations increased from Fraction 1 to Fraction 5, with Fraction 6 having slightly lower carboxyl concentration than Fraction 5. Sihombing

et al. (1996) reported a marked increase in the abundances of oxygenated and carboxylic-like structures (determined by ^{13}C -NMR) in for MW fractions of humic and fulvic acids with increasing retention time on their preparative SEC column. If ion-inclusion is the predominant process that increases the retention times of NOM solutes on SEC columns, in addition to decreasing MW, then SEC chromatograms are themselves distributions of z/MW .

Conversely, the semi-analytical SEC used to determine the MW distributions in Fractions 1-7 were performed at two different pHs at a concentration of 30 mg L^{-1} ($1/130^{\text{th}}$ the concentration of the preparative SEC), and the weighted sums of the chromatograms almost exactly replicated the SEC chromatograms of the unfractionated SRNOM. If extreme charge-charge interactions do occur, even in highly buffered mobile phases, they would be favored at the extremely high concentrations. It seems improbable that the low concentrations of sample used in the semi-analytical SEC would exhibit the same phenomenon at two different pHs. This is speculative.

Chapter 7.

CONCLUSION

7.1 Chemical Analyses.

Approximately 1 gram of Suwannee River NOM (SRNOM) was fractionated into seven fractions (Fractions 1-7) over a period of 10 weeks by a large-scale, low-pressure size-exclusion chromatography method. The division of the SRNOM into the seven fractions was performed by dividing each preparative SEC chromatogram into equal areas of absorbance. Fractions 1-6 comprised the main peak of the preparative SEC chromatograms and Fraction 7 contained all material that eluted at longer retention times after the main peak. Overall, there was a 6% loss of NOM during the fractionation and the subsequent processing of the samples. Other than the spillage of Fraction 4, the exact cause(s) of loss was not absolutely identified. The final recoveries of each fraction, based on the total recovered carbon (TOC), was poorly correlated with predicted recoveries based on their areas of absorbance. The shapes of all 70 preparative SEC chromatograms for the preparative fractionation were comparable to the chromatograms of other Suwannee River samples as determined by HPSEC.

The ranges of MWs and the average MWs were determined by a semi-analytical SEC method at pH 6.8 (using tandem UV-absorbance and online-TOC detection) and at pH 9.3 (using absorbance detection). The mode and average MWs systematically for Fractions 1-7 decreased in the order in which the fractions were collected during the preparative SEC. The tandem absorbance and TOC detection methods at pH 6.8 produced almost comparable chromatograms for the SRNOM and Fractions 1-7. There

were only slight differences between absorbance chromatograms at pH 6.8 and 9.3 for the SRNOM and Fractions 1-6. The SEC revealed that no single fraction contained a unique range of MWs that was not shared by another fraction. Instead, the preparative SEC method in this work created seven broad and overlapping segments of a MW continuum.

Fractions 1-6 tended to have very similar elemental compositions while Fraction 7 had much larger nitrogen content than the other fractions, probably due to a biologically-derived contaminant that was introduced during either the preparative SEC or the subsequent processing. The fractions had very similar elemental compositions to the well-characterized SRFA and HAs that were reported in the literature. O/C ratios tended to be inversely correlated to average MWs while N/C ratios were weakly correlated to average MWs.

The absorption of UV-visible light at pH 6.8 and 9.3 was strongly related to the average MWs of the fractions. The absorbance and SUVA values for Fraction 7 at pH 6.8 were ~30% greater than those at pH 9.3, which would explain the discrepancy between large difference in the %TOC recovery and % area of absorbance used as the criteria for the preparative fractionation. SUVA values at 254 and 280 nm were linearly correlated with the average MWs for Fractions 2-7, with Fraction 1 as an outlier. E_4/E_6 values did not correlate with average MWs, but E_4/E_6 had a strong inverse relationship to the H/C and N/C ratios of the fractions.

The acid-base chemistries of the SRNOM and Fractions 1-7 were characterized by direct titrations. Hysteresis was observed for all samples, in which the reverse titration curves always had greater charge densities than the forward titrations. The concentrations of carboxyl and phenolic groups were correlated with the average MWs of

Fractions 1-6, with Fraction 7 again being an outlier. Carboxyl content was inversely proportional to average MW while phenolic content was proportional to average MW.

The SRNOM and Fractions 1-7 were analyzed for their charge-to-size distributions by capillary electrophoresis. Electropherograms were translated toward greater negative mobilities as the pHs of the separations increased, indicating that samples were accumulating greater overall charge (Q_{pH}) and that solutes were gaining higher charges. Most electropherograms at $pH > 4$ tended to be nearly symmetrical distributions with minor tailing. Most electropherograms at all pHs contained 2-4 fingerprint peaks and 1-2 small system peaks. Electropherograms in the pH 5-6.5 range contained unusual system peaks that were most likely caused by ionic strength or pH gradients between the migrating sample zone and the carrier solution.

The SEC chromatograms (at pH 6.8 and 9.3), UV-visible spectra, and the forward and reverse titration curves for the SRNOM were reconstructed from those of Fractions 1-7. In each case, the reconstructed data very closely matched the experimental data for the SRNOM. The agreement between the reconstructed and SRNOM chromatograms, UV-visible spectra, and titration curves confirm that the physical and chemical properties of the SRNOM were conserved in Fractions 1-7 during the preparative fractionation and the subsequent processing of the fractions.

Qualitatively, Fractions 1-3 have very similar chemical characteristics to the Suwannee River humic acid. Fractions 4-6 have very similar chemical characteristics to the Suwannee River fulvic acid and the Suwannee River NOM. Fraction 7 has partially adopted the chemical characteristics of Fractions 1 and 2 because Fraction 7 contains the strongly sorbed organic matter that was flushed from the preparative SEC column during

each rinse cycle—organic matter most likely that should have been included in Fractions 1 and 2.

7.2 The Most Probable Distribution of Charge.

Data for the molecular weight distributions, electrophoretic distributions, and direct titrations were evaluated by the Charge Distribution Model (CDM) to determine the most probable distribution of charge as a function of pH and the distribution of acidic functional groups on solutes in the SRNOM and Fractions 1-7. The CDM predicted that distribution of charges on solutes, and the quantities of solutes with each charge, changes as a function of increasing pH.

At low pH, all samples have relatively high abundances of solutes with very low charges ($z = -0.5$ to -2.0). As pH increases, the abundances of the lowest charges decrease and the abundances of higher charges (> -3) increase due to the sequential deprotonation of acidic functional groups on the solutes. Fractions 1 and 2 (the fractions with the largest MWs) have significant quantities of mono-, di-, and triprotic acids—due to their relatively low carboxyl contents—but have enough solutes with >15 acidic functional groups to give them properties of ionic polymers. Fractions 1 and 2 may accrue a maximum charge of -30 (from the ionization of carboxyl and phenolic groups) on their largest solutes by pH 10-11.

Fractions 1-3 are nearly depleted in solutes with -0.5 charges by pH 7, indicating that all monoprotic acids in Fractions 1-3 are carboxylic acids. Fractions 1-3 have no monoprotic phenolic acids. 80-90% of solutes in Fractions 1-3 will contain both carboxyl and phenolic groups. Fractions 4 and 5, the most acidic samples, are nearly depleted in

solutes with the -0.5 charge by pH 5, and the -1.0 charge by pH 7-8. As a result, all probable monoprotic and diprotic acids in Fractions 4 and 5 are carboxylic acids, and will contain no phenolic groups. Phenolic groups in Fractions 4 and 5 must be on solutes that have a minimum of 2 carboxyl groups. 30-40% of solutes in Fractions 4 and 5 contain both carboxyl and phenolic groups, and 55% of solutes in Fraction 6 will contain only carboxyl groups and no phenolic groups due to its very high carboxyl:phenolic ratio. Fraction 7 is predicted to have solutes with 1 carboxyl group only or 1 phenolic group only. The monoprotic phenols in Fraction 7, which ionize above pH 8, are probably acidic amine groups from the suspected contaminant.

7.3 The Application of the Most Probable Distributions of Charge.

The ionic strength of solutions with high concentrations of NOM can be accurately calculated because the most probable distribution of charge and the mole abundances of solutes with those charges are known at a given pH. Very high concentrations of NOM, often used in laboratory experiments, overwhelm the contribution of low concentrations of 1:1 background electrolytes. The contribution of the concentrated NOM to the overall ionic strength of aqueous solutions increases with increasing pH due to the increase in z of solutes and the relative concentrations of solutes with those higher values of z .

Electrostatic models (Models V and VI and the NICA-Donnan model) that incorporate ionic strength into their empirical calculations must include the effects of concentrated NOM. Donnan volumes (V_D) as calculated in Models V and VI and the NICA-Donnan model are assumed to be independent of pH. It was shown that if NOM is

taken into consideration, V_D will be substantially smaller than predicted by the background electrolyte alone, affecting Model V and VI and the NICA-Donnan model's calculations of acidic functional groups and their mean proton or metal-binding constants.

The assumptions that Models V and VI, the NICA-Donnan model, and the Competitive Gaussian model make about the distribution of acidic functional groups or charge neglect the diversity of NOM solutes and the complexity of natural organic samples. Neither the MWs of solutes nor the charge distributions on those solutes is the same. The SRNOM and Fractions 1-7 have solutes with MWs that may range from 60 to 23,000 Da, and may have from 1 up to 30 acidic functional groups per solute.

Fractions 1-7 do not contain unique ranges of MWs, even though the SRNOM was fractionated by preparative SEC under the most optimized experimental conditions. The fractionation of the SRNOM may have been based on the charge-to-MW distribution of the SRNOM solutes rather than by MWs (Perminova et al., 1998). Ion-inclusion (Barth, 1987) is thought to be the phenomenon behind this observation and not hydrophobic interactions of solutes with the stationary phase.

7.4 Final Thoughts About the Most Probable Distribution of Charge and Future Research.

The most probabilistic distribution of charge is intended to be a concise, yet stochastic computational scheme, to further understand the acid-base chemistry, and ultimately, the metal-binding properties of natural organic matter. It is based on probability. It does not guarantee that the most probable distribution of charge and acidic functional groups presented in this work for the Suwannee River NOM is the “last word.”

The methods used this work are very labor-intensive and time-consuming, and required patience to bring about the results. To this author's knowledge, this is the first time direct titration data, molecular weight distributions, and capillary electrophoresis data have been integrated. The results in this work have shed new light on the determination of

1. The distribution of acidic functional groups in the Suwannee River natural organic matter as a function of MW.
2. The changing distributions of charge on those solutes as a function of pH.
3. The contribution of high concentrations of natural organic matter to aqueous solutions and the possible impacts of neglecting NOM.

The future work needed to verify the applicability of this research should include:

1. The integration of titration data, MW data, and electrophoresis data for a diverse suite of natural organic samples (NOM, SOM, fulvic and humic acids) from aquatic and terrestrial environments for the determination of the most probable distribution of charge.
2. The comparison of titration data for solutions of NOM at various ionic strengths (10^{-3} to 10^{-1}) and NOM concentrations when the contribution of the NOM to the ionic strength is neglected and is considered.
3. The comparison of model results for direct and metal-binding titrations with NOM at various ionic strengths (10^{-3} to 10^{-1}) and NOM concentrations when the contribution of the NOM to the ionic strength is neglected and is considered. The effect of changing ionic strengths with regard to the empirical constants and assumptions made by the electrostatic models should

also be tested.

4. The determination of activity coefficients that will adequately parameterize the activities of the largest solutes with the greatest charges (> -5) for accurate thermodynamic parameterization of NOM-metal interactions.
5. The development of new models or the revision of existing models that account for the diversity of MWs and the distribution of charges on solutes in NOM. Natural organic matter must be treated as a complex mixture.

This author anticipates that colleagues and fellow researchers will improve the CDM or develop new computational schemes dealing with this subject matter, and bring the geochemistry community closer to knowing the true acid-base chemistry of aquatic and terrestrial natural organic matter, fulvic acids, and humic acids.

APPENDIX

Table A.1. Parameters for the electrophoresis of the SRNOM.

pH	L_T	E	Q_{pH}	μ_p	k_{pH}
3.55	27	20	-2.31	-0.0122	0.466
3.75	27	25	-2.53	-0.0129	0.445
3.92	27	25	-2.73	-0.0133	0.418
4.04	37	35	-2.87	-0.0151	0.408
4.22	27	20	-3.08	-0.0161	0.454
4.44	27	20	-3.33	-0.0170	0.453
4.87	27	20	-3.82	-0.0182	0.455
5.20	27	30	-4.17	-0.0182	0.416
5.94	27	30	-4.83	-0.0180	0.361
6.34	27	30	-5.11	-0.0184	0.342
6.66	27	30	-5.30	-0.0187	0.331
7.01	27	25	-5.47	-0.0204	0.344
7.76	27	25	-5.75	-0.0205	0.338
8.62	27	25	-6.03	-0.0210	0.327
9.25	37	35	-6.35	-0.0220	0.335
9.64	37	30	-6.59	-0.0241	0.337
10.40	37	30	-6.97	-0.0243	0.334
11.25	37	25	-7.12	-0.0259	0.345

L_T : total length of capillary (cm).

E : potential (kV).

Q_{pH} : total charge density of sample (meq g⁻¹)

μ_p : peak mobility (cm² V⁻¹ min⁻¹)

k_{pH} : optimized Offord's constant.

Table A.2. Parameters for the electrophoresis of the Fraction 1.

pH	L_T	E	Q_{pH}	μ_p	k_{pH}
2.90	27	20	-0.73	-0.0042	0.552
3.18	27	20	-0.87	-0.0104	0.750
3.39	27	20	-0.98	-0.0085	0.608
3.66	27	20	-1.14	-0.0080	0.529
4.06	37	25	-1.41	-0.0160	0.641
4.30	37	20	-1.58	-0.0195	0.851
4.64	37	20	-1.83	-0.0204	0.784
4.92	37	25	-2.04	-0.0206	0.738
5.25	37	35	-2.28	-0.0196	0.645
5.42	37	35	-2.41	-0.0201	0.623
5.70	37	35	-2.60	-0.0200	0.576
6.21	27	30	-2.92	-0.0172	0.455
6.56	27	30	-3.11	-0.0175	0.433
6.87	27	30	-3.26	-0.0175	0.421
7.54	27	25	-3.53	-0.0185	0.387
7.95	27	25	-3.68	-0.0183	0.369
8.54	27	20	-3.92	-0.0196	0.361
9.25	37	30	-4.30	-0.0223	0.342
9.52	37	30	-4.47	-0.0218	0.334
10.13	37	30	-4.82	-0.0214	0.332
10.53	37	25	-4.98	-0.0226	0.343
11.35	37	25	-5.15	-0.0231	0.330

L_T : total length of capillary (cm).

E : potential (kV).

Q_{pH} : total charge density of sample (meq g⁻¹)

μ_p : peak mobility (cm² V⁻¹ min⁻¹)

k_{pH} : optimized Offord's constant.

Table A.3. Parameters for the electrophoresis of the Fraction 2.

pH	L_T	E	Q_{pH}	μ_p	k_{pH}
2.93	27	40	-1.44	-0.0056	0.342
3.04	27	40	-1.51	-0.0076	0.426
3.20	27	30	-1.63	-0.0094	0.476
3.47	37	30	-1.83	-0.0144	0.539
3.85	27	20	-2.14	-0.0133	0.443
4.15	27	30	-2.39	-0.0123	0.378
4.46	27	25	-2.66	-0.0162	0.471
4.71	27	25	-2.87	-0.0160	0.451
5.08	57	25	-3.19	-0.0218	0.551
5.43	57	25	-3.47	-0.0260	0.602
5.96	57	25	-3.87	-0.0245	0.526
6.25	57	15	-4.06	-0.0275	0.537
6.77	57	15	-4.38	-0.0283	0.519
7.22	57	20	-4.62	-0.0283	0.495
7.77	57	20	-4.89	-0.0275	0.463
8.38	57	20	-5.18	-0.0281	0.437
8.91	57	25	-5.45	-0.0277	0.415
9.33	57	35	-5.65	-0.0261	0.388
9.75	57	30	-5.83	-0.0270	0.385
10.67	57	25	-6.09	-0.0282	0.388
11.42	57	25	-6.19	-0.0290	0.380

L_T : total length of capillary (cm).

E : potential (kV).

Q_{pH} : total charge density of sample (meq g⁻¹)

μ_p : peak mobility (cm² V⁻¹ min⁻¹)

k_{pH} : optimized Offord's constant.

Table A.4. Parameters for the electrophoresis of the Fraction 3.

pH	L _T	E	Q _{pH}	μ _p	k _{pH}
3.43	27	25	-2.63	-0.0107	0.288
3.66	37	30	-2.86	-0.0128	0.332
3.96	37	30	-3.16	-0.0155	0.387
4.27	37	30	-3.48	-0.0079	0.183
4.56	37	20	-3.78	-0.0080	0.168
4.81	57	25	-4.03	-0.0211	0.422
5.14	57	25	-4.34	-0.0225	0.434
5.89	57	35	-4.99	-0.0263	0.429
6.33	57	30	-5.31	-0.0265	0.395
6.73	57	30	-5.56	-0.0267	0.395
7.17	57	20	-5.79	-0.0261	0.408
7.85	57	35	-6.09	-0.0256	0.361
8.37	57	35	-6.29	-0.0261	0.361
8.91	57	35	-6.52	-0.0263	0.354
9.24	57	35	-6.67	-0.0269	0.348
9.83	57	30	-6.89	-0.0278	0.348
10.62	57	25	-7.03	-0.0288	0.359
11.38	57	25	-7.09	-0.0296	0.354

L_T : total length of capillary (cm).

E : potential (kV).

Q_{pH} : total charge density of sample (meq g⁻¹)

μ_p : peak mobility (cm² V⁻¹ min⁻¹)

k_{pH} : optimized Offord's constant.

Table A.5. Parameters for the electrophoresis of the Fraction 4.

pH	L_T	E	Q_{pH}	μ_p	k_{pH}
3.33	37	30	-2.44	-0.0115	0.388
3.66	37	30	-2.81	-0.0125	0.335
3.90	37	25	-3.09	-0.0145	0.347
4.22	37	20	-3.46	-0.0174	0.399
4.64	57	20	-3.94	-0.0183	0.381
4.86	57	20	-4.19	-0.0219	0.442
5.67	57	25	-5.00	-0.0262	0.445
6.38	57	35	-5.54	-0.0235	0.405
6.97	57	35	-5.89	-0.0246	0.377
7.54	37	20	-6.13	-0.0223	0.322
7.86	57	30	-6.25	-0.0267	0.386
8.11	57	20	-6.33	-0.0289	0.411
8.68	57	25	-6.52	-0.0273	0.382
9.24	57	25	-6.73	-0.0280	0.380
9.82	57	20	-6.95	-0.0308	0.395
10.48	57	20	-7.10	-0.0297	0.378
11.35	37	15	-7.18	-0.0302	0.375

L_T : total length of capillary (cm).

E : potential (kV).

Q_{pH} : total charge density of sample (meq g⁻¹)

μ_p : peak mobility (cm² V⁻¹ min⁻¹)

k_{pH} : optimized Offord's constant.

Table A.6. Parameters for the electrophoresis of the Fraction 5.

pH	L_T	E	Q_{pH}	μ_p	k_{pH}
4.10	27	35	-3.36	-0.0094	0.236
4.24	27	35	-3.56	-0.0105	0.291
4.52	37	30	-3.86	-0.0165	0.350
4.92	37	25	-4.31	-0.0201	0.426
5.34	37	20	-4.75	-0.0213	0.413
6.25	37	35	-5.53	-0.0198	0.338
6.71	37	25	-5.82	-0.0222	0.359
7.25	37	25	-6.10	-0.0224	0.347
7.60	37	25	-6.24	-0.0236	0.357
7.75	37	25	-6.29	-0.0228	0.342
8.07	37	30	-6.40	-0.0232	0.334
8.26	37	20	-6.47	-0.0239	0.342
8.88	37	30	-6.68	-0.0230	0.321
9.25	37	25	-6.83	-0.0236	0.317
9.76	37	25	-7.02	-0.0245	0.320
10.35	37	20	-7.18	-0.0259	0.347
10.66	37	20	-7.22	-0.0263	0.348
11.25	27	25	-7.27	-0.0115	0.154

L_T : total length of capillary (cm).

E : potential (kV).

Q_{pH} : total charge density of sample (meq g⁻¹)

μ_p : peak mobility (cm² V⁻¹ min⁻¹)

k_{pH} : optimized Offord's constant.

Table A.7. Parameters for the electrophoresis of the Fraction 6.

pH	L_T	E	Q_{pH}	μ_p	k_{pH}
3.95	27	30	-3.25	-0.0081	0.228
4.20	27	25	-3.57	-0.0124	0.370
4.51	37	30	-3.95	-0.0181	0.428
4.96	37	20	-4.47	-0.0195	0.420
5.50	37	25	-5.00	-0.0197	0.417
5.88	37	30	-5.31	-0.0197	0.397
6.36	37	30	-5.62	-0.0209	0.398
6.64	37	30	-5.77	-0.0206	0.366
7.67	37	30	-6.13	-0.0211	0.352
8.45	37	30	-6.30	-0.0221	0.358
8.86	37	30	-6.40	-0.0221	0.363
9.26	37	20	-6.52	-0.0239	0.397
9.90	37	20	-6.74	-0.0243	0.374
10.59	57	30	-6.90	-0.0274	0.413
11.31	57	30	-6.96	-0.0267	0.398

L_T : total length of capillary (cm).

E : potential (kV).

Q_{pH} : total charge density of sample (meq g⁻¹)

μ_p : peak mobility (cm² V⁻¹ min⁻¹)

k_{pH} : optimized Offord's constant.

Table A.8. Parameters for the electrophoresis of the Fraction 7.

pH	L_T/L_D	E	Q_{pH}	μ_p	k_{pH}
3.56	27	20	-2.84	-0.0043	0.088
3.80	27	35	-2.97	-0.0090	0.270
4.01	27	20	-3.09	-0.0115	0.343
4.42	37	30	-3.31	-0.0172	0.532
4.72	37	30	-3.46	-0.0175	0.533
4.92	37	20	-3.56	-0.0194	0.567
5.10	37	25	-3.65	-0.0185	0.548
5.68	37	30	-3.91	-0.0194	0.564
6.00	37	30	-4.05	-0.0202	0.555
6.57	37	30	-4.29	-0.0210	0.547
6.80	37	25	-4.38	-0.0183	0.524
7.16	27	25	-4.52	-0.0188	0.415
7.84	27	20	-4.78	-0.0199	0.416
8.49	27	20	-5.04	-0.0212	0.416
9.00	37	30	-5.25	-0.0215	0.437
9.84	37	25	-5.64	-0.0237	0.474
10.62	37	20	-6.06	-0.0244	0.455
11.33	37	20	-6.48	-0.0252	0.439

L_T : total length of capillary (cm).

E : potential (kV).

Q_{pH} : total charge density of sample (meq g⁻¹)

μ_p : peak mobility (cm² V⁻¹ min⁻¹)

k_{pH} : optimized Offord's constant.

Table A.9. The parameters for the 3-Gaussian-3-Lorentzian (3-GL) model for the SRNOM.

pH	Gaussian Functions			Lorentzian Functions		
	A	μ	σ	A	μ	σ
3.55	2.00E-06	-1.80E-02	4.00E-04	1.77E-05	-3.71E-03	5.00E-03
	7.00E-05	-1.00E-02	3.08E-03	6.50E-07	-2.04E-03	1.00E-04
	4.24E-05	-1.54E-02	2.28E-03	7.50E-07	-6.00E-03	3.12E-04
3.75	1.57E-05	-1.84E-02	1.33E-03	1.09E-05	-3.25E-03	2.35E-03
	9.35E-05	-9.91E-03	3.33E-03	1.00E-07	-1.97E-03	1.00E-04
	5.05E-05	-1.51E-02	2.17E-03	1.57E-07	-7.15E-03	7.44E-04
3.92	5.22E-05	-1.66E-02	2.23E-03	1.00E-07	-6.50E-03	8.00E-03
	1.21E-04	-9.50E-03	4.88E-03	1.00E-07	-1.99E-03	1.00E-04
	3.66E-05	-1.27E-02	2.04E-03	1.00E-07	-1.09E-02	5.99E-03
4.04	1.03E-04	-1.21E-02	3.31E-03	3.00E-06	-1.82E-03	5.00E-04
	1.07E-05	-1.93E-02	1.09E-03	1.00E-07	-2.26E-02	9.98E-04
	4.59E-05	-1.65E-02	1.99E-03	5.38E-05	-3.93E-03	7.81E-03
4.22	9.15E-05	-1.10E-02	3.53E-03	1.00E-07	-2.57E-02	2.49E-02
	4.59E-05	-2.02E-02	2.06E-03	4.77E-06	-2.27E-02	1.92E-03
	1.34E-04	-1.62E-02	2.72E-03	1.84E-05	-2.96E-03	3.71E-03
4.44	2.35E-05	-9.50E-03	3.02E-03	1.00E-07	-1.76E-02	6.63E-04
	1.06E-04	-1.79E-02	3.19E-03	3.00E-06	-2.29E-02	1.63E-03
	9.13E-05	-1.61E-02	3.64E-03	1.98E-06	-3.40E-03	6.45E-04
4.87	1.00E-07	-1.32E-02	1.00E-04	6.78E-07	-1.74E-02	3.37E-04
	5.42E-05	-1.88E-02	2.09E-03	3.30E-06	-2.33E-02	1.82E-03
	9.98E-05	-1.80E-02	4.00E-03	1.00E-07	-1.91E-02	6.30E-04
5.20	1.38E-07	-1.31E-02	1.00E-04	3.29E-05	-1.74E-02	2.44E-04
	7.81E-05	-1.87E-02	1.86E-03	1.00E-07	-2.32E-02	1.53E-03
	2.21E-05	-1.75E-02	3.53E-03	1.96E-05	-1.91E-02	6.27E-04
5.94	1.19E-07	-1.32E-02	1.00E-04	2.34E-05	-1.63E-02	2.28E-04
	1.23E-04	-1.88E-02	1.91E-03	5.72E-06	-2.32E-02	1.53E-03
	2.09E-05	-1.66E-02	3.48E-03	1.32E-05	-1.98E-02	5.93E-04

Table A.9 (Continued). The parameters for the 3-Gaussian-3-Lorentzian (3-GL) model for the SRNOM.

pH	Gaussian Functions			Lorentzian Functions		
	A	μ	σ	A	μ	σ
6.34	1.00E-07	-9.40E-04	1.00E-04	2.56E-05	-1.65E-02	4.30E-04
	8.75E-05	-1.90E-02	1.91E-03	5.56E-06	-2.40E-02	2.11E-03
	4.50E-05	-1.73E-02	4.20E-03	1.62E-05	-1.98E-02	8.17E-04
6.66	1.00E-07	-1.11E-03	3.06E-02	1.02E-05	-1.61E-02	2.37E-04
	1.15E-04	-1.91E-02	1.84E-03	2.20E-06	-2.50E-02	1.19E-03
	4.06E-05	-1.80E-02	3.27E-03	7.28E-06	-1.23E-02	3.43E-03
7.01	4.32E-05	-6.91E-03	1.08E-02	6.77E-06	-1.73E-02	2.87E-04
	1.35E-04	-2.05E-02	2.40E-03	4.77E-06	-2.57E-02	1.53E-03
	1.81E-05	-1.91E-02	4.03E-03	7.86E-06	-1.20E-02	1.67E-03
7.76	1.67E-05	-2.07E-02	1.20E-03	7.21E-06	-1.76E-02	6.01E-04
	7.90E-05	-2.20E-02	2.69E-03	3.41E-06	-2.73E-02	2.12E-03
	4.17E-05	-1.80E-02	4.21E-03	1.35E-06	-1.23E-02	3.68E-04
8.62	5.30E-06	-2.63E-02	1.00E-03	2.80E-06	-1.70E-02	6.83E-04
	8.43E-05	-2.15E-02	2.30E-03	4.08E-07	-2.80E-02	1.00E-04
	4.38E-05	-1.87E-02	5.25E-03	1.00E-06	-1.20E-02	6.00E-04
9.25	6.54E-06	-2.67E-02	1.44E-03	1.75E-06	-2.18E-02	6.00E-04
	6.31E-05	-2.28E-02	2.38E-03	1.51E-06	-2.79E-02	1.00E-04
	8.54E-06	-1.64E-02	3.80E-03	3.18E-07	-1.32E-02	6.00E-04
9.64	1.09E-06	-2.70E-02	6.09E-04	4.39E-06	-2.97E-02	1.38E-03
	6.34E-05	-2.37E-02	2.17E-03	2.19E-06	-2.76E-02	4.09E-04
	1.07E-05	-1.70E-02	3.44E-03	1.00E-07	-1.32E-02	1.19E-03
10.40	1.32E-05	-2.65E-02	7.85E-04	1.38E-05	-2.99E-02	1.37E-03
	3.78E-05	-2.41E-02	3.02E-03	8.29E-06	-3.20E-02	1.22E-03
	8.29E-05	-2.36E-02	2.09E-03	4.40E-06	-2.45E-02	8.02E-04
11.25	1.41E-04	-2.64E-02	3.49E-03	2.53E-06	-1.58E-02	4.60E-04
	1.00E-07	-1.52E-02	1.21E-02	4.35E-07	-3.45E-02	1.00E-04
	6.81E-06	-2.49E-02	9.93E-04	2.30E-06	-2.66E-02	5.75E-04

Table A.10. The parameters for the 3-Gaussian-3-Lorentzian (3-GL) model for Fraction 1.

pH	Gaussian Functions			Lorentzian Functions		
	A	μ	σ	A	μ	σ
2.90	1.61E-07	-8.30E-03	3.07E-04	1.00E-07	-9.59E-03	7.09E-03
	1.00E-07	-9.59E-03	7.92E-03	4.96E-06	-3.36E-03	2.75E-03
	4.67E-06	-6.31E-03	1.81E-03	1.00E-07	-6.66E-03	5.53E-03
3.18	1.00E-07	-6.23E-03	4.41E-04	5.52E-06	-1.34E-02	1.62E-03
	1.11E-05	-1.09E-02	1.69E-03	1.23E-07	-3.93E-03	1.00E-04
	3.05E-05	-6.59E-03	3.38E-03	1.00E-07	-7.38E-03	6.01E-03
3.39	1.00E-07	-5.59E-03	1.00E-04	3.54E-06	-1.34E-02	2.97E-03
	9.35E-06	-1.15E-02	2.06E-03	1.00E-07	-5.59E-03	1.00E-04
	3.99E-05	-6.06E-03	3.62E-03	1.00E-07	-7.45E-03	6.01E-03
3.66	1.00E-07	-1.56E-02	1.38E-02	2.10E-06	-1.78E-03	3.08E-04
	9.46E-05	-9.74E-03	2.63E-03	1.00E-07	-1.56E-02	1.38E-02
	5.25E-05	-4.86E-03	1.78E-03	1.00E-07	-7.56E-03	6.00E-03
4.06	4.69E-06	-2.05E-02	1.07E-03	1.67E-05	-5.98E-03	1.72E-03
	1.00E-07	-2.31E-02	2.66E-03	8.67E-06	-1.83E-02	2.62E-03
	5.11E-05	-1.54E-02	3.02E-03	1.07E-04	-8.88E-03	7.93E-03
4.30	1.92E-05	-1.97E-02	2.09E-03	4.13E-07	-6.60E-03	4.00E-04
	1.00E-07	-2.32E-02	3.57E-04	1.00E-07	-1.82E-02	1.00E-04
	4.13E-05	-1.65E-02	6.00E-03	1.61E-07	-9.41E-03	3.50E-04
4.64	5.79E-05	-2.05E-02	1.98E-03	1.28E-06	-6.51E-03	7.05E-04
	7.37E-06	-2.33E-02	1.48E-03	1.53E-07	-1.92E-02	3.11E-03
	5.15E-05	-1.55E-02	4.10E-03	1.95E-07	-9.39E-03	3.00E-04
4.92	6.67E-05	-2.01E-02	1.74E-03	1.68E-05	-2.04E-02	1.84E-03
	5.97E-06	-2.32E-02	1.04E-03	1.00E-07	-1.92E-02	3.07E-03
	4.67E-05	-1.54E-02	4.06E-03	2.72E-05	-2.13E-02	2.13E-03
5.25	5.64E-05	-1.90E-02	1.65E-03	2.18E-07	-1.99E-02	3.18E-04
	4.78E-06	-2.29E-02	9.63E-04	6.64E-05	-1.96E-02	7.21E-04
	4.07E-05	-1.47E-02	3.69E-03	8.14E-06	-2.20E-02	1.67E-03

Table A.10 (Continued). The parameters for the 3-Gaussian-3-Lorentzian (3-GL) model for Fraction 1.

pH	Gaussian Functions			Lorentzian Functions		
	A	μ	σ	A	μ	σ
5.42	5.60E-05	-1.92E-02	1.94E-03	2.72E-05	-2.01E-02	3.69E-04
	1.07E-05	-2.30E-02	1.45E-03	5.60E-05	-1.96E-02	1.08E-03
	2.56E-05	-1.49E-02	3.41E-03	4.90E-06	-2.20E-02	1.67E-03
5.70	2.58E-05	-1.92E-02	2.58E-03	5.30E-05	-1.99E-02	7.60E-04
	3.14E-05	-2.04E-02	2.47E-03	3.59E-05	-1.91E-02	1.80E-03
	1.97E-05	-1.46E-02	4.28E-03	1.71E-06	-2.45E-02	1.32E-03
6.21	5.81E-05	-1.74E-02	1.02E-03	7.56E-06	-1.94E-02	2.43E-03
	9.87E-05	-1.70E-02	3.59E-03	4.98E-05	-1.72E-02	2.50E-04
	5.93E-05	-1.04E-02	5.76E-03	2.46E-06	-2.34E-02	1.00E-04
6.56	5.78E-05	-1.79E-02	9.02E-04	3.86E-05	-1.95E-02	2.93E-03
	9.86E-05	-1.70E-02	3.69E-03	5.27E-05	-1.75E-02	2.86E-04
	6.00E-05	-9.62E-03	5.66E-03	2.28E-06	-2.65E-02	1.00E-04
6.87	9.00E-05	-1.84E-02	1.18E-03	3.55E-05	-2.12E-02	3.31E-03
	8.17E-05	-1.60E-02	3.86E-03	2.85E-05	-1.75E-02	2.68E-04
	6.84E-05	-1.08E-02	1.10E-02	4.00E-06	-2.73E-02	1.00E-04
7.54	9.22E-05	-1.87E-02	1.24E-03	9.20E-05	-2.11E-02	4.09E-03
	3.04E-05	-1.57E-02	2.30E-03	2.18E-06	-1.75E-02	1.00E-04
	1.12E-04	-1.32E-02	6.67E-03	1.28E-06	-2.97E-02	1.00E-04
7.95	9.49E-05	-1.88E-02	1.76E-03	1.13E-04	-2.13E-02	4.92E-03
	4.49E-05	-1.44E-02	3.01E-03	8.09E-06	-1.74E-02	5.14E-04
	8.86E-05	-1.03E-02	8.37E-03	1.00E-06	-2.91E-02	5.00E-05
8.54	1.29E-04	-2.03E-02	2.17E-03	9.39E-05	-1.83E-02	9.14E-03
	1.00E-07	-2.78E-03	1.00E-04	8.04E-05	-1.40E-02	9.40E-03
	2.99E-05	-2.78E-03	1.07E-02	1.47E-06	-3.01E-02	1.16E-04
9.25	1.00E-04	-2.22E-02	1.70E-03	2.10E-04	-1.92E-02	9.79E-03
	1.36E-07	-1.95E-03	1.00E-04	8.81E-05	-1.11E-02	1.24E-02
	1.00E-07	-2.62E-03	1.03E-04	1.71E-06	-2.90E-02	1.00E-04

Table A.10 (Continued). The parameters for the 3-Gaussian-3-Lorentzian (3-GL) model for Fraction 1.

pH	Gaussian Functions			Lorentzian Functions		
	A	μ	σ	A	μ	σ
9.52	9.98E-05	-2.21E-02	1.70E-03	2.08E-04	-1.92E-02	9.78E-03
	1.18E-07	-1.95E-03	1.00E-04	7.06E-05	-1.11E-02	1.24E-02
	1.31E-07	-2.62E-03	1.00E-04	2.96E-06	-2.97E-02	1.00E-04
10.13	1.00E-07	-3.13E-03	2.59E-02	5.97E-05	-2.01E-02	3.52E-03
	1.00E-07	-3.13E-03	1.00E-04	9.00E-05	-2.20E-02	2.39E-03
	1.00E-07	-3.13E-03	1.00E-04	2.43E-05	-1.43E-02	6.16E-03
10.53	1.00E-07	-2.45E-03	2.96E-02	9.08E-05	-9.03E-03	1.24E-02
	1.00E-07	-2.28E-03	2.97E-02	4.65E-04	-2.28E-02	5.13E-03
	1.00E-07	-1.39E-03	2.89E-02	4.23E-06	-1.53E-02	9.20E-04
11.35	1.41E-04	-2.33E-02	1.85E-03	6.62E-06	-1.82E-02	1.96E-03
	9.39E-05	-1.75E-02	7.64E-03	1.00E-07	-1.39E-02	8.05E-03
	1.00E-07	-2.70E-02	9.79E-03	1.64E-07	-6.79E-03	2.01E-04

Table A.11. The parameters for the 3-Gaussian-3-Lorentzian (3-GL) model for Fraction 2.

pH	Gaussian Functions			Lorentzian Functions		
	A	μ	σ	A	μ	σ
2.93	1.69E-05	-5.46E-03	9.59E-04	1.61E-06	-1.49E-03	7.01E-04
	1.88E-05	-7.94E-03	1.83E-03	2.32E-06	-3.87E-03	9.94E-04
	4.51E-07	-1.23E-02	1.19E-02	4.95E-06	-2.21E-03	1.10E-03
3.04	1.22E-04	-7.93E-03	2.41E-03	2.62E-05	-2.22E-03	2.71E-03
	4.24E-05	-1.19E-02	1.81E-03	4.68E-05	-4.27E-03	3.91E-03
	4.02E-06	-1.42E-02	9.11E-04	2.25E-06	-1.54E-03	4.24E-04
3.20	1.83E-04	-7.76E-03	2.19E-03	3.77E-05	-2.59E-03	2.73E-03
	1.96E-04	-1.12E-02	2.17E-03	3.29E-06	-4.21E-03	2.85E-04
	3.36E-05	-1.47E-02	1.18E-03	3.68E-06	-8.84E-03	3.70E-04
3.47	1.84E-05	-1.78E-02	1.42E-03	2.52E-05	-2.18E-03	5.91E-03
	5.59E-05	-1.19E-02	3.10E-03	5.41E-06	-6.20E-03	2.24E-03
	1.16E-05	-1.52E-02	1.36E-03	2.66E-07	-1.16E-02	1.00E-04
3.85	1.24E-04	-1.37E-02	3.20E-03	7.04E-06	-1.84E-02	2.72E-03
	4.08E-07	-7.47E-04	9.17E-03	1.60E-05	-2.00E-03	3.60E-03
	6.44E-05	-7.93E-03	3.56E-03	1.67E-06	-1.33E-02	1.84E-04
4.15	4.04E-05	-1.30E-02	2.91E-03	3.30E-07	-1.81E-02	1.00E-04
	9.24E-05	-1.22E-02	2.89E-03	1.00E-07	-2.43E-03	6.11E-03
	6.06E-05	-6.69E-03	4.62E-03	1.00E-07	-1.19E-02	2.07E-03
4.46	1.00E-07	-2.34E-02	2.94E-03	1.00E-07	-1.54E-02	2.03E-02
	1.08E-04	-1.65E-02	2.28E-03	1.00E-07	-1.20E-02	6.09E-03
	5.52E-05	-1.30E-02	4.76E-03	6.79E-06	-1.19E-02	2.06E-03
4.71	1.00E-07	-2.37E-02	2.04E-03	1.48E-05	-1.57E-02	2.02E-02
	1.50E-04	-1.62E-02	1.94E-03	1.79E-05	-1.33E-02	5.00E-03
	2.63E-05	-1.00E-02	7.75E-03	2.66E-07	-1.23E-02	1.00E-04
5.08	4.42E-05	-2.22E-02	1.89E-03	1.00E-07	-2.59E-02	2.69E-04
	1.61E-05	-1.96E-02	3.15E-03	2.20E-07	-2.26E-02	7.54E-04
	3.25E-06	-9.77E-03	9.52E-03	1.00E-07	-1.30E-02	1.00E-04

Table A.11 (Continued). The parameters for the 3-Gaussian-3-Lorentzian (3-GL) model for Fraction 2.

pH	Gaussian Functions			Lorentzian Functions		
	A	μ	σ	A	μ	σ
5.43	4.48E-05	-2.59E-02	1.59E-03	4.35E-06	-2.62E-02	7.99E-04
	1.35E-07	-2.33E-02	1.00E-04	1.00E-07	-2.08E-02	1.00E-03
	1.24E-05	-2.32E-02	3.30E-03	7.94E-07	-2.35E-02	1.75E-03
5.96	3.48E-05	-2.51E-02	1.39E-03	1.35E-07	-2.93E-02	1.00E-04
	1.00E-07	-2.34E-02	4.03E-03	3.49E-05	-2.46E-02	1.50E-04
	1.00E-07	-2.35E-02	1.00E-04	1.28E-05	-2.76E-02	3.13E-03
6.25	2.80E-05	-2.57E-02	1.69E-03	2.50E-07	-2.92E-02	1.00E-04
	8.68E-06	-2.66E-02	6.67E-04	1.07E-05	-2.76E-02	1.31E-04
	1.00E-07	-2.25E-02	1.00E-04	9.55E-06	-2.73E-02	5.64E-04
6.77	5.33E-06	-2.81E-02	2.33E-04	1.05E-05	-2.83E-02	1.21E-04
	1.51E-05	-2.77E-02	1.98E-03	1.51E-05	-2.75E-02	1.49E-03
	1.00E-07	-2.26E-02	1.00E-04	7.85E-07	-3.01E-02	3.86E-04
7.22	8.60E-07	-2.79E-02	1.00E-04	1.32E-05	-2.82E-02	1.75E-04
	1.08E-05	-2.78E-02	1.55E-03	2.15E-05	-2.76E-02	2.33E-03
	1.00E-07	-2.32E-02	1.00E-04	1.81E-06	-3.05E-02	4.84E-04
7.77	1.00E-07	-2.46E-02	1.00E-04	1.25E-05	-2.74E-02	2.59E-04
	6.59E-05	-2.80E-02	2.33E-03	3.37E-07	-2.90E-02	3.00E-04
	1.00E-07	-2.38E-02	5.99E-04	8.52E-07	-1.88E-02	1.00E-04
8.38	2.50E-05	-2.46E-02	1.97E-02	6.98E-06	-2.60E-02	2.43E-04
	6.72E-05	-2.80E-02	2.25E-03	2.06E-07	-3.50E-02	7.35E-04
	2.53E-06	-2.38E-02	2.02E-02	3.41E-07	-1.80E-02	1.00E-04
8.91	3.61E-06	-2.45E-02	1.97E-02	1.58E-06	-2.54E-02	1.00E-04
	5.54E-05	-2.78E-02	2.03E-03	2.46E-06	-3.18E-02	2.10E-03
	1.98E-06	-2.38E-02	2.02E-02	4.22E-07	-1.80E-02	1.00E-04
9.33	5.76E-05	-2.43E-02	1.99E-02	6.95E-06	-3.12E-02	1.00E-04
	8.02E-05	-2.65E-02	1.78E-03	1.00E-07	-3.17E-02	3.39E-04
	1.00E-07	-2.38E-02	1.97E-02	1.00E-07	-1.67E-02	4.00E-04

Table A.11 (Continued). The parameters for the 3-Gaussian-3-Lorentzian (3-GL) model for Fraction 2.

pH	Gaussian Functions			Lorentzian Functions		
	A	μ	σ	A	μ	σ
9.75	2.72E-05	-2.35E-02	1.21E-02	1.00E-07	-2.35E-02	1.21E-02
	5.42E-05	-2.91E-02	1.72E-03	1.00E-07	-2.90E-02	3.00E-04
	1.08E-05	-2.35E-02	1.21E-02	1.00E-07	-2.35E-02	1.17E-02
10.67	1.00E-07	-2.24E-02	1.39E-02	1.00E-07	-2.18E-02	1.39E-02
	9.73E-05	-2.83E-02	1.58E-03	4.31E-05	-3.14E-02	3.50E-03
	1.00E-07	-2.25E-02	1.39E-02	1.00E-07	-2.28E-02	1.39E-02
11.42	1.41E-05	-2.43E-02	1.99E-02	2.44E-06	-3.38E-02	2.42E-04
	7.44E-05	-2.72E-02	1.74E-03	1.80E-06	-3.25E-02	3.27E-04
	1.18E-07	-2.38E-02	1.97E-02	1.41E-07	-1.67E-02	1.86E-04

Table A.12. The parameters for the 3-Gaussian-3-Lorentzian (3-GL) model for Fraction 3.

pH	Gaussian Functions			Lorentzian Functions		
	A	μ	σ	A	μ	σ
3.43	4.34E-05	-1.09E-02	2.37E-03	1.57E-06	-9.04E-03	1.37E-04
	1.33E-05	-1.34E-02	1.43E-03	1.33E-06	-2.01E-03	3.00E-04
	6.47E-05	-6.38E-03	3.29E-03	2.18E-06	-1.37E-03	9.91E-04
3.66	1.97E-05	-1.04E-02	1.93E-03	8.22E-07	-1.64E-02	1.00E-04
	3.88E-05	-1.45E-02	2.15E-03	1.64E-07	-3.15E-03	1.00E-04
	2.58E-05	-6.28E-03	3.25E-03	3.30E-06	-1.33E-03	8.93E-04
3.96	4.68E-05	-1.69E-02	2.53E-03	5.07E-07	-2.75E-03	3.00E-04
	2.22E-05	-1.25E-02	2.15E-03	1.00E-07	-3.89E-03	1.00E-04
	1.51E-05	-8.22E-03	3.63E-03	1.00E-07	-5.18E-03	3.00E-04
4.27	2.82E-06	-7.55E-03	6.32E-04	1.00E-07	-7.58E-03	1.00E-04
	2.51E-06	-8.54E-03	4.79E-04	1.00E-07	-8.37E-03	1.00E-04
	3.73E-06	-6.35E-03	1.28E-03	5.09E-07	-5.73E-03	5.96E-03
4.56	4.65E-06	-7.61E-03	9.52E-04	1.00E-07	-9.56E-03	8.29E-03
	3.65E-06	-8.42E-03	5.87E-04	1.00E-07	-9.56E-03	3.05E-03
	7.68E-06	-6.50E-03	1.62E-03	1.00E-07	-9.56E-03	2.63E-03
4.81	2.60E-07	-1.65E-02	3.00E-03	4.21E-07	-2.29E-02	2.66E-03
	2.88E-05	-2.16E-02	1.73E-03	1.00E-07	-1.30E-02	1.00E-04
	2.40E-05	-1.74E-02	3.00E-03	1.93E-07	-2.40E-02	4.20E-04
5.14	4.24E-06	-1.70E-02	3.00E-03	1.17E-05	-2.30E-02	2.02E-03
	4.46E-05	-2.17E-02	2.48E-03	1.00E-07	-1.33E-02	1.00E-04
	3.45E-06	-2.46E-02	8.11E-04	2.29E-07	-2.42E-02	3.34E-04
5.89	1.17E-05	-2.76E-02	1.25E-03	6.81E-05	-2.47E-02	1.90E-03
	5.65E-06	-2.37E-02	2.48E-03	6.38E-07	-1.88E-02	1.98E-03
	4.72E-06	-2.49E-02	9.90E-04	1.37E-05	-2.41E-02	1.56E-04
6.33	6.48E-06	-2.73E-02	1.75E-03	7.50E-06	-2.65E-02	3.02E-04
	7.39E-05	-2.42E-02	1.87E-03	1.51E-07	-1.71E-02	1.37E-04
	1.00E-07	-2.42E-02	1.00E-04	1.96E-05	-2.39E-02	1.69E-04

Table A.12 (Continued). The parameters for the 3-Gaussian-3-Lorentzian (3-GL) model for Fraction 3.

pH	Gaussian Functions			Lorentzian Functions		
	A	μ	σ	A	μ	σ
6.73	1.92E-05	-2.69E-02	1.10E-03	4.20E-05	-2.38E-02	2.11E-03
	5.60E-05	-2.65E-02	2.20E-03	3.39E-07	-1.67E-02	1.00E-04
	7.05E-07	-2.54E-02	5.82E-04	7.76E-06	-2.39E-02	1.15E-04
7.17	5.98E-06	-2.87E-02	9.89E-04	2.96E-06	-3.27E-02	2.16E-03
	7.04E-05	-2.80E-02	2.30E-03	2.19E-07	-1.81E-02	1.00E-04
	1.12E-05	-2.54E-02	5.81E-04	1.34E-05	-2.61E-02	1.49E-04
7.85	5.32E-05	-2.62E-02	3.00E-03	1.09E-06	-3.25E-02	1.00E-04
	1.44E-05	-1.94E-02	5.91E-03	1.00E-07	-1.60E-02	1.00E-04
	5.35E-05	-2.58E-02	1.46E-03	1.08E-06	-2.23E-02	1.00E-04
8.37	4.69E-05	-2.66E-02	3.05E-03	1.94E-06	-3.26E-02	1.00E-04
	1.23E-05	-1.74E-02	1.52E-02	5.24E-07	-1.62E-02	1.00E-04
	5.77E-05	-2.63E-02	1.53E-03	6.34E-07	-2.25E-02	1.00E-04
8.91	3.68E-05	-2.72E-02	3.03E-03	3.09E-06	-3.26E-02	1.00E-04
	6.88E-06	-1.75E-02	1.53E-02	7.76E-07	-1.64E-02	1.00E-04
	6.18E-05	-2.66E-02	1.60E-03	1.00E-07	-1.29E-02	6.34E-04
9.24	2.41E-05	-2.65E-02	3.00E-03	4.63E-06	-3.18E-02	1.00E-04
	3.48E-05	-1.75E-02	1.53E-02	3.12E-07	-1.63E-02	1.00E-04
	8.29E-05	-2.69E-02	1.71E-03	2.50E-06	-3.18E-02	5.67E-04
9.83	4.69E-07	-3.55E-02	5.30E-04	3.29E-07	-3.52E-02	1.00E-04
	8.27E-06	-2.03E-02	1.53E-02	5.45E-06	-3.25E-02	2.84E-03
	7.61E-05	-2.78E-02	1.78E-03	1.59E-06	-2.76E-02	5.34E-04
10.62	1.00E-07	-3.78E-02	2.55E-02	3.33E-07	-1.75E-02	1.00E-04
	1.00E-07	-8.82E-03	1.05E-02	2.56E-05	-3.37E-02	3.66E-03
	1.59E-04	-2.92E-02	2.09E-03	1.83E-05	-1.90E-02	1.04E-02
11.38	3.88E-05	-3.83E-02	2.49E-02	1.00E-07	-1.34E-02	2.49E-02
	1.00E-07	-2.00E-02	2.49E-02	1.00E-07	-1.34E-02	2.49E-02
	8.40E-05	-2.94E-02	2.12E-03	4.48E-07	-1.79E-02	1.00E-04

Table A.13. The parameters for the 3-Gaussian-3-Lorentzian (3-GL) model for Fraction 4.

pH	Gaussian Functions			Lorentzian Functions		
	A	μ	σ	A	μ	σ
3.33	1.00E-07	-1.47E-02	6.13E-04	1.00E-07	-6.20E-03	2.19E-04
	2.55E-06	-1.13E-02	2.32E-03	1.48E-07	-1.56E-03	3.65E-04
	1.00E-07	-8.63E-03	6.16E-04	1.00E-07	-5.09E-03	1.00E-04
3.66	1.23E-06	-1.54E-02	1.74E-03	1.00E-07	-6.21E-03	1.00E-04
	3.13E-06	-1.19E-02	1.98E-03	2.49E-07	-1.79E-03	4.00E-04
	3.72E-06	-8.54E-03	3.51E-03	1.00E-07	-2.73E-03	1.84E-04
3.90	5.64E-06	-1.54E-02	1.74E-03	1.00E-07	-1.85E-02	1.00E-04
	2.78E-06	-1.19E-02	1.98E-03	1.00E-07	-1.85E-02	1.30E-02
	5.38E-06	-8.54E-03	3.51E-03	2.23E-07	-1.41E-03	1.84E-04
4.22	1.05E-05	-1.70E-02	2.02E-03	1.00E-07	-2.24E-02	2.03E-02
	2.29E-06	-1.96E-02	9.94E-04	1.00E-07	-2.24E-02	1.30E-02
	8.10E-06	-1.22E-02	3.85E-03	3.00E-07	-2.64E-03	3.00E-04
4.64	1.85E-05	-1.79E-02	2.29E-03	1.00E-07	-2.39E-02	1.43E-02
	2.88E-06	-2.03E-02	1.34E-03	1.00E-07	-2.39E-02	1.29E-02
	6.90E-06	-1.15E-02	4.36E-03	1.00E-07	-4.56E-03	1.00E-04
4.86	1.96E-07	-1.65E-02	4.28E-03	1.00E-07	-2.60E-02	1.43E-02
	9.17E-06	-2.12E-02	1.92E-03	1.00E-07	-2.60E-02	1.29E-02
	6.11E-06	-1.81E-02	4.38E-03	5.09E-06	-2.32E-02	2.63E-03
5.67	1.83E-07	-1.74E-02	6.53E-03	3.44E-05	-2.57E-02	3.39E-03
	1.66E-05	-2.38E-02	4.91E-04	2.94E-05	-2.80E-02	3.86E-03
	1.00E-07	-3.20E-02	1.00E-04	1.28E-05	-2.36E-02	1.00E-04
6.38	7.69E-06	-1.74E-02	6.55E-03	5.03E-05	-2.51E-02	2.51E-03
	2.23E-05	-2.36E-02	7.08E-04	3.55E-05	-2.76E-02	3.63E-03
	1.00E-07	-3.22E-02	2.48E-02	5.27E-06	-2.29E-02	1.00E-04
6.97	3.78E-07	-2.09E-02	4.62E-04	2.23E-05	-2.46E-02	9.56E-04
	5.40E-06	-2.22E-02	8.52E-04	8.30E-05	-2.53E-02	3.52E-03
	1.00E-07	-2.16E-02	1.96E-03	2.25E-07	-2.13E-02	1.00E-04

Table A.13 (Continued). The parameters for the 3-Gaussian-3-Lorentzian (3-GL) model for Fraction 4.

pH	Gaussian Functions			Lorentzian Functions		
	A	μ	σ	A	μ	σ
7.54	2.82E-06	-2.05E-02	1.11E-03	1.00E-07	-2.68E-02	1.00E-04
	4.38E-05	-2.22E-02	1.79E-03	5.78E-05	-2.23E-02	3.70E-03
	1.00E-07	-2.15E-02	1.72E-03	1.60E-06	-1.91E-02	1.72E-04
7.86	7.46E-06	-2.67E-02	1.43E-03	8.88E-07	-3.25E-02	1.33E-04
	4.22E-05	-2.68E-02	1.90E-03	9.38E-07	-2.26E-02	2.06E-04
	5.49E-05	-2.73E-02	4.14E-03	1.00E-07	-1.61E-02	1.00E-04
8.11	2.94E-06	-2.80E-02	1.51E-03	7.36E-07	-3.50E-02	1.46E-03
	6.35E-05	-2.96E-02	2.78E-03	1.72E-06	-2.57E-02	1.00E-04
	2.29E-05	-2.79E-02	2.99E-03	1.00E-07	-1.79E-02	1.00E-04
8.68	6.40E-05	-2.73E-02	2.03E-03	4.96E-06	-3.33E-02	5.83E-04
	2.30E-05	-3.06E-02	2.38E-03	6.79E-07	-2.30E-02	1.00E-04
	9.56E-06	-2.40E-02	2.42E-03	6.31E-07	-1.65E-02	1.00E-04
9.24	1.00E-07	-2.79E-02	1.00E-04	9.73E-06	-3.20E-02	2.03E-04
	7.81E-05	-2.82E-02	2.18E-03	1.00E-07	-3.07E-02	3.96E-04
	2.73E-05	-3.22E-02	1.09E-02	2.65E-07	-1.66E-02	1.00E-04
9.82	1.00E-07	-2.27E-02	1.00E-04	8.71E-07	-3.26E-02	2.66E-04
	8.74E-05	-3.08E-02	2.49E-03	4.86E-07	-3.08E-02	2.78E-04
	1.00E-07	-3.67E-02	1.23E-02	2.10E-06	-2.26E-02	1.38E-02
10.48	1.00E-07	-2.27E-02	1.00E-04	1.00E-07	-3.48E-02	1.00E-04
	1.68E-04	-3.00E-02	2.82E-03	5.20E-06	-3.55E-02	2.32E-03
	6.00E-07	-3.67E-02	1.23E-02	1.00E-07	-2.27E-02	1.41E-02
11.35	1.00E-07	-2.27E-02	1.00E-04	1.00E-07	-3.25E-02	1.00E-04
	6.64E-05	-3.02E-02	2.39E-03	1.00E-07	-3.57E-02	1.00E-04
	1.00E-07	-3.67E-02	1.40E-02	1.00E-07	-2.27E-02	1.40E-02

Table A.14. The parameters for the 3-Gaussian-3-Lorentzian (3-GL) model for Fraction 5.

pH	Gaussian Functions			Lorentzian Functions		
	A	μ	σ	A	μ	σ
4.10	9.32E-06	-5.31E-03	2.17E-03	1.00E-07	-4.00E-03	7.47E-04
	1.19E-05	6.30E-05	7.39E-03	1.00E-07	-6.19E-03	2.47E-03
	2.31E-05	-1.10E-02	3.49E-03	1.56E-06	-2.85E-03	1.43E-03
4.24	4.36E-06	-5.22E-03	2.12E-03	1.00E-07	-4.01E-03	7.61E-04
	1.69E-07	-7.36E-05	7.34E-03	1.00E-07	-6.20E-03	2.47E-03
	4.96E-05	-1.19E-02	4.28E-03	7.74E-07	-2.71E-03	1.45E-03
4.52	2.91E-05	-1.95E-02	2.12E-03	2.83E-07	-5.40E-03	1.00E-03
	3.36E-05	-1.52E-02	2.25E-03	1.99E-07	-9.51E-03	1.00E-04
	3.63E-05	-8.20E-03	5.00E-03	1.00E-07	-8.58E-03	1.01E-03
4.92	6.80E-05	-1.94E-02	2.83E-03	1.69E-07	-3.11E-03	1.00E-04
	1.67E-05	-2.31E-02	1.66E-03	1.17E-06	-1.08E-02	1.05E-04
	2.18E-05	-1.60E-02	8.73E-03	2.09E-06	-9.03E-03	1.00E-03
5.34	2.66E-05	-2.09E-02	1.31E-03	2.73E-05	-1.79E-02	3.10E-03
	6.35E-05	-2.29E-02	2.12E-03	1.01E-06	-1.16E-02	1.00E-04
	1.52E-05	-1.34E-02	5.52E-03	4.45E-06	-1.71E-02	1.43E-04
6.25	8.33E-05	-1.99E-02	1.07E-03	4.46E-05	-1.70E-02	2.92E-03
	5.01E-05	-2.25E-02	1.60E-03	4.15E-07	-1.17E-02	1.00E-04
	2.30E-06	-1.54E-02	4.79E-03	2.25E-06	-1.54E-02	1.00E-04
6.71	4.15E-06	-2.76E-02	1.70E-03	1.69E-06	-1.82E-02	1.56E-04
	6.47E-05	-2.24E-02	2.45E-03	2.08E-07	-1.25E-02	1.00E-04
	3.39E-06	-1.48E-02	3.42E-03	1.03E-06	-2.22E-02	4.95E-04
7.25	5.26E-06	-2.71E-02	1.42E-03	2.00E-06	-1.80E-02	3.06E-04
	6.02E-05	-2.27E-02	1.96E-03	1.54E-07	-1.27E-02	1.00E-04
	3.59E-06	-1.47E-02	3.51E-03	1.00E-07	-3.01E-02	4.46E-04
7.60	1.21E-05	-2.69E-02	2.00E-03	9.33E-07	-1.89E-02	2.42E-04
	4.29E-05	-2.34E-02	2.02E-03	1.00E-07	-1.34E-02	1.00E-04
	5.68E-06	-1.47E-02	3.63E-03	1.37E-07	-3.01E-02	2.56E-04

Table A.14 (Continued). The parameters for the 3-Gaussian-3-Lorentzian (3-GL) model for Fraction 5.

pH	Gaussian Functions			Lorentzian Functions		
	A	μ	σ	A	μ	σ
7.75	1.96E-06	-2.69E-02	1.71E-03	1.40E-06	-1.83E-02	2.00E-04
	5.92E-05	-2.31E-02	2.12E-03	1.73E-07	-1.34E-02	1.00E-04
	2.71E-06	-1.47E-02	3.63E-03	1.00E-07	-1.83E-02	1.00E-04
8.07	1.20E-05	-2.69E-02	1.72E-03	6.85E-07	-1.87E-02	1.00E-04
	5.48E-05	-2.32E-02	1.98E-03	3.61E-07	-1.34E-02	1.00E-04
	1.53E-05	-1.47E-02	3.63E-03	1.00E-07	-1.09E-02	1.00E-04
8.26	1.00E-07	-2.45E-02	5.98E-03	1.29E-06	-1.93E-02	2.50E-04
	5.84E-05	-2.40E-02	2.46E-03	1.32E-06	-1.39E-02	3.00E-04
	1.00E-07	-1.04E-02	1.46E-02	2.16E-07	-1.12E-02	1.00E-04
8.88	1.00E-07	-2.12E-02	5.98E-03	6.64E-06	-2.76E-02	4.00E-04
	8.58E-05	-2.33E-02	2.34E-03	2.34E-06	-1.31E-02	3.00E-04
	6.01E-06	-1.04E-02	1.46E-02	1.51E-05	-1.75E-02	4.90E-03
9.25	3.22E-05	-2.11E-02	1.88E-03	1.17E-05	-2.64E-02	3.06E-04
	5.56E-05	-2.39E-02	1.50E-03	2.15E-06	-1.31E-02	2.99E-04
	5.56E-05	-3.14E-03	1.54E-02	2.33E-07	-3.04E-02	3.97E-03
9.76	1.00E-07	-3.10E-02	3.04E-02	1.90E-05	-1.39E-02	1.41E-02
	7.56E-05	-2.42E-02	2.46E-03	2.15E-07	-1.36E-02	1.00E-04
	1.00E-07	-6.56E-04	1.97E-02	1.16E-06	-2.88E-02	7.88E-04
10.35	5.15E-06	-3.19E-02	2.24E-03	4.63E-06	-1.09E-02	2.52E-02
	1.98E-04	-2.67E-02	3.41E-03	3.38E-07	-1.90E-02	5.17E-03
	1.00E-07	-1.09E-02	2.59E-02	1.00E-07	-1.09E-02	1.00E-04
10.66	1.34E-05	-3.24E-02	8.62E-04	1.00E-07	-6.19E-03	6.82E-03
	1.48E-04	-2.65E-02	2.74E-03	6.63E-07	-1.91E-02	2.67E-03
	3.89E-06	-6.19E-03	9.33E-03	1.00E-07	-6.19E-03	1.00E-04
11.25	7.39E-05	-1.12E-02	2.37E-03	1.90E-06	-4.03E-03	4.00E-03
	3.01E-05	-1.46E-02	1.98E-03	4.19E-06	-8.73E-03	3.80E-03
	1.00E-07	-2.28E-03	3.83E-03	1.00E-07	-1.73E-03	1.00E-04

Table A.15. The parameters for the 3-Gaussian-3-Lorentzian (3-GL) model for Fraction 6.

pH	Gaussian Functions			Lorentzian Functions		
	A	μ	σ	A	μ	σ
3.95	1.00E-05	-8.14E-03	2.86E-03	3.74E-07	-3.17E-03	1.16E-03
	1.00E-07	-7.31E-03	2.75E-03	1.00E-07	-7.59E-03	3.00E-03
	2.92E-06	-2.16E-03	2.24E-03	1.00E-07	-1.96E-03	1.00E-04
4.20	3.12E-06	-1.25E-02	3.31E-03	1.00E-07	-3.53E-03	2.95E-04
	1.00E-07	-1.87E-02	2.72E-03	1.00E-07	-6.68E-03	4.03E-04
	2.01E-06	-1.31E-02	3.02E-03	1.00E-07	-1.93E-03	1.00E-04
4.51	2.77E-07	-1.50E-02	3.03E-03	2.82E-07	-3.05E-03	1.00E-03
	2.55E-06	-1.88E-02	1.80E-03	1.96E-07	-6.29E-03	3.45E-04
	1.28E-05	-1.57E-02	4.82E-03	1.00E-07	-1.01E-02	1.00E-04
4.96	1.00E-07	-1.32E-02	7.60E-03	1.00E-07	-2.06E-03	1.29E-04
	1.21E-05	-2.03E-02	2.47E-03	1.02E-06	-5.37E-03	3.00E-03
	8.98E-06	-1.47E-02	3.00E-03	3.75E-07	-1.03E-02	1.00E-04
5.50	9.82E-06	-1.47E-02	4.94E-03	8.51E-07	-1.23E-02	1.73E-04
	1.78E-05	-2.08E-02	2.53E-03	9.61E-06	-1.99E-02	1.46E-03
	1.34E-06	-2.33E-02	1.67E-03	1.00E-07	-1.04E-02	1.00E-04
5.88	6.68E-06	-1.45E-02	5.34E-03	5.60E-07	-1.27E-02	1.00E-04
	2.58E-05	-2.04E-02	3.07E-03	1.07E-05	-1.97E-02	3.00E-04
	1.00E-07	-2.31E-02	1.67E-03	9.22E-07	-2.50E-02	2.21E-03
6.36	5.83E-06	-1.53E-02	4.03E-03	6.81E-07	-1.44E-02	1.00E-04
	6.83E-06	-2.22E-02	2.39E-03	1.52E-07	-1.13E-02	1.88E-04
	1.28E-06	-2.32E-02	5.19E-04	2.26E-06	-2.39E-02	2.00E-04
6.64	1.70E-05	-1.77E-02	9.31E-03	6.16E-07	-1.24E-02	1.00E-04
	3.98E-05	-2.10E-02	3.97E-03	5.19E-06	-1.98E-02	2.34E-03
	3.28E-06	-2.08E-02	6.26E-04	5.17E-06	-1.78E-02	1.45E-04
7.67	2.17E-06	-1.53E-02	1.42E-03	1.73E-07	-2.67E-02	1.00E-04
	3.95E-05	-2.12E-02	2.89E-03	1.12E-06	-1.30E-02	3.30E-04
	2.29E-06	-1.16E-02	4.43E-03	2.73E-06	-1.81E-02	1.86E-04

Table A.15 (Continued). The parameters for the 3-Gaussian-3-Lorentzian (3-GL) model for Fraction 6.

pH	Gaussian Functions			Lorentzian Functions		
	A	μ	σ	A	μ	σ
8.45	5.55E-06	-2.74E-02	3.98E-03	4.05E-07	-2.66E-02	3.26E-04
	5.32E-05	-2.20E-02	3.38E-03	2.97E-06	-1.29E-02	8.31E-04
	6.02E-06	-1.12E-02	3.26E-03	8.72E-07	-1.81E-02	4.62E-04
8.86	1.00E-07	-2.35E-02	2.75E-03	7.69E-07	-2.72E-02	3.70E-04
	5.89E-05	-2.23E-02	3.85E-03	8.83E-07	-1.29E-02	6.19E-04
	3.34E-06	-1.11E-02	3.18E-03	1.00E-07	-1.77E-02	2.16E-03
9.26	2.45E-05	-2.43E-02	2.33E-03	5.01E-06	-2.75E-02	1.90E-04
	2.63E-05	-2.22E-02	4.43E-03	8.46E-07	-1.40E-02	6.92E-04
	1.31E-06	-8.53E-03	2.62E-03	5.70E-06	-2.78E-02	2.80E-04
9.90	2.52E-05	-2.51E-02	2.51E-03	3.40E-07	-2.86E-02	1.00E-04
	2.28E-05	-2.20E-02	3.80E-03	1.01E-07	-1.45E-02	1.00E-04
	3.13E-06	-8.31E-03	2.92E-03	6.61E-07	-2.96E-02	5.92E-04
10.59	2.22E-04	-2.73E-02	3.23E-03	5.15E-06	-2.91E-02	7.55E-04
	2.18E-05	-2.11E-02	3.85E-03	3.64E-07	-1.46E-02	1.00E-04
	1.60E-06	-9.11E-03	2.41E-03	5.03E-06	-3.04E-02	5.49E-04
11.31	7.13E-05	-2.71E-02	3.15E-03	2.34E-07	-1.58E-02	1.00E-04
	9.25E-06	-1.81E-02	2.80E-03	1.00E-07	-9.70E-03	3.00E-04
	2.20E-06	-1.05E-02	2.83E-03	1.00E-07	-2.31E-02	1.00E-04

Table A.16. The parameters for the 3-Gaussian-3-Lorentzian (3-GL) model for Fraction 7.

pH	Gaussian Functions			Lorentzian Functions		
	A	μ	σ	A	μ	σ
3.56	1.62E-07	-1.48E-03	1.00E-04	1.67E-06	-1.66E-03	9.54E-04
	2.34E-07	-9.79E-03	2.13E-03	1.40E-06	-2.76E-03	1.46E-03
	6.64E-06	-1.72E-03	1.23E-03	2.17E-06	-6.65E-04	4.37E-04
3.80	8.58E-06	-1.21E-02	1.27E-03	7.67E-07	-1.65E-02	5.44E-03
	3.61E-05	-8.72E-03	2.31E-03	1.12E-06	-2.50E-03	6.55E-04
	3.58E-05	-3.39E-03	2.27E-03	1.64E-06	-1.69E-03	3.26E-04
4.01	4.83E-06	-1.43E-02	1.78E-03	1.00E-07	-1.55E-02	5.14E-03
	3.04E-05	-9.50E-03	4.10E-03	1.00E-07	-3.85E-03	1.00E-04
	5.09E-06	-3.40E-03	1.05E-03	4.71E-07	-2.18E-03	1.00E-04
4.42	4.09E-05	-1.45E-02	3.22E-03	1.97E-05	-1.77E-02	3.70E-03
	1.99E-05	-7.74E-03	3.88E-03	1.58E-07	-1.07E-02	1.00E-04
	2.41E-05	-2.07E-02	1.79E-03	3.13E-07	-9.60E-03	1.00E-04
4.72	4.14E-05	-1.00E-02	4.64E-03	3.56E-06	-1.12E-02	7.62E-04
	1.03E-05	-2.23E-02	1.76E-03	1.79E-06	-9.21E-03	1.38E-03
	9.34E-05	-1.80E-02	3.00E-03	1.53E-07	-7.31E-03	1.71E-04
4.92	1.56E-05	-6.56E-03	3.14E-03	1.59E-07	-2.01E-02	2.97E-04
	3.80E-05	-2.17E-02	2.71E-03	1.67E-06	-1.23E-02	3.37E-04
	6.25E-05	-1.76E-02	4.45E-03	1.00E-07	-7.08E-03	4.52E-04
5.10	1.01E-05	-6.62E-03	3.09E-03	1.00E-07	-2.01E-02	2.96E-04
	6.01E-05	-2.00E-02	2.15E-03	1.38E-06	-1.28E-02	2.80E-04
	3.75E-05	-1.54E-02	4.13E-03	1.52E-07	-7.76E-03	3.00E-04
5.68	1.02E-05	-6.27E-03	3.50E-03	9.64E-06	-1.97E-02	2.15E-04
	3.45E-05	-2.22E-02	2.10E-03	9.54E-07	-1.33E-02	2.42E-04
	4.11E-05	-1.57E-02	4.24E-03	4.58E-05	-1.91E-02	1.80E-03
6.00	7.31E-06	-5.72E-03	2.37E-03	1.89E-05	-2.02E-02	5.25E-04
	5.91E-05	-2.22E-02	2.99E-03	3.08E-06	-2.17E-02	2.18E-03
	6.69E-05	-1.61E-02	5.42E-03	1.07E-05	-1.92E-02	1.16E-03

Table A.16 (Continued). The parameters for the 3-Gaussian-3-Lorentzian (3-GL) model for Fraction 7.

pH	Gaussian Functions			Lorentzian Functions		
	A	μ	σ	A	μ	σ
6.57	4.80E-06	-7.13E-03	1.87E-03	9.45E-06	-2.01E-02	4.53E-04
	3.55E-05	-2.28E-02	2.42E-03	1.21E-06	-2.27E-02	3.00E-04
	4.06E-05	-1.74E-02	4.33E-03	8.14E-06	-1.93E-02	1.19E-03
6.80	1.00E-07	-1.89E-02	1.00E-04	6.71E-06	-2.03E-02	5.28E-04
	6.59E-05	-2.34E-02	2.56E-03	8.30E-06	-1.97E-02	1.30E-03
	6.06E-05	-1.39E-02	6.53E-03	1.84E-05	-1.79E-02	4.38E-03
7.16	1.00E-07	-1.91E-02	1.00E-04	5.12E-06	-2.59E-02	1.72E-04
	2.01E-04	-1.89E-02	3.64E-03	7.79E-07	-1.55E-02	1.00E-04
	1.17E-04	-9.11E-03	6.08E-03	1.60E-06	-1.78E-02	6.80E-04
7.84	2.53E-05	-2.45E-02	2.53E-03	1.15E-05	-2.96E-02	4.34E-04
	1.81E-04	-1.95E-02	3.95E-03	7.81E-07	-1.34E-02	4.36E-04
	1.34E-04	-9.07E-03	7.03E-03	4.65E-06	-1.86E-02	1.14E-03
8.49	4.02E-05	-2.28E-02	3.09E-03	1.60E-05	-3.06E-02	5.85E-04
	1.12E-04	-1.99E-02	4.28E-03	1.20E-06	-2.74E-02	1.16E-03
	1.58E-04	-1.14E-02	9.56E-03	3.65E-06	-1.90E-02	1.34E-03
9.00	6.61E-05	-2.23E-02	3.12E-03	1.55E-05	-2.88E-02	2.82E-04
	6.52E-05	-2.00E-02	4.09E-03	3.71E-06	-2.71E-02	1.61E-03
	1.19E-04	-1.32E-02	8.47E-03	1.00E-07	-2.90E-02	2.42E-03
9.84	1.65E-04	-2.29E-02	3.10E-03	7.06E-06	-3.06E-02	9.23E-04
	1.03E-07	-2.15E-02	5.31E-03	1.02E-05	-2.69E-02	1.37E-03
	4.90E-05	-1.27E-02	7.28E-03	1.31E-05	-3.22E-02	1.54E-03
10.62	1.41E-04	-2.52E-02	3.08E-03	2.95E-06	-2.99E-02	1.41E-03
	5.58E-05	-1.90E-02	5.33E-03	2.59E-07	-2.32E-02	1.00E-04
	1.00E-07	-8.78E-03	3.64E-03	4.00E-07	-1.51E-02	1.00E-04
11.33	5.13E-05	-2.59E-02	2.09E-03	4.35E-06	-2.92E-02	4.02E-04
	5.39E-05	-2.36E-02	3.84E-03	7.40E-06	-3.07E-02	8.49E-04
	1.10E-05	-1.47E-02	2.54E-03	1.04E-07	-1.65E-02	4.37E-04

Chain calculation for the most probable distribution of solutes with only carboxyl groups and solutes with carboxyl and phenolic groups. The chain calculation starts at $n_{\text{COOH}} = 1$.

Distribution of carboxyl groups (Figure 5.22). This is the distribution of charge as determined at pHs 7.6 to 7.9. pH 8.0 is assigned as the uppermost pH of carboxyl acidity.

n_{COOH} = number of carboxyl groups per solute.

$\%n$ = mole % of solutes with n_{COOH} .

$\text{COOH} = n_{\text{COOH}} \times \%n$ = number of carboxyl groups.

Distribution of total acidic functional groups (Figure 5.23). This is the distribution of the total acidic functional groups (carboxyl + phenolic) as determined at pHs 11.2-11.4. By pH 12.0, all phenolic groups in the samples are ionized.

n_{TOT} = number of acidic functional groups per solute.

$\%n$ = mole % of solutes with n_{TOT} .

$\text{TOT} = n_{\text{TOT}} \times \%n$ = number of acidic functional groups (COOH + ArOH).

Leaving COOH groups. This is the number of carboxyl groups that are predicted to be on solutes with a minimum of 1 phenolic group. These solutes will be represented at $n_{\text{TOT}} > n_{\text{COOH}}$.

$$\Delta\text{COOH} = \text{if}[(n_{\text{COOH}} \geq n_{\text{TOT}}), (n_{\text{COOH}} - n_{\text{TOT}}), n_{\text{COOH}}]$$

Gain of COOH groups. This is the increase of carboxyl groups from solutes from the distribution of carboxyl groups from the nTOT-1 class of solutes. The predicted increase of n between nCOOH and nTOT is calculated as the ratio of Q1/Q2 assuming that the carboxyl-to-phenolic ratio holds true for solutes with 3 or more carboxyl groups.

$$\Delta\text{COOH}^* = \text{if} \left[(n\text{COOH}_{n-1} > \Delta\text{COOH}_{n-1}), \Delta\text{COOH}_{n-1}, n\text{TOT} \times \left(\frac{Q_1}{Q_2} \right) \right]$$

Number of phenolic groups. The number of phenolic groups in each class of nTOT is calculated as the product of the predicted number of gained COOH groups from the nCOOH class into the higher nTOT + 1 class and the phenolic-to-carboxyl ratio.

$$n\text{ArOH} =$$

$$\text{if} \left[(\Delta\text{COOH}_{n-1} \leq 2), \Delta\text{COOH}_{n-1} \times \left(\frac{1}{n\text{COOH}_{n-1}} \right), \Delta\text{COOH}^* \times \left(\frac{Q_2}{Q_1} \right) \right]$$

Balance of carboxyl groups on solutes with only carboxyl groups. The number of excess carboxyl groups that are not balanced by the predicted number of gained COOH and the Q2/Q1 ratio.

$$x\text{COOH} = n\text{TOT} - \Delta\text{COOH}^* - n\text{ArOH}$$

Table A.17. Chain calculation for the most probable distribution of solutes with on carboxyl groups and solutes with carboxyl and phenolic groups in the SRNOM.

Distribution of carboxyl groups (Figure 5.21)										
n_{COOH}	1	2	3	4	5	6	7	8	9	10
%n	8.9	19.4	13.2	11.5	10.6	9.1	7.3	5.6	4.0	2.9
n_{COOH}	8.9	38.7	39.5	46.1	53.0	54.6	51.2	44.4	36.4	28.8
Distribution of total acidic functional groups (Figure 5.22)										
n_{TOT}	1	2	3	4	5	6	7	8	9	10
%n	5.7	15.8	13.5	10.6	10.1	9.4	8.2	6.8	5.4	4.1
n_{TOT}	5.7	31.6	40.4	42.4	50.6	56.2	57.3	54.2	48.2	40.8
Leaving carboxyl groups (n_{COOH} → n_{TOT} = n_{COOH} + ≥ 1 ArOH)										
ΔCOOH	3.2	13.5	17.1	26.5	37.9	49.1	51.2	44.4	36.4	28.8
Gain of carboxyl groups from n_{COOH} – 1.										
ΔCOOH*	0	3.2	13.5	17.1	26.5	37.9	40.7	37.0	33.3	28.5
Number of phenolic groups.										
n_{ArOH}	0	3.2	4.5	5.8	8.9	12.8	16.6	17.3	15.0	12.3
Balance of carboxyl groups on solutes with only carboxyl groups.										
x_{COOH}	5.7	25.3	22.4	19.6	15.2	5.5	0.0	0.0	0.0	0.0
Sum of acidic functional groups. (Double check)										
COOH	5.7	28.4	35.9	36.7	41.7	43.4	40.7	37.0	33.3	28.5
ArOH	0.0	3.2	4.5	5.8	8.9	12.8	16.6	17.3	15.0	12.3
TOT	5.7	31.6	40.4	42.4	50.6	56.2	57.3	54.2	48.2	40.8
%n of solutes with carboxyl only and carboxyl and phenol.										
COOH only	5.7	12.6	7.5	4.9	3.0	0.9	0.0	0.0	0.0	0.0
COOH and ArOH	0.0	3.2	6.0	5.7	7.1	8.4	8.2	6.8	5.4	4.1
TOT	5.7	15.8	13.5	10.6	10.1	9.3	8.2	6.8	5.4	4.1

REFERENCES

- Aiken G.R. and Malcolm R.L. (1987) Molecular weight of aquatic fulvic acids by vapor pressure osmometry. *Geochim. Cosmochim. Acta* **51**, 2177-2184.
- Alberts J.J. and Takacs M. (2004) Total luminescence spectra of IHSS standard and reference fulvic acids, humic acids, and natural organic matter: comparison of aquatic and terrestrial source terms. *Org. Geochem.* **35**, 243-256.
- Antweiler R.C. (1991) The hydrolysis of Suwannee River fulvic acid. In *Organic Substances and Sediments in Water. Volume 1: Humics and Soils* (Ed. R.A. Baker). pp. 163-177, Lewis Publishers, Chelsea, MI.
- Aoustin E., Schäfer A.I., Fane A.G., and Waite T.D. (2001) Ultrafiltration of natural organic matter. *Sep. Purif. Technol.* **22/23**, 63-78.
- Assemi S., Newcombe G., Hepplewhite C., and Beckett R. (2004) Characterization of natural organic matter fractions separated by ultrafiltration using flow field-flow fractionation. *Wat. Res.* **38**, 1467-1476.
- Baes A.U. and Bloom P.R. (1990) Fulvic acid ultraviolet-visible spectra: Influence of solvent and pH. *Soil Sci.* **54**, 1248-1254.
- Barbosa J., Barron D., and Jimenez-Lozano E. (1999) Electrophoretic behavior of quinolones in capillary electrophoresis. Effect of pH and evaluation of ionization constants. *J. Chrom. A* **839**, 183-192.
- Barth H.G. (1987) Nonsize exclusion effects in high-performance size exclusion chromatography. In: *Detection and Data Analysis in Size Exclusion Chromatography*. (ed. T. Provder) pp. 29-41. ACS press, Washington, DC.
- Bartschat B.M., Cabaniss S.E., and Morel F.M.M. (1992) Oligoelectrolyte model for cation binding by humic substances. *Environ. Sci. Technol.* **26**, 84-294.
- Beck K.C., Reuter J.H., and Perdue E.M. (1974) Organic and inorganic geochemistry of some coastal plain waters of the southeastern United States. *Geochim. Cosmochim. Acta* **38**, 341-364.
- Beckers J.L. (1994) System peaks and disturbances to the baseline UV signal in capillary zone electrophoresis. *J. Chrom. A* **662**, 153-166.
- Beckers J.L. and Boček P. (2003) The preparation of background electrolytes in capillary zone electrophoresis: golden rules and pitfalls. *Electrophoresis* **4**, 518-535.

- Beckett R., Jue Z., and Giddings J.C. (1987) Determination of molecular weight distribution of fulvic and humic acids using flow field-flow fractionation. *Environ. Sci. Technol.* **21**, 289-295.
- Bello M. S. (1996) Electrolytic modification of a buffer during a capillary electrophoresis run. *J. Chrom. A* **774**, 81-91.
- Benedetti M., Ranville J.F., Ponthieu M., and Pinheiro J.P. (2002) Field-flow fractionation characterization and binding properties of particulate and colloidal organic matter from the Rio Amazon and Rio Negro. *Org. Geochem.* **33**, 269-79.
- Benedetti M.F., van Riemsdijk W.H., and Koopal L.K. (1996) Humic substances considered as a heterogeneous Donnan gel phase. *Environ. Sci. Technol.* **30**(6), 1805-1813.
- Blom L., Edelhäusen L., Van Krevelen D.W. (1957) Chemical structure and properties of coal XVII--Oxygen groups in coal and related products. *Fuel* **36**, 135-153.
- Boden J. and Bächmann K. (1996) Investigation of matrix effects in capillary zone electrophoresis. *J. Chrom. A* **734**, 319-330.
- Bowles E.C., Antweiler E.C., and MacCarthy, P. (1989) Acid-base titrations and hydrolysis of fulvic acid from the Suwannee River. In *Humic Substances in the Suwannee River, GA: Interaction, Properties, and Proposed Structures*. (Eds. R.C. Averett *et al.*), pp. 209-229. USGS Open File Report 87-557.
- Brady B. and Pagenkopf G.K. (1978) Cadmium complexation by soil fulvic acid. *Can. J. Chem.* **56**, 2331-2336.
- Brooks J.D. and Sternhell, S. (1957) Chemistry of brown coals. *Aus. J. Appl. Sci.* **8**, 206.
- Buffle J., Greter F.-L., Haerdl W. (1977) Measurements of complexation properties of humic and fulvic acids with lead and copper ion-selective electrodes. *Anal. Chem.* **49**(2), 218-222.
- Cabaniss S.E. and Shuman M.S. (1988a) Copper binding by dissolved organic matter: I. Suwannee River fulvic acid equilibria. *Geochim. Cosmochim. Acta* **52**, 185-193.
- Cabaniss S.E. and Shuman M.S. (1988b) Copper binding by dissolved organic matter: I. Variation in type and source of organic matter. *Geochim. Cosmochim. Acta* **52**, 195-200.
- Cabaniss S.E., Zhou Q., Maurice P.A., Chin Y.-P., and Aiken G.R. (2000) A log-normal distribution model for the molecular weight of aquatic fulvic acids. *Environ. Sci. Technol.* **34**(6), 1103-1109.
- Cameron R.S., Swift R.S., Thornton B.K., and Posner A.M. (1972) Calibration of gel

- permeation chromatography materials for use with humic acid. *J. Soil Sci.* **23(3)**, 342-349.
- Chen Y., Senesi N., and Schnitzer M. (1977) Information provided on humic substances by E_4/E_6 ratios. *Soil Sci. Soc. Am. J.* **41**, 352-358.
- Chin Y.-P., Aiken G.R., and O'Loughlin E. (1994) Molecular weight, polydispersity, and spectroscopic properties of aquatic humic substances. *Environ. Sci. Technol.* **28(11)**, 1853-1858.
- Chin Y.-P. and Gschwend P.M. (1991) The abundance, distribution, and configuration of porewater organic colloids in recent sediments. *Geochim. Cosmochim. Acta* **55**, 1309-1317.
- Christensen J.B., Tipping E., Kinniburgh D., Gron C., and Christensen T.H. (1998) Proton binding by groundwater fulvic acids of different age, origins, and structure modeled with the Model V and NICA-Donnan model. *Environ. Sci. Technol.* **32(21)**, 3346-3355.
- Christl I. and Kretzschmar R. (2001) Relating ion binding by fulvic and humic acids to chemical composition and molecular size. 1. Proton binding. *Environ. Sci. Technol.* **35(12)**, 2505-2511.
- Clesceri L.S., Greenberg A.E., and Trusell R.R. (eds) (1989) *Standard Methods for the Examination of Water and Wastewater*. 17th ed. American Public Health Association, Washington D.C.
- Colovos G., Pansesar M.R., and Perry E.P. (1976) Linearizing the calibration curve in determination of sulfate by the methylthymol blue method. *Anal. Chem.* **48(12)**, 1893-1896.
- Colyer C.L., Oldham K.B., and Sokirko A.V. (1995) Electroosmotically transported baseline perturbations in capillary electrophoresis. *Anal. Chem.* **67**, 3234-3245.
- Croue J.P., Violleau D., Bodaire C., and Legube B. (1999) Removal of hydrophobic and hydrophilic constituents by anion exchange resin. *Wat. Sci. Technol.* **40(9)**, 207-214.
- Davies C.W. (1962) *Ion Association*, Butterworths, London.
- Davis H. and Mott J.B. (1981) Titrations of fulvic acid fractions I: Interactions influencing the dissociation/reprotonation equilibria. *J. Soil Sci.* **32**, 379-391.
- Davis W.M., Erickson C.L., Johnston C.T., Delfino J.J. and Porter J.E. (1999) Quantitative Fourier transform infrared spectroscopic investigation of humic substance functional group composition. *Chemosphere* **38(12)**, 2913-2928.
- De Haan H., Jones R.I., and Salonen. (1987) Does ionic strength affect the configuration of

- aquatic humic substances, as indicated by gel filtration? *Freshwat. Biol.* **17**, 453-459.
- de Wit C.M., van Riemsdijk W.H., and Koopal L.K. (1993) Proton binding to humic substances. 1. Electrostatic effects. *Environ. Sci. Technol.* **27(10)**, 2005-2014.
- De Nobili M. and Chen Y. (1999) Size exclusion chromatography of humic substances: limits, perspectives, and prospectives. *Soil Sci.* **164(11)**, 825-833.
- De Nobili M., Bragato G., and Mori A. (1999) Capillary electrophoretic behaviour of humic substances in physical gels. *J. Chrom. A* **863**, 195-204.
- Dobbs J.C., Susetyo W., Carreira L.A., and Azarraga L.V. (1989) Competitive binding of protons and metal ions in humic substances by lanthanide ion probe spectroscopy. *Anal. Chem.* **61(14)**, 1519-1524.
- Dubach P., Mehta N.C., Jakab T., and Martin F. (1964) Chemical investigations on soil humic substances. *Geochim Cosmochim Acta* **28**, 1567-1578.
- Duxbury J.M. (1989) *Studies of the molecular size and charge of humic substances by electrophoresis. In Humic Substances II. In Search of Structure.* (eds. M.B.H Hayes *et al.*). pp. 593-620. John Wiley & Sons, Ltd, New York.
- Dycus P.J.M., Healy K.D., Stearman G.K., and Wells M.J.M. (1995) Diffusion coefficients and molecular weight distributions of humic and fulvic acids determined by flow field-flow fractionation. *Sep. Sci. Technol.* **30(7-9)**, 1435-1453.
- Egeberg P.K. and Alberts J.J. (2003) HPSEC as a preparative fractionation technique for studies of natural organic matter (NOM). *Environ. Int.* **24**, 309-318.
- Ephraim J.H., Pettersson C., and Allard B. (1996) Correlation between acidity and molecular size distribution of an aquatic fulvic acid. *Environ. Int.* **22(5)**, 475-483.
- Ephraim J., Alegret S., Mathuthu A., Bicking M., Malcolm R.L., and Marinsky J.A. (1986) A unified physicochemical description of the protonation and metal ion complexation equilibria of natural organic acids (humic and fulvic acids). 2. Influence of polyelectrolyte properties and functional groups heterogeneity on the protonation equilibria of fulvic acid. *Environ. Sci. Technol.* **20**, 354-366.
- Everett C.R., Chin Y.-P. and Aiken G.R. (1999) High-pressure size exclusion chromatography analysis of dissolved organic matter isolated by tangential-flow ultrafiltration. *Limnol. Oceanogr.* **44(5)** 1316-1322.
- Foret F., Krivánková L., and Boček P. (1993) *Capillary Zone Electrophoresis*. Weinheim, New York.
- Friedel W., Reijenga J.C., and Kenndler E. (1995) Ionic strength and charge number

- correction of multivalent organic anions in capillary electrophoresis. *J. Chrom. A* **709**, 163-170.
- Garrison A.W., Schmitt-Kopplin P., and Kettrup A. (1995) Capillary electrophoresis for the characterization of humic substances. *Wat. Res.* **29(9)**, 2149-2159.
- Gaš B. and Kenndler E. (2004) System zones in capillary electrophoresis. *Electrophoresis* **5**, 3901-3912.
- Gebauer P. and Boček P. (1997) Predicting peak symmetry in capillary zone electrophoresis: the concept of the peak shape diagram. *Anal. Chem.* **69**, 1557-1563.
- Ghassemi M. and Christman R.F. (1968) Properties of the yellow organic acids of natural waters. *Limnol. Oceanogr.* **13**, 583-597.
- Gjessing E.T. and Lee F. (1967) Fractionation of organic matter in natural waters on Sephadex gels. *Environ. Sci. Technol.* **1(8)**, 631-638.
- Glück S.J., Steel K.P., and Benkö M.H. (1996) Determination of acidity constants of monoprotic and diprotic acids by capillary electrophoresis. *J. Chrom. A* **745**, 117-125.
- Gregor H.P., Luttinger L.B., and Loeb E.M. (1955) Metal-polyelectrolyte complexes. I. The polyacrylic acid-copper complexes. *J. Phys. Chem.* **59**, 34-39.
- Grimm D.M., Azarraga L.V., Carreira L.A., and Susetyo W. (1991) Continuous multiligand distribution model used to predict the stability constant of Cu(II) metal complexation with humic material from fluorescence quenching data. *Environ. Sci. Technol.* **25**, 1427-1431.
- Gustafsson J.P. (2001) Modeling the acid-base properties and metal complexation of humic substances with the Stockholm humic model. *J. Colloid Interface Sci.* **244**, 102-112.
- Hall K.J. and Lee G.F. (1972) Molecular size and spectral characterization of organic matter in a meromictic lake. *Wat. Res.* **8**, 239-251.
- Hatcher P.G., Schnitzer M., Dennis L.W., and Maciel G.F. (1981) Aromaticity of humic substances in soils. *Soil Sci. Soc. Am. J.* **45**, 1089-1094.
- Her N., Amy G., Foss D., and Cho J. (2002) Variations of molecular weight estimation by HP-size exclusion chromatography with UVA vs. online DOC detection. *Environ. Sci. Technol.* **36**, 3393-3399.
- Her N., Amy G., McKnight D.M., Sohn J., and Yoon Y. (2003) Characterization of DOM as a function of MW by fluorescence EEM and HPLC-SEC using UVA, DOC, and fluorescence detection. *Wat. Res.* **37**, 4295-4303.

- Hoffstetter-Kuhn S., Paulus A., Gassmann E., and Widmer H.M. (1991) Influence of borate complexation on the electrophoretic behavior of carbohydrates in capillary electrophoresis. *Anal. Chem.* **63**, 1541-1547.
- Holtzclaw K.M. and Sposito G. (1979) Analytical properties of the soluble, metal-complexing fractions in sludge-soil mixtures: IV. Determination of carboxyl groups in fulvic acid. *Soil Sci. Soc. Am. J.* **43**, 318-323.
- Huber W., Huber S., Gremm T., and Frimmel F.H. (1990) Chromatographic fractionation of natural organic matter with UV, fluorescence, and DOC/TOC detection without sample preconcentration: selection of separation phases for aqueous samples. *Vom Wasser* **75**, 331-342.
- Huber S.A. and Frimmel F.H. (1994) Direct gel chromatography characterization and quantification of marine dissolved organic carbon using high-sensitivity DOC detection. *Environ. Sci. Technol.* **28**(6), 1194-1197.
- Huber S.A. and Frimmel F.H. (1996) Size-exclusion chromatography with organic carbon detection (LC-OCD): a fast and reliable method for the characterization of hydrophilic organic matter in natural waters. *Vom Wasser*, **86**, 277-290.
- Janos P. (2003) Separation methods in the chemistry of humic substances. *J. Chrom. A*, **983**, 1-18.
- Katchalsky A. and Spitnik P. (1947) Potentiometric titrations of polymethylacrylic acid. *J. Polymer Sci.* **2**, 432-446.
- Kinniburgh D.G., Milne C. J., Benedetti M.F., Pinheiro J.P., Filius J., Koopal L.K., and Van Riemsdijk W.H. (1996) Metal ion binding by humic acid: application of the NICA-Donnan model. *Environ. Sci. Technol.* **30**, 1687-1698.
- Kemp A.L.W. and Wong H.K.T. (1974) Molecular weight distributions of humic substances from Lakes Ontario and Erie sediments. *Chem. Geol.* **14**, 15-22.
- Khalaf K.Y., MacCarthy P., and Gilbert T.W. (1975) Application of thermometric titrations to the study of soil organic matter. II. Humic acids. *Geoderma* **14**, 331-340.
- Khanna S.S. and F.J. Stevenson (1962) Metallo-organic complexes in soil: I. Potentiometric titration of some soil organic matter isolates in the presence of transition metals. *Soil Sci.* **93**, 298-305.
- Kudryavtsev A.V., Perminova I.V., and Petrosyan V.S. (2000) Size-exclusion chromatographic descriptors of humic substances. *Anal. Chim. Acta* **407**(1-2), 193-202.
- Kuhn R. and Hoffstetter-Kuhn S. (1993) *Capillary Electrophoresis: Principles and Practice*. Springer-Verlag, Berlin.

- Kuo C.-Y. and Provder T. (1987) An overview of size-exclusion chromatography for polymers and coatings. In: *Detection and Data Analysis in Size Exclusion Chromatography*. pp. 3-28. (ed. T. Provder) ACS press, Washington, DC.
- Leenheer J.A., Wershaw R.L., and Reddy M.M. (1995) Strong-acid, carboxyl groups structures in fulvic acid from the Suwannee River, Georgia. 1. Minor structure. *Environ. Sci. Technol.* **29**(2), 393-398.
- Lin C.-E. and Chen Y.-T. (2000) Migration behavior and separation of benzenediamines, aminophenols, and benzenediols by capillary zone electrophoresis. *J. Chrom. A* **871**, 357-366.
- Li J., Perdue E.M., and Gelbaum L.T. (1998) Using cadmium-113 NMR spectrometry to study metal complexation by natural organic matter. *Environ. Sci. Technol.* **32**, 483-487.
- Ma H., Allen H.E., and Yin Y. (2001) Characterization of isolated fractions of dissolved organic matter from natural waters and a wastewater effluent. *Wat. Res.* **35**, 985-996.
- Machesky M.L. (1993) Calorimetric acid-base titrations of aquatic and peat-derived fulvic and humic acids. *Environ. Sci. Technol.* **27**, 1182-1189.
- Marshall S.J., Young S.D., and Gregson K. (1995) Humic acid-proton equilibria: a comparison of two models and assessment of titration error. *Eur. J. Soil Sci.* **46**, 471-480.
- Miller J.M., Blackburn A.C., Shi Y., Melzak A.J., and Ando H.Y. (2002) Semi-empirical relationship between effective mobility, charge, and molecular weight of pharmaceuticals by pressure-assisted capillary electrophoresis: Applications in drug discovery. *Electrophoresis* **23**, 2833-2841.
- Milne C.J., Kinniburgh D.G., and Tipping E. (2001) Generic NICA-Donnan model parameters for proton binding by humic substances. *Environ. Sci. Technol.* **35**(10), 2049-2059.
- Moore S. and Stein W.H. (1954) A modified ninhydrin reagent for the photometric determination of amino acids and related compounds. *J. Biol. Chem.* **211**, 907-913.
- Morel F.M.M. and Hering J.G. (1997) *Principles and Applications of Aquatic Chemistry*. John Wiley & Sons, New York.
- Mrestani Y., Neubert R., Munk A., and Wiese M. (1998) Determination of dissociation constants of cephalosporins by capillary zone electrophoresis. *J. Chrom. A* **803**, 373-378.
- Müller M.B. and Frimmel F.H. (2002) A new concept for the fractionation of DOM as a

- basis for its combined chemical and biological characterization. *Wat. Res.* **36**, 2643-2655.
- Müller M.B., Schmitt D., and Frimmel F.H. (2000) Fractionation of natural organic matter by size exclusion chromatography—properties and stability of fractions. *Environ. Sci. Technol.* **34**(23), 4867-4872.
- Offord R.E.(1966) Electrophoretic mobilities of peptides on paper and their use in the determination of amide groups. *Nature* **211**, 591- 593.
- O'Loughlin E. and Chin Y.-P. (2001) Effect of detector wavelength on the determination of the molecular weight of humic substances by high-pressure size exclusion chromatography. *Wat. Res.* **35**(1), 333-338.
- Orlov D.S. (1966) Spectroscopic analysis of humic substances. *Sov. Soil Sci.* **6**, 1278-1286.
- Paxeus N. and Wedborg M. (1985) Acid-base properties of aquatic fulvic acid. *Anal. Chim. Acta* **169**, 87-98.
- Pelekani C., Newcombe G., Snoeyink V.L., Hepplewhite C., Assemi S., and Beckett R. (1999) Characterization of natural organic matter using high performance size exclusion chromatography. *Environ. Sci. Technol.* **33**(16), 2807-2813.
- Perdue E.M. (1985) Acidic functional groups of humic substances. In: *Humic Substances in Soil, Sediment, and Water. Geochemistry, Isolation, and Characterization.* G.R. Aiken *et al.*, Eds. pp 493-532. John Wiley & Sons, Inc.
- Perdue E.M., Reuter J.H., and Parrish R.S. (1984) A statistical model of proton binding by humus. *Geochim. Cosmochim. Acta* **48**, 1257-1263.
- Perdue E.M. and Lytle C.R. (1983) Distribution model for binding of proton and metal ions by humic substance. *Environ. Sci. Technol.* **17**(11), 654-660.
- Perdue E.M., Reuter J.H., and Ghosal M. (1980) The operational nature of acidic functional group analyses and its impact on mathematical descriptions of acid-base equilibria in humic substances. *Geochim. Cosmochim. Acta* **44**, 1841-1851.
- Perdue E.M. and Ritchie J.D. (2003) Dissolved organic matter in freshwaters. pp 273-318. In: *Surface and Ground Water, Weathering, and Soils* (ed. J.I. Drever) Vol. 5 *Treatise on Geochemistry* (eds. H.D. Holland and K.K. Turekian), Elsevier-Pergamon, Oxford.
- Perminova I.V., Frimmel F.H., Kudryavtsev A.V., Kulikova N.A., Abbt-Braun G., Hesse S., and Petrosyan V.S. (2003) Molecular weight characteristics of humic substances from different environments as determined by size-exclusion chromatography and their statistical evaluation. *Environ. Sci. Technol.* **37**(11), 2477-2485.

- Perminova I.V., Frimmel F.H., Kovalevskii D.V., Abbt-braun G., Kudrayavtsev A.V., and Hesse S. (1998) Development of a predictive model for calculation of molecular weight of humic substances. *Wat. Res.* **32(3)**, 872-881.
- Peuravuori J. and Pihlaja K. (1997) Molecular size distribution and spectroscopic properties of aquatic humic substances. *Anal. Chim. Acta* **337**, 133-149.
- Poppe H. (1992) Overloading and interaction phenomena in electrophoretic separations. *Anal. Chem.* **64**, 1908-1919.
- Randhawa N.S. and Broadbent F.E. (1965) Soil organic matter-metal complexes: 6. Stability constants of zinc-humic acid complexes at different pH values. *Soil Sci.* **99**, 362-366.
- Rasyid U., Johnson W.D., Wilson M.A., and Hanna J.V. (1992) Changes in organic structural group composition of humic and fulvic acids with depth in sediments from similar geographical but different depositional environments. *Org. Geochem.* **18(4)**, 521-529.
- Reid P.M., Wilkinson A.E., Tipping E., and Malcolm R. (1987) Determination of molecular weights of humic substances by analytical (UV scanning) ultracentrifugation. *Geochim. Cosmochim. Acta* **54**, 131-138.
- Reijenga J.C., Verheggen T.P.E.M., Martens J.H.P.A., and Everaerts F.M. (1996) Buffer capacity, ionic strength, and heat dissipation in capillary electrophoresis. *J. Chrom. A* **744**, 147-153.
- Reuter J.H. (1980) Chemical and Spectroscopic Characterization of Humic Substances Derived from River Swamps in the Floodplains of Southeastern U.S. Coastal Streams. Technical Completion Report USDI/OWRT Project No. B-132-GA.
- Rickard E.C., Strohl M.M., and Nielsen R.G. (1991) Correlation of electrophoretic mobilities from capillary electrophoresis with physicochemical properties of proteins and peptides. *Anal. Biochem.* **197**, 197-207.
- Ritchie J.D. and Perdue E.M. (2003) Proton-binding study of standard and reference fulvic acids, humic acids, and natural organic matter. *Geochim. Cosmochim. Acta* **67(1)**, 85-96.
- Robertson A.P. and Leckie J.O. (1999) Acid/base, copper binding, and $\text{Cu}^{2+}/\text{H}^{+}$ exchange properties of a soil humic acid, an experimental and modeling study. *Environ. Sci. Technol.* **33**, 786-795.
- Santos E.B.H., Esteves V.I., Rodrigues J.P.C., and Duarte A.C. (1999) Humic substances' proton binding equilibria: Assessment of errors and limitations of potentiometric data. *Anal. Chim. Acta* **392**, 333-341.

- Schimpf M.E. and Petteys M.P. (1997) Characterization of humic materials by flow field-flow fractionation. *Coll. Surf. A* **120**, 87-100.
- Schmitt-Kopplin P., Freitag D., Kettrup A., Schoen U., and Egeberg P.K. (1999a) Capillary zone electrophoretic studies on Norwegian surface water natural organic matter. *Environ. Int.* **25(2/3)**, 259-274.
- Schmitt-Kopplin P., Fischer K., Freitag D., and Kettrup A. (1998a) Capillary electrophoresis for the simultaneous separation of selected carboxylated carbohydrates and their related 1,4-lactones. *J. Chrom. A* **807**, 89-100.
- Schmitt-Kopplin P., Garmesh A.V., Kudryavtsev A.V., Perminova I.V., Hertkorn N., Freitag D., Petrosyan V.S., and Kettrup A. (2001) Quantitative and qualitative precision improvements by effect mobility-scale data transformation in capillary electrophoresis analysis. *Electrophoresis* **22**, 77-87.
- Schmitt-Kopplin P., Garrison A.W., Perdue E.M., Freitag D., and Kettrup A., (1998b) Capillary electrophoresis in the analysis of humic substances. Facts and artifacts. *J. Chrom. A* **807**, 101-109.
- Schmitt-Kopplin P., Hertkorn N., Garrison A.W., Freitag D., and Kettrup A. (1998c) Influence of borate buffers on the electrophoretic behavior of humic substances in capillary zone electrophoresis. *Anal. Chem.* **70**, 3798-3808.
- Schmitt-Kopplin P., Hertkorn N., Freitag D., Kettrup A., Garmash A.V., Kudryavtsev A.V., Perminova I., and Petrosyan V.S. (1999b) Mobility distribution of synthetic and natural polyelectrolytes with capillary zone electrophoresis. *J. AOAC Int.* **82(6)**, 1594-1603.
- Schmitt-Kopplin P. and Junkers J. (2003) Capillary zone electrophoresis of natural organic matter. *J. Chrom. A* **998**, 1-20.
- Schnitzer M. and Gupta U.C. (1965) Determination of acidity in soil organic matter. *Soil Sci. Soc. Proc.* **29**, 274-277.
- Schnitzer M. and Khan S.U. (1972) *Humic Substances in the Environment*. M. Dekker, New York.
- Schnitzer M. and Skinner S.I.M. (1962) Organo-metallic interactions in soils: 1. Reactions between a number of metal ions and the organic matter of a podzol Bh horizon. *Soil Sci.* **96**, 86-93.
- Schnitzer M. and Skinner S.I.M. (1968) Gel filtration of fulvic acid, a soil humic compound. In: *The Use of Isotopes and Radiation in Soil Organic Matter Studies*. pp 41-55.
- Senesi N., Miano T.M., Provenzano M.R., and Brunetti G. (1989) Spectroscopic and compositional comparative characterization of IHSS reference and standard fulvic and

- humic acids of various origins. *Sci. Tot. Environ.* **81/82**, 143-156.
- Serkiz S.M. and Perdue E.M. (1990) Isolation of dissolved organic matter from the Suwannee River using reverse osmosis. *Wat. Res.* **7**, 911-916.
- Shuman M.S. (1992) Dissociation pathways and species distribution of aluminum bound to an aquatic fulvic acid. *Environ. Sci. Technol.* **26(3)**, 593-589.
- Sierra M.M.D., Fernandes A.N., and Szpoganicz B. (2004) Influence of amide linkages on acidity determinations of humic substances. Testing with model-mixtures. *Talanta* **62**, 687-693.
- Sihombing R., Greenwood P.F., Wilson M.A., and Hanna J.V. (1996) Composition of size-exclusion fractions of swamp water humic and fulvic acids as measured by solid state NMR and pyrolysis-gas chromatography-mass spectrometry. *Org. Geochem.* **24(8/9)**, 859-873.
- Smith D.S., Bell R.A., and Kramer J.R. (2002) Metal speciation in natural waters with emphasis on reduced sulfur groups as strong metal binding sites. *Comp. Biochem. Physiol. C* **133**, 65-74.
- Specht C.H. and Frimmel F.H. (2000) Specific interactions of organic substances in size-exclusion chromatography. *Environ. Sci. Technol.* **34(11)**, 2361-2633.
- Sposito G., and Holtzclaw K.M. (1979) Copper(II) complexation by fulvic acid extracted from sewage sludge as influenced by nitrate versus perchlorate background media. *Soil Sci. Soc. Am. J.* **43**, 47-51.
- Sposito G., Holtzclaw K.M., and Keech D.A. (1977) Proton binding in fulvic acid extracted from sewage sludge-soil mixtures. *Soil Sci. Soc. Am. J.* **41**, 1119-1125.
- Sposito G., Holtzclaw K.M., and LeVesque-Madore S. (1978) Calcium ion complexation by fulvic acid extracted from sewage sludge-soil mixtures. *Soil Sci. Soc. Am. J.* **42**, 600-606.
- Stevenson F.J. (1994) *Humic Substances: Genesis, Composition, Reactions*. 2nd Edition. John Wiley & Sons, New York.
- Stevenson F.J. (1977) Nature of divalent metal complexes of humic acids as revealed by a modified potentiometric titration method. *Soil Sci.* **123(1)**, 10-17.
- Stumm W. and Morgan J.J. (1996) *Aquatic Chemistry : Chemical Equilibria and Rates in Natural Waters*. John Wiley & Sons, New York.
- Steelink C., Mikita M.A., and Thorn K.A. (1983) Magnetic resonance studies of humates and related model compounds. In: *Aquatic and Terrestrial Humic Materials* (eds. R.F.

- Christman and E.T. Gjessing), pp. 83-106. Ann Arbor Science, Ann Arbor.
- Sun L., Perdue E.M., and McCarthy J.F. (1995) Using reverse osmosis to obtain organic matter from surface and ground waters. *Wat. Res.* **29(6)**, 1471-1477.
- Sutheimer S.H., Ferraco M.J., and Cabaniss S.E. (1995) Molecular size effects on carboxyl acidity: implications for humic substances. *Anal. Chim. Acta* **304**, 187-194.
- Swift R.S. (1989) Molecular weight, size, shape, and charge characteristics of humic substances: some basic considerations. In: *Humic Substances II*. (eds. M.B.H Hayes *et al.*) pp. 449-465. John Wiley & Sons, Ltd, New York.
- Swift R.S. (1999) Macromolecular properties of soil humic substances: Fact, fiction, and opinion. *Soil Sci.* **164(11)**, 790-802.
- Swift R.S. and Posner A.M. (1971) Gel chromatography of humic acid. *J. Soil Sci.* **22(2)**, 237-249.
- Thang N.M., Geckeis H., Kim J.I., and Beck H.P. (2001) Application of the flow field-flow fractionation (FFFF) to the characterization of aquatic humic colloids: evaluation and optimization of the method. *Coll. Surf. A* **181**, 89-301.
- Thorn K.A. (1989) Nuclear-magnetic-resonance spectrometry investigations of fulvic and humic acids from the Suwannee River. In *Humic Substances in the Suwannee River, GA: Interaction, Properties, and Proposed Structures*. (Eds. R.C. Averett *et al.*), pp. 141-181. USGS Open File Report 87-557.
- Thurman E.M. (1985) *Organic Geochemistry of Natural Waters*. Martinus Nijhoff/Dr. W. Junk Publishers, Lancaster.
- Thurman E.M. and Malcolm R.L. (1981) Preparative isolation of aquatic humic substances. *Environ. Sci. Technol.* **15**, 463-466.
- Thurman, E.M., Wershaw R.L., Malcolm R.L., and Pinckney D.J. (1987) Molecular size of aquatic humic substances. *Org. Geochem.* **4**, 27-35.
- Tipping E. (1998) Humic ion-binding Model VI: an improved description of the interactions of protons and metal ions with humic substances. *Aq. Geochem.* **4**, 3-18.
- Tipping E. (1994) WHAM—a chemical equilibrium model and computer code for waters, sediments, and soils incorporating a discrete site/electrostatic model of ion-binding by humic substances. *Comp. Geosci.* **20**, 973-1023.
- Tipping E. and Hurley M.A. (1992) A unifying model of cation binding by humic substances. *Geochim. Cosmochim. Acta* **56**, 3627-3641.

- Tombácz E. (1999) Colloidal properties of humic acids and spontaneous changes in their colloidal state under variable solution conditions. *Soil Sci.* **164(11)**, 814-824.
- van der Moolen J.N., Boelens H.F.M., Poppe H., and Smit H.C. (1996) Origin and correction of bias caused by sample injection and detection in capillary zone electrophoresis. *J Chrom. A.* **744**, 103-113.
- Van Dijk H. (1966) Some physio-chemical aspects of the investigation of humus. In *The Use of Isotopes in Soil Organic Matter Studies*. pp. 129-141. Pergamon Press, Oxford.
- Varga B., Kiss G., Galambos I., Gelencser A., Hlavay J., and Krivacsy Z. (2000) Secondary structure of humic acids. Can micelle-like conformation be proved by aqueous size exclusion chromatography? *Environ. Sci. Technol.* **34(15)**, 3303-3306.
- Varney M.S., Mantoura R.F.C., Whitfield M., Turner D.R., and Riley J.P. (1983) Potentiometric and conformational studies of the acid-base properties of fulvic acids from natural waters. In *Trace Metals in Seawater*. (Eds. Wong C.S. *et al.*), pp. 751-772. Plenum, Oxford.
- Westerhoff P., Aiken G., Amy G., and Debroux J. (1999) Relationships between the structure of natural organic matter and its reactivity towards molecular ozone and hydroxyl radicals. *Wat. Res.* **33(10)**, 265-276.
- Woolard C.D. and Linder P.W. (1999) Modeling the cation binding properties of fulvic acids: an extension of the RANDOM algorithm to include nitrogen and sulfur donor sites. *Sci. Tot. Environ.* **226**, 35-46.
- Yemm E.W. and Cocking E.C. (1955) The determination of amino acids with ninhydrin. *Analyst* **80**, 209-213.
- Zanardi-Lambardo E., Clark C.D., and Zika R.G. (2001) Frit inlet/frit outlet flow field-flow fractionation: methodology for colored dissolved organic material in natural waters. *Anal. Chim. Acta* **443**, 171-181.
- Zhou Q., Cabaniss S.E., and Maurice P.A. (2000) Considerations in the use of high-pressure size exclusion chromatography (HPSEC) for determining molecular weights of aquatic humic substances. *Wat. Res.* **34(14)**, 3505-3514.

VITA

Jason D. Ritchie was born on May 12, 1972 and grew up in Frostburg, Maryland, a coal mining and railroad town in the Allegheny Mountains of Western Maryland. He earned his bachelor's degree in earth science, with a minor in chemistry, at Frostburg State University in May 1994. After graduation, he worked for two years as a junior manager at a high-end retail store, followed by a very short time working as a retail fashion coordinator for a major designer clothing manufacturer. He returned to Frostburg State University in 1997 for one year in the Chemistry Department to prepare for graduate school. In 1998, Jason started to pursue his Ph.D. degree in the School of Earth and Atmospheric Sciences at Georgia Institute of Technology. During his tenure at Georgia Tech, Jason focused on the chemical characterization of aquatic natural organic matter. Jason instructed four different undergraduate laboratory courses each fall and spring semester, co-authored two publications, made oral presentations at three regional ACS meetings, and participated in the collection of the new Suwannee River humic and fulvic acids for the IHSS. After completing his Ph.D. degree, Jason anticipates a postdoctoral research position.